Assessment of Static Spinal Stability and Muscle Activation Strategies: A Comprehensive Approach via a Novel Validated Finite Elements Spine Model Inclusive of Thoracolumbar Facia, Intramuscular Pressure, and Intra-abdominal Pressure

Ibrahim Kamal El Bojairami

Department of Mechanical Engineering

McGill University, Montreal

April 2022

A thesis submitted to McGill University in partial fulfillment of the requirements of the degree of Doctor of Philosophy in Mechanical Engineering

© Ibrahim El Bojairami, 2022

ABSTRACT

Low back dysfunctions, among which are potentially low back pain (LBP) episodes, continue to prevail as burdensome conditions due to their socioeconomic repercussions and unknown causes. A common understanding in the scientific community is that a significant portion of these problems is of mechanical origin, often referred to as *spinal instability*.

Growing literature suggests that the coactivation and engagement of spinal tissues tend to maintain an upright spinal posture and enhance stability through restoring the spine's initial position following an external perturbation. As such, the present research seeks to further interpret stability achieved by the coactivation of paraspinal muscles, active engagement of intramuscular pressure (IMP) and intra-abdominal pressure (IAP), and support provided by the thoracolumbar fascia (TLF). Thus, the central focus of this thesis was to develop and validate an accurate, fully representative, spine model, to then assess novel theorems of contributors towards spinal stability and underlying muscle activation patterns.

To achieve this, specific objectives were identified: 1) create and validate the first scalable biphasic muscle finite elements (FE) model inclusive of an IMP-based enclosed fluidic field; 2) develop and validate a fully representative FE spine model inclusive of IMP-based muscles from objective 1, IAP, and TLF; 3) exploit the FE spine model, from objectives 1 and 2, to investigate soft tissues' contribution to spinal stability; 4) exploit the FE spine model and stability results, from objectives 1, 2, and 3, to devise IMP-based muscle activation strategies.

Results of objective 1 exhibited linearly correlated muscle forces and IMP. This exemplified a valid novel approach to simulate fluid-filled muscle contraction. This was then integrated into objective 2 to develop a comprehensive spine model, which comprised 273 soft tissues including all those known to contribute to spinal loadings. The model was then shown valid considering *in silico* and *in vivo* comparator tests. The accurate modelling and inclusion of more representative biological soft tissues, in a comprehensive spine model, allowed for a better assessment of spine

physiology, while remaining within targeted validation scope. This led to the third objective whereby individual and collective contributions of muscles, TLF, and IAP toward spinal stability were assessed. Combined synergistic activations showed a 93% increase in defined stability. TLF appeared to dissipate and store excessive loads, IAP limited movements, and muscles acted as antagonistic to external perturbations. This begged the question of what governed such underlying muscle activations. As such, in objective 4, conventional and novel IMP-based muscle activation strategies were explored, which suggested an optimized region of IMP within which tasks are efficiently executed while maintaining a stable spine position.

Many findings have been achieved in the context of this thesis. The developed FE muscle and spine models provide accurate approaches to exploring spinal stability and spine-related pathologies. The models can potentially be leveraged to assess injuries and analyze medical devices. Lastly, investigated activation strategies can greatly inform motion analysis, device design for spine pathologies, rehabilitation, and functional electrical stimulation of muscles.

RÉSUMÉ

La Lombalgie Chronique (LC) continue de prévaloir en tant que condition pénible en raison de ses répercussions socio-économiques et de ses causes inconnues. Un consensus scientifique est qu'une partie importante du problème est d'origine mécanique, souvent appelée instabilité vertébrale.

La littérature suggère que la coactivation et l'engagement des tissus rachidiens ont tendance à maintenir une posture vertébrale droite et à améliorer la stabilité en récupérant la position initiale de la colonne vertébrale suite à une perturbation externe. En tant que tel, la présente recherche cherche à interpréter davantage la stabilité par la coactivation des muscles paraspinaux, l'engagement actif de la pression intramusculaire (PIM) et de la pression intra-abdominale (PIA) et le soutien fourni par le fascia thoraco-lombaire (FTL). Ainsi, l'objectif central de cette thèse était de développer et de valider un modèle de colonne vertébrale précis et pleinement représentatif, afin de mieux évaluer la stabilité de la colonne vertébrale et les modèles d'activation musculaire sous-jacents.

Pour y parvenir, des objectifs spécifiques ont été identifiés : 1) créer et valider le premier modèle d'éléments finis (EF) musculaire biphasique évolutif incluant un champ fluidique fermé basé sur l'PIM ; 2) développer et valider un modèle de colonne vertébrale EF entièrement représentatif comprenant les muscles basés sur l'PIM de l'objectif 1, PIA et FTL ; 3) exploiter le modèle EF de la colonne vertébrale, des objectifs 1 et 2, pour étudier la contribution des tissus mous à la stabilité de la colonne vertébrale ; 4) exploiter le modèle de colonne vertébrale EF et les résultats de stabilité, des objectifs 1, 2 et 3, pour concevoir des stratégies d'activation musculaire basées sur l'PIM.

Les résultats de l'objectif 1 présentaient des forces musculaires et une PIM linéairement corrélées. Cela illustre une nouvelle approche valide pour simuler la contraction musculaire remplie de liquide. Cela a ensuite été intégré à l'objectif 2 pour développer un modèle de colonne

vertébrale complet, qui comprenait 273 tissus mous, y compris tous ceux connus pour contribuer aux charges vertébrales. Le modèle s'est ensuite montré valide compte tenu des tests de comparaison in silico et in vivo. La modélisation précise et l'inclusion de tissus mous biologiques, dans un modèle de colonne vertébrale complet, ont permis une meilleure évaluation de la physiologie de la colonne vertébrale, tout en restant dans le cadre d'une validation ciblée. Cela a conduit au troisième objectif dans lequel les contributions individuelles et collectives des muscles, du FTL et de l'PIA à la stabilité de la colonne vertébrale ont été évaluées. Les activations synergiques combinées ont montré une augmentation de 93% de la stabilité. Le FTL a semblé se dissiper les charges excessives, l'PIA a limité les mouvements et les muscles ont agi comme antagonistes aux perturbations externes. Cela a soulevé la question de savoir ce qui gouvernait ces activations musculaires sous-jacentes. En tant que tel, dans l'objectif 4, des stratégies d'activation musculaire conventionnelles et nouvelles basées sur l'PIM ont été explorées, ce qui a suggéré une région optimisée de l'PIM dans laquelle les tâches sont exécutées efficacement tout en maintenant une position stable de la colonne vertébrale.

Une multitude d'avancées ont été réalisées dans le cadre de cette thèse. Les modèles musculaires et rachidiens développés par EF fournissent des approches précises pour explorer la stabilité de la colonne vertébrale et les pathologies liées à la colonne vertébrale. Les modèles peuvent être potentiellement exploités pour évaluer les blessures et analyser les dispositifs médicaux. Enfin, les stratégies d'activation étudiées peuvent grandement éclairer l'analyse du mouvement, la conception de dispositifs pour les pathologies de la colonne vertébrale, la rééducation et la stimulation électrique fonctionnelle des muscles.

DEDICATION

I dedicate this work to my parents, Amal Al Eleish and Kamal El Bojairami, as well as my brother, Mahmoud El Bojairami, whom I share with a very special bond, for their endless support, motivation, and unconditional love. Mom, Dad, and Mahmoud, this is but a minute symbol of gratitude for the sacrifices you have made, the hardships you had to go through, and the effort you made to seek a better future for me.

To Mahmoud, you are who taught me to perform all of life's tasks, no matter how big or small, to the best of my ability, and without complaint. You are who I will always aspire to be.

To my future wife, sit tight. I promise, I am one step closer to you.

Finally, to my future kids .. you little hypothetical beauties, I love you so much. There is no roof to your ambitions, your goals will always be within your reach. Aim as high as you impossibly can.

The human body is nothing but a perfectly tuned musical instrument in an environment of chaos, disorder, instability, randomness, and uncertainty. It is the negentropy to entropy.

ACKNOWLEDGMENTS

In the name of Allah, the Most Gracious, the Most Merciful

First and foremost, I would like to express my sincere gratitude and appreciation to my research director, supervisor, and mentor Professor Mark Driscoll for his tremendous guidance, support, kindness, understanding, patience, and motivation throughout my doctoral degree. It was, and will always be, an absolute honor that I will always carry with me, in my professional career, to have had the chance to learn spine and musculoskeletal biomechanics from Professor Driscoll. The exceptional skills I acquired from Professor Driscoll's vast academic and industrial career will always be the foundation I lean on tackling future endeavors. Words will fail me and truly undermine my blissful experience with you, Professor Driscoll.

Furthermore, I would like to thank Professor Mathias Legrand and Dr. Julie Côté for never hesitating to discuss and help guide my research.

I was exceptionally lucky to have been surrounded by wonderful friends and colleagues, at the musculoskeletal biomechanics research lab and the orthopaedic research lab during my studies. To this, a warm and special thanks goes to both, Dr. Khaled El-Monajjed and Dr. Brahim Brahmi, for all the time we spent, work we collaborated, and future plans we drew. My sincere gratitude extends to the rest of the team for their consistent support and collaboration especially Dr. Natasha Jacobson, Emily Newell, Brittany Stott, Trevor Cotter, Sneha Patel, and Tianqi Wang. I would also like to thank my university friends for all the laughs we shared, meals we had, and amazing time we spent, namely Jamil El-Najjar, Ahmed Abdelbaki, and Osaid Matar.

In addition, I would like to dedicate a special appreciation for the Fonds de Recherche du Québec - Nature et Technologies (FRQNT), the Mechanical Engineering Department at McGill University, and the Natural Science and Engineering Research Council of Canada (NSERC) for their financial support. There is no way this work would have been successful without this.

I would like to extend my thanks to my mother and father who believed, supported, and never had a doubt in my potentials. I would like to also extend my sincere thanks and love to my dear brother, Mahmoud, who stands as my backbone, always had faith in my capabilities, and without hesitation supported my decision to pursue a PhD. I also consider myself to be an extremely lucky person for having wonderful friends outside of academia, back home in Lebanon and here in Canada, who were always there in times of need. Finally, it goes without saying that this work would have never been slightly possible without the blessings of Almighty Allah, the Most Beneficent, the Most Gracious, the most Merciful. Alhamdulellah for this great achievement.

CONTENTS

LIST OF TABLES

LIST OF FIGURES

NOMENCLATURE

1D	One Dimension
2D	Two Dimensions
3D	Three Dimensions
APDL	Algorithmic Processor Description Language
AW	Abdominal Wall
AWTh	Abdominal Wall Thickness
ASME	American Society of Mechanical Engineers
α	Neo-Hookean fractional exponent
BMI	Body Mass Index
C	Planar stiffness
C_{ab}	Abdominal Compliance
CAD	Computer-Aided Design
CAX4R	Linear quadrilateral elements
COXAX4	Cohesive linear quadrilateral elements
CoU	Context of Use
d	Moment arm
D	Array of cohesive parameters
$\boldsymbol{D}$	The deformation gradient tensor
$\overline{\boldsymbol{D}}$	The modified deformation gradient tensor
ε	Strain
$\hat{\varepsilon}$	Error function
E	Young's modulus
E_{nn}	Normal elastic modulus
E_{ss}	Tangential elastic modulus

EMG	Electromyography
f_p	Insertion force
f_{friction}	Friction force
f_{cutting}	Tissue cutting force
$f_{\text{stiffness}}$	Tissue deformation reaction force
$\boldsymbol{F}$	Deformation gradient
F	Force
F_{TLF}	Thorcolumbar Fascia's reaction forces
F_{IAP}	Abdominal reaction forces
FE	Finite Elements
FEA	Finite Elements Analysis
FEM	Finite Element Model
G	Shear modulus
$\boldsymbol{G_c}$	Fracture toughness
GDM	Gradient Descent Method
GPU	Graphics Processing Unit
HDSP	Hydrostatic Pressure Node
HSFLD242	Hydrostatic Fluid Elements
IMP	Intra-Muscular Pressure
IAP	Intra-Abdominal Pressure
IAV	Intra-Abdominal Volume
IVD	Intervertebral Disc
I	Intertransversarius muscles
$\boldsymbol{J}$	Muscle bulk modulus
K	Crack elastic opening
LBP	Low Back Pain
L	Longissimus muscle
MC	Muscle Centroid
MFR	Muscle Relative Force

ML	Muscle Length
MLS	Muscle Longitudinal Strain
MRI	Magnetic Resonance Imaging.
M	Multifidus muscle
M_x	Stress couple in the axial direction
M_θ	Stress couple in the circumferential direction
$M_{x\theta}$	Stress couple in the x-θ plane
M_{Bending}	Bending moment
NS	Average Normal Stress
N_x	Normal stress resultant in the axial direction
N_θ	Normal stress resultant in the circumferential direction
$N_{x\theta}$	Shear stress resultant in the the x-θ plane
P	Psoas major muscle
p	Shell's enclosed hydrostatic pressure field
$\bar{p}$	Chi's pressure field solution
Q_x	Transverse stress resultant in the axial direction
Q_θ	Transverse stress resultant in the circumferential direction
R	Muscle radius
R_{in}	Inner muscle shell radius
R_{out}	Outer muscle shell radius
S	Overall stiffness
t	thickness
t_n	Normal traction
t_s	Shear traction
T_0	Cohesive element original thickness
TLF	Thoracolumbar Fascia
TP	Test Points
u_x	Axial displacement
u_r	Radial displacement

u_θ	Circumferential displacement
U	Average spine displacement
VB	Vertebral Body
VR	Virtual Reality
WSACS	World Society on Abdominal Compartment Syndrome
$\widetilde{W}_C$	The complementary stored-energy function
W_{ext}	External work
$\widehat{W}_{\text{f}}$	Frictional work
$\widehat{W}_E$	Strain energy
$\widehat{W}_{\text{cr}}$	Work required for crack propagation
x	Deformed position vector
χ	Strain potential
v	Poisson's ratio
σ	Stress
σ_{mn}	Normal nominal stress
σ_{ms}	Shear nominal stress
μ_i	Muscle layer shear modulus
δ_n	Normal separation
$\delta_{n,i}^0$	Crack initial displacement
$\delta_{n,i}'$	Crack failure displacement
δ_s	Shear separation
λ	Shell stretch ratio
λ_i	Principal stretches
θ_i	Expression weights
$<\ldots>$	Macaulay bracket operator

AUTHORS CONTRIBUTION

I, Ibrahim El Bojairami, hereby certify that I am the primary author for all the manuscripts and chapters within this dissertation. Under the supervision of Professor Mark Driscoll, I designed the 3D finite elements models to address the undermentioned hypotheses realizing the notion of equilibrium spinal stability and muscle activation strategies. In specifics, I developed the 3D skeletal muscle model and explored the correlation between intramuscular pressure and muscle force. Furthermore, in occasional collaboration with Dr. Khaled El-Monajjed, I developed, verified, and extensively validated the 3D full-scale finite elements spine model with which I executed biomechanical simulations. I then designed and conducted the case specific scenarios to address the contribution of spinal muscles, thoracolumbar fascia, and abdominal pressure to spinal stability. In addition, I was the primary investigator to the two additional studies, in occasional collaboration with Dr. Natasha Jacobson and Dr. Amirhossein Hamedzadeh, in which I explored the feasibility of reverse-engineering the material properties of soft tissues and the effects of abdominal physiological changes on abdominal compliance. Moreover, I devised and executed the muscle activation strategies presented herein in the objective of achieving equilibrium spinal stability. Finally, I take full responsibility for all the programs, codes, scripts, and material presented herein, and hereby certify that I am the primary developer and designer of all biomechanical case studies and scenarios conducted.

ORIGINAL CONTRIBUTION

The research reported within this dissertation consists of novel architecture and ideas to construct a finite element spine model in order to evaluate equilibrium spinal stability. In essence, the research consisted of the following contributions to knowledge towards the field of spine biomechanics:

1. First 3D scalable, custom-coded, and biphasic finite element model of a skeletal muscle inclusive of an intramuscular pressure enclosed fluidic field, with which the correlation between muscle contractile force and intramuscular pressure was explored and validated.
2. First extensively validated and verified, full-scale, physiologically representative finite element model of the spine inclusive of major spine muscles along their enclosed intramuscular pressure, thoracolumbar fascia, and abdominal pressure.
3. Examination of the feasibility of extracting the material properties of soft tissues using a hybrid finite elements and optimization approach by utilizing fracture mechanics during needle insertion procedures.
4. First extensive evaluation of equilibrium spinal stability as achieved by a coordination between spinal muscles, thoracolumbar fascia, and abdominal pressure.
5. Examination of physiological abdominal changes on abdominal compliance and equilibrium spinal stability.
6. First study to devise and explore pressure-based muscle activation strategies, as well as conventional patterns, in efforts of maintaining equilibrium spinal stability.

Correspondingly, the aforementioned contributions were further disseminated through the following published and submitted scientific journal articles:

1. El Bojairami, I. & Driscoll, M. Correlating Skeletal Muscle Output Force and Intramuscular Pressure via a 3-Dimensional Finite Element Muscle Mode. *J. Biomech. Eng.* (2021).

2. El Bojairami, I., El-Monajjed, K. & Driscoll M. Development and validation of a timely and representative finite element human spine model for biomechanical simulations. *Sci. Rep.* (2020).
3. El Bojairami, I., Hamedzadeh, A. & Driscoll, M. Feasibility of extracting tissue material properties via cohesive elements: a finite element approach to probe insertion procedures in non-invasive spine surgeries. *Med. Biol. Eng. Comput.* (2021).
4. El Bojairami, I. & Driscoll, M. Coordination Between Trunk Muscles, Thoracolumbar Fascia, and Intra-Abdominal Pressure Toward Static Spine Stability. *Spine* (2021).
5. El Bojairami, I., Jacobson, N. & Driscoll, M. Development and evaluation of a numerical spine model comprising intra-abdominal pressure for use in assessing physiological changes on abdominal compliance and spinal stability. *Clin. Biomech.* (Under review).
6. El Bojairami, I. & Driscoll, M. Formulation and Exploration of Novel, Intramuscular Pressure Based, Muscle Activation Strategies in a Spine Stability Model. *Computers in Biology and Medicine* (Accepted).

Furthermore, the findings were disseminated and presented in the following conferences (peer-reviewed published abstracts):

1. El Bojairami, I. & Driscoll, M. A 3-Dimensional Finite Element Muscle Model to Predict Forces in the Clinic. *Canadian Society of Biomechanics 'CSB',* (2018).
2. El Bojairami, I. & Driscoll, M. Development and Validation of a Representative Finite Element Spine Model for Accurate Biomechanical Simulations. *Canadian Society of Biomechanics 'CSB-SCB' 2020/21,* (2021).
3. El Bojairami, I. & Driscoll, M. A Validated State of the Art Human Spine Finite Element Model for Accurate Biomechanical Simulations. *Global Spine Congress 'GSC'* (2021).
4. El Bojairami, I. & Driscoll, M. Role of Muscles, Abdominal Pressure, and Thoracolumbar Fascia in Thoraco-Lumbar Spine Stability. *Global Spine Congress 'GSC'* (2021).
5. El Bojairami, I. & Driscoll, M. Credibility Assessment of a Physiologically Representative Finite Elements Spine Model: Verification and Validation. *Orthopaedic Research Society 'ORS'* (2022).

6. El Bojairami, I. & Driscoll, M. Devise and investigate a novel, intramuscular pressure based, muscle activation strategy in a spine stability model. *22nd Annual Scientific Conference of the Canadian Spine Society 'CSS'* (2022).
7. El Bojairami, I. & Driscoll, M. Assessment of elasticity changes on abdominal compliance and spinal stability: A numerical spine model approach inclusive of intra-abdominal pressure. *International Society for the Advancement of Spine Surgery 'ISASS'* (Accepted).
8. El Bojairami, I. & Driscoll, M. Assessment of static spine stability and relative implications of trunk muscles, thoracolumbar fascia, and intra-abdominal pressure. *37th North American Spine Society 'NASS' conference* (Accepted).
9. El Bojairami, I. & Driscoll, M. Integration of intramuscular pressure with novel muscle activation strategies in a spine model. *37th North American Spine Society 'NASS' conference* (Accepted).

INTRODUCTION

"If you would seek health, look first to the spine" – Socrates. No wonder the spine continues to catch significant research attention; this natural prodigy is literally the backbone of every task we execute. The synchronization of the tissues comprising the spine is uncanny (Fig. 0–1), as if it is a naturally existing, perfectly tuned, musical instrument. One string goes out of sync and the spine becomes dysfunctional with apparent repercussions ranging from injuries, deformities, herniated discs, vertebral fractures, and most commonly, low back pain (LBP).

Figure 0–1: Human spine schematic (obtained on December 1st 2021 from https://pixabay.com/photos/spine-bone-back-pain-vertebrae-3220105/).

Pain is a thousand-year-old paradoxical topic. It is a mental state interpreted *via* active stimulants; yet, is highlighted as a physical state pointing to a tangible body tissue, thus suggesting

its philosophically paradoxical nature. LBP is no different; it is a highly subjective condition, to which 90% of its cases have not been associated to a specific cause. With a lifetime prevalence between 75% and 84%, LBP is considered the number one cause of disability in the world. The nature of the condition, however, remains broad with significant research efforts consistently put to understand its pathomechanism.

The biomechanics surrounding the human spine is a study of equilibrium, stability, motion, and deformation of the structure itself. It is the result of internal and external forces, generated and transferred by spinal tissues. At its fundamental level, equilibrium spinal stability is still an extremely challenging concept to define and quantify. From an engineering perspective, the ability of the spinal tissues to keep the spine within its original status of equilibrium lends significant insights into overall equilibrium spinal stability. Therefore, spinal stability can be assessed *via* biomechanical parameters stemming from major spinal tissues, namely paraspinal muscles activation, muscles internal pressure, or what is referred to as intramuscular pressure (IMP), abdominal pressure, and thoracolumbar fascia. The accurate modelling of these physiologies could provide a pathway to objectively analyze their role and contribution to equilibrium spinal stability presented and defined herein.

The emergence of the biomechanics-applied finite elements (FE) field made the development of precise biomechanical models possible. FE is a numerical approximation technique used to solve redundant and physically complex systems. It is a widely applied method in biomechanics used to design medical devices, assess injuries, interpret biomechanical parameters, track the development of deformities, and complement clinical data. However, available muscle and spine FE models most often include substantial simplifications ranging from omitting muscles' fluidic constituent, focusing on selective spine parts, and/or not including the effects of intra-abdominal pressure and thoracolumbar fascia. While these assumptions may be valid in select contexts and lead to insightful findings, methodical investigations to accurately assess engineering spinal stability necessitates a representative spine model with fundamentals entailing major, mentioned, spine tissues.

In such a case, an accurate depiction of muscle constituents governing physiological contraction, coupled with a comprehensive spine model representative of vertebral bodies, intervertebral discs, major spinal muscles, thoracolumbar fascia, and intra-abdominal pressure may fill that void on the

condition that it provides timely, physiological, and realistic results. As such, this requires a tissue by tissue modelling procedure that respects the governing mechanics, as well as a dedicated FE method that would virtually waive the numerical complexity of such a detailed model.

Therefore, the general objective of this doctoral project was to develop, verify, and validate a comprehensive and state-of-the-art finite element model of the spine in order to assess engineering static spine stability and underlying muscle activation strategies. To achieve this endeavor, a methodical review was conducted on the anatomical and mechanical characterization of underlying tissues, developed spine models and their use-cases, and muscle activations in efforts of understanding spinal stability. As a result, a novel scalable model of a skeletal muscle, inclusive of intramuscular pressure, was then developed to allow for accurate depiction of muscle contraction, as well as characterize and devise IMP-based muscle activation strategies. Furthermore, representative models of the intra-abdominal pressure and thoracolumbar fascia were integrated in the full spine model in efforts of understanding and quantifying equilibrium stability of the spine.

The dissertation is composed of eight chapters as shown in Fig. 0–2. Relevant and selective, rather than exhaustive, literature was first reviewed (chapter 1), followed by explicitly identifying specific research objectives and corresponding hypotheses (chapter 2). The void in literature then led to publishing two scientific manuscripts, presented in chapters 3 and 4, which led to developing the representative spine model. Chapter 3 further presents an additional third published manuscript on the feasibility of extracting tissue material properties in the absence of *in vivo* testing. Consequently, chapter 5 presents a fourth published manuscript on developed spine model's conceived tissues to maintain spinal stability. An additional, fifth, submitted manuscript is also presented in chapter 5 to closely examine abdominal activation and physiological changes effect on equilibrium spinal stability. Finally, in a sixth submitted manuscript, chapter 6 addresses muscle activation strategies bound by spinal stability objective functions. The explored six scientific manuscripts were lastly bound under a general discussion in chapter 7 while chapter 8 concludes this dissertation and provides further perspectives.

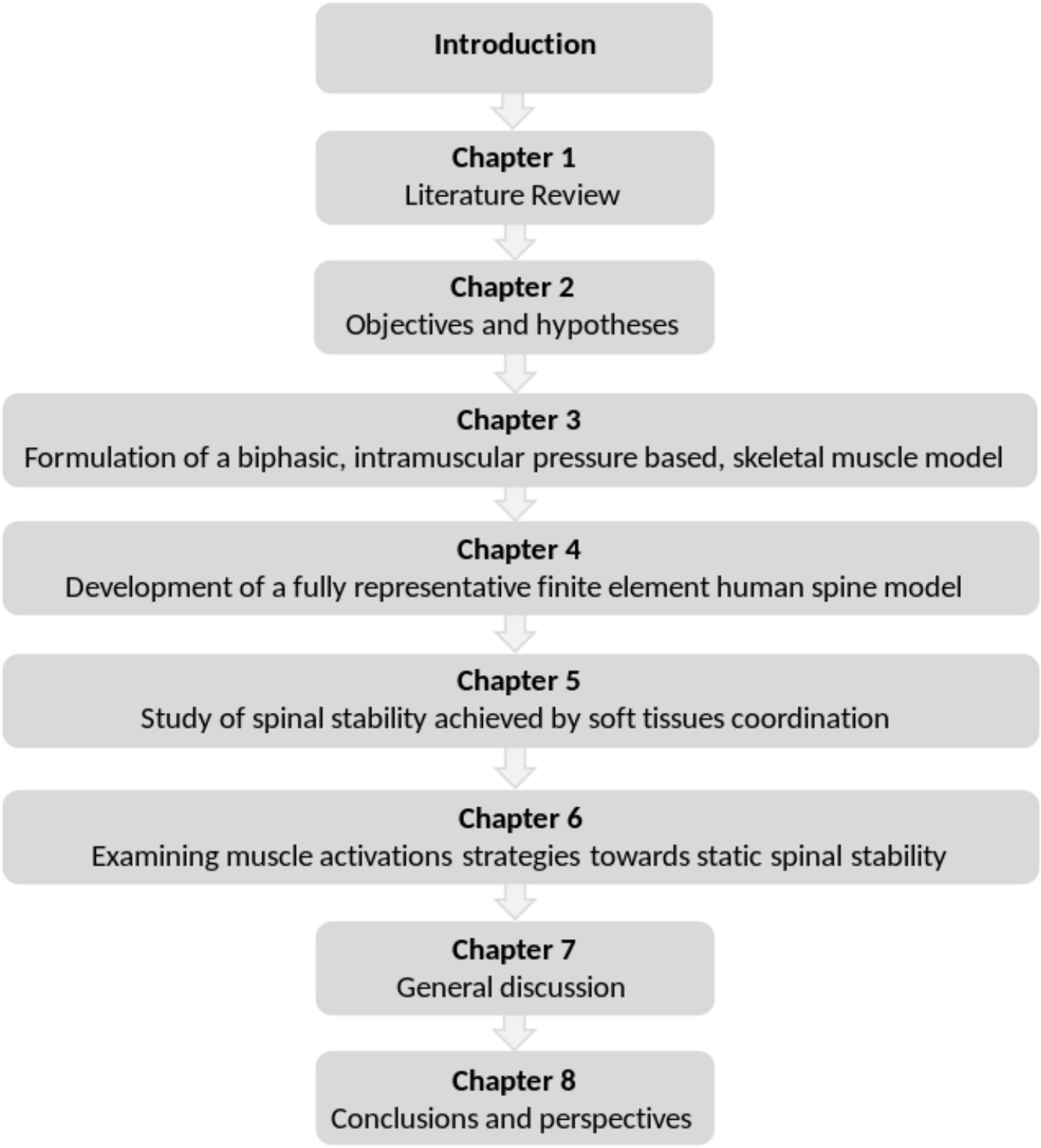

Figure 0–2: Thesis structure.

1

LITERATURE REVIEW

1.1. ANATOMY, BIOMECHANICS, AND MECHANICAL CHARACTERIZATION OF THE SPINE

The spine, vertebral column, spinal column, torso, trunk, or backbone are different names referring to the same anatomy; a bony structure that extends the length of the human back, connecting the head to the pelvis, and encloses the spinal cord[1]. Its utmost neurological function is to protect the spinal cord, one of the body's central nervous systems and a pathway for messages between the brain and the rest of the body[1]. In addition to this, the spine has a multitude of biomechanical functions including supporting the mass of the body[2], resisting external forces[3], protection against sudden impacts[4], and perhaps most importantly, granting mobility and flexibility for the body[5].

The spine consists of vertebral bodies, or vertebrae, connected by intervertebral discs, forming five distinct regions, namely, the cervical spine, the thoracic spine, the lumbar spine, the sacrum, and the coccyx, as shown in Fig. 1–1. Radially, numerous muscles surround and insert to the spine *via* tendon attachments. The frontal spine is further engulfed and enclosed by abdominal and thoracic cavities. Lastly, the spine connects to a ligamentous and fascial subsystem, which in addition to tendons, includes spinal ligaments and thoracolumbar fascia. Those can be grouped into an *active system*, comprising active muscles and abdominal cavity contraction, and a *passive system*, comprising passive contribution of muscles, vertebral bodies, intervertebral discs, ligaments, tendons, and fascia[6]. The coordination and harmony between such systems is what facilitates spine's previously mentioned functions.

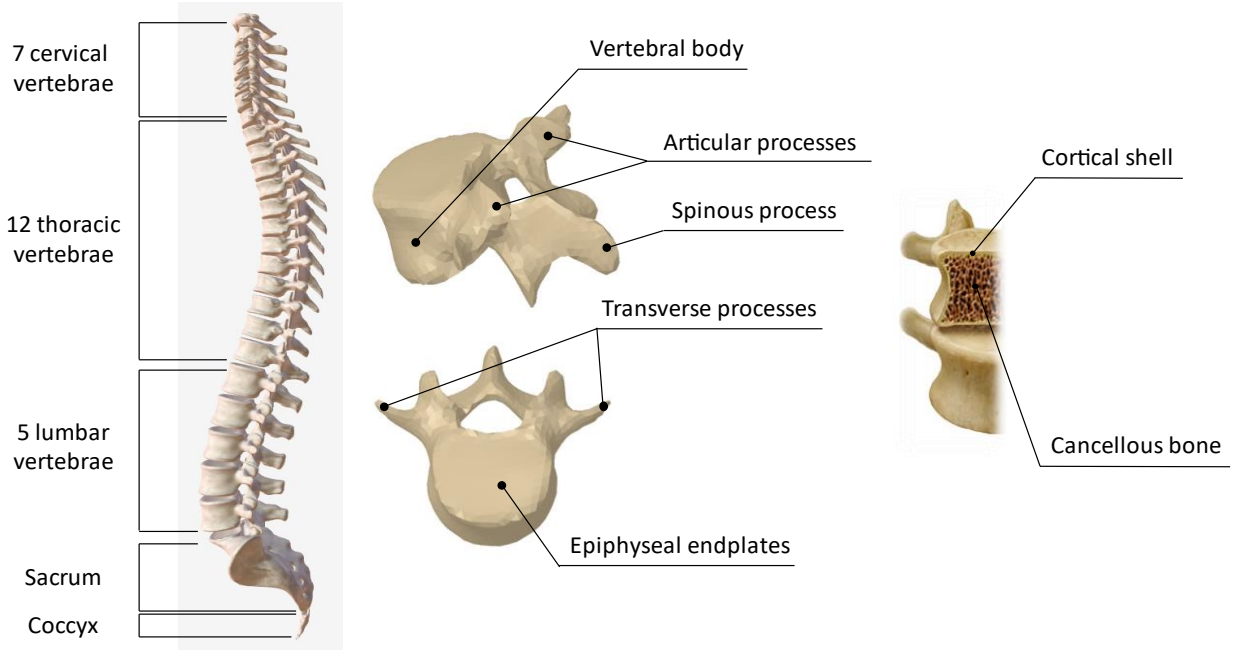

Figure 1–1: Vertebral bodies anatomy (obtained and modified on December 1st 2021 from https://commons.wikimedia.org/wiki/File:A-B-C_degenerative_changes.webp).

1.1.1. VERTEBRAL BODIES

When viewed from the side, the spine has a natural S-shaped curve (Fig. 1–1), consisting of around 33 vertebrae, depending on skeletal maturity. The first 7 comprise the cervical spine (C1-C7), the part that supports the weight and enables movement of the head[7]. This is followed by 12 vertebrae forming the thoracic spine (T1-T12), the part that is mainly responsible for holding the rib cage and protecting the heart and lungs[8]. Next are 5 vertebrae forming the lumbar spine (L1-L5), the region which bears the largest portion of the weight of the body[9]. The spinal column inferiorly ends with 5 fused vertebrae that forms the sacral elements (S1-S5), which connect the spine to the hip bones, followed by 4 more fused vertebrae that make up the coccyx (Co1-Co4), which provide attachments for ligaments and muscles of the pelvic floor[7,10].

Each of those vertebrae is made up of a thin cortical shell of almost 0.29 mm thickness[11] enclosing the vertebral body, which is made of cancellous, or trabecular, bone[10]. The top and bottom of each vertebrae is bordered by endplates, each of approximately 0.62mm thickness[12].

The posterior elements, also called vertebral processes, are distinct in shape and size throughout the spine depending on their function[13].

Biomechanical characterization of cortical bone and cancellous matrix show viscoelastic response and dependency on strain rate due to water content[14]. However, under small strains and static conditions, viscoelastic effects are less noticeable and the material behaves as almost linear elastic[15], commonly defined by an elasticity modulus (E), a Poisson's ratio (ν), and/or a shear modulus (G). Those can be either directional (defined by a planar stiffness 'C') or bulk properties depending on material's isotropy. In numerical analyses, such as finite elements (FE), accurate assignment of material laws has a significant effect on conceived results, whereby the validity of the choice depends on the scope of the study. Numerous studies attempted to characterize vertebrae *via* mechanical tests; conceived mechanical properties were thus collected and are summarized in Tables 1–1 and 1–2.

1.1.2. INTERVERTEBRAL DISCS

An intervertebral disc (IVD) is a cartilaginous tissue situated in between each two adjacent vertebrae[51]. It is mainly composed of three sub-elements: the nucleus pulposus, the annulus fibrosus, and two endplates (Fig. 1–2). On a microstructural level, no clear separation seems to exist between the boundaries of the nucleus pulposus and annulus fibrosus[52]. Thus, these substructures interact in a continuum to serve overall IVDs' functions. In general, IVDs are fluid-heavy tissues that exhibit large deformations to allow for spinal flexibility[51]. Specifically, they are almost 20-30% of the total spine length, and reflect highly important functions including, but not limited to, reducing stress caused by sudden impacts[53], enabling relative movement between adjacent vertebrae[10], cushioning excessive spinal loads[54], and acting as a nutrients passage to the spine and the spinal cord fluid[51].

Biomechanical characterization of the IVDs is usually governed by biphasic models due to the fluidic behavior of the tissue[55]. Thus, a healthy IVD is expected to exhibit a viscoelastic response under different strain rates. On the other hand, the structural element of typical literature IVD models follows a composite material analogy due to the presence of strong collagen fibers, especially in the annulus fibrosus[56]. Thus, under dynamic time-dependent effects, an IVD material

Table 1–1: Mechanical characterization of cortical bone.

Cortical shell	
Material law	**Constitutive properties**
Isotropic	$E = 5$ GPa; $v = 0.3$[16–18]
	$E = 10$ GPa; $v = 0.3$[19–21]
	$E = 12$ GPa; $v = 0.3$[22–36]
	$E = 11.3$ GPa; $v = 0.2$[37]
	$E = 17$ GPa; $v = 0.3$[38]
Transversely isotropic	$E_L = 16.6$ GPa; $E_T = 9.55$ GPa; $G_L = 4.74$ GPa; $G_T = 3.28$ GPa; $v_L = 0.37$[39]
	$E_{xx} = 11.3$ GPa; $E_{yy} = 11.3$ GPa; $E_{zz} = 22$ GPa; $G_{xy} = 3.8$ GPa; $G_{yz} = 5.4$ GPa; $G_{xz} = 5.4$ GPa; $v_{xy} = 0.48$; $v_{yz} = 0.2$; $v_{xz} = 0.2$[40–42]
	$E_{11} = 12.8$ GPa; $E_{22} = 12.8$ GPa; $E_{33} = 20.3$ GPa; $G_{12} = 4.8$ GPa; $G_{13} = 6.32$ GPa; $G_{23} = 6.38$ GPa; $v_{12} = 0.35$; $v_{13} = 0.28$; $v_{23} = 0.27$; $v_{21} = 0.35$; $v_{31} = 0.43$; $v_{32} = 0.42$[43]
Orthotropic	$E_x = 11.3$ GPa; $E_y = 13.8$ GPa; $E_z = 19.4$ GPa; $v_{xy} = 0.274$; $v_{yz} = 0.237$; $v_{xz} = 0.237$[44]
	$E_1 = 9.36$ GPa; $E_2 = 9.23$ GPa; $E_3 = 16.21$ GPa; $G_{12} = 3.15$ GPa; $G_{13} = 4.16$ GPa; $G_{23} = 4.14$ GPa; $v_{12} = 0.48$; $v_{13} = 0.24$; $v_{23} = 0.21$; $v_{21} = 0.47$; $v_{31} = 0.41$; $v_{32} = 0.38$[45]
Stiffness Tensor Coefficients	$C_{11} = 20.1$ GPa; $C_{33} = 29.5$ GPa; $C_{13} = 12$ GPa; $C_{44} = 6\ GPa$; $C_{66} = 4.5\ GPa$; All others are zeros[46]
	$C_{11} = 20.3$ GPa; $C_{22} = 20.2$ GPa; $C_{33} = 31.7$ GPa; $C_{12} = 10.7$ GPa; $C_{13} = 13.4$ GPa; $C_{23} = 13.4$ GPa; $C_{44} = 6.38$ GPa; $C_{55} = 6.32$ GPa; $C_{66} = 4.8$ GPa; All others are zeros[43]
	$C_{11} = 21.2$ GPa; $C_{22} = 21$ GPa; $C_{33} = 29$ GPa; $C_{12} = 11.7$ GPa; $C_{13} = 11.1$ GPa; $C_{23} = 12.7$ GPa; $C_{44} = 6.3$ GPa; $C_{55} = 6.3$ GPa; $C_{66} = 5.4$ GPa; All others are zeros[47]

Table 1–2: Mechanical characterization of cancellous bone.

Cancellous bone	
Material law	**Constitutive properties**
Isotropic	$E = 10$ MPa; $v = 0.2$[16,17,27,32,34,35,40,42]
	$E = 150$ MPa; $v = 0.3$[36]
	$E = 350$ MPa; $v = 0.25$[38]
	$E = 500$ MPa; $v = 0.2$[18]
Transversely isotropic	$E_{xx} = 140$ MPa; $E_{yy} = 140$ MPa; $E_{zz} = 200$ MPa; $G_{xy} = 48.3$ MPa; $G_{yz} = 48.3$ MPa; $G_{xz} = 48.3$ MPa; $v_{xy} = 0.45$; $v_{yz} = 0.32$; $v_{xz} = 0.32$[40]
	$E_1 = 140$ MPa; $E_2 = 140$ MPa; $E_3 = 250$ MPa; $G_{12} = 48$ MPa; $G_{13} = 77$ MPa; $G_{23} = 77$ MPa; $v_{12} = 0.45$; $v_{13} = 0.18$; $v_{23} = 0.32$[48,49] 1 is the coronal plane horizontal direction. 2 is the sagittal plane horizontal direction, and 3 is the axial direction
	$E_x = 112$ MPa; $E_y = 112$ MPa; $E_z = 340$ MPa; $G_{xy} = 52$ MPa; $G_{yz} = 53$ MPa; $G_{xz} = 53$ MPa; $v_{xy} = 0.3$; $v_{yz} = 0.1$; $v_{xz} = 0.1$[28,29]
Orthotropic	$E_x = 346.8$ MPa; $E_y = 457.2$ MPa; $E_z = 1107.1$ MPa; $v_{xy} = 0.05$; $v_{yz} = 0.01$; $v_{xz} = 0.322$[44]
Stiffness Tensor Coefficients	$C_{11} = 245.4$ MPa; $C_{22} = 243.6$ MPa; $C_{12} = 49.9$ MPa; $C_{33} = 64.9$ MPa; All others are zeros[50]

behavior is subdivided into three modes interacting in a continuum: a quasi-incompressible fluid representing the nucleus pulposus, a ground substance representing a composite annulus fibrosus matrix, and reinforced fibers accounting for heavy collagen present in the annulus fibrosus. Although time-dependent analyses necessitate such a fluid-structure interaction material behavior, under static conditions and small deformations, IVDs can be approximated by a bulk linear elastic behavior as the sub-elemental distinctions and nonlinearities mostly appear at high strain values[57]. As such, previous investigations modelling the IVDs as linear elastic have been collected as shown in Table 1–3.

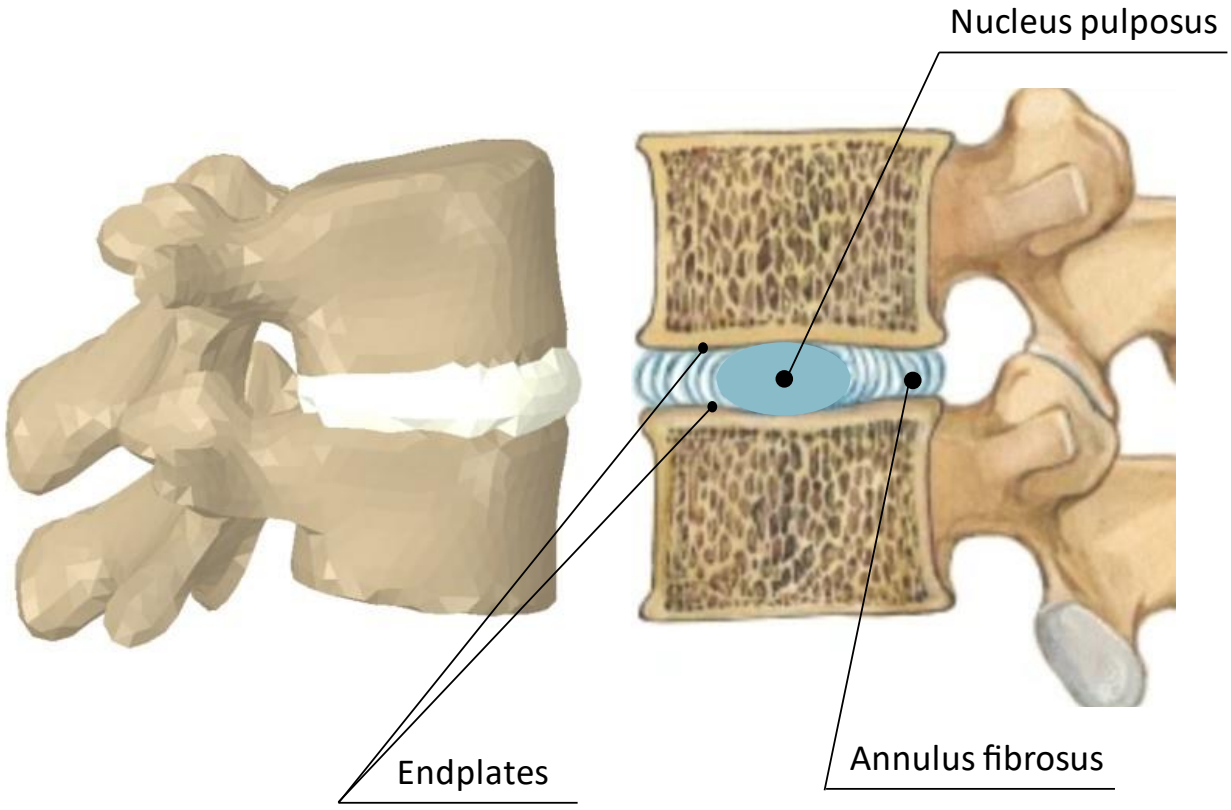

Figure 1–2: Intervertebral discs anatomy (obtained and modified on December 1st 2021 from https://commons.wikimedia.org/wiki/File:A-B-C_degenerative_changes.webp).

Table 1–3: Mechanical characterization of the intervertebral discs

Intervertebral discs	
Material law	**Constitutive properties**
Isotropic	$E = 8$ MPa; $v = 0.45$[58]
	$E = 175$ MPa; $v = 0.45$[42]
	$E = 450$ MPa; $v = 0.45$[17,34]
	$E = 500$ MPa; $v = 0.45$[16,30,36,40,59,60]
	$E = 904$ MPa; $v = 0.3$[61]
	$E = 8000$ MPa; $v = 0.3$[62]

1.1.3. SPINAL MUSCLES

It is the current consensus that most of the spine's support and stability comes from the numerous muscles surrounding it[63]. Those are skeletal, striated, muscles controlled by the brain through nerve impulses[10]. They are composed of groups of actin and myosin muscle fibers, enclosed in fascicle shells[64]. Their activation is commonly believed to follow the "sliding-filament" theory, *i.e.*, in response to a nervous stimulus, actin and myosin pull upon each other causing the contraction of the whole muscle[65]. Their contractive force is integrated to the vertebral column through tendons. Unlike ligaments, tendons connect muscles to bones and are made up of more collagen type I fibers[66].

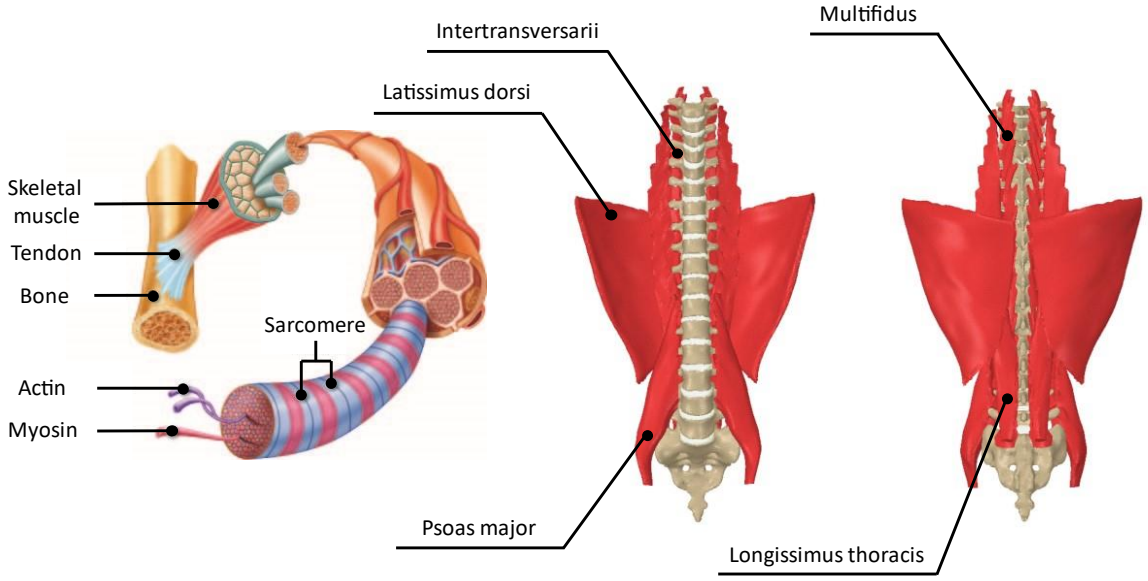

Figure 1–3: Skeletal muscle anatomy and major spinal muscles (obtained and modified on December 1st 2021 from https://courses.lumenlearning.com/cuny-csi-ap-1/chapter/muscular-levels-of-organization/).

One of the most dominant spine muscles, referred to as intrinsic muscle group, is the erector spinae[67]. This group controls spine's forward flexion and is subdivided into the spinalis, longissimus, and iliocostalis, among which the longissimus thoracis dominates. Anterior to the erector spinae is the multifidus, a smaller deep muscle but with highly pennate and stiff fibers, as well as shorter sarcomeres which may enable its high muscle strength[68]. One of the strongest muscles in the lumbar spine is the psoas major, a muscle that activates the lumbar region during

forward bending and lifting[69]. Other important spinal muscles are the intertransversarius, which connect the posterior elements of the vertebrae together and activate spine axial loads[70], and the latissimus dorsi, which attaches to the thoracolumbar fascia in effort of stabilizing and activating the latter[71].

Muscle biomechanical characterization is often dominated by either a biophysical or a phenomenological model[72]. Although phenomenological models, such as Hill's famous elastic-contractile model, are useful in performance analyses[73,74], biophysical are more appropriate for macroscopic characterization such as the inclusion of intramuscular pressure[75,76]. Time-independent material properties previously used to describe skeletal muscles biophysical response were collected as shown in Table 1–4.

Table 1–4: Mechanical characterization of skeletal muscles.

Skeletal muscle	
Material law	**Constitutive properties**
Linear elastic	$E = 7 - 127$ N/m[77]
	$E = 22 - 363$ kPa[78]
	$E_{multifidus} = 33 - 91$ kPa[68,79,80]
	$E_{longissimus} = 32 - 63$ kPa[79,80]
	$E_{iliocostalis} = 37 - 59$ kPa[79,80]
	$E_{psoas\ major} = 34 - 520$ kPa[80,81]
	$E_{rectus\ abdominis} = 520$ kPa[81]
	$E_{transversus\ abdominis} = 1.03$ MPa[81]
	$E_{tibialis\ anterior} = 4$ MPa; $v = 0.45$[82]
Hyperelastic	$Mooney - Rivlin\ 2 - parameters$: $c_1 = c_2 = 0.01$ MPa[83]
	$Mooney - Rivlin\ 5 - parameters$: $C_{10} = 64.3$ kPa; $C_{01} = -38$ kPa; $C_{11} = -0.043$ kPa; $C_{20} = 5.4$ kPa; $C_{02} = 0.005$ kPa; $\rho\ (density) = 1000\ Kg/m\text{^}3; Bulk\ modulus = 50$ MPa[84]
	$Yeoh\ model$: $c_1 = 6750$ Pa; $c_2 = 0.0278$ Pa; $c_3 = -0.001975$ Pa[84]
Viscoelastic	$Single\ mode\ Ogden\ model$: $\mu = 9.32 - 20.6$ kPa; $\alpha = 17.2 - 29.8$; $\gamma = 0.498 - 0.63$; $\tau = 5.5 - 6.53$ s[85]
	$1st\ order\ Ogden\ model$: $\gamma_1 = 0.0715$; $\gamma_2 = 2.49$; $\gamma_3 = 0.277$; $\tau_1 = 0.015$ ms; $\tau_2 = 0.0015$ ms; $\tau_3 = 0.00015$ ms; $K = 20$ MPa; $c = 0.001685$ MPa; $m = 15.43$[86]

1.1.4. THORACOLUMBAR FASCIA

The thoracolumbar fascia (TLF) is a set of thin fascial layers between the paraspinal muscles supporting the spine during unloading[87]. In addition to having very strong fibers, the TLF is highly flexible, enabling it to transmit muscular forces to ease movements and support contraction and relaxation of the back muscles[88]. Anatomically, the TLF extends between the paraspinals while it inserts to the vertebrae, posteriorly, and to the ribs, laterally. Its fibers run and overlap diagonally to create a bulk diamond-like shape in the back. It further subdivides into three anterior, middle, and posterior layers, wrapping the paraspinals, multifidus, and psoas major, while also attaching to the latissimus dorsi[87].

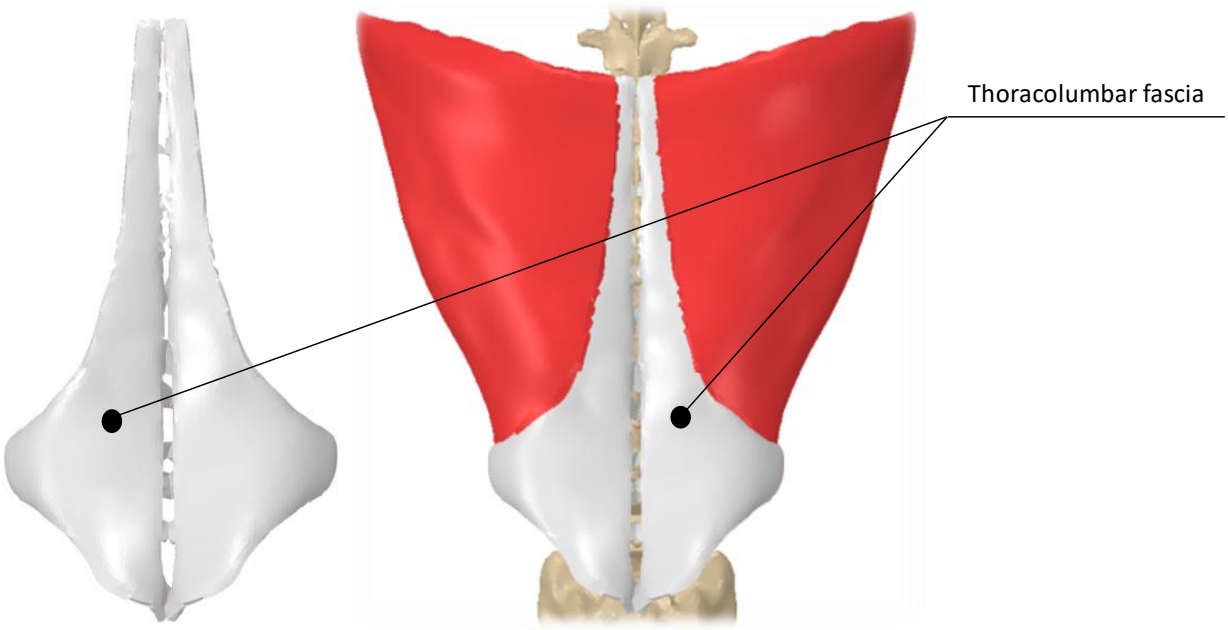

Figure 1–4: Thoracolumbar fascia model showing approximate anatomy.

Arguably, the TLF provides central support to the spine while transmitting muscular forces during coordinated movements[89,90]. Gracovetsky conducted a series of static computational analyses to suggest that the mechanical properties of the TLF permit storing sufficient energy to support the spine under excessive loadings[91]. This was later supported by Moorhouse and Granata who observed an increased spine stiffness under tensional muscular forces resisted by the TLF[92]. It has also been shown, experimentally, that when the TLF layers are placed under tension, they

tend to impart tensional forces on the spinal processes, which may augment segmental stiffness[93–95]. Thus, investigations support that the TLF can provide additional stability component to the spine, thus explaining the motivation and rising interest to understand its mechanics.

Being a relatively new topic, few studies have attempted to mechanically characterize the bulk behavior of the TLF. This is also due to its composite structure as well as the different biomechanical response of its layers[96]. Nonetheless, studies who have successfully characterized the TLF, and other human fascia to that matter, are summarized in Table 1–5.

Table 1–5: Mechanical characterization of human fascia.

Skeletal muscle	
Material law	**Constitutive properties**
Linear elastic	$G\ (shear\ modulus)\ = 117 - 137$ kPa[97]
	$E\ =\ 7.1$ MPa[98]
	$E_{transcersalis\ fascia}\ =\ 1 - 27$ MPa[81,99]
	$E_{plantar\ fascia}\ =\ 350$ MPa[100]
	$E_{fascia\ lata}\ =\ 397.5$ MPa[100]
	$E_{fascia}\ =\ 450$ MPa[100,101]

1.1.5. ABDOMINAL WALL & PRESSURE

In theory, the activation of abdominal pressure, enclosed in the abdominal cavity by the abdominal wall, suggests an additional role of supporting and stabilizing the spine[102–104]. This explains the rising recent interest in literature to model and describe abdominal pressurization. The abdominal wall is a fascial lining encapsulating the abdominal cavity; a space commonly attributed with the activation of abdominal pressure[105]. It is a space activated laterally, dorsally, and ventrally by the abdominal muscles, namely external oblique, internal oblique, and transverse abdominis.

This coordinated activation results with a continuous positive pressure inside the abdominal cavity normally ranging between 2 to 30 mmHg[106], rising to as high as 150 mmHg[107]. This pressure is countered by the abdominal wall which, as a result, is under continuous strains[108]. With only a handful of biomechanical investigations on the abdominal wall, mechanical characterizations of this structure are summarized in Table 1–6.

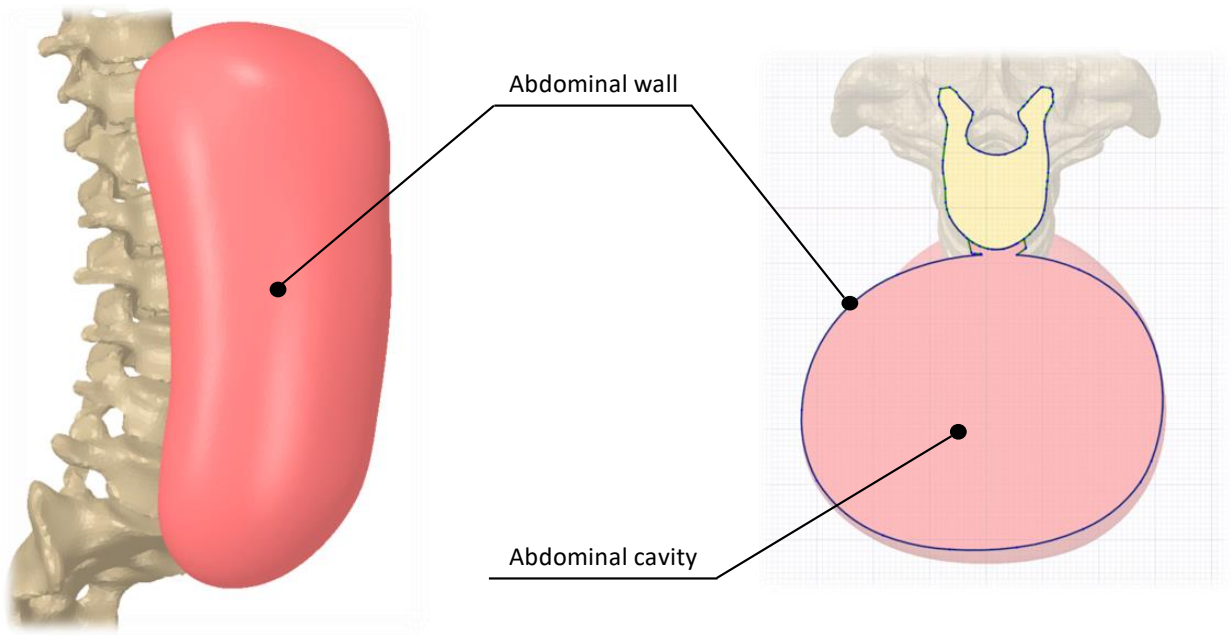

Figure 1–5: Abdominal cavity model showing approximate anatomy.

Table 1–6: Mechanical characterization of the abdominal wall

Skeletal muscle	
Material law	**Constitutive properties**
Linear elastic	$E = 21 - 27.7$ kPa; $thickness = 7.4 - 12.1$ mm[109]
	$E = 20 - 51.5$ kPa[110]
	$E = 32 - 80$ kPa[81]
	$thickness = 23.94 - 33.882$ mm[106]
	$thickness = 16 - 20$ mm[111]

1.2. SPINE AND MUSCLES MODELLING

The history of modelling in the biomechanics field dates back to Borelli's balance body model in the 1600s[112]. Later, scientists like Harvey, Weber brothers, Carlet, Marey, Muybridge, Eduard, and Whilhelm built upon, and put the fundamentals behind biomechanical modelling[112–114]. Due to system's redundancies involving different degrees of freedom, multiple input loads, numerous joints, muscles, and soft tissues, biomechanical modelling has never been a straightforward task

as it is indeterminate at its foundation[115]. Therefore, since the era of Borelli and up until this time, investigators have always had to simplify their models' variables. This would include: simplifying gravitational loads/kinematics/anatomy/passive properties, neglecting inherent nonlinear behavior of different tissues, grouping muscles as synergic sets, straight line of action assumptions for dominant trunk muscles (representing them with force vectors), and introducing cost functions or limited surface EMG data[116–119]. Due to similar assumptions and redundancies, the FE field presents itself as a plausible solution to such complex problems.

Finite element analysis (FEA) was first proposed by Richard Courant in 1922[120], in an era where it wasn't yet practical due to the arduous process of solving a system of linear equations by hand. It was the invention of the digital computer in 1942 that made this method applicable[121]. Like other numerical techniques, the FE method converts a complex problem into hundreds, thousands, and millions of simple problems that abide by the same physical and mathematical laws[122]. The first biomechanics FE application was reported in 1972 by Brekelmans[123]. Based on Fagan *et al.*, there are four ways where FE can be used in the context of the spine: "(1) provide assessment of the spine in health, (2) provide assessment of the spine as altered by disease, degeneration, ageing, trauma, or surgery, (3) provide assessment of the spine with spinal instrumentation, and (4) assist in the design and development of spinal instrumentation."[124].

FE models developed to analyze spinal loadings, injuries, and mechanical tolerances are abundant in literature. Such models varied from simple spine models using just a few elements[125–127], to vertebral and IVDs models simplifying organs other than the vertebrae and IVDs [124,128,129], to more involved models including simple muscle anatomical physiologies[130–132]. However, only a few studies were successful in including the effect of either the intramuscular pressure (IMP), intra-abdominal pressure (IAP), or thoracolumbar fascia (TLF). Still, studies which did so have only accounted for such effects using simplified approaches[133–135], such as including IMP in a basic muscle geometry rather than an anatomical representation.

1.2.1. SKELETAL MUSCLES MODELLING

In depth understanding of skeletal muscles biomechanics and contribution to human locomotion is ongoing research which attracted the attention of many researchers. Historically, muscle length-

tension curves have been the primary resource to describe skeletal muscles biomechanical response[136]. In other words, the level to which a skeletal muscle stretches or shortens dictates its ability to produce maximal force. Recently though, investigations started to complement this with another effect, namely the pressure that builds up inside skeletal muscles upon contraction (Fig. 1–6)[137].

IMP has been shown to correlate to muscle force, with a correlation coefficient reaching 89-98%[138,139]. This correlation, as well as other insightful biomechanical parameters, were merely extracted from experimentation done on animals, most commonly on rabbits[137,140]. Few were actually performed on humans, but have documented results in terms of external applied loads, which does not consider the actual load carried by the muscle of interest[141,142]. That is, a reference model able to discover this link for any skeletal muscle is still missing and numerous similar experiments on different muscles are still required to arrive at an accurate set of data that can be integrated to human muscles. Thus, the availability of a muscle model inclusive of a force-IMP relation that can easily be fine-tuned to meet the behavior, mechanics, and environment of a specific muscle remains of interest for researchers in biomechanics.

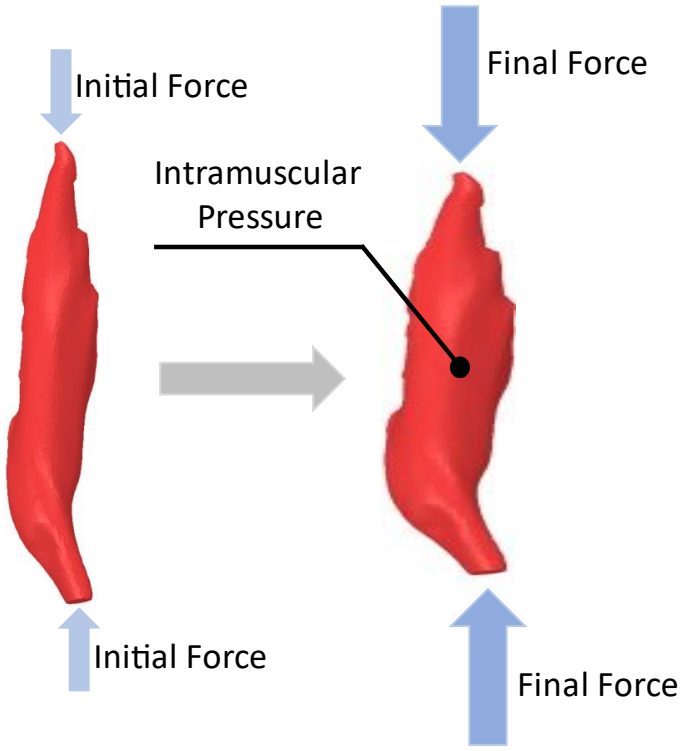

Figure 1–6: Intramuscular pressure build-up upon contraction.

In-vivo measurements of biomechanical parameters would not be always feasible, especially when clinicians are faced with severe injuries. Measurements in such cases would be dangerous, which raises the importance of modelling[65]. Skeletal muscles computational models are usually based on either the microscopic, filaments-based, processes or on simplified phenomenological models focusing on the overall biomechanical response of skeletal muscles. In other words, existing skeletal muscle models can be divided into two broad categories: (i) biophysical and (ii) phenomenological[72] models. Biophysical models allow for the assessment of skeletal muscles response, mainly muscle force, by analyzing their intrinsic physiological properties[143,144]. On the other hand, phenomenological models describe the relations between input and output parameters based on mathematical representations[145,146].

Phenomenological models give important insights into the capability and validity of input-output relations on larger scales. They often use experimental results to describe input-output relations and, as such, are less suitable for examining hypotheses on the single skeletal muscle scale[72]. Hill's model (Fig. 1–7) is considered one of the first mathematical-based models[145]. Hill's phenomenological approach is derived from force-velocity measurements, representing muscles as simple spring-dashpot mechanical systems. One improvement to Hill's model, suggested by Hatze[147], was to include the influence of muscle fiber length on the muscle activation process. Further extensions were also later proposed[148–150].

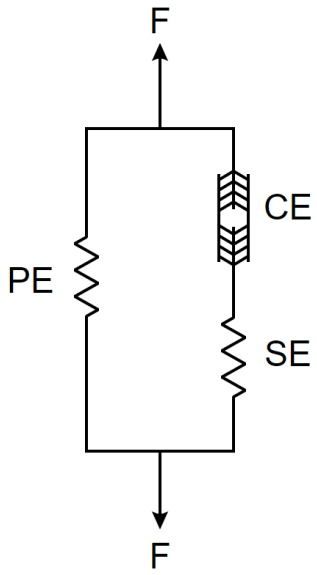

Figure 1–7: Hill's phenomenological muscle model (obtained on December 1st 2021 from https://commons.wikimedia.org/wiki/File:Hill_muscle_model.svg).

Phenomenological and micromechanical-based models are usually used to investigate the contraction of the muscle as a whole, such as in multibody dynamics movement and performance analyses, where hundreds of muscles are combined in a simulation[73,74,151–155]. Although such mathematical models can be used to study force generation relationships of a skeletal muscle in the global musculoskeletal system, they are obviously not suitable to investigate muscles' intrinsic force generation properties. Furthermore, such models simplify the muscle into a force acting between an insertion and an origin point, as well as not accounting for the three-dimensional complexity of the skeletal muscle of interest, which eliminates muscle pressure and prevents incorporating muscle interaction with surrounding tissues.

To assess complex geometrical aspects of skeletal muscles, numerous planimetric and 3D models exist[156–165]. Such models, as well as the others that exist in literature, provide better understanding of muscle force distribution. Their well-documented physiological depiction allows analyzing dynamic muscles changes[160], which cannot be explored *via* simpler 1D models. The principles of continuum mechanics are what cover these models with the focus on macroscopic mechanisms rather than any cellular-level properties. Even those well-documented complex muscle models have not been typically formulated to simulate IMP during skeletal muscle contraction. Still, due to the fact that muscles are incompressible, muscle contraction causes a reversible distortion of its architecture and an increase in hydrostatic pressure in the fluid within[75]. Thus, the development of a skeletal muscle model inclusive of the strong link between muscle force and IMP remains a critical clinical concern.

In an attempt to solve the aforementioned shortcomings, the field of FE modelling presents itself as a potential solution. FE can be used to analyze complex engineering and biomechanical problems to retrieve various results[166]. Besides, in the context of muscles, FE makes the modelling of different contraction types - isometric, concentric, and eccentric - possible[167,138]. Further, numerous FE software packages, such as ANSYS (Canonsburg, Pennsylvania, United States, https://www.ansys.com/), exist that can be manipulated, by way of custom coding, to integrate physiological constitutive models and behavior.

In light of the emergence of this field, previous muscle FE models incorporating muscle force and mathematically modelling or *in-situ* measuring IMP were successfully developed using simple geometries[75,76]. Some focused on deriving the mechanical response in the passive state with an

anisotropic hyperelastic response, derived a strain-energy density function, and found the stress-stretch ratio relations in different muscle pulling directions[168]. Others advanced this to integrating the model with a simple geometry, accounted for IMP, and studied the passive stresses and pressure as a function of fiber strains[76]. However, neither muscle output forces, nor a baseline were documented. Another novel perspective was to include the muscle's active state[169]. This model considered nonlinear, rate dependent, properties, applied on a simplified 3D geometry, to model the muscle as a composite material of fibers and muscle matrix. Using this model, strains and deformations were studied. However, these did not consider fluid content and failed to capture whole muscle behavior.

Such omissions should be re-examined as they are expected to be more significant than previously thought during tendon transfer surgeries for example[76], in which the muscle-tendon complex is elongated and fixed at a constant length. IMP is also believed to influence muscle performance by directly opposing sarcomere shortening forces[170]. Besides, it is an important metric in tissue nutrition, viability, and diagnosis of compartment syndrome fields[171–173]. Thus, an accurate representation of a human 3D muscle model that incorporates IMP may grant a multitude of advantages in musculoskeletal research such as spine-focused research. The development of such a quantitative model, to the best of the author's knowledge, would allow scaling to major spinal muscles, in efforts of better representing them, as well integrating such effects with intra-abdominal pressure and the thoracolumbar fascia. Such an endeavour opens the gates to the new assessments of underlying implications on spinal stability.

1.2.2. SPINE MODELLING

Whether driven by economic and social burdens of spine pathologies, or due to the significance of protecting the spinal cord, modelling the spine has always been a captivating field that eluded researchers. Over the years, an overwhelming number of spine mathematical, biophysical, phenomenological, and numerical models have been developed depending on their context of use. As a result, in this review, only selective literature that serve the purpose of this dissertation, namely spine FE models focused on spinal stability, have been discussed.

In addition to skeletal muscles combined with their enclosed IMP, the pressure developed inside the abdominal cavity (Fig. 1–5), or intra-abdominal pressure, may provide assistive support to improve spinal stability[102]. This caught research interests to integrate conventional spine FE models with representative depictions of IAP. Some FE models introduced the effect of IAP as vectorized forces acting on surrounding tissues, without accounting for the actual inflation in the diaphragm/abdomen[135], which overestimated IAP values. On the other hand, a more comprehensive approach to account for IAP was developed by Dietrich *et al*[174]. In this study, non-linear anisotropic viscoelastic material laws were used to model the vertebrae, cartilage, intervertebral discs, ligaments, and muscles, whereas IAP was modelled as an incompressible fluid embedded in a closed cavity. The overall model consisted of 2640 elements and 13107 algebraic equations[175]. Furthermore, Arjmand *et al.* developed a FE model based on another mathematical model built by Daggfeldt and Thorstensson[176], whereby they modelled the abdominal cavity as encapsulated by back and abdominal muscles. The final form of the model developed by Arjmand *et al.* mimicked the mechanics of a piston-cylinder, in which a top plate displaces vertically to simulate the role of the diaphragm, and thus, generate IAP. As such, they predicted a 7.35 mmHg quiet standing position IAP at a plate displacement of 3.15 mm while a 29.627 mmHg at partial valsalva maneuver by subsequently increasing muscle stiffness along all muscle fibers[106]. On the other hand, Meijer *et al.* was perhaps the first to build a relatively comprehensive FE model of the torso to include the spine, ribcage, and the abdominal cavity[177]. Later, in a study developed by Ouaaid *et al.*, an iterative kinematic-driven deformable-rigid body FE model to compute muscular forces under different IAP levels was investigated[178]. IAP values were assumed to increase up to 75.006 mmHg in extension and 187.515 mmHg in flexion and produced an extensor moment at a lever arm of 5 cm. However, the effect was modelled as an upward force using a rigid link element applied on the 12th thoracic vertebrae, T12, following an applied movement. They observed that spinal compression and shear loads increased with muscle activation but decreased with increasing IAP values.

Among other tissues, the thoracolumbar fascia, shown in Fig. 1–4, has interested researchers due to its apparent role in transferring loads while providing foundational support to contacting tissues[87,179]. The contribution of the TLF to spinal stability is gaining in acceptance as explored by means of mathematical models[133] and simplified geometries[180]. This is supported by a recent review conducted by Vleeming *et al.* whereby they noticed a point of equal tension between the

muscles by force transfer through the TLF[181]. In addition, a series of tests conducted by Tesh *et al.* showed that the TLF may stabilize the spine by withstanding a force up to 335N[133]. Adam and Dolan later found that the tensile loading ability of the TLF can actually go beyond Tesh's observation to reach almost 1000N[134]. Therefore, these investigations and models suggest a stabilizer role of the TLF and show the importance of including it in stability-based FE models.

Although representative spine FE models seem to necessitate physiological considerations such as IMP, IAP, and TLF, simple models focusing only on vertebral bodies and IVDs are abundant in literature. Although such studies tend to overestimate *in-vivo* results, they provide impactful insights on spinal loadings. A great example is a well-designed study between 16 senior groups, focused on spine research, comparing 8 different FE spine models that they developed for the lumbar spine (5 vertebrae with their 4 corresponding IVDs)[182]. The models are very distinct in the sense that only Schmidt's[183] represented muscle *via* simplified geometries while all others simulated muscles' behavior *via* means of force vectors. In addition, Little *et al.* and Goel *et al.*[184,185] did not include the spinous processes of the vertebrae, Chen *et al.* study[42] accounted for cartilage effect, while the models of Rohlmann *et al.*, Shirazi-Adl, Puttlitz *et al.*, and Kim *et al.*[31,183,186] were only representative of the vertebrae and IVDs anatomies. Thus, fascia, tendons, IMP, and IAP effects were excluded from the explored models. Loading conditions in these investigations consisted of a pure bending moment of 7.5 N.m applied in all anatomical planes. As a result, all models showed a maximum discrepancy of 5^{o} rotation from *in vitro* data (median: 17^{o}; range 11^{o}-22^{o}). In another part, under same loading conditions, all models recorded approximately similar facet joint forces of 38N in extension, 14N in lateral bending, and 60N in axial rotations. However, forces were considerably different across all FE models under flexion[182]. The result of this comparative study thus suggests increased confidence in reporting biomechanical parameters, such as facet joint forces and spine's displacements, for appropriately validated models, in the presence of simplifications, assumptions, and anatomical differences across integrated models. That is, considering the wide differences in model form across all models, simulated results were within good agreement, thus lending further credibility to undertaken assumptions.

Arguably, validation and verification are important steps when developing numerical models. It even becomes more critical in biomechanics as the field involves inherent discrepancies due to patient-to-patient variabilities. Thus, validation of simulated results and verification of numerical

approaches become essential in order to report data with high confidence levels. Essentially, a model is said to be validated if the results it predicts matches experimental observations[182]. Verification is "the assessment of the numerical accuracy, that is, how well the computational model output represents the solutions to the underlying mathematical equations"[187]. Sensitivity studies, on the other hand, is the process of ensuring that the model is robust, i.e. predicts repeatable results, upon changing main input parameters such as the mesh size, quality, and material properties[188]. When speaking of biomechanical systems, such analyses may be considered controversial due to the complexity and high level of variabilities imbedded. Although validation, verification, and sensitivity analyses are essential in biomechanics FE investigations, especially for spinal stability case-studies, their level of accuracy is still debatable due to limited access to accurate anatomies of the complete human spine[124,189,190].

Spinal validation usually undergoes either a direct method by comparing FE results to *in-vitro* experiments on cadaveric spinal tissues, or indirectly by matching model's predicted data to published *in-vivo* and *in-situ* observations[191]. It is the process of potentially ensuring that the model appropriately represents the reality of interest. This may include assessing the fundamental and mathematical formulation of the model (model form), as well as the input parameters used in model's conditions and configuration (model inputs). It can be also essential to validate comparators' aspects including the quantity, range, and uncertainties of test samples and test conditions, as well as the equivalency and agreement of input and output parameters. On the other hand, verification of an FE model is usually done by altering model's mesh, refining or coarsening it, and then checking if the model produces repeatable results[192]. This is calculation verification which may also include numerical solver error and use error. Code verification is often an important step if new constitutive tissue models are proposed and employed in the simulation. Model robustness against input parameters is perhaps the final crucial step to conclude the development of an FE model. That is, upon changing input variables such as material properties or behavior, if the model predicts relatively close results, the model can then be said to be insensitive to studied inputs[193]. This step is particularly important in biomechanics studies because FE indirect validation is usually conducted against animals' experimental data. This means that, the FE model cannot yet be relied on to simulate human scenarios such as human spinal flexion, muscle contraction, and stability analyses. However, once the model is shown to be robust against

main input parameters, it can then be scaled up to human physiology, architecture, and material response with high confidence that it would be able to predict human biomechanics.

1.3. SPINAL STABILITY, MUSCLE ACTIVATIONS, AND LOW BACK PAIN

Chronic low back pain (LBP) is a well-recognized problem in today's society due to its profound socioeconomic repercussions (Figs. 1–8)[194–197]. It has always been a common problem whereby the earliest surviving surgical text discussing it is the Edwin Smith papyrus that dates back to about 1500 BC[198]. There is a 60-80% chance of a person having LBP in his or her lifetime[199], and it usually begins at working age[200]. In 1999 in Canada, 17% of the people under the ages of 39, and 20% of the people between the ages of 40 and 49 reported having LBP[201]. Furthermore, in 2001 in Alberta, out of 37927 work loss claims, 26.8% were associated with LBP[200]. In such industrialized societies, LBP is an expensive condition that costs the Canadian government around 16$ billion[200] and the US from 15$ to 50$ billion annually[63,202]. It is an expensive condition which costs keep rising due the challenges of attributing it to specific causes[6]. It is instead attributed to general causes relating to negative social interaction[203] (dissatisfaction at work), poor ergonomics[204] (jerky movements or prolonged vibrations), psychological conditions[205,206] (stress or depression), inadequate habits[207] (obesity, drinking, smoking, improper posture), and injuries[208,209] (soft tissues such as intervertebral discs, sacroiliac joints, ligaments, tendons, muscles). On the other hand, although its sense of definition is broad, one of the well-established and reliable interpretations of low back dysfunctions, and potentially LBP, is mechanical and clinical instability[63,203,210]. In fact, Panjabi associates LBP to clinical instability and hypothesize a relationship between LBP and abnormal intervertebral motion[63]. Panjabi claims that this is the basis to treating low back patients and examines this hypothesis *via* applying an external fixator to observe an average decrease of 39.3% in range of motion[63]. He concludes his results with a "ball-in-a-bowl" analogy to explain how stability is achieved and the spine becomes in a pain-free state[63]. Nevertheless, current clinical procedures address LBP using diagnostic methods[211–214] trying to tailor treatment which usually start with awareness, then followed with therapy, and finishing with physiotherapy[215]. In cases where the pain becomes unbearable or disabling, surgical interventions become necessary[216,217], although their result might often be unplausible.

Figure 1–8: Depiction of low back pain (obtained on December 1st 2021 from https://thenounproject.com/icon/lower-back-pain-638290/ and from https://commons.wikimedia.org/wiki/File:Lower_back_pain.svg).

As highlighted, accurate assessments of low back dysfunctions are challenging due to the general or non-specific causes of instabilities defined earlier. In short, similar to any mechanical system, the ability of the musculoskeletal system to perform its normal functions relies on its state of stability, or commonly known as spinal stability. However, researchers are not yet able to give a clear definition of stability, admitting to the challenge when attempting to quantify it[218]. Clinical stability was defined by White *et al.* as the spine's ability to limit the set of displacements to within normal ranges of motion to protect the spinal cord[219]. McGill *et al.* gave a more general definition where they conceived the foundation of stability to be directly related to potential energy by first illustrating the concepts of both, potential and elastic potential energy, in the context of mechanical structures stability[220]. They then elaborated on the clinical implications of this, and one example they gave was, during a task such as picking a pencil of the ground, a change in height is translated to a change in potential energy sustained by the muscles, which stabilizes the spine again. Although many other examples were given, McGill *et al.* conceded that the way the change in potential energy stabilizes the spine is still not fully understood[220]. The American Academy of Orthopedic Surgeons referred to spinal stability as the "capacity of the vertebrae to remain cohesive and to preserve the normal displacements in all physiological body movements"[221]. However, those normal physiological displacements are still questionable due to difficulties correlating standard references with clinical and radiological findings[222]. In fact, there exists numerous other definitions

of spinal stability; however, researchers like Panjabi *et al.* did compelling studies towards understanding spinal stability through its instabilities. In general, Panjabi and Pope consider an unstable structure to be one that is not in an optimal state of equilibrium[223]. This optimal state is the configuration in which the structure is in static equilibrium under the action of external forces subjected to it [223,224]. The authors used the analogy and behavior of a cone sitting on a horizontal surface to explain the characteristics of a structure's optimal equilibrium state. They argue that optimal stability is similar to the cone resting on its base; if it is displaced, it maintains its equilibrium state. On the other hand, a cone sitting on its side is in neutral equilibrium stability; if it is displaced, it rolls to a new equilibrium resting position. Only when the cone is sitting on its tip it becomes in unstable equilibrium whereby the smallest displacement causes it to fall on its side, shifting the cone from unstable to a neutral equilibrium stability state. Equilibrium stability of this inherently unstable cone resting on its tip can be maintained by tethering ropes to it; *i.e.* when the cone is displaced, the tension in the ropes returns the cone to its original position, and thus, maintains its stability. Similarly, although the spine is inherently unstable, tensional and compressive forces in the tissues surrounding and attaching to it maintain its equilibrium stability[223,224]. In the spine, instability initiates when the restraints offered by ligaments, muscles, and other soft tissues are damaged or lost part of their stiffness[223]. Panjabi *et al.* further reflected on instability as the loss of the ability of the spine to preserve its range of motion in a way to prevent pain and major deformities[225]. Driscoll *et al.* discussed the adverse effects of spinal deformities, considered one end of the instability spectrum, and presented novel spinal screw designs as a corrective treatment of such deformities[226,227].

In addition to loading and range of motion, motion type has been reported as another parameter reflecting on spinal stability[228]. That is, the question whether static or dynamic conditions are a more important factor in spinal stability became debatable[229]. Static spinal stability was defined as the role played by spinal tissues, such as the effect of IAP, to stabilize the spine under external stimulations[230,231]. Three mechanisms have been proposed for the role of IAP in the biomechanics of the spine and whether that alone can increase the stiffness, and further, static spinal stability[191,230,232,233]. First, it was proposed that IAP influences spinal stability by exerting a static force up on the diaphragm and down on the pelvic floor[232]. A second theory was that the build-up of IAP increases the stiffness in the abdominal cavity, which in turn limits intervertebral translation and rotation, increasing spinal static stability as alluded by Dr. McGill in his discussion[233]. One

last possibility was that IAP prevents the abdominal muscles from shortening, therefore maintaining the hoop-like geometry of these muscles around the abdominal cavity, maintaining their ability to generate tensile forces, thus preserving spinal static stability[191,230]. Nevertheless, it was investigated that normal IAP under resting conditions to be around 5-7 mmHg[234]. Interestingly, the first to propose that IAP assists in spinal unloading was Sir Arthur Keith, in 1923, where he suggested that upon pressurizing the abdomen, a stiff cylindrical compartment was observed of pressure values between 100-150 mmHg[235]. It was also noted that a power-lifter carrying a load of 890N can create a discal stress of 8900N while an IVD fails at 1500-6200N[236]. A later study built on this finding and recorded a peak IAP value of 200mmHg, concluding, rather simplistically, that this reduced the stress on the spine and the lumbosacral disc by 30%[237]. Furthermore, McGill *et al.* also suggested that IAP build-up provides a resistive type of support by limiting intervertebral displacements, thus statically stabilizing the spine[233]. However, the exact mechanism of how IAP builds up remains debatable[177] and its exact role in maintaining spinal static stability requires further investigations. Lastly, the ligamentous system in combination with the fascia, especially the TLF, was examined by Dr. Gracovetsky through simple static computations, which suggested that their mechanical properties allow storing sufficient tension to permit the spine to overcome the extra forces applied by the muscles[91].

On the other hand, spinal stability has been dynamically defined by Reeves and Cholewicki as situation-dependent; understanding the dynamic characteristic of the spine to demonstrate the qualitative definition of stability regarding spinal initial state and suggest performance and robustness studies as crucial when studying stability[238]. Further, in addition to potential energy, kinetic energy is a critical parameter to assess spinal dynamic stability[239,240]. That is, accounting for the energy of movement dynamics as well as the time-dependent dynamic neural feedback in controlling spinal stability[241]. Meakin *et al.* introduced a novel mathematical model of the spine, taking into account the intrinsic nature of the spinal muscles; the Euler pendulum model[242]. "Flexion and extension of the spine were considered as oscillations of an Euler column in which the frequency is determined by the length of the column, its bending stiffness, and the supported mass"[242]. It was further shown by Moorhouse and Granata that the tensile force applied by the spinal muscles, when resisting an applied flexion force, increases the stiffness of the spine[92]. In addition, rather than having a solely passive nature, in an interesting study, Schleip *et al.* proposed an evidence that fascia may be actively contracting in a smooth muscle-like manner, and hence

may influence the dynamics of the musculoskeletal system[243]. He presented observatory, biomechanical *in vitro*, and pharmacological *in vitro* evidences of the presence of contractile cells, myofibroblasts, in fascia[243]. Although it is an important finding[244], Schleip *et al.* suggest that this is still a hypothesis and requires further research through quantitative immunohistochemical examinations for example.

As highlighted, skeletal muscles are key players in spinal stability, to which they seem to contribute actively and passively. However, the spine is considered a statically undetermined system, with muscles exceeding its kinematic degrees of freedom[245], to which there exists an infinite number of ways to conduct a motor task[246]. This has led to the development muscle activation strategies based on optimization methods; to assume a specific muscle activation pattern in a way to optimize an objective function under physiological constraints[247]. Although there exists other techniques to determine individual muscle forces, optimization methods are often adopted because they are easy to use, easy to develop, and can produce highly accurate results under normal physiological constraints[104,248].

In the context of maintaining spinal stability, numerous muscle activation objective functions have been examined. Those included: minimizing muscle effort as perceived by the sum of muscle forces[249] or muscle stress[250], minimizing lumbar compression as perceived by intervertebral discs forces[251], maintaining equilibrium and stability at all physiological costs[252], as well as minimizing and reversing a spinal deformity[248]. In addition, examining combinations of these functions for an overall stability objective was explored[247]. However, to the author's knowledge, no optimization model to date has accounted for muscle internal pressure, let alone investigating spinal stability achieved by intramuscular pressure-based optimization objective functions. Thus, assessment of equilibrium static spine stability as provided by IAP, TLF, muscle recruitment, activation, and force optimization analyses, remains to be explored in the present literature.

1.4. LITERATURE LIMITATIONS

It is evident from the presented literature review that the assessment of equilibrium spine stability and underlying activation strategies is a challenging endeavour. It is with no surprise that

researchers and previous investigators struggle to define and quantify such notions. This problem, however, can be traced back to its roots whereby available methods are inadequate or cannot suffice for this context of use. In other words, methods explored in literature provide insightful interpretation about spinal stability and involved tissues, but do not permit its exploration inclusive of additional surrounding and engaged tissues.

The simplified representation of skeletal muscles, mainly excluding IMP and overlooking tissue-specific physiologies, creates limitations to the application of such muscle models. The inclusion and appropriate linkage between muscle's enclosed pressure and external force properties might potentially fill the gap of realizing more representative contraction properties. This may further permit exploring pressure-based muscle activation strategies in the effort of stabilizing the spine.

In addition, spine models are very selective in literature in the sense of accounting for the direct interaction of specific sets of tissues or effects. In other words, to the best of author's knowledge, there remains a pressing need for physiological spine FE models that would incorporate more exhaustive and primary stability effects. As highlighted in the literature review, such effects are the different contraction phases of muscles, the inclusion of TLF, and the depiction of abdominal pressure. These omissions are perhaps due to accompanied computational complexities as the accurate modelling of the aforementioned effects would result in an infeasible numerical discretization. As such, exploring and optimizing mesh options applied to spinal tissues applications is another area which may be improved.

2

RESEARCH RATIONALE, OBJECTIVES, AND HYPOTHESES

The use of numerical methods, including FE, to model and analyze biological soft tissues has advanced the realm of biomechanics into an innovative state of providing preliminary assessments prior to moving forth with *ex vivo* and *in vivo* testing. The successful development and validation of representative models have permitted the analyses of spinal loading, physiologies, and conditions to a high level of accuracy. This further advanced the field to designing mechanical-based medical instrumentation, by means of numerical analyses, in a timely manner. However, due to selective methodologies and computational cost, the applications of such models are limited to the validated and explored context of use. That is, with a number of physiological simplifications, assessment of biomechanical spine notions, such as equilibrium stability and underlying activation strategies, did not seem possible using available models. This is due to undertaken decisions such as not including a physiological representation of intramuscular pressure, abdominal pressure, and thoracolumbar fascia. As such, there remains a pressing need to put forth more physiologically representative and accurate full-scale spine models to facilitate conducting such *in silico* assessments. Moreover, the progressive evolution of the FE-biomechanics applied field, which adopts innovative numerical technologies and tools, created a need for physiological assessments to better understand inner-body mechanics.

Thus, the ***central focus*** of this doctoral thesis was the development and validation of physiologically representative finite element models of spinal muscles and soft tissues, to generate an integrated spine model, in efforts of better assessing equilibrium spinal stability and underlying muscle activation patterns.

In order to address this primary objective, accurate physiological representation, by means of FE modelling, of primary spinal tissues known to contribute to spinal stability were first needed to be developed. At the core of this is the development of pressure-based skeletal muscle models rather than the often-used force vector representations. Integrating these partial models would then allow to formulate a novel full-scale FE spine model with which biomechanical simulations of interest can be conducted. The successful development of this would necessitate extensive verification and validation against *ex vivo*, *in vivo*, and *in situ* experimentation comparators. With proper validation, the model can then be numerically manipulated by means of loading and boundary conditions to explore the central objective of assessing spinal stability and muscle activation strategies. Consequently, the primary objective was subdivided into the following 4 objectives:

Objective 1: Create and validate the first scalable, custom-coded, biphasic FE muscle model inclusive of an intramuscular pressure enclosed fluidic field;

Objective 2: Develop and validate a fully representative, full-scale, FE model of the spine, inclusive of the intramuscular pressure-based muscle model from objective 1, intra-abdominal pressure, and thoracolumbar fascia;

Objective 3: Exploit the FE spine model, from objectives 1 and 2, to objectively investigate soft tissues contribution to equilibrium spinal stability; and

Objective 4: Exploit the FE spine model and stability results, from objectives 1-3, to explore conventional activation strategies as well as devise intramuscular pressure-based muscle activation strategies.

The ***central theme*** addressed in this dissertation is:

Spinal stability, governed by the coordination of spinal soft tissues and coactivation of spinal muscles, may be better quantified and understood by modelling and validating physiological fundamentals of engaged tissues and adopting representative loading and boundary conditions. This central theme was subdivided into the following hypotheses:

Hypothesis 1: A relationship between muscle force and intramuscular pressure can be represented in a biphasic volumetric finite elements muscle model within a 10% validation accuracy and 20% results repeatability;

Hypothesis 2: The integration of pressurized spinal muscles, abdominal pressure, and thoracolumbar fascia in a uniform spine model creates a framework to conduct biomechanical simulations with a range of 15% validation accuracy;

Hypothesis 3: The activation of spinal muscles, intra-abdominal pressure, and passive tensioning of the thoracolumbar fascia contribute to at least 80% of overall spine's equilibrium stability;

Hypothesis 4: Minimizing muscular pressure, in a spine stability-based model, yields at least 25% decrease in intramuscular pressure, while staying within a 10% force margin from the minimal muscle force conventional strategy; and

Hypothesis 5: Maximizing muscular pressure, in a spine stability-based model, results with at least twice the engagement of thoracolumbar fascia passive forces, while staying within a 20% force margin from the absolute stability conventional strategy.

The objectives and corresponding hypotheses of this doctoral dissertation were explored and assessed sequentially as presented in Fig. 2–1. The validation of the *in silico* muscle model allowed to successfully accomplish objective 1, confirm hypothesis 1, and initiate objective 2. Integrating spinal tissues with the muscle model attained in objective 1 allowed for the full-scale spine *in silico* model. Extensive verification and methodical validation of the model, against *in vivo*, *ex vivo*, and *in situ* experimentation comparators, allowed to affirm hypothesis 2; which, marked the completion of objective 2. The models of objectives 1 and 2 were then exploited to confirm hypothesis 3, to which stability results yielded the accomplishment of objective 3. Collective findings of all objectives were then utilized to formulate novel muscle activation strategies, explore and affirm hypotheses 4 and 5, evaluate significance of including pressure, and thus, successfully completing objective 4. This linear path between objectives and hypotheses concluded with novel findings pertaining to equilibrium spinal stability. As a result, 6 manuscripts were submitted and published in peer-reviewed journals detailed in chapters 3 to 6. Finally, to resume and integrate these studies, a general discussion is found in chapter 7 followed by conclusions proclaimed in chapter 8.

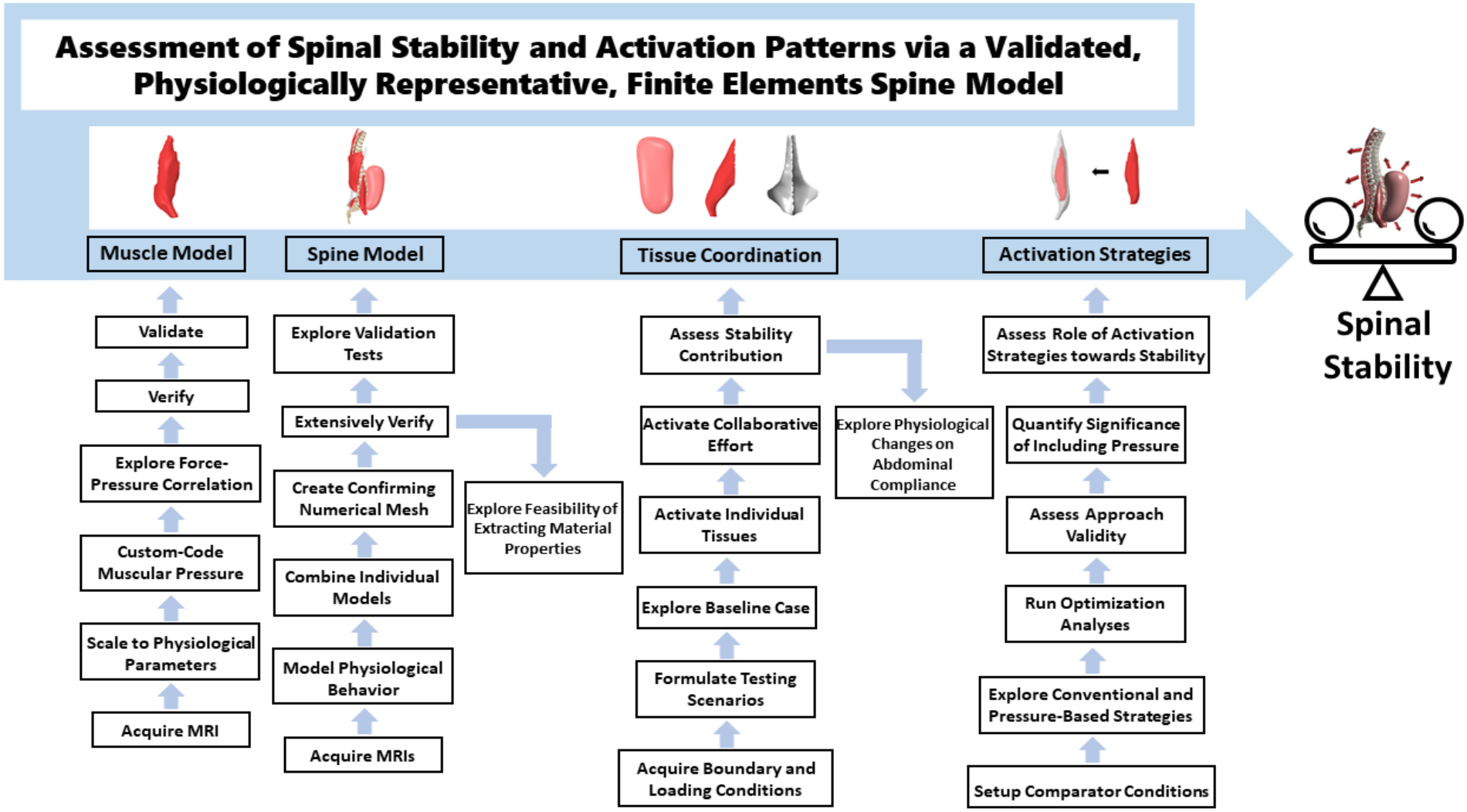

Figure 2–1: Thesis workflow and methodical research steps.

3

DEVELOPMENT OF A BIPHASIC MUSCLE MODEL INCLUSIVE OF ENCLOSED INTRAMUSCULAR PRESSURE

3.1. FRAMEWORK OF THE FIRST ARTICLE

This study was the steppingstone for the rest of the thesis in terms of serving as a reliable and representative approach to modelling skeletal muscles. In order to fulfill subsequent objectives of quantifying stability, perceived by muscle activations, the development of an accurate, reliable, scalable, and representative volumetric model of a skeletal muscle was necessary. This would serve as a scalable modelling procedure to primary spine muscles, to complement a fully representative spine model readily available for biomechanical simulations. As such, this study aimed to build and validate a FE model of the tibialis anterior muscle inclusive of enclosed muscular pressure, namely intramuscular pressure. Although muscles are inherently rich in fluids, whereby the pressure build-up upon contraction reaches significant levels, few attempts were made to consider IMP in skeletal muscles FE models. Therefore, in this study, a clear distinction between muscle's shell and fluid content, representative of IMP, was created, *via* a fluid-shell mixed field, to represent muscle mechanics during contraction while respecting fluidic behavior. The study sought to achieve this using a simple numerical model and a soft FE mesh in order to minimize computational time and enable scaling the procedure to the full spine model discussed in chapter 4. With IMP previously shown to linearly correlate to skeletal muscle force, the model put forth was validated in light of this relationship which further served to characterize muscle forces in subsequent studies. Since IMP needed to be quantified in FE terms, a special attention was given to muscles' enclosed regions. In specific, those were modelled using custom coded pressure

elements, allowing to directly extract enclosed IMP, as a response to a generated muscle force, from a centroidal hydrostatic pressure node. This permitted exploring correlations between generated muscular forces, perceived as model inputs, and resultant IMP, as well as validating those in the context of the tibialis anterior. Hence, this study provided insightful implications on the inclusion of IMP, in numerical models of skeletal muscles, as a novel and valid approach to simulate fluid-filled muscle contraction. The attainment of objective 1 and exploration of hypothesis 1 are presented in the manuscript entitled “Correlating Skeletal Muscle Output Force and Intramuscular Pressure *via* a 3-Dimensional Finite Element Muscle Model” for which the contribution of the first author is considered to be 85%. This manuscript was published in the journal of *Biomechanical Engineering* on November 3, 2021.

3.2. ARTICLE 1: CORRELATING SKELETAL MUSCLE OUTPUT FORCE AND INTRAMUSCULAR PRESSURE *VIA* A 3-DIMENSIONAL FINITE ELEMENT MUSCLE MODEL

Ibrahim El Bojairami[1]; Mark Driscoll, Ph.D., P.Eng.[1]

[1]*Musculoskeletal Biomechanics Research Lab, Department of Mechanical Engineering, McGill University, Montréal, Quebec, Canada*

Address for notification, correspondence, and reprints:

Mark Driscoll, Ph.D., P.Eng., Assistant Professor

Associate Member, Biomedical Engineering

Canada NSERC Chair Design Engineering for Interdisciplinary Innovation of Medical Technologies

Department of Mechanical Engineering

817 Sherbrooke St. West

Montréal, QC, H3A 0C3 Canada

T : +1 (514) 398 – 6299

F : +1 (514) 398 – 7365

E-Mail : mark.driscoll@mcgill.ca

3.2.1. ABSTRACT

Purpose: The inclusion of muscle pressure in muscle models may have important implications in biomechanics. This notion builds from the known correlation between muscle contractile force and internal pressure. However, this relation is often omitted in numerical models leveraged to

study biomechanics. Thus, the purpose of this study was to develop and validate a method of modeling muscles, via finite elements, inclusive of the correlation between muscle contractile force and intramuscular pressure. *Methods*: A MRI-scanned tibialis anterior muscle was modelled via a simple, yet easily scalable, mixed shell and pressure finite element model. Then a validation study was conducted on intramuscular pressure, resulting from applied muscle contractile force, through leveraging special fluid elements type. *Results*: The fluid-structure based model and adopted methods exhibited muscle forces and intramuscular pressure that were highly linearly correlated. Indirect validation was achieved with a maximum discrepancy of 7.25%. Furthermore, force-length curves followed a trend similar to documented conventional muscle data, which added to the model's validity. Mesh, material properties, and tendon stiffness sensitivity studies supported model's robustness. *Conclusion*: This study has introduced a novel 3-dimensional finite element modelling method that respects the physiological force and intramuscular pressure relationship. Although similar models have been previously explored, their complex physiological representation and time-consuming solvers make their scalability and real-time implementation questionable. Thus, the developed model may address such limitations while improving the realism of volumetric finite element models inclusive of muscle contribution.

Keywords: Muscle modelling, finite element modelling, intramuscular pressure, muscle forces.

3.2.2. INTRODUCTION

Considerable research efforts have been carried out to understand the mechanics of skeletal muscles and their contribution to biomechanics. This endeavor is challenging provided numerous skeletal muscles, tendons, and joints interact together to produce a specific movement[1]. Specifically, determining individual muscle force remains a challenging clinical endeavor as available methods do not directly measure muscle force and are subject to variability from multiple muscle contributions[2]. Thus, the capability of muscle to produce a specific amount of force remains of great interest as it often defines performance and, on the other end of the spectrum, helps in the medical assessments of muscular diseases[3].

Conventionally, skeletal muscle physiology has been commonly described by the muscle length-tension curves[4]. Recently, studies have further shown that intramuscular pressure (IMP) correlates linearly with muscles contractile force (F). This correlation was motivated by Laplace's law and Hill's phenomenological model which describe that muscle fibers in contraction results with an inward produced pressure, based on muscle tension magnitude and geometric characteristics[5]. The correlation coefficient (R) between these two parameters reached a range of 0.89-0.98[6,7], mostly extracted from animal experiments, especially rabbits[7,8]. Furthermore, the measure of IMP has benefited from improvements of pressure microsensor technologies which encourages force estimation from IMP a potentially promising field[1,8,9]. Moreover, IMP is suggested to influence muscle performance by directly opposing sarcomere shortening forces[10]. It is also considered an important metric in tissue nutrition, viability, and diagnosis of compartment syndrome[11–13]. Thus, developing a numerical method to correlate IMP to muscle force could be of clinical interest as an approach to assess physiological parameters and estimate individual muscle forces[2].

In-vivo measurements of biomechanical parameters are not always feasible, especially in cases of severe injuries. This poses challenges in a clinical setting, which raises the importance of modelling[14] as a quick assessment tool to aid or guide clinicians. Available computational models of skeletal muscles generally focus on either the microscopic, sarcomere-based, processes or on simplified phenomenological models focusing on the global behavior of skeletal muscles. These models are divided into two broad categories of biophysical and phenomenological[15]. Biophysical models allow for the evaluation of a skeletal muscle output, mainly muscle force, by analyzing its intrinsic physiological properties[16,17]. Phenomenological models focus on mathematical representations to describe the relationships between input and output parameters[18,19]. Although phenomenological models can be used to investigate multibody dynamics and performance analyses[20–26], they are not suitable to study the muscle's intrinsic force generation properties due to anatomic simplifications such as excluding IMP and muscle interaction with surrounding tissues. As a result, numerous biophysical, planimetric, and 3-D models have been developed[27–36], to which investigating force generation and distribution became possible. In particular, finite elements (FE) has shown to be a promising approach to integrate physiological constitutive models and behavior, including muscle force and IMP[37,38].

The research put forth was motivated by previous successfully developed, representative, and novel IMP-based muscle models[2,38], as well as the variational principle with fluid-structure interaction field to model muscles' incompressibility while preventing the problematic phenomenon of volumetric locking[39]. Furthermore, the fine line between accuracy and simplicity allowed to develop a fast computational model with the advantage of being quickly scalable to all other skeletal muscles. As such, the central focus of this paper was to incorporate the effect of IMP through building and validating a finite element model of the Tibialis Anterior (TA) muscle coupled with this IMP effect. The adopted novel approach was to attempt to create a distinction between muscle shell and fluid content, representative of IMP, via a fluid-shell mixed field while maintaining simple model extremities and FE mesh. The goal was to achieve this while accurately representing interior muscle fluidic behavior, minimizing computational time, and enabling for ease of scalability.

3.2.3. METHODS

A. Continuum Mechanics Modelling

A 3-D model of the Tibialis Anterior was created having an inner volume, representative of fluid, and an outer shell, representative of the outer muscle epimysium layer (Fig. 3–1).

Sanders' thin shell theory[40], where strains vanish for small rigid-body motion, was leveraged for this model. However, in this study, muscle's outer shell was modelled using a combination of classic finite elements and Sanders' shell theory. The FE formulation was based on the circumferential frustrum-like structure of the tibialis anterior muscle shell, constructed of two nodal cylindrical-like shell layers.

For an infinitesimal shell element, the relations of static equilibrium, comprising stress couples and resultants, are well-known and can be found in the report put forth by Sanders[40]. By virtue of the principle of virtual work, surface integrating the equilibrium equations, and applying inherent shell boundary conditions, strain-displacements relations can be found to be[40]:

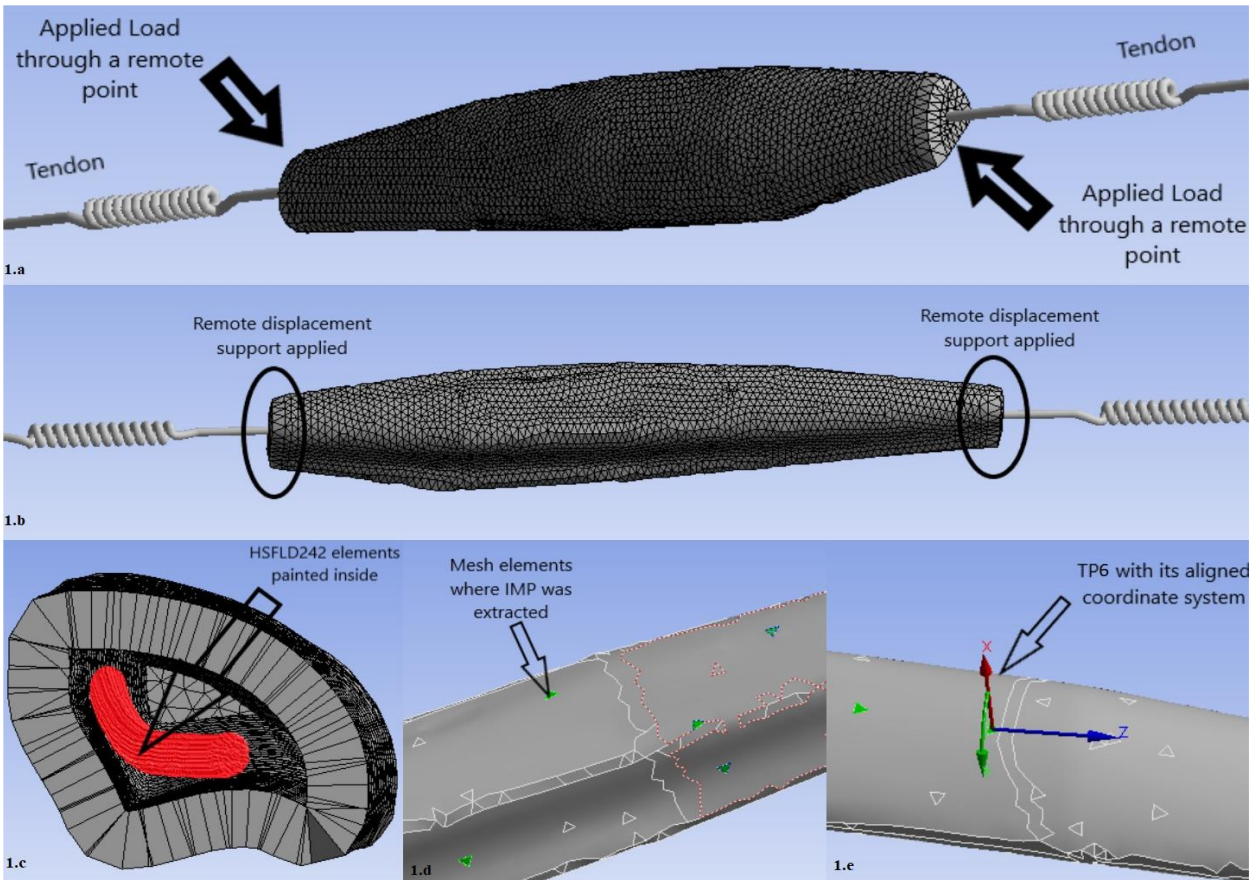

Figure 3–1: Finite element model of the muscle. 1(a): Top view of the meshed model with tendons attachments and force application region. 1(b): Bottom view of the meshed model with tendons attachments and remote displacement supports application region. 1(c): Hollow muscle cross-section showing how the hydrostatic fluid elements (HSFLD242) will be applied. 1(d): Bottom view of five regions used to extract IMP from the model mesh. 1(e): Top view of test point 6 (TP6), and its aligned coordinate system, which produced the most accurate results.

$$\begin{pmatrix} \varepsilon_x \\ \varepsilon_\theta \\ \varepsilon_{x\theta} \\ \gamma_x \\ \gamma_\theta \\ \gamma_{x\theta} \end{pmatrix} = \begin{pmatrix} \dfrac{\partial u_x}{\partial x} \\ \dfrac{1}{R}\dfrac{\partial u_\theta}{\partial \theta} + \dfrac{u_r}{R} \\ \dfrac{1}{2}\left(\dfrac{\partial u_\theta}{\partial x} + \dfrac{1}{R}\dfrac{\partial u_x}{\partial \theta}\right) \\ -\dfrac{\partial^2 u_r}{\partial x^2} \\ -\dfrac{1}{R^2}\dfrac{\partial^2 u_r}{\partial \theta^2} + \dfrac{1}{R^2}\dfrac{\partial u_\theta}{\partial \theta} \\ -\dfrac{1}{R}\dfrac{\partial^2 u_r}{\partial \theta \partial x} + \dfrac{3}{4R}\dfrac{\partial u_\theta}{\partial x} - \dfrac{1}{4R^2}\dfrac{\partial u_x}{\partial \theta} \end{pmatrix} \tag{3.1}$$

where u_x, u_r, and u_θ are the axial, radial, and circumferential displacements, respectively.

Based on Kirchoff-Love's approximation, for an isotropic shell, the elasticity tensor is:

$$[\boldsymbol{E}] = \begin{bmatrix} At & Atv & 0 & 0 & 0 & 0 \\ Atv & At & 0 & 0 & 0 & 0 \\ 0 & 0 & \frac{B}{2}t & 0 & 0 & 0 \\ 0 & 0 & 0 & \frac{A}{12}t^3 & \frac{A}{12}t^3 v & 0 \\ 0 & 0 & 0 & \frac{A}{12}t^3 v & \frac{A}{12}t^3 & 0 \\ 0 & 0 & 0 & 0 & 0 & \frac{B}{24}t^3 \end{bmatrix} \tag{3.2}$$

where $A = \frac{E}{1-v^2}$ and $B = \frac{E}{1+v}$; whereas t, v, and E are the muscle shell thickness, Poisson's ratio, and Young's modulus, respectively.

The stress-strain relation for an isotropic shell then becomes:

$$[\boldsymbol{\sigma}] = [\boldsymbol{E}]\{\varepsilon\} \tag{3.3}$$

As such, without going deep into the derivations and mathematics, substituting Eqs. (3.1) and (3.2) into Eq. (3.3), a system of linear partial differential equations is obtained. Assigning the boundary conditions detailed in section *3.2.3.C* results with a well-posed boundary value problem, which can then be solved through any numerical method of interest. For this study, the finite element method using the commercial software ANSYS Static Structural (v. 19.1, Canonsburg, Pennsylvania, United States) was used.

B. Internal Pressure Modelling

As the material properties of muscle approaches the incompressibility limit, a problematic phenomenon, usually referred to as volumetric locking[39], appears. This means that, the variational principle involving only the displacement field will perform poorly under standard finite element methods. As a remedy, variational principles with multiple fields can be used[41,42]. In other words, a mixed fluid structure interaction field becomes necessary to describe the whole muscle mechanics. Thus, a connection between the shell displacement field and the contained pressure resulting from the muscle shell deformation was realized. The adopted formulation was motivated by Heng Chi, who derived a similar two-field variational principle from the principles of minimum potential energy, which is valid for elastic materials with any level of compressibility[39].

Based on Chi's derivation of the expansion of a cylindrical shell in a mixed fluid-structure variational field[39], for an incompressible Neo-Hookean material, the stored energy function is defined by:

$$\widetilde{W}_C(\bar{\boldsymbol{D}}, \boldsymbol{D}) = -\frac{G}{2}(\bar{\boldsymbol{D}}\colon \boldsymbol{D} - 3) \tag{3.4}$$

where $G = \frac{E}{2(1+v)}$. G, $\boldsymbol{D}$, and $\bar{\boldsymbol{D}}$ are the shear modulus, standard, and modified deformation gradient tensors, respectively.

By definition of the Cauchy stress tensor, the hydrostatic pressure field is given by:

$$p = \bar{p} - \frac{1}{3\det \boldsymbol{D}} \frac{\partial \widetilde{W}_C}{\partial \boldsymbol{D}} : \boldsymbol{D} \tag{3.5}$$

Solving Eqs. (3.4) and (3.5), the analytical expression of the muscle's pressure field is derived as[39]:

$$p(R,\lambda) = -\frac{2G}{3}[r'(R)]^2 + \frac{G}{3}\left\{\frac{[r(R)]^2 + R^2}{R^2}\right\} + \frac{G(\lambda^2 - R_{out}^2)(R^2 - R_{in}^2)}{(\lambda^2 - R_{out}^2 + R^2)(\lambda^2 - R_{out}^2 + R_{in}^2)} + G.\ln\left(\frac{R.r(R_{in})}{R_{in}.r(R)}\right) \tag{3.6}$$

where R is the muscle shell radius at which local shell pressure, resulting from the contained hydrostatic pressure, is calculated (Fig. 3–2). The notation $r' = \frac{dr}{dR}$ is utilized for convenience and $r(R)$ is defined by the following expression:

$$r(R,\lambda) = \sqrt{R^2 + \lambda^2 - R_{out}^2} \tag{3.7}$$

Eq. (3.6) has multiple implications, some of which are beyond the scope of this research but are still noteworthy. It enables one to estimate the resultant uniform pressure contained within the muscle shell as well as the local elemental pressure load in the muscle shell elements, both resulting from the shell stretch ratio due to an external load. In other words, external loads cause muscle deformation, expressed by the shell stretch ratio, which IMP and shell elemental pressure depend on. For the scope of this research, and since the modelled muscle has a very thin shell, the pressure distribution, produced a residual stress at the muscle shell elements, is not of interest (pressure resultant internal load at a radius R shown in Fig. 3–2). However, especially for

subsequent modelled human muscles, which are much thicker in nature, the formulated variational principle allows exploring such pressure distribution, which is of high clinical significance.

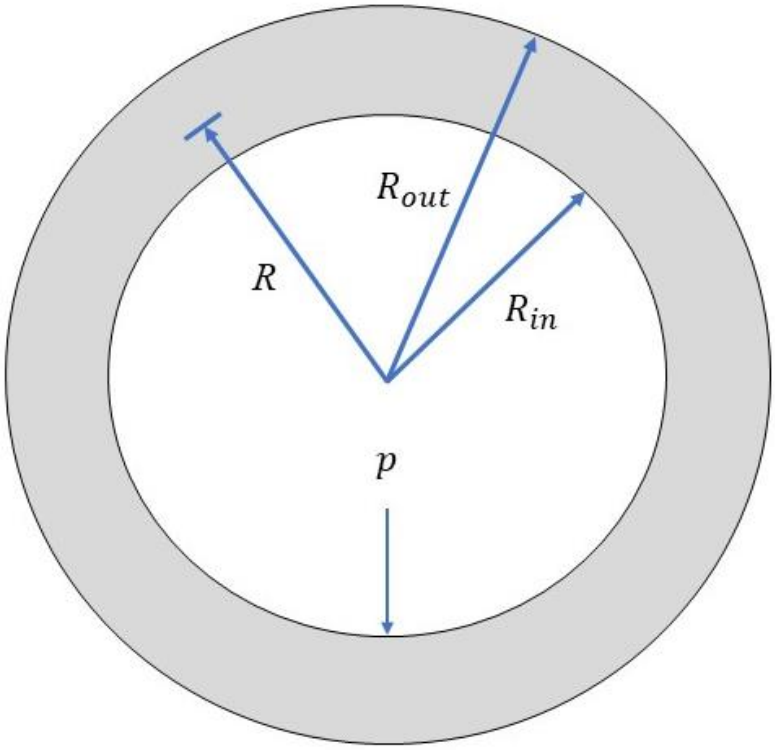

Figure 3–2: A cross-sectional cylindrical element schematic.

As such, for a uniform pressure field contained within a muscle shell, all shell radius (R) dependent terms vanish, resulting in the following analytical solution for the hydrostatic pressure field confined within the muscle shell:

$$p(\lambda) = \frac{G(\lambda^2 - R_{out}^2)(-R_{in}^2)}{(\lambda^2 - R_{out}^2)(\lambda^2 - R_{out}^2 + R_{in}^2)} \tag{3.8}$$

Combining Eqs. (3.3) and (3.8) *via* the radial deformation allows linking both fluid and structure fields, to which muscle shell stresses, displacements, and internal IMP can be all accordingly found. For the purpose of this study, being a medically applied model, the pressure field was introduced through the commercial software ANSYS Mechanical APDL by implementing a special type of hydrostatic pressure elements called HSFLD242 with a pressure node placed at muscle's centroid as illustrated in the next section and shown in Fig. 3–3.

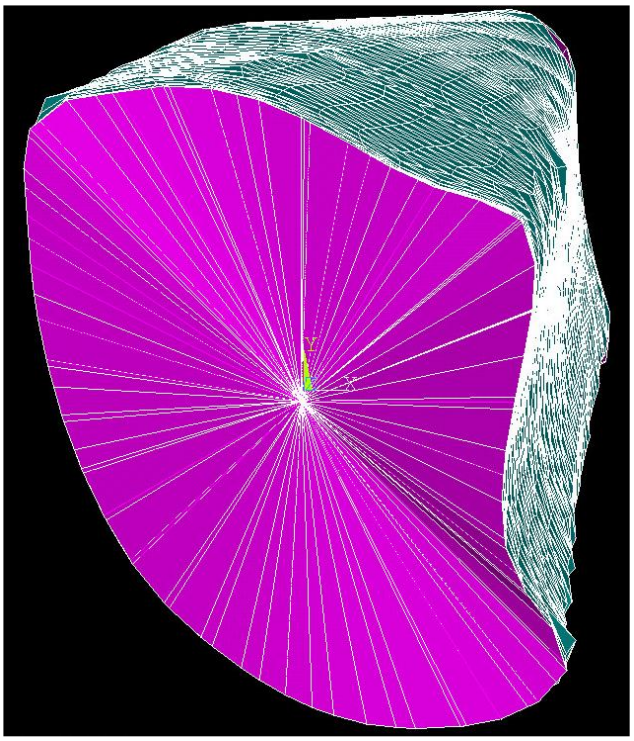

Figure 3–3: A cross-sectional view of the finite element muscle model showing the interaction between both the fluid, HSFLD242, and the shell elements, as well as the hydrostatic, HDSP, pressure node from which IMP was extracted.

C. Finite Elements Software Modelling

The TA muscle was downloaded from an anatomography website, a database of 3-dimensional MRI-scanned human body parts called 'BodyParts3D/Anatomography'. It was then processed in ANSYS SpaceClaim and ICEM CFD software packages to feature that of a male New Zealand White Rabbit (Rabbit mass of 3.6 Kg): unipennate and specific architectural dimensions[43] for validation purposes. In particular, a polygonal mesh (OBJ file) was downloaded, imported to SpaceClaim, and patched with surfaces created via splines. The generated volume was altered via surface and edge features, and then shrink-wrapped to 1 mm triangular edge size, 56.1 mm tendon-to-tendon length, and 3363 mm^3 volume. An equilateral triangular computational shell mesh was then generated from facets in ICEM with refining the extremities, hard-edges, and sharp angles. The resultant mesh was of 1 mm size with 0.46 minimum quality and aspect ratio. The model was then imported to ANSYS Mechanical modeler and solver, whereby the muscle shell was modelled based on its epimysium envelope, which was assigned a 1 mm thickness[44]. Material properties

were taken from a previous study that developed a nonlinear hyperelastic incompressible material law for muscles[45]. This study identified linear behavior in the first portion of the stress-strain curve. Fitting that part to a linear material law gave a Young's Modulus of $E = 4\ MPa$ and a Poisson's Ratio of $v = 0.45$, which were adopted in this study.

Aponeurosis/tendons were modelled by placing two deformable springs, of 1.945 N/mm longitudinal stiffness[46], attaching each muscle's extremity to a virtual ground, with the connection defined for all nodes present at each tendon attachment site. Frictionless and remote displacement supports were also defined for the same nodes to model neighboring organs. Implementing IMP, the shell model was coupled with confined pressure elements, mainly HSFLD242 elements to model a fluid-filled muscle. Those are special fluid elements in ANSYS Mechanical APDL that can be only applied to closed structures to mimic contained fluid behavior and simulate fluid-structure interaction. The elements share hydrostatic pressure, HDSP node, from which the IMP values were retrieved, and from where the HSFLD242 elements initiate and extend to each element on the surface of the shell. In this model, the HDSP node was put at muscle's centroid to distribute uniform hydrostatic pressure from that position to the HSFLD242 elements painted over the whole interior shell mesh.

A remote point was also defined at muscle's centroid and remote muscle forces (F) were internally applied from the nodes of tendon attachments at a pennation angle of 2.5 degrees[2]. In other words, muscle forces were modelled as internal remote muscle loads, acting from internal muscle elements, towards the remote point defined at the centroid. This was to model the behavior of sarcomeres and actin-myosin muscle fibers during contraction. Input F was then parametrized and increased from 2 to 12N, in increments of 0.5, to simulate IMP output. Although model's capabilities extend below 2N and beyond 12N, the muscle was simulated within this range for validation purposes as studies against which model's results were indirectly validated have this force range in common[1,47]. Thereafter, the F-IMP curve of interest was directly extracted from ANSYS Static Structural, which was then exported and post-processed in MATLAB (MathWorks, v. R2020a).

To further verify the results of the HDSP nodal method described above, another reverse-engineered method of assessing intramuscular pressure build-up was picking eight selective mesh elements in different locations along muscle's circumference. A cylindrical coordinate system was

created for each of those elements with changing the principal angles until one of the principal axes is perpendicular to the picked mesh element. Then, the radial normal stress contours were extracted from the bottom side of each element. This mimics the gauge pressure inside the muscle as the radial stress for thick-walled cylinders is equal and opposite to the gauge pressure on the inside surface[48]. Intramuscular pressure was then found by taking the average value of the stress contours at the element of interest. This was merely conducted to verify model's HDSP node IMP results. Figs. 3–1 and 3–3 show the muscle model with its boundary conditions.

Changes in muscle length, enabled by relation between pressure and adopted material properties, as a function of force were also investigated by measuring the directional deformation in the axial direction. Results were then normalized and reported in terms of a percentage of longitudinal strain (MLS) and percentage of force relative to the maximum applied (MFR). This was conducted as another model verification step by comparing the behavior of these results to conventional skeletal muscles length-tension curves.

Lastly, model's sensitivity to nonlinear large deformation effects, different finer meshes, and the range of different tendon stiffnesses collected from literature[46] was investigated. In particular, the first sensitivity study investigated model's response against nonlinear effects and large deformations, whereby results were compared to the linear case. Furthermore, in efforts of investigating model's response to other computational meshes, two finer triangular meshes of 0.1 and 0.25mm edge-size were created by inflating, pinching, and face-meshing regions of stress concentration, to which IMP results were then compared against the original courser mesh. Mesh convergence was also conducted by retrieving IMP variations, for the first 20 iterations, at 11N F. Finally, IMP sensitivity to other tendon stiffness values was investigated by simulating the range of 1.51 to 2.77 N/mm[46] at a constant 12N muscle force.

3.2.4. RESULTS

A. Main Findings

In response to increased F from 2 to 12 N, IMP measured at the Muscle Centroid (MC) by the HDSP node showed a linear increase from 5.25 to 31.73 mmHg (Fig. 3–4). To validate this linear

correlation, plotting the experimental values of both the studies of Davis *et. al* and Degens *et. al* on the same graph showed an increase from 7.5 to 32.91 mmHg and from 7.4 to 34.21 mmHg, respectively. Deviations from the linear mode for the same force range values were also reported in Fig. 3–4. A maximum discrepancy of 3.6% was registered between the muscle model, at MC, and the investigation of Davis *et. al* at a 12 N muscle force; whereas for the investigation of Degens *et. al*, it was 7.25%.

On the other hand, to verify IMP values, radial stresses were collected (Fig. 3–5). Upon increasing F from 2 to 12 N, radial stress increased linearly from [5.07, 6.35] to [32.46, 37.36] mmHg interval values for the eight different mesh elements test points (TPs), as shown in Fig. 3–4. Comparing those radial stresses to the IMP measured at the Muscle Centroid (MC) by the HDSP node, a strong agreement was observed with a maximum difference of 15.07% recorded between the radial stress measured at TP7 at a 12 N applied muscle force (Fig. 3–4).

Using the MC HDSP node, a linear correlation between IMP and TA muscle output forces was found to be:

$$F\ [N] = A \times IMP\ +\ B \tag{3.9}$$

with a R^2 statistical regression value of: $R^2 = 0.9913$. $A\ =\ 0.03811$ N/mmHg, IMP is intramuscular pressure in units of mmHg, and $B\ =\ 0.02104\ (\pm 0.132)$ N.

Lastly, under passive isometric contraction conditions, increasing muscle force from 0.01 to 12 N, muscle axial deformation decreased, enabled by relation between pressure and adopted material properties, from 40 to 31.8 mm (Fig. 3–6). The normalized results in terms of MLS and MFR are also shown in Fig. 3–6. A quadratic correlation between muscle length (ML) and force was found to be:

$$F\ [N] = C \times ML^2 + D \times ML + E \tag{3.10}$$

with a R^2 statistical regression value of: $R^2 = 0.9865$. $C\ =\ -0.1848$ N/mm^2, ML is muscle length in units of mm, $D\ =\ 11.94$ N/mm, and $E\ = -181.06$ mm.

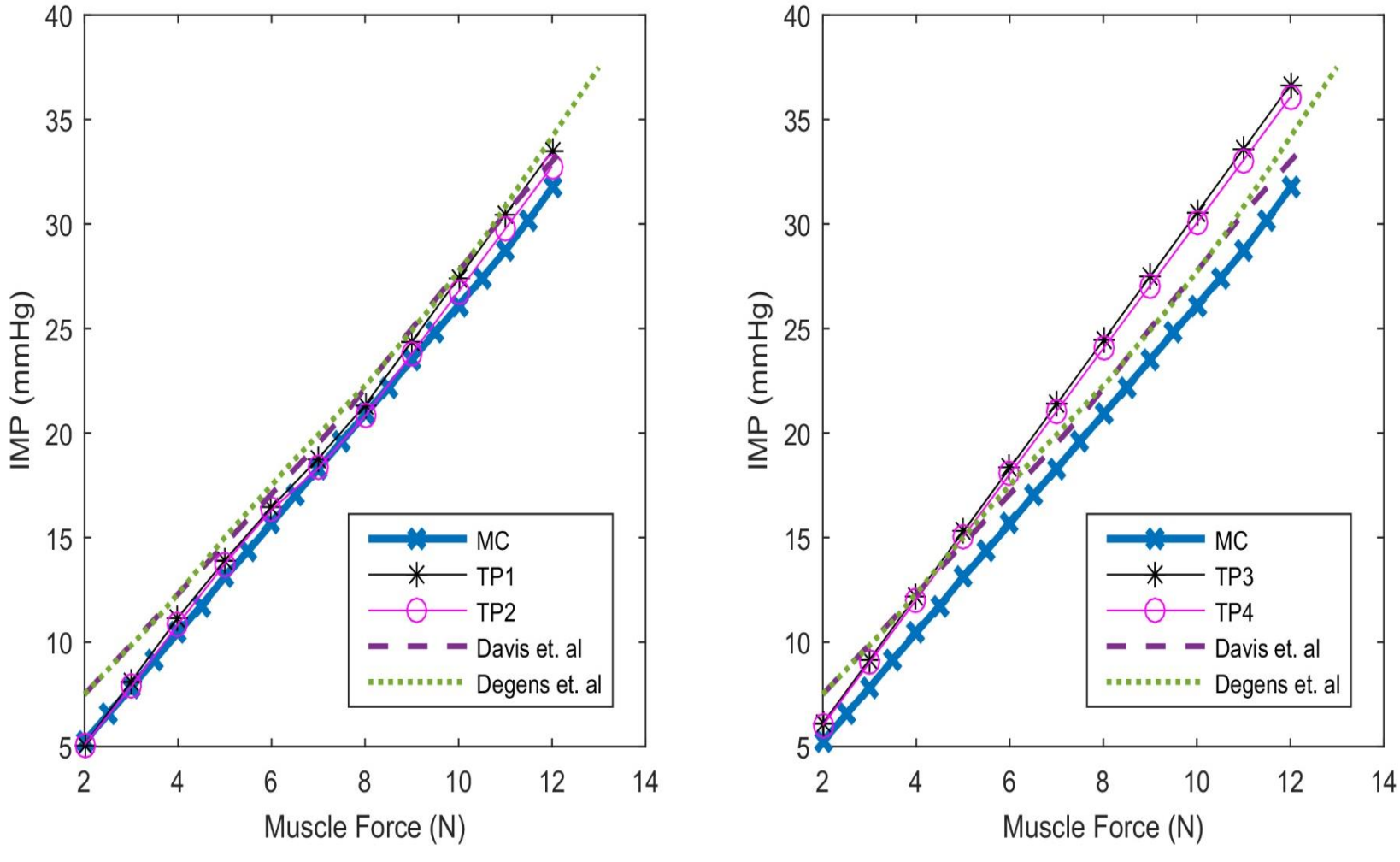

Figure 3–4: Relation between muscle forces [N] and IMP [mmHg] extracted from the hydrostatic pressure node HDSP, the eight different test points (TP1, TP2, TP3, TP4, TP5, TP6, TP7, and TP8) picked along muscle surface in different locations, and literature results used for validation. Each plot includes the HDSP node results, two of the selective mesh elements, and the experimental literature results of Davis *et. al.* and Degens *et. al*[1,47].

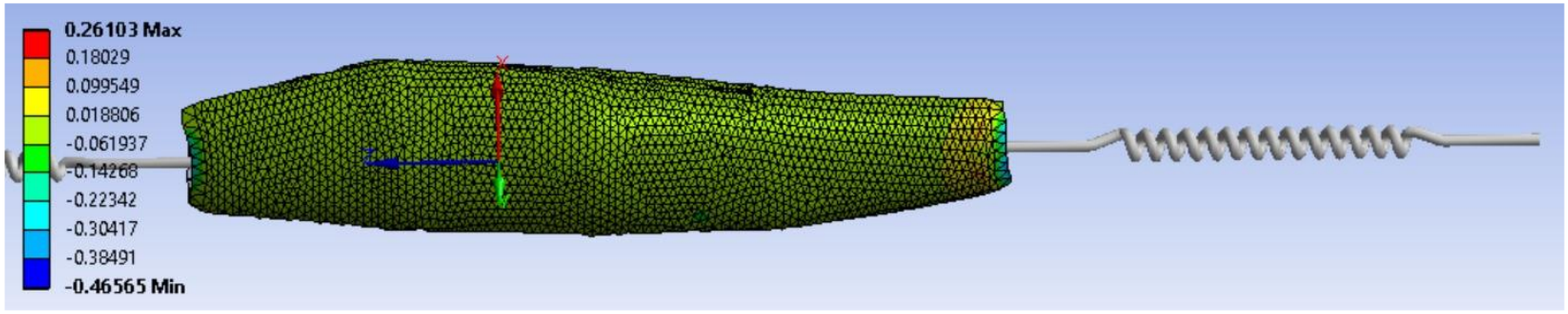

Figure 3–5: Normal, radial, stress distribution results [MPa] used to extract and verity IMP values.

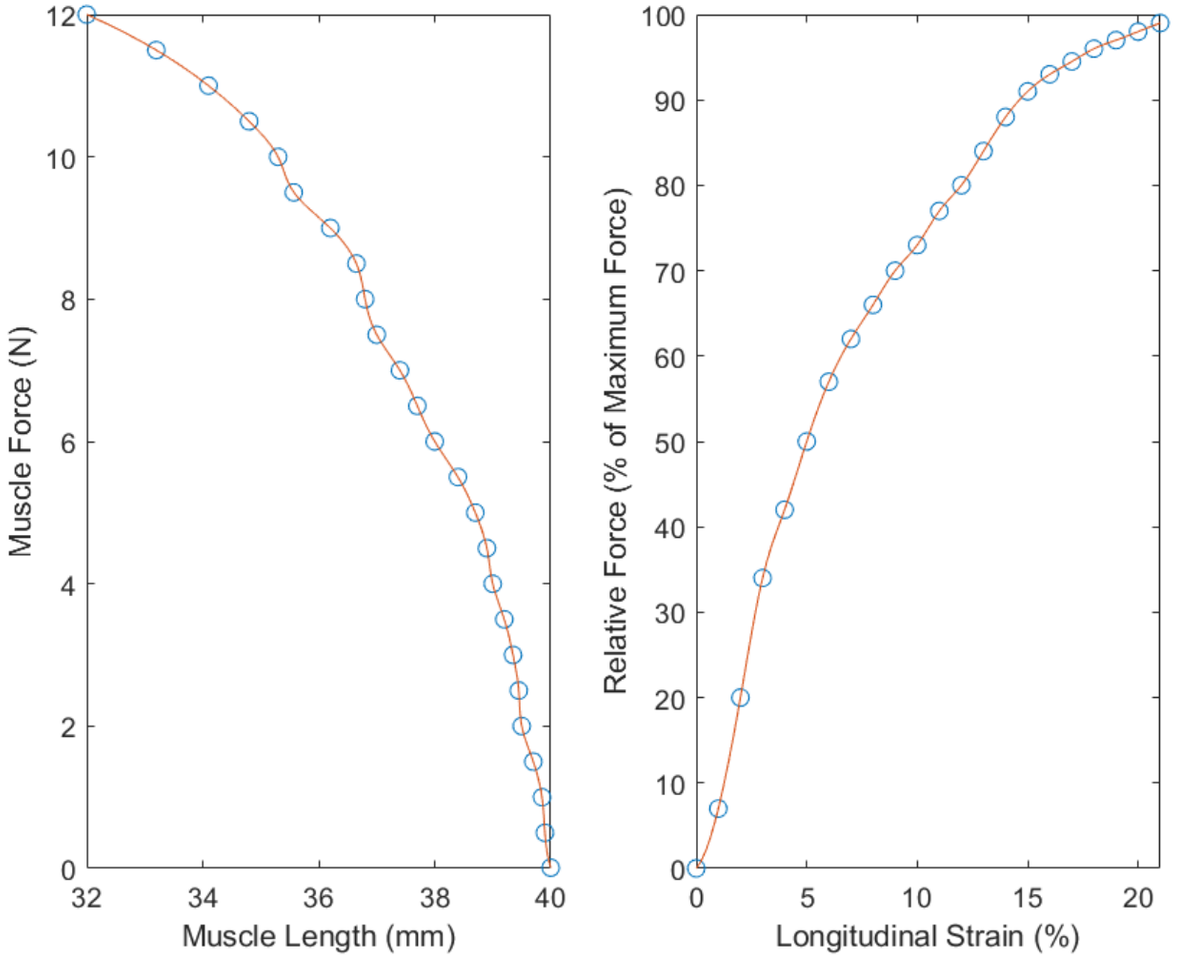

Figure 3–6: Muscle length-force results.

B. Sensitivity Study

B.1. Model response to nonlinearities

Adopting non-linear effects and large deformations, simulating the range of 2 to 12 N, showed a maximum IMP discrepancy of 9.6% between the linear and nonlinear cases, recorded at 12 N force (Fig. 3–7a).

B.2. Model response to different meshing techniques

Simulating the three produced meshes resulted in a maximum IMP discrepancy of 11.2%, recorded between the original 1 mm coarse and the finest 0.1 mm mesh (Fig. 3–7b). Results also revealed that IMP reached its plateau limit, at 11 N force within the first 5 iterations for the coarser mesh, while it took at least 10 iterations for the other finer meshes, with only slight increases afterwards (Fig. 3–7c).

B.3. Model response to different tendon stiffnesses

Upon simulating the range of tendon stiffnesses from 1.51 to 2.77 N/mm, IMP values barely changed over the entire interval with a maximum difference of 6.5% between the lowest (1.51 N/mm) and highest (2.77 N/mm) stiffness values (Fig. 3–7d).

3.2.5. DISCUSSION

The purpose of this study was to develop and validate a novel detailed finite element model of a muscle inclusive of a validated internal pressure and contractile force (F-IMP) relationship. This served to directly quantify the relationship between IMP and muscle's force through a three-dimensional finite element model of an MRI-scanned tibialis anterior muscle. The present study successfully achieved this by developing a custom coded, mixed fluid-shell field, FE model of a muscle.

In the past, rabbit tibialis anterior was used often to investigate different parameters, including IMP, with little research on human muscles to this regard. Previous investigators[49–52] have implied that muscle tension and IMP were correlated. However, to the authors' knowledge, a three-

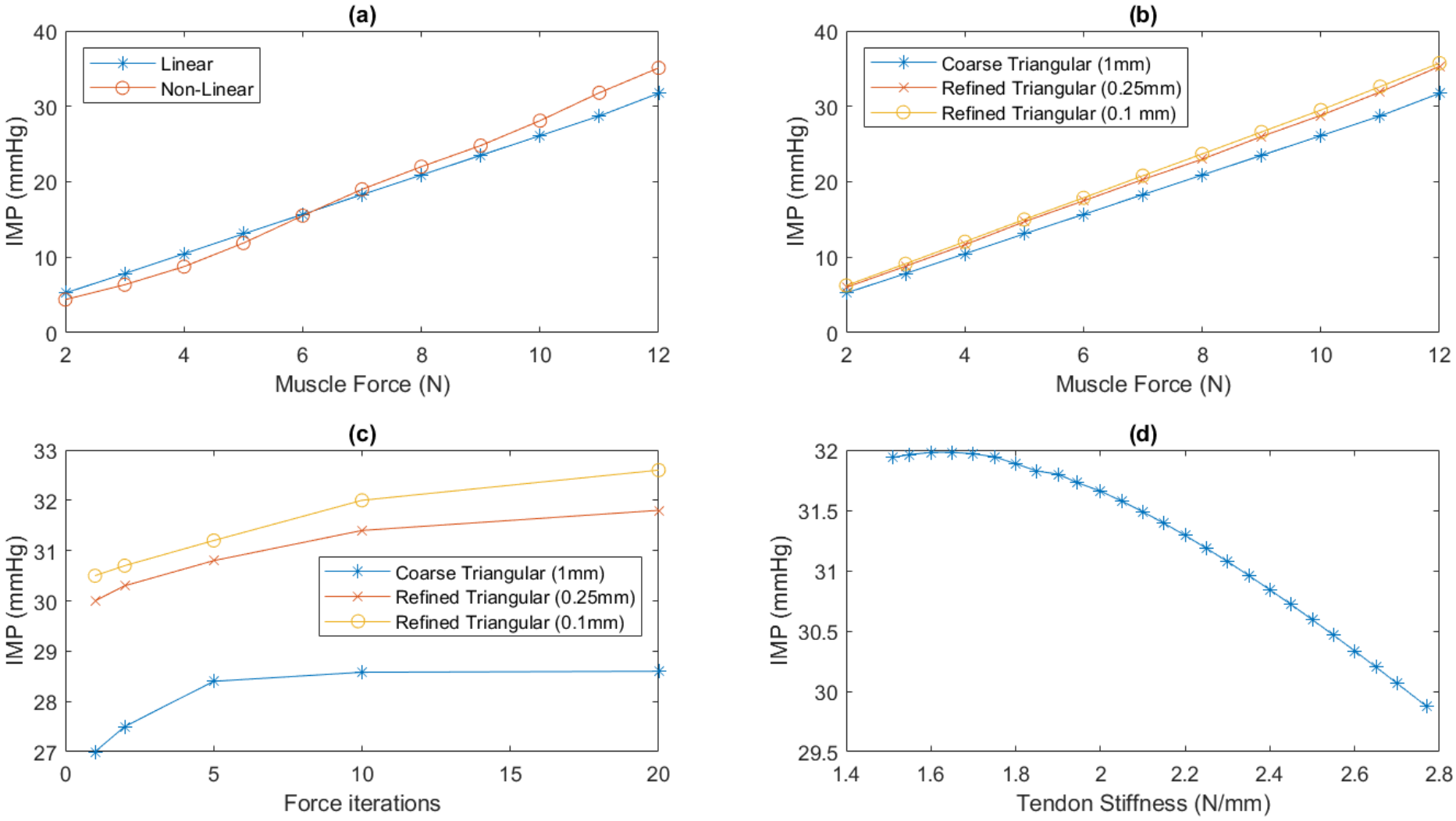

Figure 3–7: Model's sensitivity studies. (a): Model's sensitivity to non-linearities; (b): Model's sensitivity to different meshes; (c): Mesh convergence; (d): Model's sensitivity to different values of tendon stiffnesses.

dimensional muscle model that accurately includes muscle fluid responsible for generating its internal pressure, has the potential to interact with neighboring human tissues *via* ease of scalability, and considerably enhance computational times does not yet exist. The modeling approach of IMP in the present study may potentially be used by clinicians to estimate individual muscle force or in biomechanical models seeking a more physiological muscle representation compared to commonly employed vectoral type muscle models.

A. Linear F-IMP Relation & Model Validation

The use of 3D confined hydrostatic fluid (HSFLD242) elements, explained in detail in the methods section, coupled with a hydrostatic pressure HDSP nodes in a closed epimysium muscle shell, allowed for the accurate representation of a mixed fluid-filled muscle field using the finite element numerical approach. The use of those fluid elements was of high interest because of their capability to simulate any closed system involving fluid structure interaction, such as the case of human muscles and other soft tissues, without the need of combining those fields in a highly complex analysis. Upon doing so, a linear correlation between muscle forces and intramuscular pressure was realized. To further verify this, the IMP value measured at the hydrostatic pressure node at the muscle's centroid was compared to the measured stresses at different selective elements distributed in different regions across the muscle's surface. It was revealed that the same direct linear F-IMP relationship existed at all test points. As one may expect, there were discrepancies between the results of the HDSP node IMP and the different test points (TPs), and among those TPs themselves. This was expected as each test point was chosen from a different section of the muscle. The reported discrepancies are best explained by the muscle's geometric complexity given that the force introduced at extremities may have impacted adjacent element stress values before being uniformly distributed across all other muscle elements (Fig. 3–5). That is, other stress components might have accumulated and affected collecting the accurate radial stress at each selected element nearby the tendons. Despite this slight deviation, as shown in Fig. 3–4, the measured data have a strong correlation with each other as well as with the compared experimental data.

Indirect validation, by comparing the FE results to previous published experimental data, was carried out relevant to the content of use. Essentially, reported results agreed with literature values

closely with a maximum discrepancy of 3.6% registered between MC IMP and the study of Davis *et. al.* while 7.25% for the study of Degens *et. al*, both at 12N force. These small differences are perhaps related to the fact that literature correlations appeared to diverge from being linear at high IMP values where the percentage error got higher (Fig. 3–4). Furthermore, it was reported that those studies did not end up with a direct linear correlation due to human experimental errors[47], where it was suggested that sensors might have displaced a bit upon successive insertions and removals[1]. One more reason that might have deteriorated simulation values was the coarser mesh used to enhance computational time (running the simulation for one force input took around 12 seconds to solve for the course 1 mm mesh, 21 seconds for the 0.25 mm mesh, while 51 seconds for the finest 0.1 mm mesh). However, the reported errors are not considered significant, especially in the mid-range IMP values. Therefore, the implemented methodology has been shown to be valid, with a minimal discrepancy, and has the potential to be scaled to any human muscle dimension.

Furthermore, a linear F-IMP correlation was established with a very small margin of error (± 0.13 N). Hence, exhibiting the capability of predicting muscle forces from IMP and providing a realistic muscle modeling method that may be employed in subsequent biomechanical studies. It was also observed that acquired pressure data most closely agree with literature values near the center of the muscle. This was because the associated mesh element was on the smoothest section of the muscle with no stress concentrations existing around that region. This describes its ability to record more accurate pressure values. It is therefore conceivable that experimentally, if a muscle's centroid is not accessible for pressure measurements, such values can be also predicted by the radial stress in the muscle mid-region.

On the other hand, based on the sliding filament theory, since muscle fibers shortening is in direct relation with muscle forces, another useful correlation between muscle length and force was established in the passive muscle state. The developed FEM produced a curve that followed a similar trend as the contraction part, inclusive of passive element, of documented length-tension curves, which supports model's capability to simulate the passive state, as well as adds to the validity and accuracy of the developed model. Normalizing those values into a longitudinal strain and force, the collected curve follows the same trend as the passive contraction part of documented muscle force-strain curves as well (Fig. 3–6). The nonlinearities of this correlation were best

described by fibers strengthening. As muscle fibers, actin and myosin, stiffen, muscle forces increased, which was reflected in finite elements terms as the non-linear stiffening of the shell mesh elements. As a result, muscle's axial deformation decreased, with respect to previous applied force, which is reflected by the decline in slope going up the curve.

B. Robust Model to Input Parameters

As part of studying model's sensitivity, changing material behavior to nonlinear and to include large deformations was not considered significant. Thus, it can be suggested that the model was robust when it came to material behaviors. Further, non-linearities increase computational time by at least five folds (in this case, running the simulation for one force input took the linear model around 12 seconds while the non-linear one around 64 seconds). Both times are not considered significant; however, when considering muscle models with numerous muscles, computational time becomes of a concern. Further, the addition of FE contacts and coupling them with a non-linear material behavior would also considerably increase simulation time. Both, number of muscles and contacts, effects were shown by the authors in a subsequent study to deteriorate simulation time[53]. It was further shown that their treatment would not cause any loss in accuracy. Thus, it can be argued that it is preferable to stay away from nonlinearities, to keep computational time as reasonable as possible, whenever the linear model is capable of producing accurate results and simulating the actual biomechanics of the human body. Such confidence levels must be kept in mind according to the content of use of the model. On the other hand, mesh sensitivity did not also result in considerable differences. The reason courser mesh was adopted in the present study was to reduce computational time. Lastly, since tendon stiffness values differed greatly in literature, assessing model's sensitivity to different tendon stiffness was essential. Results showed that IMP values barely changed over the entire interval which was also not considered a significant discrepancy. This suggests, and further proves, an essential role of tendons, which is to solely transmit forces generated by muscles, redistribute them over the available joints, and seldom generate any force.

C. Limitations

Although the developed model proved to predict accurate F-IMP results, there remains some limitations. The fact that the model is linear is an assumption compared to the inherent properties of tissues being anisotropic and hyperelastic. Viscoelasticity is not an issue here since this behavior only appears when investigating tissue dynamics, whereas the developed model represented imposing conditions that are analogous to concentric contraction under isometric static conditions. However, as previously shown by the authors in a strains sensitivity analysis[53], such assumption is valid as the simulated range of motion falls within the linear part of the stress-strain curves. Another limitation was that the model adapted MRI-scanned tibialis anterior muscle to rabbit's muscle geometry and physiology, which was required to perform validation comparisons. Representing all inter-biomechanics inside the muscle by IMP is considered a limitation as well. It is true that the developed model did not consider an accurate representation of muscle fibers, fascicles, and how they are packed; however, the aim was to produce an accurate physiological representation of a muscle behavior inclusive of IMP. The inclusion of IMP instead of the actual elements inside a muscle allowed for the modelling of the presence of those elements. That is, the final model's behavior mimics the actual physiology of muscles and provides a validity that can be scaled to play the role of a reference model for other human muscles.

D. Future Work

Proving the validity of the developed model, the next step would be to incorporate muscle dynamics. That is, expanding the constitutive model to include nonlinearities, mainly hyperelastic and viscolelastic effects, as well as to include muscle fibers-IMP interaction inside the muscle. It would be of interest to check the validity of the F-IMP relationship and then apply the same procedure to a group of muscles in the spine region to study the effect of muscle packing, for which the authors have successfully built a state-of-the-art fully representative spine model for this purpose[53].

3.2.6. CONCLUSION

In conclusion, this study developed and validated a novel 3-dimensional volumetric finite element muscle model that includes an accurate physiological correlation between its contractile force and internal pressure. The model was indirectly validated with in-vivo data. Subsequently, two correlations relating muscle output force to IMP and muscle length were established. Lastly, the model was shown to be robust in light of sensitivity studies. The developed model exemplifies a novel method to simulate fluid-filled muscle finite element models, which has been shown to be easily integrated in biomechanical studies[53]. Moreover, potentially following further research and validation, the model may be used to estimate individual muscle forces in a clinical setting spanning from empirical measurements of IMP. Lastly, again building on further studies, the model's linearities and scalable characteristics may enable one to make appropriate adjustments towards conducting patient-specific analyses.

3.2.7. ACKNOWLEDGMENTS

We gratefully acknowledge funding by McGill University (MEDA), the Fonds de Recherche du Québec – Nature et Technologies (FRQNT), and the Natural Sciences and Engineering Research Center (NSERC). The authors also acknowledge that the 3D CAD model is based on a parametric 3D model from the Japanese Database 'BodyParts3D/Anatomography'.

3.2.8. REFERENCES

1. Davis, J., Kaufman, K. R. & Lieber, R. L. Correlation between active and passive isometric force and intramuscular pressure in the isolated rabbit tibialis anterior muscle. J. Biomech. (2003). doi:10.1016/S0021-9290(02)00430-X

2. Wheatley, B. B., Odegard, G. M., Kaufman, K. R. & Haut Donahue, T. L. Modeling Skeletal Muscle Stress and Intramuscular Pressure: A Whole Muscle Active-Passive Approach. J. Biomech. Eng. (2018). doi:10.1115/1.4040318

3. Barry, D. T., Gordon, K. E. & Hinton, G. G. Acoustic and surface EMG diagnosis of pediatric muscle disease. Muscle Nerve (1990). doi:10.1002/mus.880130403

4. Speich, J. E. et al. Adjustable passive length-tension curve in rabbit detrusor smooth muscle. J. Appl. Physiol. (2007). doi:10.1152/japplphysiol.00548.2006

5. Sejersted, O. M. & Hargens, A. R. Intramuscular pressures for monitoring different tasks and muscle conditions. Advances in Experimental Medicine and Biology (1995). doi:10.1007/978-1-4899-1016-5_27

6. Evertz, L. Q., Bulstra, L. F., Shin, A. Y. & Kaufman, K. R. Evaluate muscle tension using intramuscular pressure device in rabbit tibialis anterior model for improved tendon transfer surgery. Physiol. Meas. (2017). doi:10.1088/1361-6579/aa6739

7. Winters, T. M. et al. Correlation between isometric force and intramuscular pressure in rabbit tibialis anterior muscle with an intact anterior compartment. Muscle and Nerve (2009). doi:10.1002/mus.21298

8. Go, S. A. et al. Design Considerations of a Fiber Optic Pressure Sensor Protective Housing for Intramuscular Pressure Measurements. Ann. Biomed. Eng. (2017). doi:10.1007/s10439-016-1703-6

9. Ward, S. R., Davis, J., Kaufman, K. R. & Lieber, R. L. Relationship between muscle stress and intramuscular pressure during dynamic muscle contractions. Muscle and Nerve (2007). doi:10.1002/mus.20828

10. Daggfeldt, K. Muscle bulging reduces muscle force and limits the maximal effective muscle size. J. Mech. Med. Biol. (2006). doi:10.1142/s0219519406001947

11. Hargens, A. R., Mubarak, S. J., Owen, C. A., Garetto, L. P. & Akeson, W. H. Interstitial fluid pressure in muscle and compartment syndromes in man. Microvasc. Res. (1977). doi:10.1016/0026-2862(77)90136-4

12. Matsen, F. A., Mayo, K. A., Sheridan, G. W. & Krugmire, R. B. Monitoring of intramuscular pressure. Surgery (1976). doi:10.5555/uri:pii:0039606076902385

13. Hargens, A. R. et al. Tissue fluid pressures: From basic research tools to clinical applications. J. Orthop. Res. (1989). doi:10.1002/jor.1100070617

14. Smith, D. A. The theory of sliding filament models for muscle contraction. III. Dynamics of the five-state model. J. Theor. Biol. (1990). doi:10.1016/S0022-5193(05)80372-8

15. Röhrle, O., Davidson, J. B. & Pullan, A. J. A physiologically based, multi-scale model of skeletal muscle structure and function. Front. Physiol. (2012). doi:10.3389/fphys.2012.00358

16. Hodgkin, A. L. & Huxley, A. F. A quantitative description of membrane current and its application to conduction and excitation in nerve. J. Physiol. (1952). doi:10.1113/jphysiol.1952.sp004764

17. Huxley, A. F. Muscle structure and theories of contraction. Prog. Biophys. Biophys. Chem. (1957). doi:10.1016/s0096-4174(18)30128-8

18. Hill, A. V. The Heat of Shortening and the Dynamic Constants of Muscle. Proc. R. Soc. B Biol. Sci. 126, 136–195 (1938).

19. Winters, J. M. & Stark, L. Muscle models: What is gained and what is lost by varying model complexity. Biol. Cybern. (1987). doi:10.1007/BF00318375

20. Semwal, S. K. & Hallauer, J. J. Biomechanical modeling: Implementing line-of-action algorithm for human muscles and bones using generalized cylinders. Comput. Graph. (1994). doi:10.1016/0097-8493(94)90121-X

21. Nussbaum, M. A., Chaffin, D. B. & Rechtien, C. J. Muscle lines-of-action affect predicted forces in optimization-based spine muscle modeling. J. Biomech. (1995). doi:10.1016/0021-9290(94)00078-I

22. Delp, S. L. et al. An Interactive Graphics-Based Model of the Lower Extremity to Study Orthopaedic Surgical Procedures. IEEE Trans. Biomed. Eng. 37, 757–767 (1990).

23. Chao, E. Y. S., Lynch, J. D. & Vanderploeg, M. J. Simulation and animation of musculoskeletal joint system. J. Biomech. Eng. 115, 562–568 (1993).

24. Gatton, M., Pearcy, M. & Pettet, G. Modelling the line of action for the oblique abdominal muscles using an elliptical torso model. J. Biomech. (2001). doi:10.1016/S0021-9290(01)00079-3

25. Pandy, M. G. Computer Modeling and Simulation of Human Movement. Annu. Rev. Biomed. Eng. (2001). doi:10.1146/annurev.bioeng.3.1.245

26. Dong, F., Clapworthy, G. J., Krokos, M. A. & Yao, J. An anatomy-based approach to human muscle modeling and deformation. IEEE Trans. Vis. Comput. Graph. (2002). doi:10.1109/2945.998668

27. Johansson, T., Meier, P. & Blickhan, R. A finite-element model for the mechanical analysis of skeletal muscles. J. Theor. Biol. (2000). doi:10.1006/jtbi.2000.2109

28. Oomens, C. W. J., Maenhout, M., Van Oijen, C. H., Drost, M. R. & Baaijens, F. P. Finite element modelling of contracting skeletal muscle. in Philosophical Transactions of the Royal Society B: Biological Sciences (2003). doi:10.1098/rstb.2003.1345

29. Blemker, S. S., Pinsky, P. M. & Delp, S. L. A 3D model of muscle reveals the causes of nonuniform strains in the biceps brachii. J. Biomech. (2005). doi:10.1016/j.jbiomech.2004.04.009

30. Lemos, R. R., Rokne, J., Baranoski, G. V. G., Kawakami, Y. & Kurihara, T. Modeling and simulating the deformation of human skeletal muscle based on anatomy and physiology. in Computer Animation and Virtual Worlds (2005). doi:10.1002/cav.83

31. Röhrle, O. & Pullan, A. J. Three-dimensional finite element modelling of muscle forces during mastication. J. Biomech. (2007). doi:10.1016/j.jbiomech.2007.05.011

32. Böl, M. & Reese, S. Micromechanical modelling of skeletal muscles based on the finite element method. Comput. Methods Biomech. Biomed. Engin. (2008). doi:10.1080/10255840701771750

33. Blemker, S. S. & Delp, S. L. Three-dimensional representation of complex muscle architectures and geometries. Ann. Biomed. Eng. (2005). doi:10.1007/s10439-005-1433-7

34. Röhrle, O., Davidson, J. B. & Pullan, A. J. Bridging scales: A three-dimensional electromechanical finite element model of skeletal muscle. SIAM J. Sci. Comput. (2008). doi:10.1137/070691504

35. Böl, M., Kruse, R., Ehret, A. E., Leichsenring, K. & Siebert, T. Compressive properties of passive skeletal muscle-The impact of precise sample geometry on parameter identification in inverse finite element analysis. J. Biomech. (2012). doi:10.1016/j.jbiomech.2012.08.023

36. Siebert, T., Till, O. & Blickhan, R. Work partitioning of transversally loaded muscle: Experimentation and simulation. Comput. Methods Biomech. Biomed. Engin. (2014). doi:10.1080/10255842.2012.675056

37. Jenkyn, T. R., Koopman, B., Huijing, P., Lieber, R. L. & Kaufman, K. R. Finite element model of intramuscular pressure during isometric contraction of skeletal muscle. Phys. Med. Biol. (2002). doi:10.1088/0031-9155/47/22/309

38. Wheatley, B. B., Odegard, G. M., Kaufman, K. R. & Haut Donahue, T. L. A validated model of passive skeletal muscle to predict force and intramuscular pressure. Biomech. Model. Mechanobiol. (2017). doi:10.1007/s10237-016-0869-z

39. Chi, H., Talischi, C., Lopez-Pamies, O. & Paulino, H. G. Polygonal finite elements for finite elasticity. Int. J. Numer. Methods Eng. (2015). doi:10.1002/nme.4802

40. Sanders, J. L. An Improved First-Approximation Theory for Thin Shells. NASA Technical Report R-24 (1959). doi:TR R-24

41. Herrmann, L. R. Elasticity equations for incompressible and nearly incompressible materials by a variational theorem. AIAA J. (1965). doi:10.2514/3.3277

42. Atluri, S. N. & Reissner, E. On the formulation of variational theorems involving volume constraints. Comput. Mech. (1989). doi:10.1007/BF01047050

43. Lieber, R. L. & Blevins, F. T. Skeletal muscle architecture of the rabbit hindlimb: Functional implications of muscle design. J. Morphol. (1989). doi:10.1002/jmor.1051990108

44. Nishimura, T., Hattori, A. & Takahashi, K. Ultrastructure of the Intramuscular Connective Tissue in Bovine Skeletal Muscle. Cells Tissues Organs (1994). doi:10.1159/000147671

45. Metan, S., Mohankumar, G. C. & Krishna, P. FEM an Effective Tool to Analyse the Knee Joint Muscles during Flexion. Am. J. Biomed. Eng. (2016).

46. Behfar, M., Sarrafzadeh-Rezaei, F., Hobbenaghi, R., Delirezh, N. & Dalir-Naghadeh, B. Enhanced Mechanical Properties of Rabbit Flexor Tendons in Response to Intratendinous Injection of Adipose Derived Stromal Vascular Fraction. Curr. Stem Cell Res. Ther. (2012). doi:10.2174/157488812799859874

47. Degens, H., Salmons, S. & Jarvis, J. C. Intramuscular pressure, force and blood flow in rabbit tibialis anterior muscles during single and repetitive contractions. Eur. J. Appl. Physiol. Occup. Physiol. (1998). doi:10.1007/s004210050381

48. Roylance, D. Pressure vessels and piping papers published in 1988 Contents of volume 31. Int. J. Press. Vessel. Pip. 36, i–xi (1989).

49. Sadamoto, T., Bonde-Petersen, F. & Suzuki, Y. Skeletal muscle tension, flow, pressure, and EMG during sustained isometric contractions in humans. Eur. J. Appl. Physiol. Occup. Physiol. 51, 395–408 (1983).

50. Sejersted, O. M. et al. Intramuscular fluid pressure during isometric contraction of human skeletal muscle. J Appl Physiol Respir Env. Exerc Physiol 56, 287–295 (1984).

51. Aratow, M. et al. Intramuscular pressure and electromyography as indexes of force during isokinetic exercise. J. Appl. Physiol. 74, 2634–2640 (1993).

52. Ballard, R. E. et al. Leg intramuscular pressures during locomotion in humans. J. Appl. Physiol. 84, 1976–1981 (1998).

53. El Bojairami, I., El-Monajjed, K. & Driscoll, M. Development and validation of a timely and representative finite element human spine model for biomechanical simulations. Sci. Rep. (2020). doi:10.1038/s41598-020-77469-1

3.3. SUMMARY

The central idea in this chapter was to advance the physiological behavior of skeletal muscles by accounting for enclosed muscular pressure. This was achieved by formulating two custom, separate fields, modelling the structural and volumetric behavior of muscles and the fluidic pressure enclosed within. The model was then developed based on the anatomy of the tibialis anterior muscle, realizing a link between both fields. This produced a biphasic, fluid-structure interaction, model by which monitoring muscle forces and intramuscular pressure became possible. Upon successful model development, a linear correlation was observed between these two physiological parameters which was validated against two comparators. The model also underwent parameters verification *via* sensitivity studies, which potentially showed a robust model with slight changes in results against input parameters.

A number of research and application advances were accomplished due to model's novelties. Firstly, the model put forth exhibited a direct and accurate physiological link between force generation and internal mechanism transcribed by intramuscular pressure. These permit replicating inner-body radial interaction between muscles and surrounding tissues. In essence, the build-up of intramuscular pressure exerts radial loads which might limit or support neighboring tissues and can be captured by the model put forth. Lastly, the model can be scaled to all paraspinal muscles, capturing the physiology of spinal muscles contraction, in order to complement a full-scale spine model as proposed and achieved in chapter 4.

4

NOVEL SPINE MODEL DEVELOPMENT AND PARAMETRIC VALIDATION

4.1. FRAMEWORK OF THE SECOND ARTICLE

Achieving the biphasic muscle model discussed in chapter 3, with an accurate depiction of the biomechanical physiological interaction between enclosed fluid and epimysium muscle shell, along with quantifying inner intramuscular pressure, is an advancement in the simulation of volumetric muscle contraction. This has a multitude of merits in numerical biomechanics, among which is the improvement in physiological reality which may allow improved understanding of the spine's underlying mechanics and pathomechanisms. However, the spine is a highly redundant structure possessing numerous kinematic degrees of freedom, to which conducting a task requires the engagement and coactivation of a very high number of spinal soft tissues. As such, a realistic representation of a spinal motion requires not only an accurate depiction of muscles' mechanisms, but also detailed models of other primary effects and tissues surrounding the spine. Thus, this study aimed to develop a parametric, detailed, 3-dimensional, and comprehensive finite element model of the spine by scaling the muscle model developed in chapter 3 to major spinal muscles, coupled with detailed models of the thoracic and lumbar vertebral bodies, intervertebral discs, associated tendons, thoracolumbar fascia, and intra-abdominal pressure. The inclusion of these tissues was motivated by their collective potential to better assess spinal stability as perceived in the research presented herein. The resulting spine model consisted of 273 soft tissues comprised of a computationally exhaustive number of numerical nodes, elements, and contacts. As such, to enable feasibility and ease of simulating an otherwise extremely complex model, a dedicated finite elements meshing method was employed by manually manipulating nodes at their connection

levels, to overcome the need for contact-based computations while maintaining high accuracy. Such a method has not been employed in such a complex physiological model before to the author's knowledge. A comprehensive and parametric set of indirect validation tests against prominent *in silico*, *ex vivo*, and *in vivo* models were carried out, to which all results closely resembled documented data. Therefore, this study achieved a state-of-the-art finite elements spine model inclusive of most physiological tissues known to contribute to spinal loadings. This model is considered an important advancement in numerical-applied biomechanics with numerous merits, among which is the accurate numerical representation of spinal tissues and the rendering of a reliable, fast, and validated spine model. Chapters 5 and 6 present a fundamentally clear vision on the exact use-cases of the novel model put forth in terms of a better assessment of spinal stability and muscle activation strategies; however, it possesses more far-reaching merits such as being a clinical complementary assessment tool, allowing for timely examination of spine-related pathologies, assessing injuries, evaluating surgical treatments, and performing medical device analyses prior to moving forth with *in situ* and *in vivo* testing. The outcome of this chapter marked the completion of objective 2 and examination of hypothesis 2, as presented in the manuscript entitled "Development and validation of a timely and representative finite element human spine model for biomechanical simulations" for which the contribution of the first author is considered to be 75%. This manuscript was published in the *Scientific Reports* open access journal by *Nature Research* on December 9, 2020.

4.2. ARTICLE 2: DEVELOPMENT AND VALIDATION OF A TIMELY AND REPRESENTATIVE FINITE ELEMENT HUMAN SPINE MODEL FOR BIOMECHANICAL SIMULATIONS

Ibrahim El Bojairami[1]; Khaled El-Monajjed, Ph.D, Jr.Eng.[1]; Mark Driscoll, Ph.D., P.Eng.[1]

[1]*Musculoskeletal Biomechanics Research Lab, Department of Mechanical Engineering, McGill University, Montréal, Quebec, Canada*

Address for notification, correspondence, and reprints:

Mark Driscoll, Ph.D., P.Eng., Assistant Professor

Associate Member, Biomedical Engineering

Canada NSERC Chair Design Engineering for Interdisciplinary Innovation of Medical Technologies

Department of Mechanical Engineering

817 Sherbrooke St. West

Montréal, QC, H3A 0C3 Canada

T: +1 (514) 398 – 6299

F: +1 (514) 398 – 7365

E-Mail: mark.driscoll@mcgill.ca

4.2.1. ABSTRACT

Numerous spine Finite Element (FE) models have been developed to assess spinal tolerances, spinal loadings and low back pain-related issues. However, justified simplifications, in terms of tissue composition and inclusion, for such a complex system may result in overlooking crucial

information. Thus, the purpose of this research was to develop and validate a comprehensive and representative spine FE model inclusive of an accurate representation of all major torso elements. A comprehensive model comprised of 273 tissues was developed via a novel FE meshing method to enhance computational feasibility. A comprehensive set of indirect validation tests were carried out to validate every aspect of the model. Under an increasing angular displacement of 24-41^{o}, the lumbar spine recorded an increasing moment from 5.5 to 9.3 Nm with an increase in IVD pressures from 0.41 to 0.66 MPa. Under forward flexion, vertical vertebral displacements simulated a 6% and 13% maximum discrepancy for intra-abdominal and intramuscular pressure results, all closely resembling previously documented *in silico* measured values. The developed state-of-the-art model includes most physiological tissues known to contribute to spinal loadings. Given the simulation's accuracy, confirmed by its validation tests, the developed model may serve as a reliable spinal assessment tool.

Keywords: Human spine model, finite element modelling, muscle pressure, abdominal pressure, thoracolumbar fascia.

4.2.2. INTRODUCTION

Chronic Low Back Pain (LBP) prevails as a burdensome restrictive condition given its persistent apparent socioeconomic repercussions[1–4]. In industrialized societies, such as Canada and the United States, medical expenditures and consequential losses spiral up to $50 Billion USD annually[5,6]. Such incurred costs develop from the challenges present in the accurate assessments of LBP as a result of the broadness of its most common defined cause, sustaining both, mechanical and clinical instabilities[7–9]. In essence, the ability of the musculoskeletal system to perform its normal functions relies on its capability to maintain an upright structure, commonly known as 'Spinal Stability'. In general, engineering stability pertains to a system's ability to restore itself and maintain its initial state when perturbed. This in part aligns with the widely accepted definition of clinical spinal stability, perhaps best explained by Panjabi[7], which attests that the spine maintains its three main functionalities which include protecting spinal cord and nerve roots, carrying loads, and enabling motion. The deterioration in spinal stability results in numerous

problems, most commonly LBP, which motivates the necessity to better understand the spinal system mechanism and pain pathomechanisms.

Due to the system's redundancies involving different degrees of freedom, multiple input loads, complex joint-muscle connectivity, and intricate soft tissues, assessing the musculoskeletal system has always been a challenging venture. In such a case, modelling presents itself as a plausible strategy to tackle elaborate systems such as the spine[10–12]. One conceivable, widely used, modelling tool is the finite elements method, which was first proposed by Richard Courant in 1922[13]. Since then, numerous biomechanical FE models have been developed[14–17] and used in various applications. One interesting example pertaining to spine biomechanics is the model developed by Driscoll *et. al*, in which he discussed the adverse effects of spinal deformities, considered to be on the end of the instability spectrum, which conceived a platform to analyze novel spinal screw designs as a corrective treatment of such deformities[18,19].

Numerous FEMs have been reported in literature to analyze spinal loading profiles, injuries, and its mechanical tolerances. Such models vary from a simple spine model which utilizes just a few elements[15,20,21], to models detailing only the vertebral bodies (VB) and intervertebral discs (IVD)[14,22,23], to more involved models that include simplified muscle geometries[24–26]. Other studies developed more physiologically realistic models by including the effects of intra-abdominal pressure (IAP) by using force vectors without the actual inflation in the diaphragm/abdomen[16]. However, this may tend to overestimate IAP values in certain areas due to the imbalance resulting from a fixed value of a varying fluidic IAP effect which changes with the muscular contraction. One of the most involved studies of including IAP was developed by Dietrich, Kedzior, and Zagrajek[27]. In their study, they modelled the bones, cartilages, discs, ligaments, and muscles as non-linear anisotropic viscoelastic with the IAP as an incompressible fluid embedded in a closed cavity, producing 2640 elements and 13107 algebraic equations[28]. Similarly, Arjmand *et. al.* developed an FE model based on mathematical representations which were constructed by Daggfeldt and Thorstensson[29]. Specifically, they represented the abdominal cavity as being encapsulated by three membrane layers to achieve a 7.35 mmHg baseline IAP elevating to a maximum of 29.627 mmHg IAP value during a partial valsalva maneuver[30].

In addition to the IAP, the pressure build-up in the spinal muscles, or in any other skeletal muscle to that matter, upon contraction (known as the muscle-balloon effect)[31], is believed to play a role

in spinal stability as put forth by the authors of the present study. As such, research efforts have been carried out to understand the mechanics of skeletal muscles, including their intramuscular pressure (IMP), and their overall contribution to human locomotion. Such a task is highly challenging due to the fact that numerous skeletal muscles, tendons, and joints interact together to produce a specific movement[32]. A well-developed and validated IMP-based FEM of a single muscle was put forth by El Bojairami and Driscoll[33], in which the authors realized the existence of linear correlation between muscle forces and IMP. However, to the authors' knowledge, incorporating the IMP in a full spine model has not yet been performed or studied.

One may argue that a reliable spine model should potentially incorporate all loading-assistive tissues attached to the spine[34–37]. That is, in addition to the spinal VBs, IVDs, IAP, and IMP effects, there remains an interest in including the ligamentous system that is believed to provide passive stiffness to the spine structure at limiting positions. In an interesting study, the ligamentous system in combination with the fascia, especially the thoracolumbar fascia (TLF), was examined by Gracovetsky through static computations[37]. It was suggested that their mechanical properties allow storing sufficient energy to permit the spine to overcome the extensive forces applied by the muscles. This was further developed by Moorhouse and Granata who observed that the tensile force applied by the spinal muscles, when resisting an applied flexion force, increases the stiffness of the spine[34]. In a complementing study, El-Monajjed and Driscoll simulated effects of varying IMP and IAP in a 2D TLF model. They suggested that the IAP tended to realize a rather balancing role within the body during asymmetric postures[38]. Thus, the inclusion of all the aforementioned effects in a comprehensive spine FE model to examine the influence of such tissues would potentially permit performing detailed investigations.

Other reliable spine FE models tailored towards VBs and IVDs only, are abundant in literature, which like most models include some level of physiological simplification[17,39,40]. Such studies provide a great deal of insight into spinal loading, albeit the predicted values may be over-estimated in comparison with empirical data. In a well-executed study, sixteen senior groups that perform spinal investigations collaborated to compare 8 FE models of the lumbar spine (5 lumbar vertebral bodies and their 4 corresponding IVDs)[17]. Distinctions between the models were present such that Little *et. al.* and Goel *et. al.*[39], [41] included only the cylindrical part of the vertebral bodies with no spinous processes while Chen *et. al.*[42] included cartilages between vertebral bodies. In

contrast, the other models[40,43,44] represented the actual anatomical shape of the vertebral bodies and the IVDs. Furthermore, Schmidt *et. al.*[40] included the representation of muscles through simplified geometries, while the other 7 models modelled the muscles' effect as vector forces. All other fascia, tendons, IMP, or IAP effects were excluded from these studies. For the first part, pure bending of 7.5 Nm was applied in all anatomical planes and all FE models simulated a maximum difference of 5^o rotation which aligns with *in-vitro* data (median: 17^o; range 11^o-22^o). Additionally, facet joint forces were predicted under the same loading condition. All FE models reported approximately 38N in extension, 14N in lateral bending, and 60N in axial rotation; however, forces were considerably different between the models under flexion[17]. In conclusion, the comparative study suggested that combining different FE models improves the prediction to estimate biomechanical parameters, especially if such models individually involve different simplifications and assumptions.

It is evident that predictions conceived via FE analysis would not be worth interpreting unless the model was verified and validated. Essentially, a model is said to be validated if the results it predicts matches experimental observations[17]. Verification assesses the numerical accuracy of the underlying model to ensure that the computational model output properly represents the solutions to the corresponding mathematical equations[45]. Sensitivity, on the other hand, is the process of ensuring that the model is robust, *i.e.* predicts repeatable results, upon changing main input parameters such as the mesh size and quality[46].

Thus, the purpose of this paper was to develop a detailed 3-dimensional comprehensive finite element model of the spine integrating the effects of IMP, IAP, and TLF. A series of tasks were executed via a diversified validation process to validate the model segment by segment against multiple published studies. In addition, a novel meshing technique was developed and utilized to compensate for the inevitable exceedingly high element count given the inclusion of the VBs, IVDs, all major spinal muscles with their IMP, IAP, connecting tendons, and TLF.

4.2.3. METHODS

A.1. Creating the Base Model

The developed spine FEM was based on MRI-scans acquired from an anatomography; a database of 3D MRI-based human body parts, namely, "BodyParts3D/Anatomography". The model of interest included the VBs from T_1 to S_2 joined together by IVDs. The major spinal muscles comprised of the longissimus, multifidus, psoas major, and lateral intertransversarius and were designated as force generators. Soft tissues, mainly the TLF and tendons, were also included to transmit muscle forces as well, due to their critical role of storing excess forces and stresses. Lastly, the IAP was further integrated modelled within a pressurized cavity enclosed by the abdominal muscles.

The acquired MRI-based model components were initially organized then processed into CAD supported files in SpaceClaim (v.19.1, Concord, Massachusetts) to achieve a full-scale model consisting of a total of 302 parts. Numerous modules within the FE software, ANSYS (v.19.1, Canonsburg, Pennsylvania), were employed to build the project. The detailed model of each part's behavior and mechanical properties is described in the sections below.

A.2. Volumetric Bodies

The base model consisted of 17 VBs (12 thoracic and 5 lumbar vertebrae) linked by 16 IVDs. For the scope of this model, the cervical spine was omitted given its minimal relative effect on the employed model using the established series of tasks defined within this study. The base model components, *i.e.* the VBs and IVDs, were modelled as deformable volumetric bodies. In addition, tendons conveying muscle forces, and the TLF which are believed to provide structural support to the torso, were similarly modelled as deformable volumetric bodies. The core difference between the components was the assigned material law to each part which dictates its range of motion, resilience under an applied load, as well as the ability to store excess stress subjected to the spine. Although vertebral deformations are minimal in comparison to the other soft tissues, modelling them as deformable bodies with representative material behavior was intended to ensure the model's accuracy and serve in subsequent studies thereof.

The geometrical representations of the various soft tissues were processed in SpaceClaim whereby sharp edges, low aspect ratio elements, and other unintended features that would otherwise increase the FE model complexity were eliminated. Each part was then transformed to a polygonal mesh with an edge size of 3 mm; a relatively computationally inexpensive element

size that also enhances simulation accuracy. The detailed adopted mesh is further explained in subsection *4.2.3.B.* An example of each of the aforementioned components is depicted in Fig. 4–1a.

Under external loading, detailed later as muscle forces, defined volumetric bodies may deform, translate, and rotate in all degrees of freedom. Such movements depend on the applied load, as well as their material behavior law, which also dictates possible changes in shape and volume under loading. Different material laws may be incorporated but for the scope of this paper, *i.e.* validating the spine model, material properties were adopted from the same investigations against which the model was indirectly validated, subsection *4.2.3.C* below.

A.3. Muscles and Intra-muscular Pressure (IMP) Modelling

The presented model adopts all major muscles that significantly contribute to sagittal motion, mainly flexion, of the spinal system. These include the longissimus, multifidus, psoas major, lateral intertransversarius, and latissimus dorsi (Fig. 4–1c). The longissimus, multifidus, and psoas major were included because, under spinal loading, they account for most of the load endured by the spine[47]. Similarly, the lateral intertransversarius were incorporated for their role of supporting the posterior elements of the vertebrae under vertical compression/tension loading[48]. Finally, given the importance of including the TLF as discussed earlier, the latissimus dorsi was included as a result of its role in setting the TLF under tension[49]. Although other major muscles, such as the gluteus maximus and transversus abdominis attach to the TLF, only the latissimus dorsi was included to laterally support the posterior TLF layer.

FEMs of human skeletal muscles are abundant in literature. However, as previously discussed, IMP is believed to play an important role during muscle contraction, and a novel accurate model that relates muscle forces to IMP, taking into account the actual muscle architecture, shape, and geometric features, has been previously explored[33]. As such, the procedure of building fluid-structure finite element field, by filling the muscle shell with hydrostatic pressure elements (HSFLD242 elements available in ANSYS) has been used for the present muscles. In short, the finite elasticity formulation started with the displacement field of the muscle shell. Since muscles are inherently incompressible, a displacement field would perform poorly in describing the whole muscle's biomechanics due to a phenomenon commonly referred to as interlocking. This forces

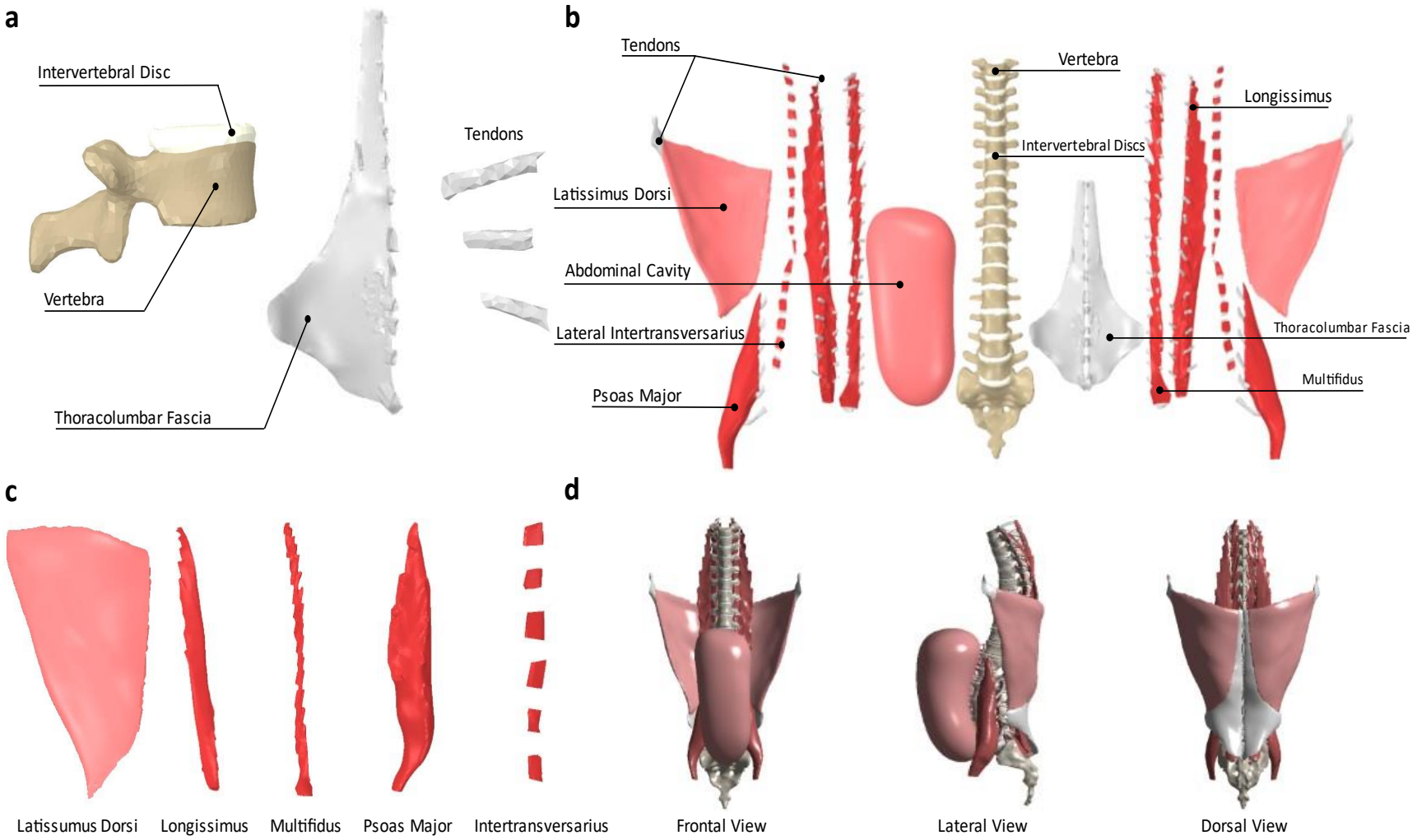

Figure 4–1: Finite element model of the spine produced via ANSYS Static Structural (v.19.1, Canonsburg, Pennsylvania, United States, https://www.ansys.com/). (a): Vertebral bodies, intervertebral discs, thoracolumbar fascia, and tendons modelled as volumetric deformable bodies; (b): Exploded view of all parts considered in the spine model; (c): Major torso muscles modelled as pressurized structures; (d): Frontal, lateral, and dorsal views of the full spine finite element model.

the researcher to build a two-field variational formulation to describe this fluid structure interaction of a muscle based on the principle of minimum potential energy. That is, to avoid the volume-locking phenomenon, in addition to the displacement field describing the muscle's shell behavior, a hydrostatic pressure field is linked from the inside. For a an incompressible Neo-Hookean material, the stored energy function, as formulated in[50], is described by:

$$\widetilde{W}_C(\bar{\boldsymbol{D}}, \boldsymbol{D}) = -\frac{G}{2}(\bar{\boldsymbol{D}}, \boldsymbol{D} - 3) \tag{4.1}$$

where $G = \frac{E}{2(1+v)}$. G, $\boldsymbol{D}$, and $\bar{\boldsymbol{D}}$ are the shear modulus, standard, and modified deformation gradient tensors, whereas E and v are Young's modulus and Poisson's ratio, respectively.

Thereafter, by definition of the Cauchy stress tensor, the hydrostatic pressure is given by:

$$p = \bar{p} - \frac{1}{3\det \boldsymbol{D}} \frac{\partial \widetilde{W}_C}{\partial \boldsymbol{D}} : \boldsymbol{D} \tag{4.2}$$

The hydrostatic pressure field, defined by equation (4.2), was then solved in ANSYS by custom coding the pressure field. Enclosed within each muscle's shell, the HSFLD242 elements share a hydrostatic pressure node (HDSP) allowing to extract IMP results, as well as introducing this pressure to stimulate muscle contraction. The novelty of such a procedure lies within the ability of relating muscle forces to their IMP, simulating one effect as a result of the other, and accounting for physiological muscle lateral growth under contraction.

A.4. Intra-abdominal Pressure (IAP) Modelling

The importance of including the IAP effect stems from investigations towards understanding its exact role. Bartelink[51] suggested that the activation of abdominal muscles translates into an IAP, which stabilizes the lumbar spine by providing an opposite unloading effect. The present model focuses on this effect, rather than its activation. As such, IAP was modelled as a pressure build-up enclosed by an abdominal cavity, defined by the abdominal muscles, soft tissues reaching the frontal part of the VBs, and the diaphragm from the top. MRI scans of existing organs in that region were processed and their surfaces were traced to create a model of the abdominal cavity. Thereafter, similar to the adopted muscle model strategy, IAP was introduced as a hydrostatic pressure effect building up in the abdominal cavity by merging the cavity's shell elements with

HSFLD242 elements enclosed inside. This cavity, along with the full spine model, is shown in Figs. 4–1b and 4–1d.

Due to the limited published data on the abdominal wall mechanical behavior, material properties were extracted from the results of the experimental study conducted by Song et. al.[52], performing ultrasound measurements of the abdominal wall. This resulted in Young's moduli: $E_{transverse} = 42.5kPa;\ E_{sagittal} = 22.5kPa$ and an average abdominal wall thickness, defined by the abdominal muscles, of: $t_{wall} = 9.7mm$.

B. Adopted Mesh

A common problem in the FE method entails a trade-off between accuracy and computational feasibility or speed. Less variability and higher reliable results generally require: (1) a representative graphical model, (2) accurate description of material behaviors, and (3) a full-scale smooth mesh that captures all model features. For a representative benchmark spine model, the first two objectives were closely met as described above. The challenge remained to create a smart, novel, computational mesh that would not elongate simulation time. For reference, a conventional 3 mm size mesh resulted in over 0.6 million elements, with approximately 311 linear and nonlinear contact objects between the modelled parts. The simulation of a trial spine under 100N flexion would take months to solve. This would not be feasible with the aim of creating a reference spine model to be implemented in the medical field.

Hence, this study adopted a non-conventional meshing technique, whereby all FEM fixed contacts computations (applying nonlinear constraints and penalty functions) would be eliminated, with all contacting bodies, having adjacent surfaces, sharing the same nodes. This would not only relax the simulations and produce more accurate results, but would also result in better approximations as conventional penalty functions would not be applied anymore[53]. The idea was to create a unitary mesh whereby under any loading condition, over contacts that are physiologically fixed, the load would distribute and travel among nodes with no barrier of iterating the mathematical equations of the contacts. This was done by leveraging ICEM CFD component of ANSYS to create shell meshes for the muscles and abdominal cavity, which were then filled with HSFLD242 fluid elements prior to simulation. Further, the multizone method in ANSYS meshing tool tetrahedral volumetric elements for the other organs. An intermediate stage of

exporting adjacent parts into Blender, a free and open-source 3D computer graphics software, was then used to merge adjacent nodes on contacting bodies together. After iterating all present bodies in the model, all mesh files were then collected by a single ANSYS mesh component to run a final compatibility check before proceeding with simulating the model. Fig. 4–2b illustrates this meshing procedure.

This time-consuming step was justified as the final version of the model took roughly 3 minutes to solve, though comprised of 398,217 elements and 547,380 nodes.

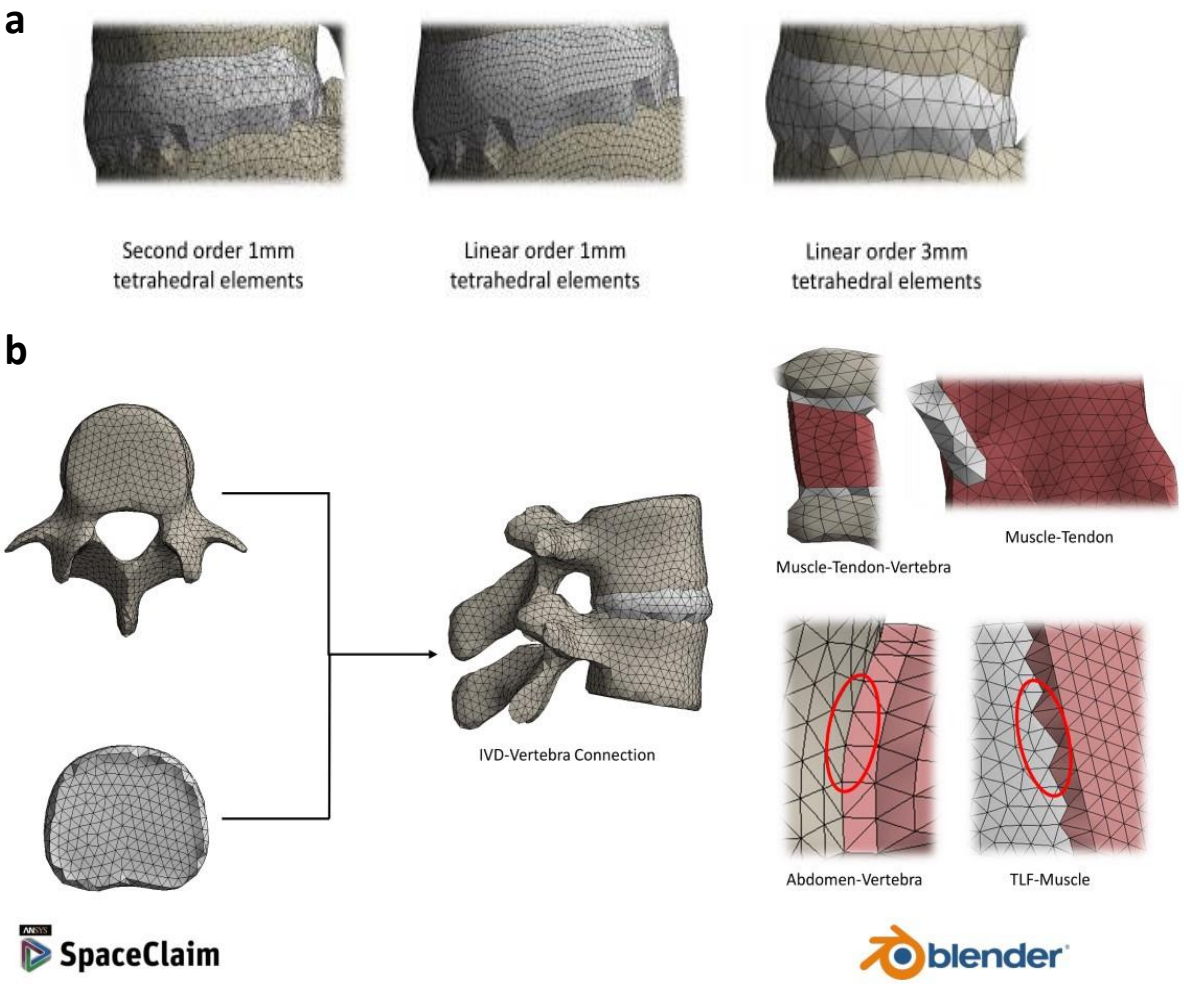

Figure 4–2: Finite element model produced mesh. (a): Three different meshes explored in the sensitivity analysis; (b): Adopted meshing technique showing conformity across contacting objects. Meshes were produced *via* the help of ANSYS SpaceClaim and ICEM CFD software packages (v.19.1, Canonsburg, Pennsylvania, United States, https://www.ansys.com/) as well as Blender (v.2.83.5, Netherlands, https://www.blender.org/).

C. Model Validation

Indirect validation of comparing the model's results against readily available literature data was carried out. Due to the model's novelty of including major tissues, IAP, and IMP effects, a complex and diversified sensitivity case-study was performed. Each component within the developed model was validated against appropriate published data in efforts to conclude on the overall validity of the present model. As such, the following validation tests were conducted:

C.1. Muscles and Enclosed Pressure

The modelling of skeletal muscles as fluid-filled structures resulted in a linear direct correlation between muscle forces and IMP. A comprehensive mesh, material behavior, and tendon stiffnesses sensitivity analyses suggested a robust model[33]. Following the linearities of the model, expanding the developed model to other skeletal muscles would maintain this IMP-force correlation, resulting in a valid modelling procedure. To investigate this, the spine-IVDs lumbar structure, with the psoas major muscle and its tendons, were isolated, as shown in Fig. 4–3a, and psoas major muscle forces, based on an EMG assisted approach coupled with force-length/velocity relationships[47], were applied across each insertion point. Dirichlet boundary conditions were applied on L1 and the sacrum, thereafter, IMP was plotted against different force levels to explore the validity of the linear IMP-force correlation. Table 4–1 summarizes the adopted material properties used in this scenario[54–58].

C.2. Lumbar Spine

A detailed comparative study between eight, novel, different lumbar spine FEMs[17], earlier detailed in the introduction section, was used to validate the lumbar part of the present model. The lumbar part of the present model was isolated to mimic the structure of those published[17] (Fig. 4–3b). Due to the wide range of material properties used, summarized in table 1 of Dreischarf *et. al*, different material properties, being those used in the first scenario, were adopted for the present model. Thereafter, inverse validation was conducted, whereby the range recorded L_1-L_5 rotations in flexion-extension (*i.e.* 24 – 41°), was applied while a reaction bending moment around the same anatomical plane was extracted from the FE model. This was done in order to investigate the

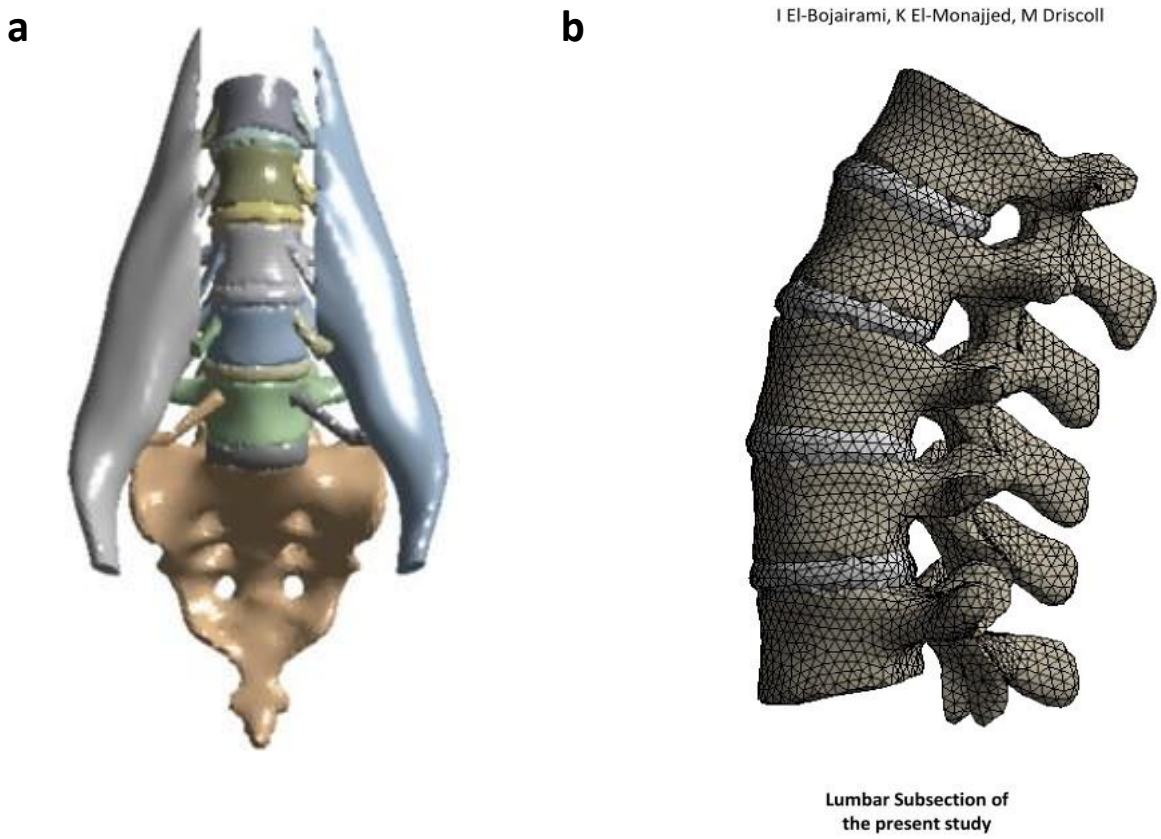

Figure 4–3: Lumbar spine finite element model. (a): Lumbar spine and psoas major muscle model isolated to perform the muscles and enclosed pressure validation; (b): Lumbar spine finite element model isolated to match the models against which validation was performed[17] (Models were developed using ANSYS, v.19.1, Canonsburg, Pennsylvania, United States, https://www.ansys.com/).

Table 4–1: Material properties for the lumbar spine test.

Component	Material properties	Thickness
Vertebral bodies	E= 12 GPa; v= 0.3[50]	-
Intervertebral discs	E= 42.7 MPa; v= 0.499 (Incompressible)[49]	-
Psoas major muscle	E= 0.52 MPa; v= 0.499 (Incompressible)[51]	2.73 mm[48]
Tendons	E= 1 GPa; v= 0.499 (Incompressible)[52]	-

resulting level of rotation with their applied 7.5 Nm bending moment. Using the same boundary conditions, Dirichlet conditions were also applied at the sacrum level, preventing any displacement in all degrees of freedom.

C.3. Intradiscal (IVD) Pressure

Using the same lumbar model, under the same loading conditions and material properties, intradiscal (IVD) pressure values were recorded to be compared to normal published range. This was done by extracting the average normal stress recorded at the surface of the IVDs. Although, previously shown that this approach approximates the pressure build-up in a structure according to the principle of pressurized vessels under static condition[33], a better IVD model that allows extracting the actual pressure within would provide more reliable results. As such, the fifth lumbar IVD was divided into its annulus fibrosis and nucleus pulposus components. The anulus fibrosis was modeled as a volumetric deformable object with a Young's modulus of E = 8MPa and a Poisson's ratio of $\nu = 0.45$[59], while the nucleus pulposus was modelled as shell structure enclosed with hydrostatic HSFLD242 pressure elements with the shell assigned a 1mm thickness[60], Young's modulus: E = 1MPa, and a quasi-incompressible Poisson's ratio of $\nu = 0.49$[17]. Thereafter, the pressure inside the fifth lumbar vertebra was extracted and compared to the normal stress approach.

C.4. Full Spine Validation

Lastly, the VBs and IVDs of the whole model were isolated to mimic the behavior and validate against a numerical model constructed in LifeMOD[61]. Under the same loading conditions, *i.e.* recorded flexion force range of 0 to 350N, translation of VBs T_{10} to L_5 was recorded and compared to Huynh's findings. However, due to the wide difference between both models, with one being the inclusion of the actual muscles in the present model, another approach was conducted in efforts of validating the presented full spine model. This was done to ensure that the inclusion of all IMP, IAP, TLF, and the other soft tissues would result in a valid model.

The other approach consisted of applying all muscular contribution detailed by the EMG recorded data of Cholewicki *et. al.* and Hansen *et. al.*[5,47] by the included muscle, thus simulating spine flexion caused by muscles contraction. Following this, the model's extremities, including T_1, were fixed and the load resulting on T_1 was measured. Thereafter, according to documented muscular proportions, muscle forces were varied until they resulted in the minimum applied forward flexion force of 50N[61]. Thereafter, muscle forces were increased in 5 increments and a similar curve of the resultant values of T_1 load vs. T_{10}–L_5 vertebral translations was plotted and

compared to the previous one. By doing so, the present model would ensure the incorporation of the additional effects resulting mainly from the IMP, IAP, and TLF contribution, rather than such effect being completely passive. Again, Dirichlet's boundary conditions were also applied at the sacrum and the tendons attached to the latissimus dorsi. The material properties employed are summarized in Table 4–2[38,52,54–58,62].

Table 4–2: Material properties for the full spine validation test.

Component	Material properties	Thickness
Vertebral bodies	E= 12 GPa; v= 0.3[50]	-
Intervertebral discs	E= 42.7 MPa; v= 0.499 (Incompressible)[49]	-
Psoas major muscle	E= 0.52 MPa; v= 0.499 (Incompressible)[51]	2.73 mm[48]
Multifidus muscle	E= 36.87 KPa MPa; v= 0.499 (Incompressible)[58]	~4.5 mm[48]
Longissimus muscle	E= 36.87 KPa MPa; v= 0.499 (Incompressible)[58]	4.03 mm[48]
Latissimus dorsi muscle	E= 36.87 KPa MPa; v= 0.499 (Incompressible)[58]	~4.5 mm[48]
Intertransversarius muscles	E= 36.87 KPa MPa; v= 0.499 (Incompressible)[58]	~1 mm[48]
Tendons	E= 1 GPa; v= 0.499 (Incompressible)[52]	-
Thoracolumbar fascia	E= 450 MPa; v= 0.499 (Incompressible)[57]	-
Abdominal wall	E= 25 KPa; v= 0.45[56]	9.7 mm[56]

D. Sensitivity Case-Studies

D.1. Model Form Validation

As suggested by ASME V&V 40-2018 guidelines[63], model form validation is essential to ensure that the FE model closely captures the origin from which the model stems, being MRI scans in this case. Thus, it was essential to compare the computational mesh size to the original MRI scans size. For this, it was decided that the metric of comparison to be the volume in both cases. For simplicity, this analysis was done for the lumbar part only, i.e., L_1-L_5 with their IVDs.

D.2. Mesh Sensitivity

With the adopted mesh strategy being one of the novelties of this study, it was essential to verify the accuracy of the adopted meshing procedure. As such, two other meshes were explored: (1) a

linear tetrahedral mesh but with smaller element size, being 1mm, and refined around sharp angles and edges using the pinch and inflation features in ANSYS and (2) a second order tetrahedral mesh, with one element composed of 10 nodes instead of 4 in the case of linear tetrahedrons, with 1mm element size and properly refined as well. (Fig 4–2a)

For the purpose of comparison between those meshes, the scenario of subsection *4.2.3.C.2* above was repeated, recording the moment resulting from the levels of rotations for each of those meshes.

4.2.4. RESULTS

A. Model Validation

A.1. Muscles and Enclosed Pressure

Forces of the Psoas Major (P) previously measured via Electromyography (EMG)[47], under the documented physiological condition, recorded an average of 249N for the right P and 275N for the left P under flexion, while 74N for the right P and 75N for the left P under extension. Simulating all possible scenarios between flexion and extension, the range of 75-275N was applied in both P muscles. The resultant force-IMP curve for the right P muscle is shown in Fig. 4–4a. Results showed an approximately linear correlation ($R^2 = 0.995$), between P forces and IMP whereby the latter increased from 195 to 785mmHg as the force increased from 75 to 250N.

A.2. Lumbar Spine

In the first task, the range of rotations of 24–41° across the lumbar spine were applied as detailed in the methodology section. Thus, the resultant bending moments, defined by Eq. (4.3) as a special ANSYS command output, were recorded (Fig. 4–4b).

$$M_{Bending} = F_y . d \tag{4.3}$$

Such that:

- $M_{Bending}$: Bending moment about the transverse plane

- F_y: In-plane reaction force (sagittal plane normal vector reaction force resultant)

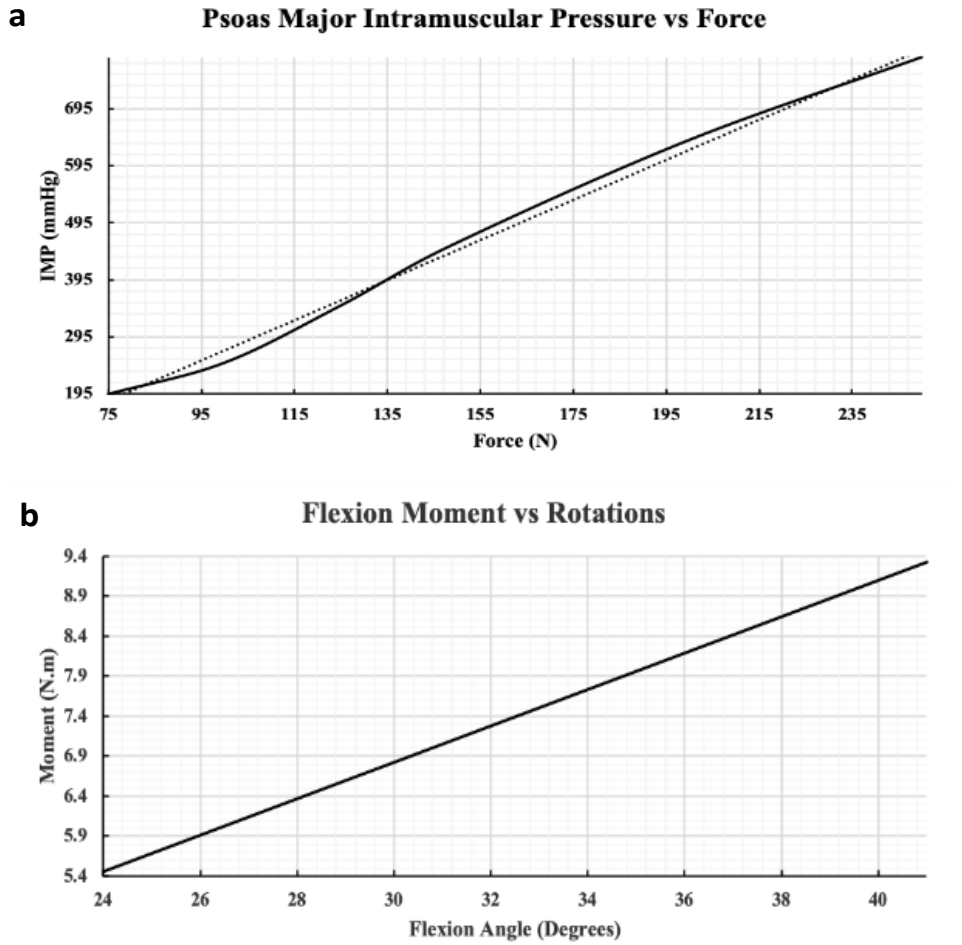

Figure 4–4: Intramuscular pressure and lumbar spine validation results. (a): Results showing the relation between muscle forces (N) and IMP (mmHg) extracted from the psoas major muscle; (b): Recorded bending moment (N.m) as a result of the lumbar spine elevation intensity (degrees).

- *d*: Moment arm defined as the distance between the reaction force and the parallel plane containing the model center of gravity

When simulating the intensity elevation (i.e. 24–41^{o}) of lumbar spine in flexion, the bending moment recorded at the level of L_5 linearly increased from 5.5 to 9.3N.m. Similarly, the *in-vitro* experimentation[17] showed that a 35 ± 2^{o} degree flexion would be the result of a 7.5N.m bending moment. Fig. 4–4b shows an output simulation result of 33^{o} flexion for the developed FE model. Furthermore, the present FE model predicted a follower compression load of 977N compared to the 1000N applied load they reported or a 98% correspondence.

A.3. Intradiscal (IVD) Pressure

Under the same loading conditions of the second task, *i.e.* increasing the flexion intensity from 24^{o} to 41^{o}, IVD pressure values in the lumbar spine increased from a range of 0.41–0.43 to 0.59–0.66MPa (Fig. 4–5a) for all IVDs (*i.e.* 1–5). The data further showed an increasing pattern for both flexion/extension at any spinal level such that the intradiscal pressure value increases inferiorly to IVD_1, with the maximum registered at IVD_5. The data closely resembled the normal physiological ranges of intradiscal pressure of 0.4 to 0.8MPa, during flexion/extension, as experimentally conducted by Wang *et. al.*[64] on 3 different subjects. Furthermore, the present data differed by 14% in comparison to the investigations conducted by Rolander *et. al.*[65] and Ranu *et. al.*[66]. By tailoring the degree of flexion to attain a compressive load similar to that applied by previous scholars, Rolander *et. al.*'s case study showed an increase in intradiscal pressure from approximately 0.37 to 0.63MPa, while an increase from a range of 0.3–0.4 to 0.6–0.8MPa for the investigation of Ranu *et. al.*

On the other hand, the approach of extracting IVD pressure as an average normal stress (NS) recorded at the surface of each IVD was compared to another more representative approach, as detailed in the methodology section, of modelling the IVD as a two-phase fluid-structure component and extracting the IVD pressure from the fluid model of the nucleus pulposus, from a hydrostatic pressure node (HDSP) assigned within. Fig. 4–5b shows that both results overlap to a great extinct, with a maximum discrepancy of approximately 4% at 34^{o} flexion.

A.4. Full Spine Validation

The final step was to validate the full model with all its components and included effects. Initially, the spine included the VBs and IVDs only and a forward flexion of 0 to 350N was applied on T_1. The caudocranial translation of each VB was then extracted and plotted as shown in Fig. 4–6a. Vertebral displacements exhibited an increasing pattern, with a flexion force, at a higher rate for the superior VBs, recording around 7.1mm and 6.5mm displacement values for T_{10} and T_{11} respectively, at a 350N flexion force. For T_{12} and L_1, the displacements reported a 4mm and 3.8mm, while such displacements were minimal for the rest VBs, especially for L_4 and L_5 with a nearly null value under all flexion forces. Such results were highly correlated to those of Huynh's

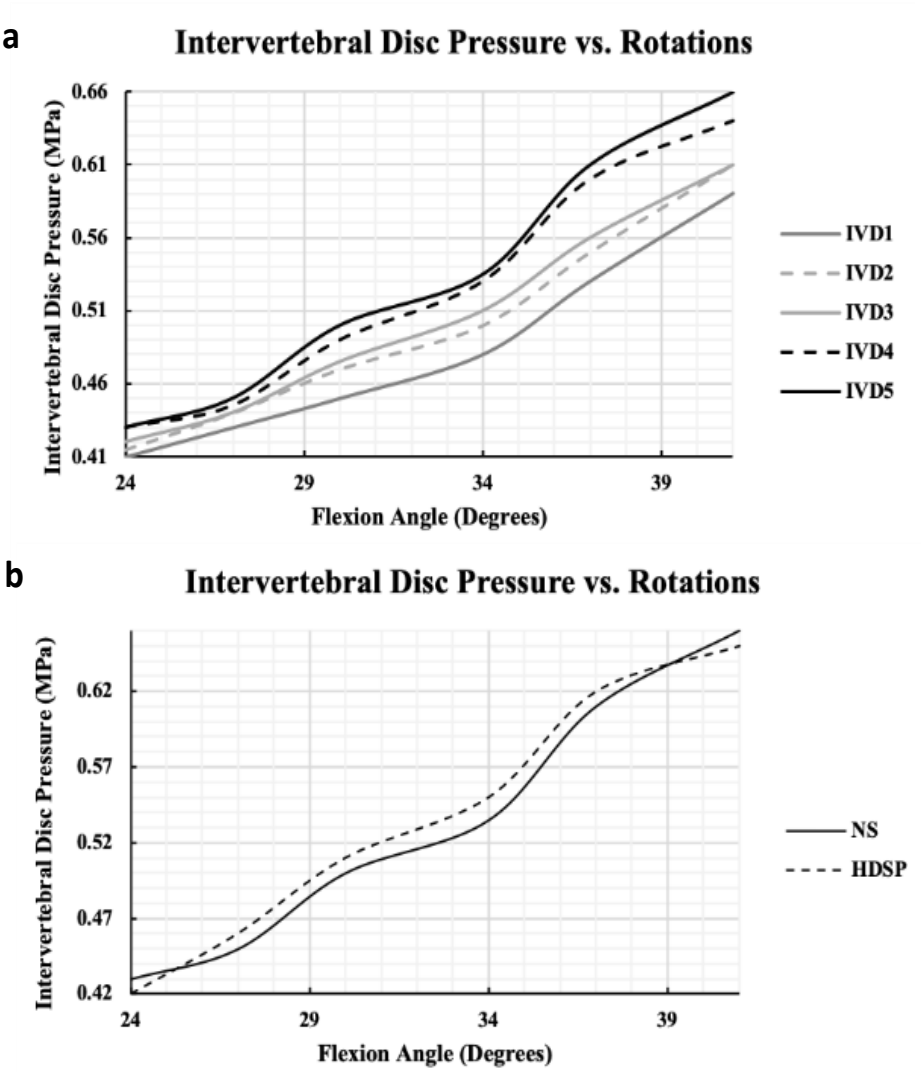

Figure 4–5: Intervertebral discs validation results. (a): Recorded lumbar intervertebral discs pressure as a result of spine flexion intensity, extracted via the average normal stress approach; (b): Verification of the normal stress approach via another two-state fluid-structure field using a hydrostatic pressure node.

et. al.[61], with a very small maximum discrepancy of approximately 6% recorded for T_{11} at a 300N force.

In the second approach, previously reported muscle forces[47] were first applied, as summarized in case 0 of Table 4–3, which caused a 382N load on T_1. Thereafter, muscle forces decreased in similar proportions until a T_1 load of approximately 50N was achieved, summarized by case 1. In subsequent cases, muscle forces increased in equal proportions, recording the resultant load on

Table 4–3: Muscle force inputs.

Muscle	Muscles forces (N)					
	Case 0	Case 1	Case 2	Case 3	Case 4	Case 5
Longissimus	210	30	85	120	185	198
Multifidus	71	15	30	45	65	71
Psoas Major	275	40	100	140	235	260
Intertransversarius	25	5	10	15	25	25
Load on T1 (N)	382	54.4	136	203	314	346

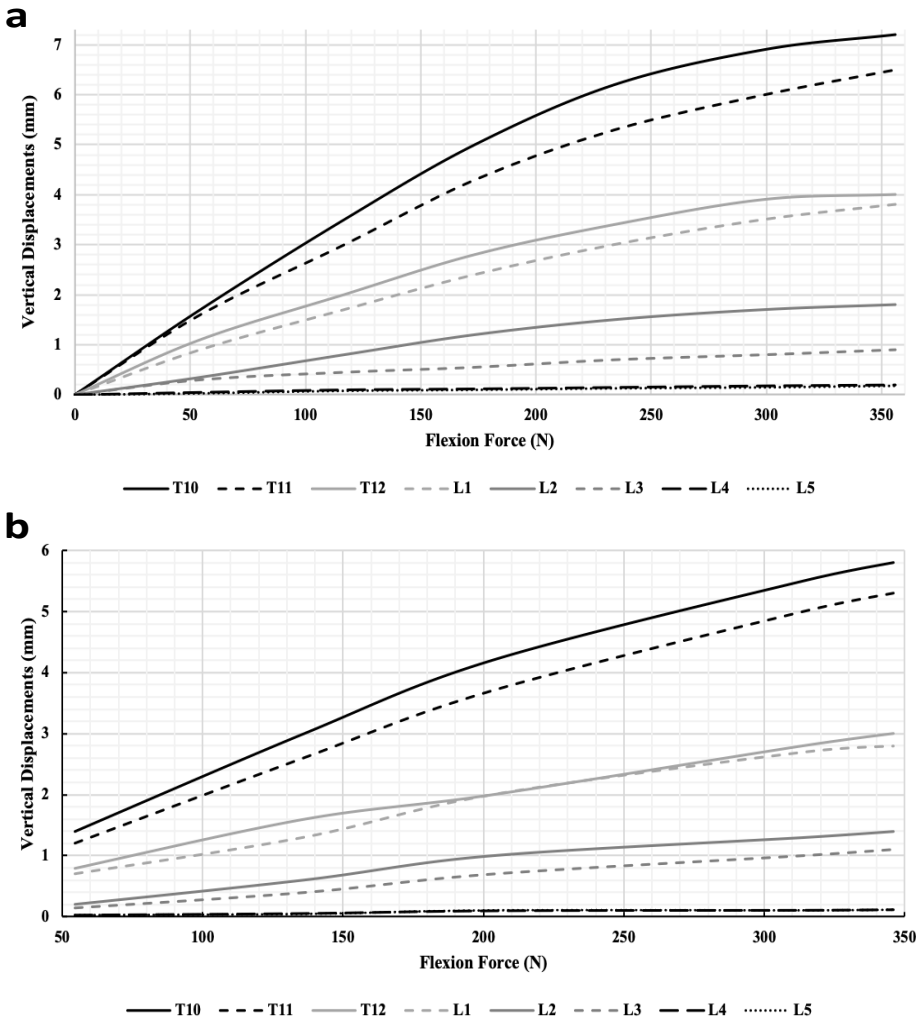

Figure 4–6: Full spine validation. (a): Recorded vertical vertebral displacements in response to an external flexion force applied on the first thoracic vertebrae; (b): Verification of the external applied flexion force via muscles active contraction approach.

T_1, until a maximum load of 346N was obtained. It was also observed that muscle forces achieved a nonlinear increase in the T_1 loading such that the more the muscle generated a force, the less the load increment was applied on T_1.

Lastly, a similar curve of vertebral displacements was generated as shown in fig. 4–6b. Interestingly, results followed the same trend as the previous findings, however, with a significant drop in the vertebral displacements at similar flexion forces. That is, vertebral displacements increased, with increasing flexion force, recording a maximum of 5.8mm and 5.3mm for T_{10} and T_{11} respectively, at 346N. For T_{12} and L_1, this was 3mm and 2.7mm, while such displacements were also minimal for the rest VBs, especially for L_4 and L_5 recording almost null values. Furthermore, IAP recorded by the HDSP pressure node inside the abdominal cavity recorded an increase in IAP from 5 to 36mmHg, and the force recorded at each TLF-VB connection showed a similar nonlinear increase from a minimum of 12N to a maximum of 139N resistive force.

B. Sensitivity Case-Studies

B.1. Model Form Validation

Table 4–4 summarizes the analysis conducted on the volumetric difference of the components within the lumbar part of the model. As depicted, the modelled mesh achieved an accurate representation of the original MRI scans with a maximum discrepancy of 6.17% registered for IVD_2.

B.2. Mesh Sensitivity

Simulating the lumbar spine section, as detailed in the methodology section, was conducted by increasing the degree of rotation from 24^o to 41^o such that the bending moment at the level of L_5 increased from 5.6N.m to 9.9N.m for the linear 1mm tetrahedral mesh. Similarly, the value increased from 5.8N.m to 10.3N.m for the second order 1mm tetrahedral mesh (Fig. 4–7). Compared to the original mesh, a maximum difference of 8.7% was registered between the original and the utmost refined second order mesh.

Table 4–4: Model's form and development sensitivity analysis.

Model's part	Model's volume (mm^3)	MRI volume (mm^3)	%Change
L_1	39675	41344	4.04%
L_2	42124	43863	3.96%
L_3	46001	47571	3.3%
L_4	44840	46478	3.52%
L_5	50861	52321	2.79%
IVD_1	7808	8082	3.39%
IVD_2	8715	9288	6.17%
IVD_3	7750	7895	1.84%
IVD4	11253	11766	4.36%

4.2.5. DISCUSSION

Advancements in the computational biomechanical field have paved the way for more accurate finite element model representations of the human torso and its biomechanical behavior. These FE models are usually constructed based on mathematical representations (*i.e.* considered case-specific), which disregard accurate geometric representations and may result in an over simplified model. Although for specific cases such approximations and assumptions are valid, such simplification leads such models astray from accurate physiological representation. For example, as of late, the effects such as the abdominal pressure, muscle pressure, and thoracolumbar fascia[38,67] have been shown to play a role in spine biomechanics and hence their inclusion in biomechanical models may be warranted if one focuses their research thereon.

In accordance with this, a three-dimensional representative novel full-scale biomechanical spine FE model has been successfully constructed and validated. The model consisted of the thoracic and lumbar vertebral bodies, intervertebral discs, abdominal wall and its intra-abdominal pressure, thoracolumbar fascia, longissimus, multifidus, psoas major, latissimus dorsi, and intertransversarius muscles, as well as their accompanying tendons.

A. Model Development

Geometric modelling has been given attention to preserve MRI-scan features. That is, multiple modelling iterations were carried out to ensure each part was modelled accurately without significant loss in quality. Models of vertebral bodies and intervertebral discs were for example generated with a quality of at least 94%. This was achieved by directly faceting those parts and preserving the enclosed volume for deformable body modelling. The abdominal wall, on the other hand, required a relatively rigorous amount of effort as it required tracing the abdominal muscles, reaching the frontal side of the vertebral bodies and the diaphragm from above.

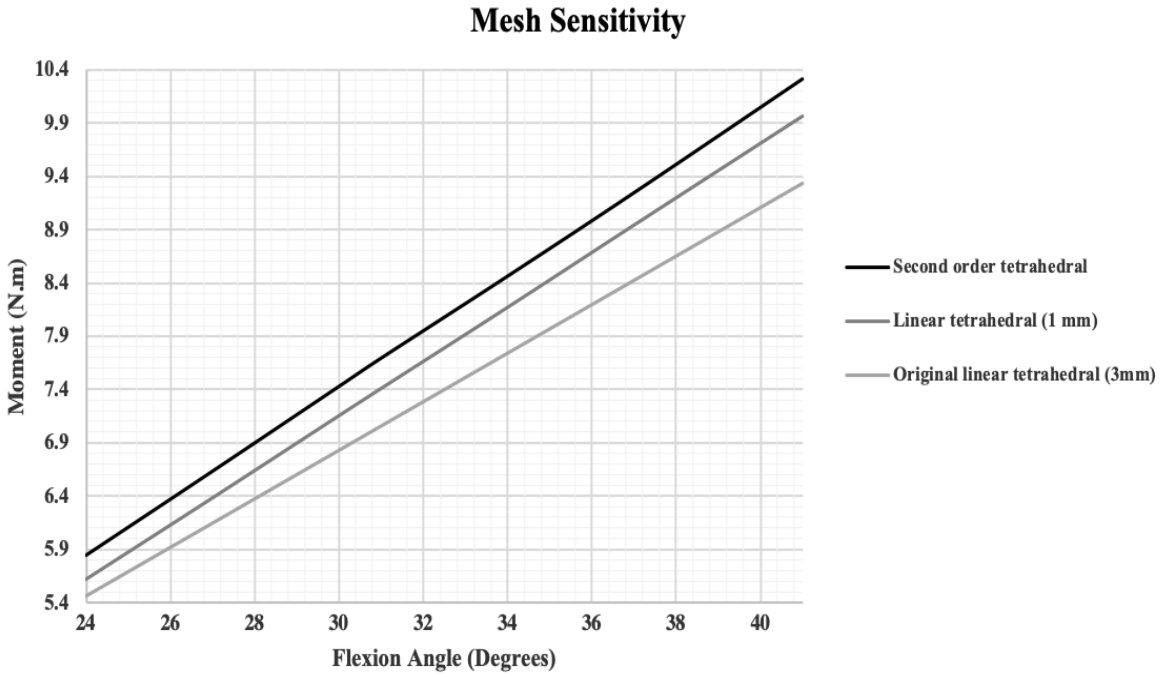

Figure 4–7: Model's sensitivity to different meshes.

This required collecting literature decisions the shape of the abdominal cavity and its biomechanical behavior. In addition, creating a representative model of muscles and their enclosed pressure was tedious which are substituted with force vectors in most developed models. As such, the first step towards building the present model was to create a tibialis anterior muscle model suited to predict muscle forces from its IMP and vice versa[33]. Nevertheless, as tendons are functional passive parts of the muscle structure, separating both parts with the intention of better

modelling two-structure anatomy required the generation and faceting of some of the lost tendons. This resulted in some loss in accuracy, especially for the multifidus muscle due to its compact nature, as the volumetric difference increased to approximately 81% compared to the original MRI-based components. Yet, this was accounted for in the tendon model and ultimately parts of the muscle itself. Finally, the thoracolumbar fascia has been recently receiving growing attention and thus its inclusion was hypothesized to play a role in the force distribution within the model. However, the original model lacked the TLF's connection to the vertebra, which required the integration of the faceted junctions at the vertebral dorsal portion. A similar 2-D planar model of the TLF has been validated and investigated by the authors[38]. Thus, the authors strived towards modeling all the components accurately.

Generating a representative computational mesh is designated as one of the most critical stages in FE modelling. Generally, researchers strive to create a mesh that reliably reproduces results yet maintains a low complexity to carry out future simulations in a reasonable amount of time. Nevertheless, initial simulations were conducted using conventional methods which resulted in a high complexity overhead, requiring months to solve. Hence, the present model was meshed using a non-conventional novel technique. As described in the methodology, surfaces of contacting bodies were manually generated. As such, nonlinear contact computations were greatly reduced, whereby the load transmission mechanism between contacting bodies followed an explicit solution rather than iterative nonlinear as with the case of nonlinear ANSYS contact algorithms. That is, the entire spinal assembly became one structure, from the meshing perspective, for which the deformation of one object directly affects neighboring components. In human body mechanics, this is, in fact, recommended to ensure a homogeneous fluidic movement of all body parts. Therefore, in comparison, this meshing technique resulted in a significant reduction in computational time (almost 3 minutes per simulation) depending on utilized material properties and boundary conditions.

B. Model Validation

In satisfying computational reliability, validation plays a key element for any constructed FE model. Given the high number of components introduced into the model, validation of the entirety of the model in a single step was not possible to achieve specifically that no such model exists to

the authors' knowledge. As such, as detailed in the methodology section, a comprehensive case study was conducted in efforts of validating the model scoped to subsections.

B.1. Muscles and Enclosed Pressure

Modelling skeletal muscles as pressurized structures provides a relatively accurate representation of muscle contraction in terms of representing both, intermuscular and intramuscular pressure. The validity of this modelling procedure stems from the proven valid representation of a two-state muscle, fluid-structure state, that was previously conducted[33]. However, it was still essential to investigate if muscle scaling would change the IMP-F relation. Under realistic muscle contractile force, collected from EMG data as illustrated previously, the Psoas Major (P) muscles produced significant spine flexion under 275N force, and extension under an opposing 75N muscle force as suggested by Cholewicki *et. al*[47]. In fact, the linear correlation between muscle forces and IMP was consistently preserved (Fig. 4–4a). Such results were highly encouraging to model all other skeletal muscles, presented in the model, using the same procedure due to the proven potential of this accurate and representative muscle model in the FE field.

B.2. Lumbar Spine

Lumbar spine models have received great attention rendering advanced investigations among biomechanical researchers. The effort done by Dreischarf *et. al*[17], comparing eight different well-developed lumbar spine FE models, was of a particular interest as validating against all of those at once would leverage the accuracy and validity of the presented lumbar spine. Thus, in forward flexion simulations, results showed a linear increase in bending moment from 5.5 to 9.3N.m with an increasing angle of flexion. Linearity, in this case, stems from the linear relation between force and bending moment, presented in Eq. (4.3). Additionally, an accurate forecast of 7.5 N.m occurred at flexion angle of 33º (Fig. 4–4b). In their investigation, in-vitro results showed that a 7.5 N.m moment would be the result of 35 ± 2^{o} flexion. Nevertheless, with the current approach of applying the range of flexion and measuring the resultant bending moment, their applied follower load would be a result rather than an input in the current investigation. As such, retrieving the compression load at the level of L_5 resulted in a 977N load mimicking their 1000N applied follower load. The main reason for simulating lumbar flexion this way is the fact that one crucial

particularity of the full model is the inclusion of the major spinal muscles. That is, for the accurate representation of muscles producing spine movement, it was of interest to minimize other approximations that would substitute any muscular effort, mainly follower load and muscles contribution modelled as force vectors.

Overall, the achieved results proved the high accuracy of the present FE model of the lumbar spine, combined with the reported material properties, when compared to the previously well-developed lumbar spine models in the literature.

B.3. Intradiscal (IVD) Pressure

As described in the introduction, low-back pain is often associated to a malfunction with the lumbar spine associated with an excessive pressurization of the lumbar discs. Standing as one of the highest causes leading to disability[68], intradiscal pressure data in conditions of low back pain cases is widely available. This permitted additional validation of the lumbar spine, mainly investigating the accuracy of the spine model to predict IVD pressure.

In the first scenario, under the normal range of flexion/extension explained in the *lumbar spine* test, IVD pressure exhibited an increase from a range of 0.41–0.43MPa to 0.59–0.66MPa (Fig. 4–5a) for the entire range of IVD_1–IVD_5. The data closely resembled multiple previous investigations[64–66] with a maximum discrepancy of 14% as illustrated in the results section. Although such a difference is not significant specifically when considered over the entire range, IVD pressure values fell within normal physiological ranges[64]. Such differences may be directly attributed to the fact that other soft tissues were eliminated from this investigation. Nevertheless, the inclusion of such components, especially the TLF, permitted storing substantial load within these soft tissues. With a smoother transition of loads, suggested by the results of the current test, less pressure is put on the IVDs, and on the spine in total, resulting in a more representative intradiscal pressure.

The estimation of IVD pressure from the average normal stress subjected to the IVD surface has been proven to be accurate in the muscle model previously investigated[33]. This is due to the fact that, for thick-walled pressurized structures, the radial stress is equal and opposite to the gauge pressure on the inside surface[69]. However, when dividing the IVD into its nucleus pulposus

and annulus fibrosis, the nucleus was modelled as a hydrostatic fluid filled structure. Results for IVD_5 pressure showed that both procedures resemble each other to a very great extent, with a maximum discrepancy of approximately 4% at 34^o flexion (Fig. 4–5b). Clearly, the second approach provides a more accurate representation of the spinal discs' biomechanics. However, as in all FE analyses, as long as a model predicts accurate results, approximations to follow the less computationally expensive approach remain applicable.

Overall, results of the intradiscal (IVD) pressure test suggest a validated model of the spinal discs. Combined with the lumbar spine test, both tests suggest a fully validated spine structure, similar to most published spine models which were composed of the vertebral bodies and intervertebral discs. In essence, this lays the foundation to advanced investigations and assessments of low-back pain which has been greatly correlated with IVD pressure[68].

B.4. Full Spine Validation

The final test was done in efforts of concluding on the validity of the full model. However, due to model's novelties, no previous model that closely resembles the present model was found. As such, the model was first validated against one of the more involved models put forward by Huynh *et. al.*[61], after which all other soft tissues were included to comment on the full validity of the model.

Initially, applying an increasingly forward flexion on the base model resulted in higher displacements of VBs T_{10}–L_5 (Fig. 4–6a). It was also noticed that such displacements decrease, until vanishing at the level of the lumbar spine, suggesting the strong support provided by the IVDs. Force–displacement results were in high agreement with those of Huynh's up until a force of 350N. However, Huynh's investigation showed that vertebral displacements plateau at 350N, thereafter they start decreasing again, which the present model was not able to predict. This was counterintuitive as, numerically, displacements are believed to ultimately increase with flexion. The results obtained by Huynh's may be attributed to the adopted coordinate system, from which it seemed that they were measuring displacements in only one direction, and with respect to a fixed coordinate system, rather than updating and measuring the directional displacement. Additionally, their spine model's excessive movement had exceeded the physiological ranges of static spine flexion, for which they continuously applied flexion until the spine became in a perpendicular

position with respect its initial one. Regardless, the base of the present model closely matched their results up to the maximum displacement point with a very small discrepancy of 6% recorded for T_{11} at 300N force.

With the model accounting for the actual structures of skeletal muscles rather than utilizing vector forces, it was more representative to replicate the flexion movement via muscles contracting. However, reasonable forces should be provided via the muscles which was the reason behind adopting previous muscle data[47]. Such data suggested a maximum flexion position with a total force of 382N at the T_1 level, which was slightly higher than the previously used maximum of 350N, yet was close enough to suggest that muscles are capable of producing accurate spine flexion. Afterwards, all parts were included to investigate the overall effect on vertebral bodies displacements. With the forces presented in Table 4–3, force–displacement results followed the same trend but with a significant drop in vertebral displacements (Fig 4–6b). That is, the correlation remained intact but suggested a significant contribution by the other soft tissues. The addition of abdominal pressure from 5 to 36mmHg played a resistive role, supporting the lumbar spine. Upon investigating such pressure values, they did not seem arbitrary. That is, they compared very well to the IAP values of Mueller's *et. al.*[70]. Furthermore, as anticipated, the thoracolumbar fascia seemed to provide an essential role supporting the spine as well. With the increased amount of flexion, the TLF built an increasing force from 12N to 139N, resisting the forward flexion motion, and thus, supporting the role of storing sufficient tension to permit the spine to withstand excessive loads. Such findings further support the 'intradiscal (IVD) pressure' test where the inclusion of other soft tissues decreases spine flexion, subjecting the spine to less compressive loads, which in turn puts less pressure on the IVDs. Combining all four tests, the model put forth shows accurate and valid results, with the potential of leveraging it to carry out spine-related investigations.

C. Sensitivity Analysis

Similar to any FE model, verifying the model's form and results repeatability against input parameters is essential. As such, the guidelines put forth by ASME V&V 40-2018 for numerical models in the biomechanics field were followed to carry out the applicable sensitivity conditions required to conclude on the verification of the model.

Investigating model form was essential to make sure that the modelled parts properly capture the MRI scans upon which the model was based. For this purpose, the best applicable metric seemed to be the volume of each part. Results showed that modelled parts were in excellent agreement with the MRI scans with a maximum difference of 6.17% recorded for IVD_2 (Table 4–4). This proves that all parts were accurately graphically modelled with a small margin of error.

Furthermore, investigating the model's sensitivity against the adopted mesh is crucial as the mesh was one of the model's novelties. Besides, a common practice in all FE models, by which researchers verify numerical result accuracy, is to run mesh sensitivity analysis. For the purpose of this model, different meshing techniques, both linear and nonlinear, where investigated (Fig. 4–7). Results showed a very good agreement, with a maximum discrepancy of 8.7% between the original and the second order tetrahedral mesh. It is worth mentioning that a high reduction in computational time upon adopting the second order mesh for the lumbar model only was observed. Arguably, with an acceptable discrepancy level, leveraging the original mesh brings a great deal of potential, due to eliminating high order of nonlinearities, for the model to be used in medical applications as a quick spine assessment tool or to run implant design optimization, as examples.

Hence, with such acceptable margins of difference, the model can be safely assumed to be robust against critical parameters, leveraging both an accurate valid and repeatable verified representative novel full spine model.

D. Limitations

Similar to any *in silico* model, limitations are inevitable due to the approximation scheme and assumptions made. However, such limitations do not hinder the model's capabilities as long as the model, with its fixed input parameters, are proven to be valid and accurate towards the content of use that is targeted in subsequent analyses. One of the limitations of the developed model described herein is the material properties and material laws used. Specifically, this investigation lacks a material property sensitivity case-study. Due to the vast number of parts incorporated, each having a wide range of acceptable material properties, conducting a sensitivity on all possible combinations would be an exhaustive measure. However, since the adopted material properties were previously validated and are adopted from studies against which the current developed model

was validated, for which results further proved a valid model, such limitation may not be considered significant.

The application of the model as a spine static stability clinical assessment tool necessitates a balance between accuracy and simulation time cost. Without significant loss in accuracy, besides the mesh created for this specific model, the adopted material laws allowed for an extreme drop in simulation time. Although those were mostly linear, given the quasi-static nature of the model, the maximum range of motion simulated still fell within the elastic regime of all components when nonlinearly modelled (hyperelasticity, multiple states interaction, and time effects). Specifically, Fig. 4–8 shows the maximum strain recorded for the VBs, IVDs, tendons, muscles, and the TLF, which were 0.14, 5.3, 3.5, 9.2, and 2.6 percent, respectively. Such results were in high agreement with the linear regime of the stress-strain curves of each of those components[25,71–75]; thus, highly supporting the validity of using linear material laws for this range of static motion.

Although the adopted mesh may be considered a smart time saving approach, it can be argued that its implementation reduces the model's accuracy by a small percentage. However, besides such discrepancy being insignificant, considering all factors, such a meshing technique has a significant application-wise potential. One being the large decrease in computational time, permitting its usage in real-life applications. It also presents a manner in numerical analysis for which redundant nonlinearities may be overcome by such careful meshing.

Lastly, validating the model was a tedious task due to the lack of literature in full-spine modelling. Specifically, the model had to be validated in subsections rather than carrying out a direct validation scheme. Even with such an approach, considerable efforts were carried out to validate the soft tissue section of the model. With literature commonly modelling such effects as force vectors, or even completely eliminating them, multiple studies had to be combined to achieve full spine validation. Even though results showed close resemblance, it may still be argued that this may not be the best approach to achieve validation due to different segregated errors integrated to the final model. Yet, with the obtained results, the authors safely assumed that such anonymous errors were eliminated, concluding with a potentially fully validated model.

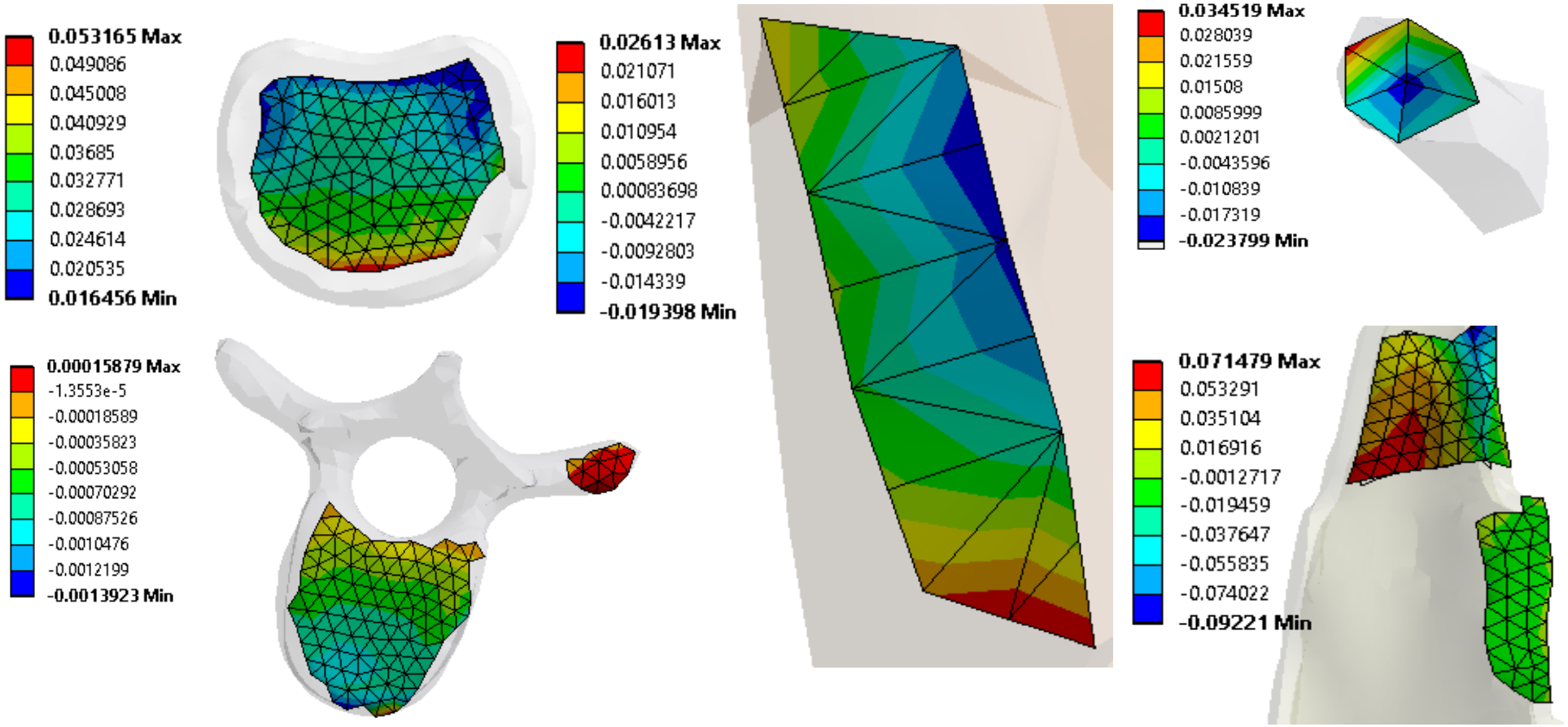

Figure 4–8: Maximum strain sensitivity analysis (Conducted and extracted from ANSYS, v.19.1, Canonsburg, Pennsylvania, United States, https://www.ansys.com/).

E. Future Work

The capabilities of this model extend beyond numerical modelling and validation. Leveraging such a model may help in various industrial and biomechanical fields from assessing spine injuries, investigating low-back pain, all the way to designing and optimizing medical devices. The authors further admit that this was the first step towards important studies that will be carried out but extend beyond the scope of this paper. Nonetheless, a more comprehensive sensitivity analysis comprising other material properties, shell thicknesses, and other modelling approaches might need to be considered if deemed essential.

F. Expected Contributions

The authors safely assume that this research may contribute to the modelling and biomechanical field. The model introduces the approach of perhaps better modelling biological tissues to fully represent human spine mechanics. The inclusion of the thoracolumbar fascia, abdominal cavity, as well as considering muscle intramuscular pressure in one spine model is, on its own, a novelty. Furthermore, this paper introduces a meshing technique applicable for any complex system that acts as a unitary structure rather than integrating the effects of using complex computations of numerical nodes and elements in contact.

In conclusion, this study developed and validated a novel 3-dimensional volumetric finite element model of the spine including the vertebral bodies, intervertebral discs, major torso muscles, accurate modelling of intra-abdominal pressure, as well as the thoracolumbar fascia. The model was meshed using a new meshing technique that permitted the elimination of redundant nonlinearities involved with contacts computations and greatly accelerated required calculation time. The model was indirectly validated against multiple previously published models in four different validation tests. All test results showed that the model produced reliable results when input parameters were accurately accounted for. Lastly, the model was proven to be robust in light of model form and mesh sensitivity analyses. This novel model provides an accurate method to simulate spine mechanics with the potential of leveraging it for various medical purposes from assessing injuries to designing or evaluating surgical treatments.

4.2.6. ACKNOWLEDGMENTS

We gratefully acknowledge funding by McGill University (MEDA), the Fonds de Recherche du Québec – Nature et Technologies (FRQNT), and the Natural Sciences and Engineering Research Center (NSERC). The authors also acknowledge that the 3D CAD model is based on a parametric 3D model from the Japanese Database 'BodyParts3D/Anatomography'.

4.2.7. REFERENCES

1. Freburger, J. K. et al. The Rising Prevalence of Chronic Low Back Pain. Natl. Institutes Heal. 169, 251–258 (2015).

2. Gatchel, R. J. Low Back Pain: Recent Advances and Perspectives.

3. Dipphysio, P. O. S. Acute Low Back Pain: Beyond Drug Therapies. (2014).

4. O'Sullivan, P., Smith, A., Beales, D. & Straker, L. Understanding Adolescent Low Back Pain From a Multidimensional Perspective: Implications for Management. J. Orthop. Sport. Phys. Ther. 47, 741–751 (2017).

5. Hansen, L. et al. Anatomy and biomechanics of the back muscles in the lumbar spine with reference to biomechanical modeling. Spine (Phila. Pa. 1976). 31, 1888–1899 (2006).

6. Epidemiological, A. N. Risk Factors in Low-Back.

7. Panjabi, M. M. Clinical spinal instability and low back pain. J. Electromyogr. Kinesiol. 13, 371–379 (2003).

8. Cholewicki, J., Juluru, K., Radebold, A., Panjabi, M. & McGill, S. Lumbar spine stability can be augmented with an abdominal belt and/or increased intra-abdominal pressure. Eur spine J 8, 388–395 (1999).

9. Panjabi, M. M. The stabilizing system of the spine. Part II. neutral zone and instability hypothesis. J. Spinal Disord. 5, 390–397 (1992).

10. Borelli & Pauwels. Iatrophysics to Biomechanics. J Bone Jt. Surg 74, 335–339 (1992).

11. Harvey, W. Exercitatio anatomica de motus cordis et sanguinis in animalibus. Frankfurt (1628).

12. Weber, W. & Weber, E. Ueber die Mechanik der menschlichen Gehwerkzeuge, nebst der Beschreibung eines Versuchs über das Herausfallen des Schenkelkopfs aus der Pfanne im luftverdünnten Raume. Ann. Phys. (1837). doi:10.1002/andp.18371160102

13. Williamson Jr, F. Richard courant and the finite element method: A further look. Historia Mathematica. 369-378 (1980).

14. Fagan, M. J., Julian, S. & Mohsen, A. M. Finite element analysis in spine research. 216, 281–298

15. Orne, D. & Liu, Y. K. A Mathematical Model of Spinal Response to Impact. 4, 49–71 (1970).

16. Stokes, I. A. F. & Gardner-Morse, M. Quantitative anatomy of the lumbar musculature. J. Biomech. (1999). doi:10.1016/S0021-9290(98)00164-X

17. Dreischarf, M. et al. Comparison of eight published static fi nite element models of the intact lumbar spine : Predictive power of models improves when combined together. J. Biomech. 47, 1757–1766 (2014).

18. Driscoll, M. et al. Biomechanical assessment of reduction forces measured during scoliotic instrumentation using two different screw designs. Spine Deform. 1, 94–101 (2013).

19. Driscoll, M. et al. Biomechanical Comparison of 2 Different Pedicle Screw Systems During the Surgical Correction of Adult Spinal Deformities. Spine Deform. 3, 114–121 (2015).

20. Prasad, P. & King, A. I. An Experimentally Validated Dynamic Model of the Spine. 546–550 (2019).

21. Williams, J. L. A Three-Dimensional Model of the Human Cervical Spine for Impact Simulation. (2017).

22. Newell, N. et al. Biomechanics of the human intervertebral disc : a review of testing techniques and results. J. Mech. Behav. Biomed. Mater. 69, 420–434 (2017).

23. Beebe, P., Bartel, D. & Graf, N. A Study of the Biomechanics of Spondylolysis. (2002).

24. Zander, T. & Bergmann, Æ. G. Comparison of the effects of bilateral posterior dynamic and rigid fixation devices on the loads in the lumbar spine : a finite element analysis. 1223–1231 (2007). doi:10.1007/s00586-006-0292-8

25. Spyrou, L. A. & Aravas, N. Muscle and Tendon Tissues: Constitutive Modeling and Computational Issues. J. Appl. Mech. 78, 041015 (2011).

26. Eberlein, R., Holzapfel, G. A. & Fro, M. Multi-segment FEA of the human lumbar spine including the heterogeneity of the annulus fibrosus. 34, 147–163 (2004).

27. Dietrich, M., Kedzior, K. & Zagrajek, T. Modeling of muscle action and stability of the human spine. in Multiple Muscle Systems 451–460 (Springer, 1990).

28. Dietrich, M., Kedzior, K. & Zagrajek, T. A Biomechanical Model of the Human Spinal System. Proc. Inst. Mech. Eng. Part H J. Eng. Med. (1991). doi:10.1243/PIME_PROC_1991_205_257_02

29. Daggfeldt, K. & Thorstensson, A. The role of intra-abdominal pressure in spinal unloading. J. Biomech. (1997). doi:10.1016/S0021-9290(97)00096-1

30. Arjmand, N., Shirazi-Adl, A. & Parnianpour, M. A finite element model study on the role of trunk muscles in generating intra-abdominal pressure. Biomed. Eng. Appl. Basis Commun. 13, 181–189 (2001).

31. Degens, H., Salmons, S. & Jarvis, J. C. Intramuscular pressure, force and blood flow in rabbit tibialis anterior muscles during single and repetitive contractions. Eur. J. Appl. Physiol. Occup. Physiol. (1998). doi:10.1007/s004210050381

32. Aratow, M. et al. Intramuscular pressure and electromyography as indexes of force during isokinetic exercise. J. Appl. Physiol. 74, 2634–40 (1993).

33. El-Bojairami, I. & Driscoll, M. Correlating Skeletal Muscle Output Force and Intramuscular Pressure via a 3-Dimensional Finite Element Muscle Model. J. Biomech. Eng. (In Submission)

34. Moorhouse, K. M. & Granata, K. P. Trunk stiffness and dynamics during active extension exertions. 38, 2000–2007 (2007).

35. Hodges, P. W., Shirley, D., Gandevia, S. C. & Physiotherapy, R. Lumbar spine stiffness is increased by elevation of intra- abdominal pressure 1. 3–5 (1999).

36. Keith, S. A. Man's Posture; Its Evolution and Disorders. (1923).

37. Gracovetsky, S., Farfan, H. F. & Lamy, C. The mechanism of the lumbar spine. Spine (Phila. Pa. 1976). (1981). doi:10.1097/00007632-198105000-00007

38. El-Monajjed, K. & Driscoll, M. A finite element analysis of the intra-abdominal pressure and paraspinal muscle compartment pressure interaction through the thoracolumbar fascia. Comput. Methods Biomech. Biomed. Engin. (2020). doi:10.1080/10255842.2020.1752682

39. Little, J. P. & Adam, C. J. Geometric sensitivity of patient-specific finite element models of the spine to variability in user-selected anatomical landmarks. Comput. Methods Biomech. Biomed. Engin. (2015). doi:10.1080/10255842.2013.843673

40. Schmidt, H., Galbusera, F., Rohlmann, A., Zander, T. & Wilke, H. J. Effect of multilevel lumbar disc arthroplasty on spine kinematics and facet joint loads in flexion and extension: A finite element analysis. Eur. Spine J. (2012). doi:10.1007/s00586-010-1382-1

41. Goel, V. K. et al. Effects of Charité artificial disc on the implanted and adjacent spinal segments mechanics using a hybrid testing protocol. Spine (Phila. Pa. 1976). (2005). doi:10.1097/01.brs.0000195897.17277.67

42. Chen, C.-S., Cheng, C.-K., Liu, C.-L. & Lo, W.-H. Stress analysis of the disc adjacent to interbody fusion in lumbar spine. Med. Eng. Phys. (2001). doi:10.1016/S1350-4533(01)00076-5

43. Shirazi-Adl, A. & Parnianpour, M. Load-bearing and stress analysis of the human spine under a novel wrapping compression loading. Clin. Biomech. (2000). doi:10.1016/S0268-0033(00)00045-0

44. Park, W. M., Kim, K. & Kim, Y. H. Effects of degenerated intervertebral discs on intersegmental rotations, intradiscal pressures, and facet joint forces of the whole lumbar spine. Comput. Biol. Med. (2013). doi:10.1016/j.compbiomed.2013.06.011

45. Jones, A. C. & Wilcox, R. K. Finite element analysis of the spine : Towards a framework of verification , validation and sensitivity analysis. 30, 1287–1304 (2008).

46. Cheung, J. T., Zhang, M., Leung, A. K. & Fan, Y. Three-dimensional finite element analysis of the foot during standing — a material sensitivity study. 38, 1045–1054 (2005).

47. Cholewicki, J., McGill, S. M. & Norman, R. W. Comparison of muscle forces and joint load from an optimization and EMG assisted lumbar spine model: Towards development of a hybrid approach. J. Biomech. 28, (1995).

48. Cave, A. J. The Innervation and Morphology of the Cervical Intertransverse Muscles. J. Anat. (1937).

49. Bogduk, N. & Macintosh, J. E. The applied anatomy of the thoracolumbar fascia. Spine (Phila. Pa. 1976). (1984). doi:10.1097/00007632-198403000-00006

50. Chi, H., Talischi, C., Lopez-Pamies, O. & Paulino, H. G. Polygonal finite elements for finite elasticity. Int. J. Numer. Methods Eng. (2015). doi:10.1002/nme.4802

51. Bartelink, D. L. The role of abdominal pressure in relieving the pressure on the lumbar intervertebral discs. J. Bone Joint Surg. Br. (1957). doi:10.1016/S0140-6736(01)35637-4

52. Song, C., Alijani, A., Frank, T., Hanna, G. & Cuschieri, A. Elasticity of the living abdominal wall in laparoscopic surgery. J. Biomech. 39, 587–591 (2006).

53. Papadopoulos, P. & Taylor, R. L. A mixed formulation for the finite element solution of contact problems. Comput. Methods Appl. Mech. Eng. (1992). doi:10.1016/0045-7825(92)90061-N

54. Brooks, J. C. & Savell, J. W. Perimysium thickness as an indicator of beef tenderness. Meat Sci. (2004). doi:10.1016/j.meatsci.2003.10.019

55. Yang, H., Jekir, M. G., Davis, M. W. & Keaveny, T. M. Effective modulus of the human intervertebral disc and its effect on vertebral bone stress. J. Biomech. (2016). doi:10.1016/j.jbiomech.2016.02.045

56. Kurutz, M. & Oroszvry, L. Finite Element Modeling and Simulation of Healthy and Degenerated Human Lumbar Spine. in Finite Element Analysis - From Biomedical Applications to Industrial Developments (2012). doi:10.5772/37384

57. Deeken, C. R. & Lake, S. P. Mechanical properties of the abdominal wall and biomaterials utilized for hernia repair. J. Mech. Behav. Biomed. Mater. 74, 411–427 (2017).

58. Harris, E. H., Walker, L. B. & Bass, B. R. Stress-strain studies in cadaveric human tendon and an anomaly in the young's modulus thereof. Med. Biol. Eng. (1966). doi:10.1007/BF02474798

59. Baroud, G., Nemes, J., Heini, P. & Steffen, T. Load shift of the intervertebral disc after a vertebroplasty: A finite-element study. Eur. Spine J. (2003). doi:10.1007/s00586-002-0512-9

60. Alonso, F. & Hart, D. J. Intervertebral Disk. Encycl. Neurol. Sci. 2, 724–729 (2014).

61. Huynh, K. T., Gibson, I., Jagdish, B. N. & Lu, W. F. Development and validation of a discretised multi-body spine model in LifeMOD for biodynamic behaviour simulation. Comput. Methods Biomech. Biomed. Engin. (2015). doi:10.1080/10255842.2013.786049

62. Ward, S. R. et al. Architectural analysis and intraoperative measurements demonstrate the unique design of the multifidus muscle for lumbar spine stability. J. Bone Jt. Surg. - Ser. A (2009). doi:10.2106/JBJS.G.01311

63. ASME. Assessing Credibility of Computational Modeling and Simulation Results through Verification and Validation : Application to Medical Devices. Asme V&V 40-2018 (2018).

64. Wang, S. et al. In vivo loads in the lumbar L3-4 disc during a weight lifting extension. Clin. Biomech. (2014). doi:10.1016/j.clinbiomech.2013.11.018

65. Rolander, S. D. Motion of the lumbar spine with special reference to the stabilizing effect of posterior fusion. An experimental study on autopsy specimens. Acta Orthop. Scand. Suppl 90:1-144 (1966).

66. Ranu, H. S., Denton, R. A. & King, A. I. Pressure distribution under an intervertebral disc-An experimental study. J. Biomech. (1979). doi:10.1016/0021-9290(79)90166-0

67. Arjmand, N. & Shirazi-Adl, A. Role of intra-abdominal pressure in the unloading and stabilization of the human spine during static lifting tasks. Eur. Spine J. (2006). doi:10.1007/s00586-005-0012-9

68. Choi, Y., Park, M. H. & Lee, K. Tissue engineering strategies for intervertebral disc treatment using functional polymers. Polymers (2019). doi:10.3390/polym11050872

69. Roylance, D. Pressure vessels and piping papers published in 1988 Contents of volume 31. Int. J. Press. Vessel. Pip. 36, i–xi (1989).

70. Mueller, G. et al. Intramuscular pressure in the erector spinae and intra-abdominal pressure related to posture and load. Spine 23, 2580–2590 (1998).

71. Keaveny, T. M., Wachtel, E. F. & Kopperdahl, D. L. Mechanical behavior of human trabecular bone after overloading. J. Orthop. Res. (1999). doi:10.1002/jor.1100170308

72. Benedict, J. V., Walker, L. B. & Harris, E. H. Stress-strain characteristics and tensile strength of unembalmed human tendon. J. Biomech. (1968). doi:10.1016/0021-9290(68)90038-9

73. Yang, T. et al. The rule of strain in different stratification of the intervertebral disc under physiologic loading. Biomed. Res. (2017).

74. Kirilova, M., Stoytchev, S., Pashkouleva, D. & Kavardzhikov, V. Experimental study of the mechanical properties of human abdominal fascia. Med. Eng. Phys. (2011). doi:10.1016/j.medengphy.2010.07.017

75. Wheatley, B. B., Odegard, G. M., Kaufman, K. R. & Haut Donahue, T. L. A validated model of passive skeletal muscle to predict force and intramuscular pressure. Biomech. Model. Mechanobiol. (2017). doi:10.1007/s10237-016-0869-z

4.3. ADDITIONAL STUDIES RELATED TO THE SPINE MODEL

The use of appropriate material properties representative of underlined mechanics is perhaps one of the most crucial decisions in FE models. In biomechanics, there exists several reasons that dictate the mechanical response of a soft tissue. These include patient age, sex, race, active injuries or injury history, medical conditions, lifestyle, food habits, external factors, and so on. In other words, the exact material properties of a patient's soft tissues are, probably, as unique as his/her DNA. Even though slight variabilities exist, the general response of each tissue is, however, best explained by a specific material model. For example, as highlighted in literature, skeletal muscles closely follow hyperelastic models with viscoelastic properties appearing as a result of time-dependent changes. As such, there exists a wide range of variabilities for the mechanical properties of soft tissues in literature, to which, it becomes a critical decision, in FE analyses, as to which material properties to use without causing significant loss in accuracy. In the spine model put forth, linear properties were used along a sensitivity analysis to show their validity for the simulated range of motion. Still, for patient-specific models, and depending on the context of use, more representative and specific properties may be required. This presented the potential for an additional study in efforts of reverse-engineering the exact material properties of a soft tissue under study.

An application of the spine model is its potential to be used in developing virtual reality simulations of several medical procedures for training purposes. The proposed framework to reverse-engineer material properties of a specific soft tissue rely on needle insertion mechanisms within that tissue during the medical procedure. That is, needle insertion can be described by fracture mechanics and crack propagation, which can be modelled in FE using cohesive elements. The traction-separation properties of those elements are then used to extract fracture properties, which if coupled with a material behavior optimization scheme, can lend insight into the bulk properties of the tissue of interest. As such, the following paper explores the feasibility of this procedure, namely extracting material properties using cohesive elements, as a potential approach to getting material behavior for patient-specific scenarios towards more accurate spine modeling. This, in turn, would allow leveraging more representative material properties in order for the presented spine model to be widely used in other applications. The outcomes of this procedure are presented in the manuscript entitled "Feasibility of extracting tissue material properties *via*

cohesive elements: a finite element approach to probe insertion procedures in non-invasive spine surgeries" for which the contribution of the first author is considered to be 60%. This manuscript was published in the *Medical & Biological Engineering & Computing* journal on August 24, 2021.

4.3.1 ARTICLE 3: FEASIBILITY OF EXTRACTING TISSUE MATERIAL PROPERTIES VIA COHESIVE ELEMENTS: A FINITE ELEMENT APPROACH TO PROBE INSERTION IN NON-INVASIVE SPINE SURGERIES

Ibrahim El Bojairami[1]; Amirhossein Hamedzadeh, Ph.D.[1]; Mark Driscoll, Ph.D., P.Eng.[1]

[1]*Musculoskeletal Biomechanics Research Lab, Department of Mechanical Engineering, McGill University, Montréal, Quebec, Canada*

Address for notification, correspondence, and reprints:

Mark Driscoll, Ph.D., P.Eng., Assistant Professor

Associate Member, Biomedical Engineering

Canada NSERC Chair Design Engineering for Interdisciplinary Innovation of Medical Technologies

Department of Mechanical Engineering

817 Sherbrooke St. West

Montréal, QC, H3A 0C3 Canada

T: +1 (514) 398 – 6299

F: +1 (514) 398 – 7365

E-Mail: mark.driscoll@mcgill.ca

4.3.1.1 ABSTRACT

Modelling the mechanical behavior of soft tissues probe insertion remains a challenging endeavor due to involved interdependent phenomena comprising tissues nonlinear deformation, contact between the probe and the tissue, crack propagation, and viscoelastic effects. To that matter, cohesive elements allow simulating crack formation and propagation, which provides a promising path to modelling the mechanical behavior of probe insertion in soft tissues. As such, the aim of the present study was to investigate the feasibility of devising and integrating an algorithm in a finite element (FE) case-study in efforts of reverse-engineering the material properties of non-homogeneous soft tissues. A layered nonlinear tissue model with a cohesive zone was created in the commercial software ABAQUS. Material properties were iteratively modified via a hybrid gradient descent optimization algorithm: Minimizing the resultant error to firstly find optimum Ogden's hyperelastic parameters, followed by obtaining the damage parameters. Perceived material properties were then compared to those obtained via experimental human cadaver testing. Under the investigated four-layered muscles model, numerical results overlapped, to a great extent, with six different force-insertion experimental profiles with an average error of $\pm$15%. The best profile fit was realized when the highest sudden force drop was less than 60% of the peak force. Lastly, the FE analysis revealed an increase in stiffness as the probe advanced inside the tissue. The optimization algorithm demonstrated its capability to reverse engineer the material parameters required for the FE analysis of real, non-homogeneous, soft tissues. The significance of this procedure lies within its ability to extract tissues material parameters, in real-time, with little to no intervention or invasive experimental tests. This could potentially further serve as a database for different muscle layers and force-insertion profiles, used for surgeons and physicians clinical training purposes.

Keywords: Finite element analysis, probe insertion, cohesive elements, tissues material properties, optimization algorithms.

4.3.1.2 INTRODUCTION

Needle insertion is a common practice in numerous medical procedures such as endoscopy[1], spine biopsy[2], and epidural lumbar puncture[3]. Traditionally, physicians and surgeons are trained on these procedures via either cadavers or anesthetized animals[4]. Considering the associated challenges, such as patient's safety and limited exposure to cadaveric samples[4], the use of virtual reality (VR) as a comprehensive training tool has gained momentum[5]. However, simulating an accurate VR environment, in terms of probe insertion, is a must to realize a precise surgical simulator tool[6].

Numerous approaches have been realized to model probe insertions, with most studies focusing on robotically controlled needle insertion and steering flexible needles in the tissue[7,8]. Other studies were concerned with obtaining the elastic and fracture properties of the tissue[9]. Generally, the insertion force f_p is subdivided into three components, namely, friction $f_{friction}$, force required to cut the tissue $f_{cutting}$, and reaction force resulting from tissue deformation $f_{stiffness}$[10], as follows:

$$f_p = f_{friction} + f_{cutting} + f_{stiffness} \tag{4.4}$$

A more convenient approach is to express the same concept in terms of energies[11,12] such that:

$$W_{ext} = \widehat{W}_f + \widehat{W}_E + \widehat{W}_{cr} \tag{4.5}$$

where W_{ext} is the external work, $\widehat{W}_f$ is the frictional work, $\widehat{W}_E$ is the strain energy, and $\widehat{W}_{cr}$ is the work required for crack propagation. Among these components, the strain energy is the only recoverable term, from elastic deformations, which makes it a primary candidate for finite element (FE) modelling as energy frameworks, based on deformations, are well-suited for FE applications.

Although FE analyses are computationally expensive in nature, their real-time application is still attractive when combined with condensation techniques[13]. In this particular case, a planar-based tissue was modelled, whereby boundary and local material conditions changes were achieved via updating the potential field and Jacobian inverse matrices, if they exist. Furthermore, the needle was modelled as a beam, comprising one-dimensional elements. This added advantage was appropriate as beam elements accommodate for large-strain deformations.

In essence, the problem of probe insertion is mechanical based, with different levels of complexity and assumptions[14]. Broadly speaking, several phenomena simultaneously happen in a quasi-static probe insertion problem, mainly tissue elastic deformation, propagation of the crack in the tissue, and hard normal and tangential contact between the probe and the tissue[15–17]. The interdependency between these phenomena further adds to the problem's complexity. For instance, the contact surface between the tissue and the probe is directly related to the crack propagation. That is, as the probe cuts through the tissue, frictional forces increase as the contact surface expands; however, if the crack propagates ahead of the probe tip, the tissue relaxes and the contact will be lost between the tissue and the probe[17].

Crack propagation is perhaps the most complex phenomenon to model due to both, the theoretical and computational aspects of the problem[18]. A well-known approach in fracture mechanics is the J-integral method, originally applied to metal plasticity[19]. In this approach, rupture is considered as a sudden crack propagation when the release rate of the strain potential surpasses the fracture toughness of the material. Under dynamic conditions where tissue viscoelastic effects are of interest, the J-integral is combined with a nonlinear Kelvin-Voigt model[20].

Another widely used approach to fracture mechanics is the use of cohesive elements, whereby the tearing is described by the surface separation of the cohesive interface[21,22]. In cohesive theories, the separation between the two surfaces is described as a displacement jump, resisted by the cohesive traction, ahead of the crack tip[23]. The conveniency of this approach has pushed researchers to exploit it in several applications including modelling aorta dissection[24] via utilizing both, the extended and classical FE methods[23]. It has been also used to investigate the effect of bevel-tip steerable needles[25], whereby a cohesive zone at the tip of the needle was adopted to simulate elements separation. The primary finding was that the forces at the tip of the needle were highly sensitive to the tissue's fracture toughness. Lastly, cohesive elements were utilized in dynamic explicit methods to simulate needle insertions[26]. The strain energy release during the crack formation was extracted from experimental data, to which the FE model was calibrated based on the needle insertion in a homogeneous phantom tissue experimental set[26]. The needle was further assumed a rigid body and a single layer of cohesive elements were placed between the

tissue elements to model the crack path. Fundamentally, the study concluded the accuracy of cohesive approaches to capture gross aspects of needle insertion operations[26].

In light of the aforementioned studies, to date, and to the best of the authors' knowledge, needle insertion FE simulations focus on controlled phantom experiments[25,26], with little to no knowledge on the feasibility of their application in real-time surgeries under unknown material properties. This in no means is to say that much advancement has not been made in the fields of modelling surgeries, biological tissues fracture, needle insertions, and tool-tissue interactions. There has rather been an exponential progress in such fields amid the emergence of powerful simulation techniques and computational power. A comprehensive review of needle insertion into soft tissues with a focus on the force measurements effect to model the interaction between needles and tissues can be found in[15]. Within this, several FE models were developed, ranging from tissues deformation during needle insertion in soft tissue[13,27,28], 2D FE modeling of needle insertion with application to prostate brachytherapy[29,30], to force feedback models relevant to epidural insertion[31–33]. Real-time simulations of tool-tissues interactions have also experienced significant improvements thanks to GPU-based implementations[34]. One critical accompanied limitation is the solution accuracy, which has been fully addressed in a recent application of corotational cut finite element method to needle insertion simulations by combining an error control method with an adaptive meshing technique[35,36]. However, retaining patient-specific material properties whilst the surgery is in effect remains a dilemma.

The purpose of the current work is to devise an algorithm, coupled with a FE probe insertion simulation, to reverse-engineer the material properties of a non-homogeneous tissue during intervertebral disc (IVD) discectomy. The study follows a recent experimental work[37], which was further used as the comparable, to investigate the feasibility of gaining access to tissues' material behavior during surgery. Although the current numerical approach follows the work of Oldfield *et. al.*[26], it differs from previous contributions as it adopts a hybrid gradient-descent algorithm to create different muscle layers with different material properties in order to fit reaction forces from the FE simulation to the experimental data set.

4.3.1.3 METHODOLOGY

A. Cohesive Elements Description

To better understand the mode of operation of cohesive elements, their constitutive response in terms of traction-separation laws is first briefly covered. In 2D problems, the nominal traction stress vector for cohesive elements has two components, t_n and t_s, representing the normal and shear tractions along the local 1-direction and the local 2-direction, respectively. The corresponding separations are denoted δ_n and δ_s. Denoting by T_0 the original thickness of the cohesive element, the nominal strains are then defined as:

$$\varepsilon_n = \frac{\delta_n}{T_0}, \varepsilon_s = \frac{\delta_s}{T_0} \tag{4.6}$$

The elastic behavior is then described by:

$$\boldsymbol{t} = \begin{Bmatrix} t_n \\ t_s \end{Bmatrix} = \begin{bmatrix} E_{nn} & E_{ns} \\ E_{sn} & E_{ss} \end{bmatrix} \begin{Bmatrix} \varepsilon_n \\ \varepsilon_s \end{Bmatrix} = \boldsymbol{E}\varepsilon \tag{4.7}$$

where E is the elastic modulus, with E_{nn} and E_{ss} being the normal and tangential elastic moduli components. In this study, uncoupled cohesive traction behavior is desired, to which the off-diagonal components, E_{ns} and E_{sn}, are zero. The element thickness is chosen to be 1 ($T_0 = 1$).

Fig. 4–9 demonstrates the linear separation-traction law for a typical cohesive element. The damage initiates at $\delta_{n,s}^0$ and progresses to the full extent when the displacement reaches $\delta_{n,s}'$. $\boldsymbol{G_c}$ is the fracture toughness denoted and is equal to the shaded area. Damage is assumed to initiate when the maximum nominal stress ratio, defined by the expression below, reaches a value of 1. Denoting σ_{mn} and σ_{ms} to be the peak values of the nominal stress when the deformation is either purely normal to the interface or purely in the shear direction, respectively, the criterion is represented as:

$$Max\left\{\frac{\langle t_n \rangle}{\sigma_{mn}}, \frac{\langle t_s \rangle}{\sigma_{ms}}\right\} = 1 \tag{4.8}$$

where $< \ldots >$ is the Macaulay brackets operator on t_n and t_s. At this point, the element loses all strength and is removed from the analysis.

B. Finite Elements Model

An axisymmetric FE model comprising the four major muscle layers encountered in lumbar IVD discectomy, namely the latissimus dorsi, iliocostalis, longissimus, and multifidus, was created in ABAQUS. The model closely followed the experimental procedures conducted by El-Monajjed and Driscoll[37] for validation and comparison purposes. A replica of a standard surgical probe tool used in spinal fusion surgeries, mimicking a ball pen dilator, was modelled (Fig. 4–10). The tool conceived a 0.5mm rounded tip, with a minor and major diameter of 1 and 4mm, respectively,

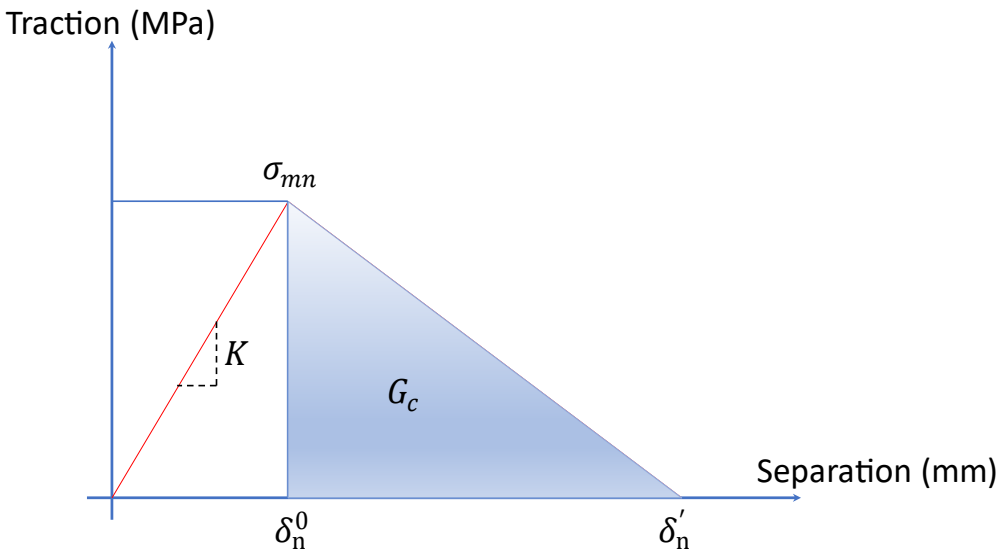

Figure 4–9: Linear separation-traction behavior for cohesive elements.

and over a 7mm length. The original tool material was medical grade stainless steel 304, which was treated as a discrete rigid body in the FE model to mimic the almost null-deformation behavior during surgeries[38]. Muscle layers were separated via a thin fascial layer to mimic lumbar muscles anatomy (Fig. 4–11). To retain the inherent nonlinear, hyperelastic, nature of human muscles, each muscle layer was modelled via an incompressible Ogden material behavior[39], due to its high level of accuracy in capturing the nonlinear steep change in soft tissues force-deformation curve[40]:

$$\chi(\boldsymbol{F}(\lambda,\alpha,\boldsymbol{J})) = \frac{2\mu}{\alpha^2}(\lambda_1^\alpha + \lambda_2^\alpha + \lambda_3^\alpha - 3) + \frac{1}{D}(\boldsymbol{J}-1)^2 \quad (4.9)$$

where χ is the strain potential, $\boldsymbol{F}$ is the deformation gradient, λ_i are the principal stretches characterized by the eigenvalues of deformation, μ is the hyperelastic shear modulus, $\boldsymbol{J}$ represents muscle's bulk modulus, α represents the fractional exponent, and D is a material constant.

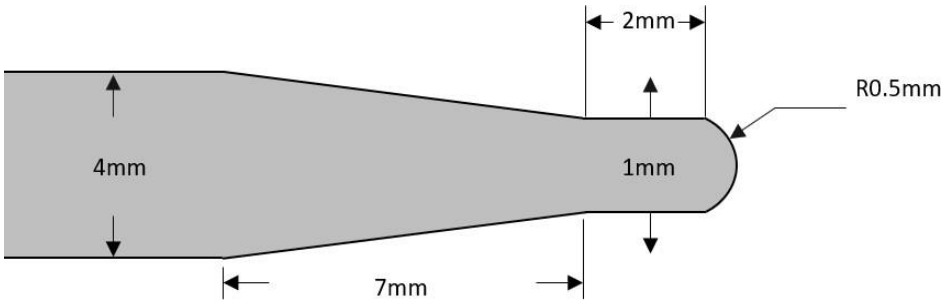

Figure 4–10: Schematic of the utilized probe.

As previously mentioned, skeletal muscles are inherently incompressible, thus, to mimic this behavior and simplify the model to a new-Hookean, the $\boldsymbol{J}$ and α parameters were set to 1 and 2, respectively[41–43]. As such, the material behavior collapses to the following 1-degree, optimization-compatible, function that follows a behavior similar to the neo-Hookean:

$$\chi(\boldsymbol{F}(\lambda)) = \frac{\mu}{2}(\lambda_1^2 + \lambda_2^2 + \lambda_3^2 - 3) \tag{4.10}$$

Modelling fracture within the cohesive zone requires careful choice of the model parameters. That is, unless one of the damage parameters of Fig. 4–9, namely σ_{mn}, $\boldsymbol{G_c}$, or K, is predefined, the optimization scheme would be ill-defined. Besides, to perform a realistic simulation of the cutting process, δ_n^0 and δ_n' need to be fundamentally constrained to the geometry of the indenter[14]. As such, δ_n' was constrained to be less than the 4mm maximum diameter of the needle while δ_n^0 was assumed to be less than or equal to its 1mm minor diameter. If these conditions are not fulfilled, a complete cut would not be achieved. All other parameters were left without bounds. On the other hand, σ_{mn} and $\boldsymbol{G_c}$ should be obtained from dedicated experiments; however, this is a challenging task due to the large strains preceding failure, dependence on strain rates, and failure stress variabilities between different muscle layers. To this matter, with the aid of conducted experiments[37], an estimate of the elastic opening of the crack, K, could be obtained. However, a bad choice of K could introduce an additional fictitious compliance to the bulk material, to which previous investigators have suggested keeping this value as high as possible[44,45]. As such, for the purpose of this study being a feasibility assessment of tissue material properties, rather than picking a random value, a maximum derivative finder was coded in Python and iterated over the experimental force-displacement curves[37] to obtain the highest possible initial stiffness as a best

estimate of K, which resulted in $K = 11.2\ MPa/mm$, a relatively high value compared to soft tissue elastic response. All other parameters were randomly assigned a positive starting point.

In line with the previously conducted experimental study[37], the modelled muscle layers had 25mm radius, whereas a 50mm depth subdivided over four torso muscles as follows: latissimus dorsi starts at 0 and ends at 16mm, iliocostalis starts at 17 and ends at 22mm, longissimus starts at 23 and ends at 30mm, and multifidus extends from 31mm to the very ends, with a 1mm fascial layer between every other muscle. A 2mm deep notch was created at the contact point between the tissue and the probe. The model was meshed via linear quadrilateral elements (CAX4R), with the

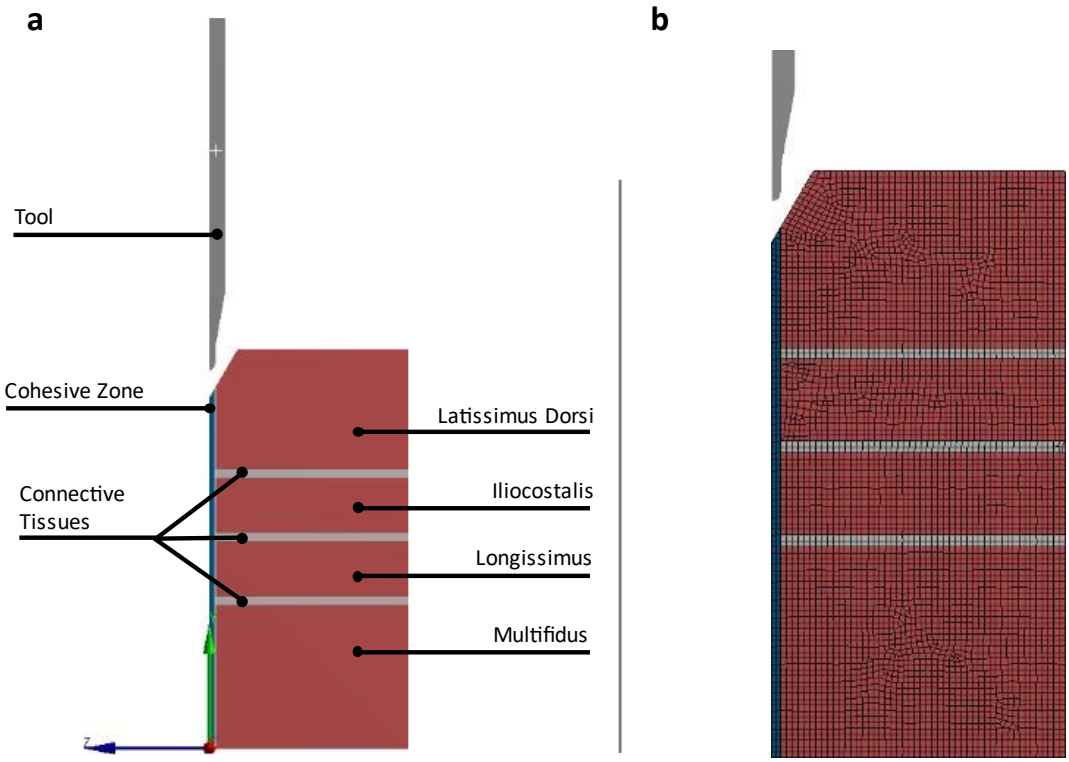

Figure 4–11: (a) Probe-muscle layers FE model. (b) Adopted FE mesh.

exception of the crack path being meshed with cohesive linear quadrilateral elements (COHAX4), both in the XY plane (Fig. 4–11b). Encastre boundary conditions in ABAQUS, commonly known as homogeneous Dirichlet, were applied to the bottom of the tissue, while a frictional contact, of 0.3 friction coefficient derived from bone-muscle interaction[46], was maintained between the tool

and tissue, especially at the cohesive zone. This has the advantage of preventing the tool from penetrating tissue elements. That is, the tool pushes on the current cohesive element until the damage criterion is met. The cohesive element is then removed from the simulation and the tool progresses to the next element. Given the time-independent nonlinear quasi-static nature of the problem, an iterative implicit solver was used.

In line with the experimental setup[37], the probe can only move along the y-axis. The experiments were designed to mimic the mechanical interaction of a multi-purpose probe to access the intervertebral disc (IVD) for a general postero-lateral, minimally invasive, spinal lumbar interbody fusion surgery. The probe punctures through the four different torso muscle layers, in a series of six different puncture tests, in efforts of gaining access to the first three lumbar IVDs (IVDs of L_1-L_2, L_2-L_3, and L_3-L_4), from both the left and right side.

C. Optimization Scheme

As previously stated, the goal of this study was to investigate the feasibility of obtaining material properties and force profiles of a probe insertion in different torso muscle layers via an optimization algorithm. The adopted algorithm is the gradient descent method (GDM)[47], a well-known optimization method vastly used in machine learning. Since the investigated study is a 2D small-scale axisymmetric problem, the use of GDM would be highly advantageous due to the method's simplicity and fast computational power per iteration[48]. Python (Python Software Foundation) was utilized to run the algorithm, whereby at each step, material behavior values were returned to ABAQUS to run the numerical case-scenario.

The error function used in this study was defined as follows:

$$\varepsilon(X, Y) = \theta_j (X_j - Y_j)^2 \tag{4.11}$$

$$\theta_j = 1 \tag{4.12}$$

where θ_js are the expression weights, whereas X_j and Y_j are the reaction forces from the FE analysis and the experimental case-studies, respectively. The error thus becomes a function of the muscle layers material properties and the damage parameters of the cohesive zone illustrated in Fig. 4–9. Therefore, the variation of the error function can be expressed as:

$$\delta\varepsilon(\boldsymbol{\mu}, \boldsymbol{D}) = \frac{\delta\varepsilon}{\delta\boldsymbol{\mu}}\delta\boldsymbol{\mu} + \frac{\delta\varepsilon}{\delta\boldsymbol{D}}\delta\boldsymbol{D} \tag{4.13}$$

$$\boldsymbol{\mu} = (\mu_0, \mu_1, \ldots, \mu_i) \tag{4.14}$$

$$\boldsymbol{D} = (K_{\boldsymbol{0}}, \sigma_{0mn}, \boldsymbol{G_{0c}}, \delta^0_{n,0}, \delta'_{n,0} \ldots, K_{\boldsymbol{i}}, \sigma_{imn}, \boldsymbol{G_{ic}}, \delta^0_{n,i}, \delta'_{n,i}) \tag{4.15}$$

where μ_i, $(i \in \mathbb{N})$, is the shear modulus of the i-th muscle layer while $K_{\boldsymbol{i}}, \sigma_{imn}$, $\boldsymbol{G_{ic}}$, $\delta^0_{n,i}$, and $\delta'_{n,i}$ $(i \in \mathbb{N})$, are the crack opening stiffness, maximum nominal stress, fracture toughness, crack initiation displacement, and critical failure displacement of the i-th cohesive layer, respectively. As previously stated, the purpose of the cohesive elements is to initiate a crack and allows for the probe to follow an incision path. As such, a homogeneous material property for the bulk modelled tissue is of interest. To fulfill this, the algorithm minimizes the error function with respect to μ of the muscle layers, restricted to positive moduli only, assuming a high 11.2MPa/mm initial crack opening stiffness, with a 10% allowance constraint during optimization, to prevent any added compliance to the bulk material, as well as constraining δ^0_n to be less than or equal to needle's 1mm minor diameter as part of geometry constraints. The set of μ_i, $K_{\boldsymbol{i}}$, and δ^0_n that minimize μ_i's error function are returned (Fig. 4–12, line 16) to form a new error function ($\hat{\varepsilon}$, Fig. 4–12, line 18), to which the weights $\theta_j s$ are then increased in value for points with critical drops. These points are identified via computing the derivative of the force-displacement profile of the experimental results. The new error function $\hat{\varepsilon}$ is then minimized with respect to the remaining critical cohesive parameters ($\boldsymbol{D}$), as explained in Fig. 4–12, to find the optimum σ_{mn}, $\boldsymbol{G_{ic}}$, and δ'_n values, under the 4mm geometric constraints set for δ'_n.

D. Experimental Case-Studies

The experimental tests[37] were conducted to mimic and characterize the mechanical interaction of a multi-purpose probe at the initial stage to achieve access to IVDs during minimally invasive, lumbar spine, interbody fusion surgery. During the surgery, the probe is manually handled by surgeons to penetrate through multiple muscle layers, mainly back spine muscles. Prior to insertion, a 10-15mm deep incision is placed at the point of access through the skin and thoracolumbar fascia (TLF). The experimental test protocols are devised to investigate probe insertion, relaxation, and extraction. The tests were conducted on a custom-made hydraulic

1: **procedure** MIN $\varepsilon(\mu, \sigma_{mn}, G_c, K, \delta^0, \delta^{'})$ ▷ Minimizing the error

2: $\mu_0 \leftarrow \mu_{\text{experimental}};\ \delta^0_{max} \leq d_{minor}; \delta'_{max} \leq d_{major}$

3: $\delta^0_0 \leftarrow \delta^0_{\text{experimental}}; \delta'_0 \leftarrow \delta'_{\text{experimental}}$

4: $K_0 \leftarrow K_{max}$ ▷ Initializing $\mu, K, \sigma_{mn}, G_c, \delta^0, \delta^{'}$

5: $\sigma_{0mn} \leftarrow \sigma_{mn,\text{experimental}}$

6: $G_{0c} \leftarrow G_{c,\text{experimental}}$

7: Choose arbitrary $\mu_1, K_1, \delta^0_1, \delta^{'}_1, \sigma_{1mn}$, & G_{1c} and initialize counter: $n \leftarrow 1$

8: **while** $\varepsilon(\mu_{n+1}, K_{n+1}, \delta^0_{n+1}, \delta'_0, \sigma_{0mn}, G_{0c}) \leq \varepsilon(\mu_n, K_n, \delta^0_n, \delta'_0, \sigma_{0mn}, G_{0c})$ **&** $(\delta^0_{max} \leq d_{minor})$ **do**

9: $\beta_n \leftarrow \frac{(\mu_n - \mu_{n\text{-}1})^T [\nabla\varepsilon(\mu_n) - \nabla\varepsilon(\mu_{n\text{-}1})]}{\nabla\varepsilon(\mu_n) - \nabla\varepsilon(\mu_{n\text{-}1})}$ ▷ Gradient descent for μ

10: $\mu_{n+1} \leftarrow \mu_n - \beta_n \nabla\varepsilon(\mu_n)$

11: $\delta^0_{n+1} \leftarrow \delta^0_n - \beta_n \nabla\varepsilon(\delta^0_n)$

12: $K_{n+1} \leftarrow K_n - \beta_n \nabla\varepsilon(K_n)$

13: $n \leftarrow n + 1$ ▷ update the counter

14: **end while**

15: **Update** $\theta_j \leftarrow \hat{\theta}_j$ ▷ new weights

16: **return** μ^*, δ^{0*}, $K^* \leftarrow \mu_n$, δ^0_n, K_n ▷ Optimized μ, δ^0, and K values

17: $\text{N} \leftarrow 1$

18: $\hat{\varepsilon}(D_{\text{N}}) \leftarrow \varepsilon(\mu^*, \delta^{0*}, K^*, \delta'_{\text{N}}, \sigma^0_{\text{N}mn}, G^0_{\text{N}c})$

19: **while** $\hat{\varepsilon}(D_{\text{N}+1}) \leq \hat{\varepsilon}(D_{\text{N}})$ **do**

20: $\beta_{\text{N}} \leftarrow \frac{(D_{\text{N}} - D_{\text{N}\text{-}1})^T [\nabla\hat{\varepsilon}(D_{\text{N}}) - \nabla\hat{\varepsilon}(D_{\text{N}\text{-}1})]}{\nabla\hat{\varepsilon}(D_{\text{N}}) - \nabla\hat{\varepsilon}(D_{\text{N}\text{-}1})}$

21: $D_{\text{N}+1} \leftarrow D_{\text{N}} - \beta_{\text{N}} \nabla\hat{\varepsilon}(D_{\text{N}})$

22: **end while**

23: **end procedure**

Figure 4–12: Gradient-descent method-based optimization and curve fitting algorithm for the finite element model.

traction/compression machine (MTS 858 BIONIX II, MTS Systems Corporation, USA). It is equipped with a 100N axial load test with a resolution of 0.02N. The probe was inserted at a constant 0.5mm/s axial speed. The overall penetration cut-off was set to 40mm displacement and 70N axial force. One trial was performed per vertebral level (L_1-L_2, L_2-L_3, and L_3-L_4) per side

(Left/Right). The cadaver was situated at an angle on the MTS machine frame at which the probe insertion was directly perpendicular to the tissue.

4.3.1.4 RESULTS

Ogden material properties parameter results, for the muscle layers under study, are shown in Table 4-5. The latissimus dorsi of L_1-L_2-L showed similar modulus, μ, to that of L_1-L_2-R, whereas the iliocostalis muscle of L_1-L_2-L was significantly stronger (73%). The same was true for the longissimus muscle, being even stiffer than the iliocostalis. Multifidus was of particular interest, conveying relatively small μ values, as compared to the other muscle layers. On the other hand, the first step optimization constraints of δ_n^0 and K, as well as the optimization of the second error function allowed for obtaining average cohesive material properties for each of the six puncture tests (Table 4-6). Fracture toughness ranged between 0.99 and 5.34KJ/m^2 whereas maximum nominal stress was between 0.71 and 3.71MPa for all puncture points. The corresponding crack opening stiffness, crack initiation displacement, and critical failure displacements are also reported in Table 4-6.

Table 4-5: Ogden material parameters for the different muscle layers

Location	**Muscle hyperelastic parameter μ_i (kPa)**				
	Latissimus Dorsi μ_1	**Iliocostalis μ_2**	**Longissimus μ_3**	**Multifidus μ_4**	**Average Error** (%)
L_1– L_2– L	9.3	45.3	52.3	0.1	12
L_1– L_2– R	9.3	26.0	26.5	7.6	14
L_2– L_3– L	6.7	43.0	42.6	8.4	12
L_2– L_3– R	6.7	30.0	31.0	12.8	11
L_3– L_4– L	4.3	45.0	50.0	0.16	13
L_3– L_4– R	7.0	8.0	8.5	0.08	17

In addition, Figs. 4–13 through 4–18 illustrate both, the FE and the experimental forces obtained from the six puncture tests on the different muscle layers. The FE results were better at predicting the first significant drop, explained by the probe transitioning from the latissimus dorsi to the

iliocostalis muscle. The force acquired by the FE L_3-L_4-R puncture test had the best agreement with the experimental results. Furthermore, although the first drop was significant for the L_1-L_2-L case (6N), the FE simulation was still able to successfully predict it; however, it overestimated the maximum force by 16%. Similarly, for the second and third drops, as the probe penetrated the longissimus and multifidus muscles, respectively, FE results were in good agreement with the experimental curves, recording an average error ranging between 11 and 17%.

Table 4-6: Cohesive zone parameters

Location	Maximum Nominal Stress σ_{mn} (MPa)	Fracture Toughness G_c (KJ/m^2)	Crack Opening Stiffness K (MPa/mm)	Crack Initiation Displacement δ_n^0 (mm)	Critical Failure Displacement δ_n' (mm)
L_1– L_2– L	9.3	45.3	52.3	0.1	12
L_1– L_2– R	9.3	26.0	26.5	7.6	14
L_2– L_3– L	6.7	43.0	42.6	8.4	12
L_2– L_3– R	6.7	30.0	31.0	12.8	11
L_3– L_4– L	4.3	45.0	50.0	0.16	13
L_3– L_4– R	7.0	8.0	8.5	0.08	17

4.3.1.5 DISCUSSION

The overarching goal of this study was to devise a FE method and an optimization algorithm to investigate the feasibility of obtaining the material properties of muscles, along replicating the experimental results, obtained from probe insertion during a general minimally invasive, lumbar spine, interbody fusion surgery. To the best of the authors' knowledge, most attempts on finite element simulation of needle insertion are focused on controlled experiments on phantom[25,26]. However, in real time analysis or during surgery, it is not viable to conduct experimental tests to obtain the material properties, required for FE simulation. Moreover, the complexity of tissue composition makes it arduous to obtain the underlying descriptive material behavior. This is due to the fact that material properties along the depth of the tissue, or across its width, can potentially drastically vary. In addition, although not perfectly bonded together, muscle layers are still encompassed by fascia and connective tissues, which in turn induce variations on muscles'

material behavior. In fact, numerous studies have shown that fascia and connective tissues possess significantly higher stiffness than adjacent muscles[49–53]. In general, they are stronger and can undergo significantly high deformations (300%). In this study, thin layers of fascia (1mm) were placed in between the muscle layers in order to investigate their effect on the overall insertion profile (Fig. 4–11). It was expected that fascia layers would have a significant effect due to their much stiffer material properties. In contrast, only local spikes were observed in the insertion force profiles (Figs. 4–13 through 4–18), which was explained by the fact that actual fascia models were replaced by thin layers to maintain the focus on muscles. So to speak, if fascia and connective tissues were properly modelled, as illustrated by previous research conducted by the current authors[49], their realistic role might have appeared. However, since the focus was merely on muscles material properties, it was decided to replace them with simpler models to ease the FE simulations.

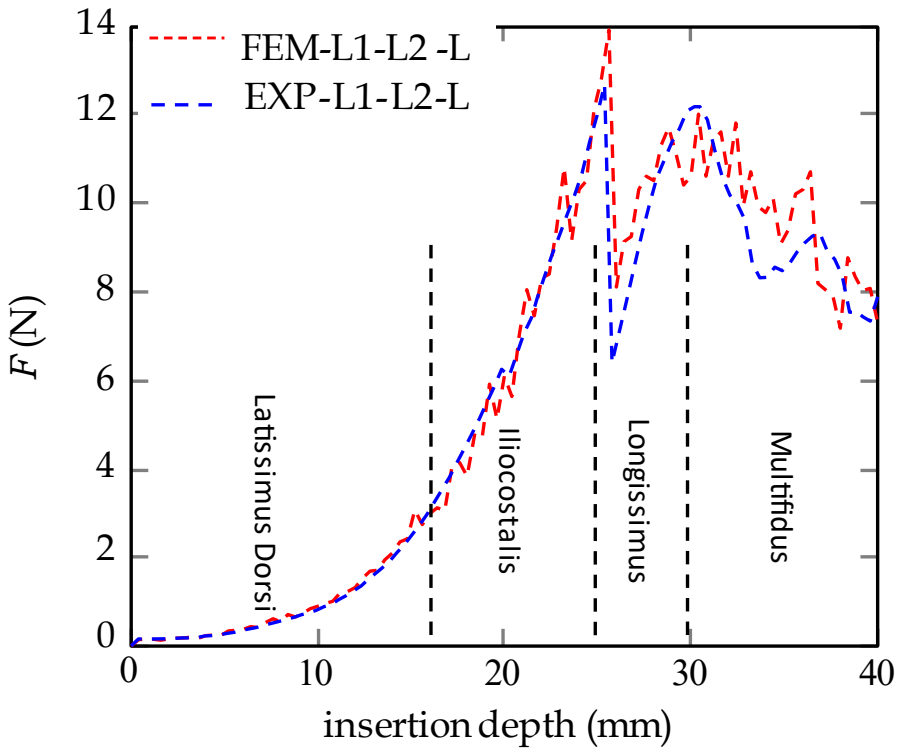

Figure 4–13: Probe insertion force-depth profile for L_1-L_2-L puncture case.

Even though this was the case, this still caused random numerical instabilities, explained by the elements distorting excessively under small loads, which can be attributed to finite sliding contact

algorithm. Generally speaking, this issue results whenever adjacent objects are not in perfect bonded contact state. For the current study, a frictional contact was placed to mimic the behavior of a tool pushing on the tissue of interest. Although accompanied with numerical instabilities in some cases, this is still highly advantageous to prevent the tool from penetrating elements that has not met the damage criterion yet. Nevertheless, such numerical instabilities were overcome by appropriately refining the mesh at the contact points. In addition, such refinements resulted in a highly compatible mesh, with global and local mesh quality exceeding 95%. This being the case, and considering that the study was a feasibility analysis, a mesh sensitivity analysis was not necessary anymore given the accuracy of the original mesh.

Force profiles (Figs. 4–13 through 4–18) showed the potential feasibility of the underlined methods to predict the material properties of soft tissues via FE techniques to a relatively high accuracy level. However, differences were still observed between the experimental and numerical results, reflected by the average errors reported in Table 4-5. In-vivo tissue biomechanics experiments are usually affected by numerous factors including age, gender, and genetics. The

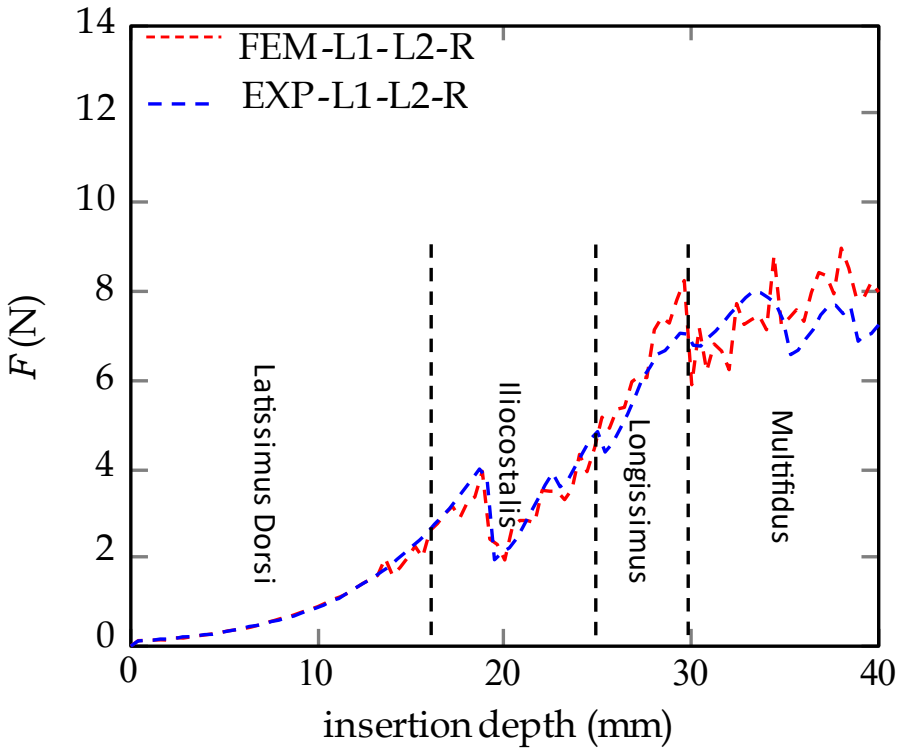

Figure 4–14: Probe insertion force-depth profile for L_1-L_2-R puncture case.

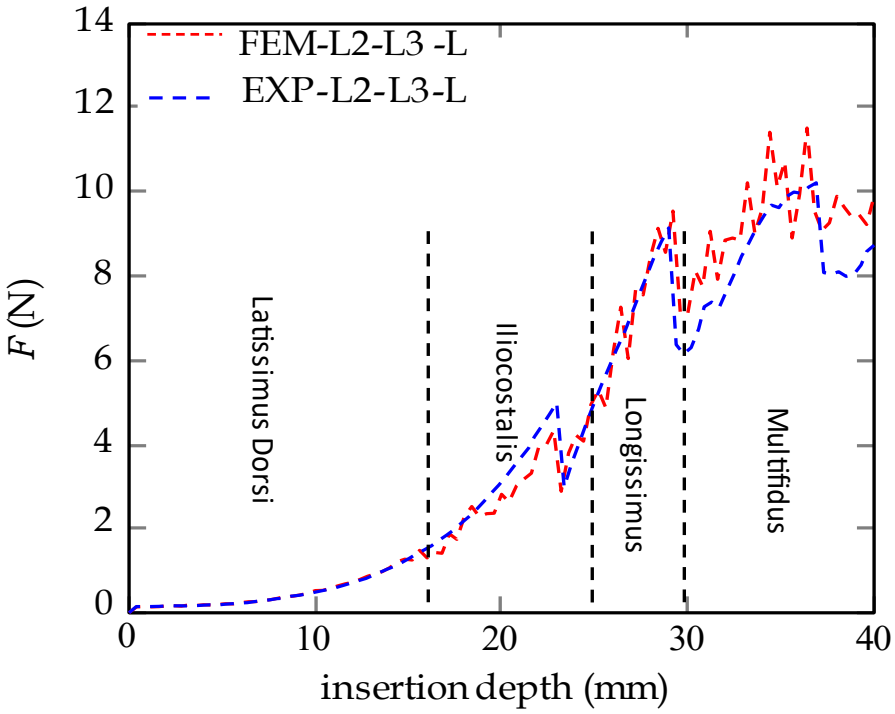

Figure 4–15: Probe insertion force-depth profile for L_2-L_3-L puncture case.

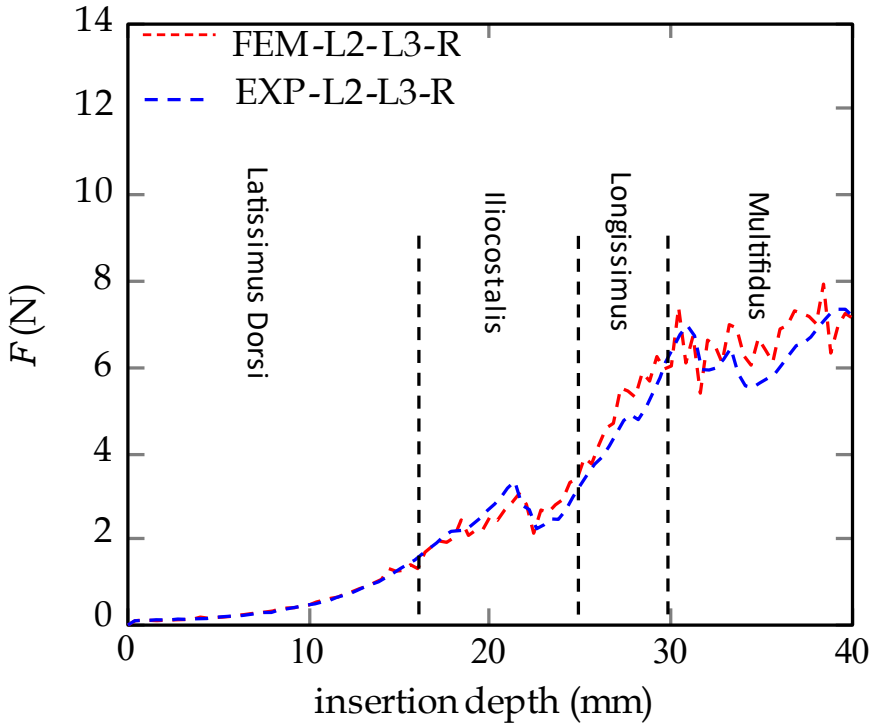

Figure 4–16: Probe insertion force-depth profile for L_2-L_3-R puncture case.

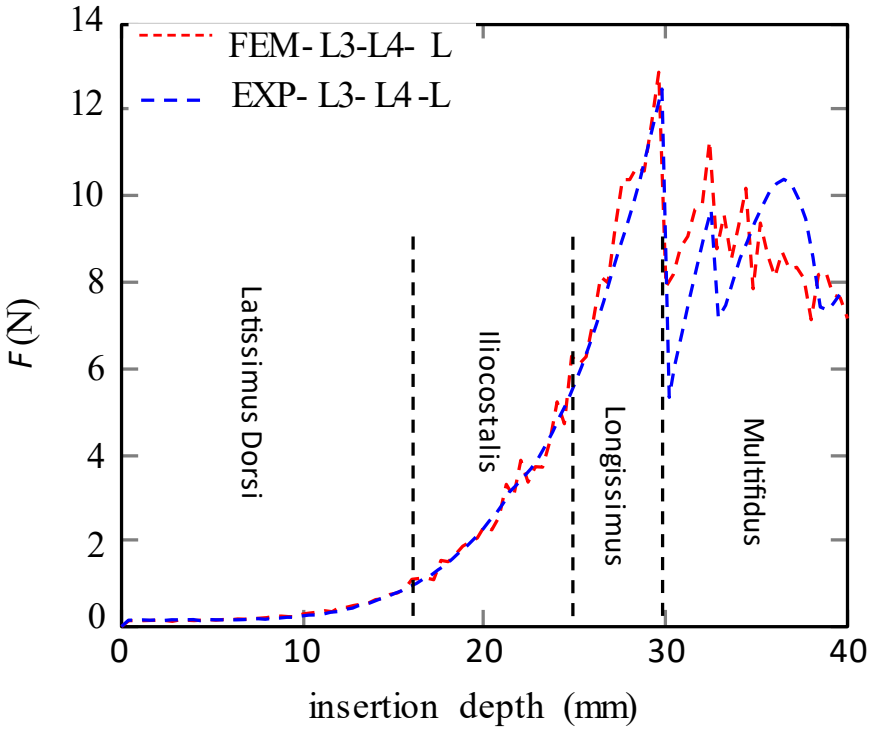

Figure 4–17: Probe insertion force-depth profile for L_3-L_4-L puncture case.

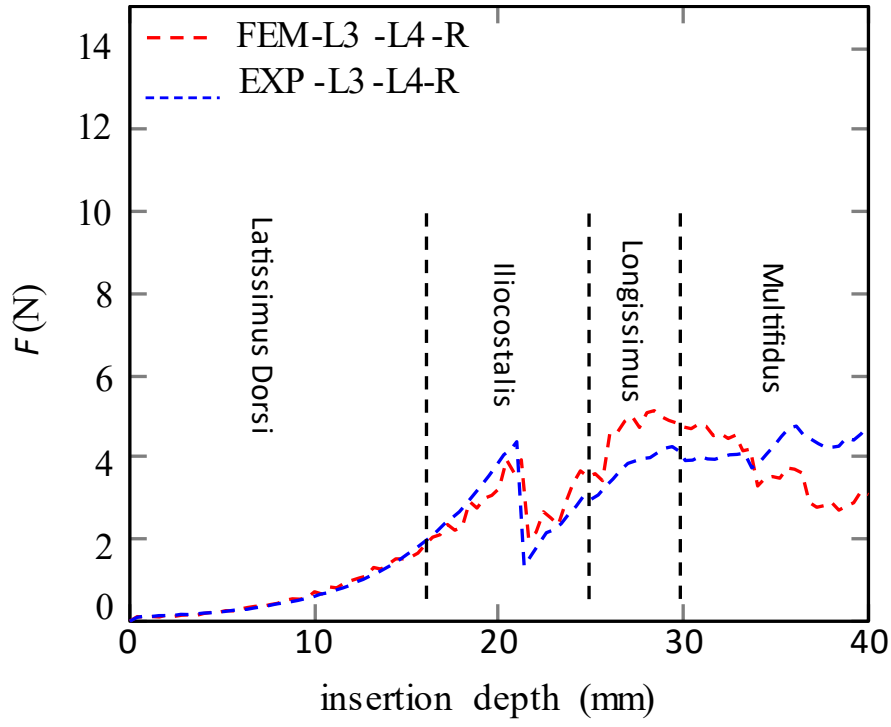

Figure 4–18: Probe insertion force-depth profile for L_3-L_4-R puncture case.

experimental tests were conducted on the same cadaver, under the same physiological condition, thus minimizing such experimental errors. On the other hand, observed errors were mainly due to simplifications realized in the FE model, mainly performing the analysis under static conditions. Other minor simplifications were assuming a rigid tool, choosing an initial stiffness starting point, and fixing some of Ogden's constitutive model parameters based on the theory and literature. However, such simplifications were reasonable and complied with literature, and although they led to marginal errors, they made the feasibility and convergence of the FE model and the optimization scheme possible.

Constraints and assumptions made regarding the cohesive zone model might have also affected material properties results. The necessity for predefining at least one damage parameter for the optimization to work drastically affected the results. Defining an initial crack opening stiffness that is both realistic and sufficiently high to avoid introducing added compliance to the material was highly challenging. Although every effort was made to extract this K value from experimental values, slight changes in this parameter might render completely different cohesive parameters, to which the authors recommend performing dedicated experiments to obtain such parameter prior to running the optimization scheme in real-time. On the other hand, although fluctuations were observed with respect to reported fracture toughness, such results were in the vicinity of similar literature experiments[9,54]. Lastly, crack initiation and failure displacements were within needle geometric constraints, showing a realistic crack propagation and cutting mechanism.

This study offered a feasible solution to bridge the gap between the mechanical behavior of the tissue and its material properties by utilizing an algorithm to reverse engineer properties required that are obtained from other mechanical tests. This is due to the complicated mechanical nature of soft tissues, as well as limitations involved not only in experimental works, but also in the theoretical realm of damage and fracture mechanics. Nevertheless, cohesive parameters (Eq. 4.15), especially fracture toughness, is a nonlocal variable, meaning that it is affected by the extent of damage at its vicinity. That is, approaches of determining fracture toughness based on single numerical elements might render inaccurate results, whereby fracture from adjacent elements affect local results. Thus, the need for more sophisticated models, such as the phase-field method, which not only consider local, but also gradient variations[55]. Nonetheless, besides being

computationally expensive, such models are incompatible with current available FE commercial software, making their real-time implementation questionable.

A. Limitations

Similar to any in silico model, limitations are always present due to the FE approximation and GDM optimization schemes. However, with assumptions kept to a minimum, this does not limit method's capabilities in assessing the feasibility of collecting real-time biomechanical behavior of tissues. For the method to converge, it assumes a static behavior, which is a valid assumption as the experiments were passively performed on isolated muscles, thus eliminating their active contraction part[56]. A thorough study was also previously conducted by the current authors on utilizing static material properties to approximate tissues realistic behavior[49]. Furthermore, as explained in the methodology, muscles are inherently incompressible, thus suggesting the values used for Ogden's $\boldsymbol{J}$ and α parameters. Although it would be ideal to also optimize these material parameters, realistic values were chosen in order for the GDM algorithm to quickly converge. Another limitation was the use of the GDM scheme instead of other faster and more accurate methods such as control gradient and fast gradient descent algorithms. However, considering that GDM does not compute any second derivates, making it inherently computationally fast per iteration, this was a reasonable choice due to model's simplicity and scale[48]. Besides, its practical use is well-developed in literature, as well as being backed by most current available commercial FE software. One last major limitation was the need for a manual initial K starting point for the algorithm to proceed. However, this did not pose any problems for the current research as this value was extrapolated from the conducted experimental case-studies. One the other hand, although this study developed a successful approach to obtain feasible tissue material properties, extensive validation and comparison against other parameters outside the presented modelling approach is still required. This is particularly important in order to investigate whether all fracture and tissue mechanisms were accurately incorporated and modelled. Thus, dedicated validation might still be essential before using the reported parameters outside the enclosed modelling problem. Nevertheless, such simplifications are potentially valid and do not hinder the method's capabilities to obtain feasible tissue material behavior.

B. Future Work

The FE-based algorithm presented in this study was capable of reverse engineering feasible parameters to model probe insertion in non-homogenous tissues. Even though the initial guess was manually tuned, the rest of the procedure was performed with little intervention. With such a promising algorithm, in future research, the authors aim to fully automate and enhance the scheme via resolving some of its major limitations, in order to implement it for surgeons training applications. As such, the method would become compatible with more detailed FE simulations, allowing to extract more advanced information, such as real-time stress distributions and muscles pressure. Another goal is to cross-examine the method's results against in-vivo experimental tests to find meaningful correlations, empirical formulas, and build material databases for the design of patient-specific probes.

4.3.1.6 CONCLUSIONS

This study investigated the feasibility of utilizing the cohesive element approach in the simulation of probe insertion in non homogenous cadaveric tissues. The study offered a gradient descent method-based algorithm to obtain feasible set of material parameters for different torso muscles. To achieve the best fit, the algorithm minimized a predefined error function with equal weights to obtain Ogden's μ shear modulus parameters of each muscle layer. The weights were then adjusted to the critical experimental drop point, intensifying their effect on the new error function, to which a second stage new error function was minimized in order to find the cohesive zone material parameters. Numerical simulation results presented good agreement with conducted experiments, showing an average difference of 15% attributed to FE limitations and simplifications necessary for the optimization to have worked. This method is potentially promising and can be used to generate realistic force-insertion curves, within the statistical variance of experimental results, for virtual surgery training applications.

4.3.1.7 ACKNOWLEDGMENT

We gratefully acknowledge funding by McGill University (MEDA), the Fonds de Recherche du Québec – Nature et Technologies (FRQNT), and the Natural Sciences and Engineering Research Center (NSERC).

4.3.1.8 REFERENCES

1. Itoi, T. et al. Experimental endoscopy: objective evaluation of EUS needles. Gastrointest. Endosc. (2009). doi:10.1016/j.gie.2008.07.017

2. Peh, W. C. G. CT-guided percutaneous biopsy of spinal lesions. Biomedical Imaging and Intervention Journal (2006). doi:10.2349/biij.2.3.e25

3. Doherty, C. M. & Forbes, R. B. Diagnostic lumbar puncture. Ulster Med. J. (2014).

4. Stefanidis, D., Yonce, T. C., Green, J. M. & Coker, A. P. Cadavers versus pigs: Which are better for procedural training of surgery residents outside the OR? Surg. (United States) (2013). doi:10.1016/j.surg.2013.05.001

5. Mccloy, R. & Stone, R. Virtual reality in surgery. BMJ (2001). doi:10.1136/bmj.323.7318.912

6. Gurusamy, K. S., Aggarwal, R., Palanivelu, L. & Davidson, B. R. Virtual reality training for surgical trainees in laparoscopic surgery. Cochrane Database of Systematic Reviews (2009). doi:10.1002/14651858.CD006575.pub2

7. Delingette, H. Toward realistic soft-tissue modeling in medical simulation. Proc. IEEE (1998). doi:10.1109/5.662876

8. Ko, S. Y., Davies, B. L. & Rodriguez Y Baena, F. Two-dimensional needle steering with a 'programmable bevel' inspired by nature: Modeling preliminaries. in IEEE/RSJ 2010 International Conference on Intelligent Robots and Systems, IROS 2010 - Conference Proceedings (2010). doi:10.1109/IROS.2010.5650859

9. Azar, T. & Hayward, V. Estimation of the fracture toughness of soft tissue from needle insertion. in Lecture Notes in Computer Science (including subseries Lecture Notes in Artificial Intelligence and Lecture Notes in Bioinformatics) (2008). doi:10.1007/978-3-540-70521-5_18

10. Okamura, A. M., Simone, C. & O'Leary, M. D. Force modeling for needle insertion into soft tissue. IEEE Trans. Biomed. Eng. (2004). doi:10.1109/TBME.2004.831542

11. Simone, C. & Okamura, A. M. Modeling of needle insertion forces for robot-assisted percutaneous therapy. in Proceedings - IEEE International Conference on Robotics and Automation (2002). doi:10.1109/robot.2002.1014848

12. Misra, S., Reed, K. B., Schafer, B. W., Ramesh, K. T. & Okamura, A. M. Mechanics of flexible needles robotically steered through soft tissue. Int. J. Rob. Res. (2010). doi:10.1177/0278364910369714

13. Dimaio, S. P. & Salcudean, S. E. Needle steering and motion planning in soft tissues. IEEE Transactions on Biomedical Engineering (2005). doi:10.1109/TBME.2005.846734

14. Terzano, M., Dini, D., Rodriguez y Baena, F., Spagnoli, A. & Oldfield, M. An adaptive finite element model for steerable needles. Biomech. Model. Mechanobiol. (2020). doi:10.1007/s10237-020-01310-x

15. Abolhassani, N., Patel, R. & Moallem, M. Needle insertion into soft tissue: A survey. Med. Eng. Phys. (2007). doi:10.1016/j.medengphy.2006.07.003

16. van Gerwen, D. J., Dankelman, J. & van den Dobbelsteen, J. J. Needle-tissue interaction forces - A survey of experimental data. Medical Engineering and Physics (2012). doi:10.1016/j.medengphy.2012.04.007

17. Taschereau, R., Pouliot, J., Roy, J. & Tremblay, D. Seed misplacement and stabilizing needles in transperineal permanent prostate implants. Radiother. Oncol. (2000). doi:10.1016/S0167-8140(00)00162-6

18. Su, X., Yang, Z. & Liu, G. Finite element modelling of complex 3D static and dynamic crack propagation by embedding cohesive elements in Abaqus. Acta Mech. Solida Sin. (2010). doi:10.1016/S0894-9166(10)60030-4

19. Rice, J. R. Inelastic constitutive relations for solids: An internal-variable theory and its application to metal plasticity. J. Mech. Phys. Solids (1971). doi:10.1016/0022-5096(71)90010-X

20. Mahvash, M. & Dupont, P. E. Mechanics of dynamic needle insertion into a biological material. IEEE Trans. Biomed. Eng. (2010). doi:10.1109/TBME.2009.2036856

21. Ortiz, M. & Pandolfi, A. Finite-deformation irreversible cohesive elements for three-dimensional crack-propagation analysis. Int. J. Numer. Methods Eng. (1999). doi:10.1002/(SICI)1097-0207(19990330)44:9<1267::AID-NME486>3.0.CO;2-7

22. Mathur, K. K., Needleman, A. & Tvergaard, V. Three dimensional analysis of dynamic ductile crack growth in a thin plate. J. Mech. Phys. Solids (1996). doi:10.1016/0022-5096(95)00087-9

23. Ferrara, A. & Pandolfi, A. A numerical study of arterial media dissection processes. in International Journal of Fracture (2010). doi:10.1007/s10704-010-9480-y

24. Gasser, T. C. & Holzapfel, G. A. Geometrically non-linear and consistently linearized embedded strong discontinuity models for 3D problems with an application to the dissection analysis of soft biological tissues. Comput. Methods Appl. Mech. Eng. (2003). doi:10.1016/j.cma.2003.06.001

25. Misra, S., Reed, K. B., Douglas, A. S., Ramesh, K. T. & Okamura, A. M. Needle-tissue interaction forces for bevel-tip steerable needles. in Proceedings of the 2nd Biennial IEEE/RAS-EMBS International Conference on Biomedical Robotics and Biomechatronics, BioRob 2008 (2008). doi:10.1109/BIOROB.2008.4762872

26. Oldfield, M., Dini, D., Giordano, G. & Rodriguez y Baena, F. Detailed finite element modelling of deep needle insertions into a soft tissue phantom using a cohesive approach. Comput. Methods Biomech. Biomed. Engin. (2013). doi:10.1080/10255842.2011.628448

27. DiMaio, S. P. & Salcudean, S. E. Interactive simulation of needle insertion models. IEEE Trans. Biomed. Eng. (2005). doi:10.1109/TBME.2005.847548

28. DiMaio, S. P. & Salcudean, S. E. Needle steering and model-based trajectory planning. Lect. Notes Comput. Sci. (including Subser. Lect. Notes Artif. Intell. Lect. Notes Bioinformatics) (2003). doi:10.1007/978-3-540-39899-8_5

29. Alterovitz, R., Pouliot, J., Taschereau, R., Joe Hsu, I. C. & Goldberg, K. Simulating needle insertion and radioactive seed implantation for prostate brachytherapy. in Studies in Health Technology and Informatics (2003). doi:10.3233/978-1-60750-938-7-19

30. Alterovitz, R., Goldberg, K., Pouliot, J., Taschereau, R. & Hsu, I. C. Needle insertion and radioactive seed implantation in human tissues: Simulation and sensitivity analysis. in Proceedings - IEEE International Conference on Robotics and Automation (2003). doi:10.1109/robot.2003.1241854

31. Hiemenz, L., Stredney, D. & Schmalbrock, P. Development of the force-feedback model for an epidural needle insertion simulator. in Studies in Health Technology and Informatics (1998). doi:10.3233/978-1-60750-894-6-272

32. Holton, L. L. H. Force models for needle insertion created from measured needle puncture data. in Studies in Health Technology and Informatics (2001). doi:10.3233/978-1-60750-925-7-180

33. Meiklejohn, B. H. The effect of rotation of an epidural needle: An in vitro study. Anaesthesia (1987). doi:10.1111/j.1365-2044.1987.tb05224.x

34. Courtecuisse, H., Allard, J., Kerfriden, P., Bordas, S. P. A., Cotin, S., & Duriez, C. Real-time simulation of contact and cutting of heterogeneous soft-tissues. Med. Image Anal. (2014). doi:10.1016/j.media.2013.11.001

35. Bui, H. P., Tomar, S. & Bordas, S. P. A. Corotational cut finite element method for real-time surgical simulation: Application to needle insertion simulation. Comput. Methods Appl. Mech. Eng. (2019). doi:10.1016/j.cma.2018.10.023

36. Bui, H. P., Tomar, S., Courtecuisse, H., Cotin, S. & Bordas, S. P. A. Real-Time Error Control for Surgical Simulation. IEEE Trans. Biomed. Eng. (2018). doi:10.1109/TBME.2017.2695587

37. El-Monajjed, K. & Driscoll, M. Analysis of Surgical Forces Required to Gain Access Using a Probe for Minimally Invasive Spine Surgery via Cadaveric-Based Experiments towards Use in Training Simulators. IEEE Trans. Biomed. Eng. (2021). doi:10.1109/TBME.2020.2996980

38. Craker, R., Johnson, B. V., Sakthivel, H. & Cappelleri, D. J. Design of a miniaturized actuation system for robotic lumbar discectomy tools. in Proceedings of the ASME Design Engineering Technical Conference (2020). doi:10.1115/DETC2020-22319

39. Fu, Y. B., R. W. O. Nonlinear Elasticity: Theory and Applications. Nonlinear Elast. Theory Appl. (2001).

40. Martins, P. A. L. S., Jorge, R. M. N. & Ferreira, A. J. M. A comparative study of several material models for prediction of hyperelastic properties: Application to silicone-rubber and soft tissues. Strain (2006). doi:10.1111/j.1475-1305.2006.00257.x

41. Mo, F. et al. In vitro compressive properties of skeletal muscles and inverse finite element analysis: Comparison of human versus animals. J. Biomech. (2020). doi:10.1016/j.jbiomech.2020.109916

42. Elyasi, N., Taheri, K. K., Narooei, K. & Taheri, A. K. A study of hyperelastic models for predicting the mechanical behavior of extensor apparatus. Biomech. Model. Mechanobiol. (2017). doi:10.1007/s10237-017-0874-x

43. Fougeron, N. et al. Combining Freehand Ultrasound-Based Indentation and Inverse Finite Element Modeling for the Identification of Hyperelastic Material Properties of Thigh Soft Tissues. J. Biomech. Eng. (2020). doi:10.1115/1.4046444

44. de Borst, R. Numerical aspects of cohesive-zone models. Eng. Fract. Mech. (2003). doi:10.1016/S0013-7944(03)00122-X

45. Scheider, I. Cohesive model for crack propagation analyses of structures with elastic – plastic material behavior. GKSS Res. center, Geesthacht (2001).

46. Shacham, S., Castel, D. & Gefen, A. Measurements of the static friction coefficient between bone and muscle tissues. J. Biomech. Eng. (2010). doi:10.1115/1.4001893

47. Michalewicz, Z. Genetic Algorithms, Numerical Optimization, and Constraints. Proc. sixth Int. Conf. Genet. algorithms (1995).

48. El Mouatasim, A. Fast gradient descent algorithm for image classification with neural networks. Signal, Image Video Process. (2020). doi:10.1007/s11760-020-01696-2

49. El Bojairami, I., El-Monajjed, K. & Driscoll, M. Development and validation of a timely and representative finite element human spine model for biomechanical simulations. Sci. Rep. (2020). doi:10.1038/s41598-020-77469-1

50. Eng, C. M., Pancheri, F. Q., Lieberman, D. E., Biewener, A. A. & Dorfmann, L. Directional differences in the biaxial material properties of fascia lata and the implications for fascia function. Ann. Biomed. Eng. (2014). doi:10.1007/s10439-014-0999-3

51. Yahia, L. H., Pigeon, P. & DesRosiers, E. A. Viscoelastic properties of the human lumbodorsal fascia. J. Biomed. Eng. (1993). doi:10.1016/0141-5425(93)90081-9

52. Dora, C. D., Dimarco, D. S., Zobitz, M. E. & Elliott, D. S. Time dependent variations in biomechanical properties of cadaveric fascia, porcine dermis, porcine small intestine submucosa, polypropylene mesh and autologous fascia in the rabbit model: Implications for sling surgery. J. Urol. (2004). doi:10.1097/01.ju.0000121377.61788.ad

53. Schleip, R., Zorn, A. & Klingler, W. Biomechanical properties of fascial tissues and their role as pain generators. J. Musculoskelet. Pain 18, 393–395 (2010).

54. Taylor, D., O'Mara, N., Ryan, E., Takaza, M. & Simms, C. The fracture toughness of soft tissues. J. Mech. Behav. Biomed. Mater. (2012). doi:10.1016/j.jmbbm.2011.09.018

55. Gültekin, O. & Holzapfel, G. A. A brief review on computational modeling of rupture in soft biological tissues. in Computational Methods in Applied Sciences (2018). doi:10.1007/978-3-319-60885-3_6

56. Bosboom, E. M. H. et al. Passive transverse mechanical properties of skeletal muscle under in vivo compression. J. Biomech. (2001). doi:10.1016/S0021-9290(01)00083-5

4.4. SUMMARY

The central idea in this chapter was to advance the realm of physiology-based finite elements spine models by accounting for major tissues known to contribute to spine's locomotion. This was achieved by accurate and representative anatomy-based numerical models of vertebrae, intervertebral discs, major spinal muscles, tendons, thoracolumbar fascia, and abdominal pressure. Muscles and abdominal cavity followed the same pressure-based modelling procedure formulated in chapter 3. Other tissues were modelled as flexible bodies, all with assigning material properties indicative of their physiology. Model's complexity, involving interaction between numerous tissues, necessitated appropriate decisions to ease simulation time. One of which was the elimination of contact computations by means of developing a conforming mesh between adjacent objects. This followed the valid assumption that tissues interacting with the spine experience little to no sliding or separation. Thereafter, several verification tests were conducted in terms of model's form, discretization, and utilized material properties for the simulated range of motion. Lastly, extensive, structure-by-structure, validation by means of four different tests were carried out against distinct comparators which potentially showed a valid model.

Furthermore, a case-study was conducted on the feasibility of reverse-engineering material properties of soft tissues. This was motivated by the limitations realized in the spine model upon deciding which properties to use given the wide range in literature, as well as the significance of underwent verification tests. In essence, the use of needles in surgeries to gain access to a specific tissue presented the potential of modelling this mechanism, using fracture mechanics, *via* cohesive elements in finite methods. Integrating those with a hybrid gradient descent optimization algorithm allowed to minimize the resultant materials-based error function. This permitted optimizing and

retrieving the cohesive zone fracture properties, namely maximum nominal stress, fracture toughness, crack opening stiffness, crack initiation displacement, and critical failure displacement. Following this, hyperelastic shear modulus of each muscle layer was optimized for and extracted. Therefore, this explored context of use demonstrated the capability of extracting material properties required for FE analyses of non-homogeneous soft tissues, as the case of skeletal muscles.

This chapter successfully completed objective 2, to which several research and application advances were achieved by means of confirming hypothesis 2. Firstly, the state-of-the-art, novel, developed spine model underlines a breakthrough in biomechanics finite elements frameworks given the anatomical and physiological inclusion of most soft tissues known to contribute to spinal loadings. Secondly, the developed numerical mesh allows for feasibility of such complex biomechanical models given spine's uniform mechanics. In addition, considering the wide range of literature variabilities when reporting material response of soft tissues, the formulated hybrid algorithm permits extracting patient-specific material properties in surgical environments for virtual reality training applications. Such advancements open the gates to numerous potentials among which are to non-invasively simulate spine mechanics, assess injuries, evaluate surgical treatments, and design spinal instrumentation. Lastly, the availability of such a full-scale FE spine model, representative of the physiology of major spinal tissues, presents an appropriate foundation to examine equilibrium spinal stability, as proposed and achieved in chapter 5.

5

ASSESSMENT OF SPINE STABILITY ACHIEVED BY SPINAL TISSUES

5.1. FRAMEWORK OF THE FOURTH ARTICLE

The successful completion of chapter 4 resulted in a novel, validated, and fully representative model of the spine, with which conducting accurate biomechanical simulations to arrive at physiological results became promising. In this context, one of the most burdensome restrictive conditions affecting the spine is low back pain. Although the condition remains a research debate with unknown causes thus far, a growing consensus in the scientific community is that a significant portion of the problem is of mechanical origin, more specifically, a deteriorated or loss in spinal stability. An aspect of equilibrium spinal stability can be thought of as the capability of a specific set of soft tissues to retrieve the spine to within the vicinity of its initial position following an external perturbation. Although little research has been conducted on the subject, growing literature supports that this type of stability can be achieved through the coordination of spinal tissues. Thus, this study aimed to interpret the stability of the spine as perceived by the coordination between major spine soft tissues, *i.e.* the coactivation of paraspinal muscles, active engagement of intramuscular and intra-abdominal pressure, and passive support provided by the thoracolumbar fascia. Individual and collective effort of these tissues were examined through different activation case-scenarios while assessing the achieved level of stability. The study yielded good insights on the contribution of the examined soft tissues toward stability, thoracolumbar fascia's role in dissipating excessive loads, intra-abdominal pressure's movement limiting role, and muscles' antagonistic behavior to external perturbations. The outcome of this chapter marked the completion of objective 3 and hypothesis 3, as presented in the manuscript entitled "Coordination

Between Trunk Muscles, Thoracolumbar Fascia, and Intra-Abdominal Pressure Toward Static Spine Stability" for which the contribution of the first author is considered to be 85%. This manuscript was published in *Spine*, a leading journal in the field of spine, by *Lippincott Williams & Wilkins* international publisher on September 20, 2021.

5.2. ARTICLE 4: COORDINATION BETWEEN TRUNK MUSCLES, THORACOLUMBAR FASCIA, AND INTRA-ABDOMINAL PRESSURE TOWARD STATIC SPINE STABILITY

Ibrahim El Bojairami[1]; Mark Driscoll, Ph.D., P.Eng.[1]

[1]*Musculoskeletal Biomechanics Research Lab, Department of Mechanical Engineering, McGill University, Montréal, Quebec, Canada*

Address for notification, correspondence, and reprints:

Mark Driscoll, Ph.D., P.Eng., Assistant Professor

Associate Member, Biomedical Engineering

Canada NSERC Chair Design Engineering for Interdisciplinary Innovation of Medical Technologies

Department of Mechanical Engineering

817 Sherbrooke St. West

Montréal, QC, H3A 0C3 Canada

T: +1 (514) 398 – 6299

F: +1 (514) 398 – 7365

E-Mail: mark.driscoll@mcgill.ca

5.2.1. ABSTRACT

Study Design: Numerical in-silico human spine stability finite element analysis.

Objective: The purpose of this study was to investigate the contribution of major torso tissues towards static spine stability, mainly the thoracolumbar fascia (TLF), abdominal wall with its intra-abdominal pressure (IAP), and spinal muscles inclusive of their intramuscular pressure.

Summary of Background Data: Given the numerous redundancies involved in the spine, current methodologies for assessing static spinal stability are limited to specific tissues and could lead to inconclusive results. A three-dimensional finite element model of the spine, with structured analysis of major torso tissues, allows for objective investigation of static spine stability.

Methods: A novel previously fully validated spine model was employed. Major torso tissues, mainly the muscles, TLF, and IAP were individually, and in combinations, activated under a 350N external spine perturbation. The stability contribution exerted by these tissues, or their ability to restore the spine to the unperturbed position, was assessed in different case-scenarios.

Results: Individual activations recorded significantly different stability contributions, with the highest being the TLF at 75%. Combined or synergistic activations showed an increase of up to 93% stability contribution when all tissues were simultaneously activated with a corresponding decrease in the tensile load exerted by the tissues themselves.

Conclusion: This investigation demonstrated torso tissues exhibiting different roles towards static spine stability. The TLF appeared able to dissipate and absorb excessive loads, the muscles acted as antagonistic to external perturbations, and the IAP played a role limiting movement. Furthermore, the different combinations explored suggested an optimized engagement and coordination between different tissues to achieve a specific task, while minimizing individual work.

Keywords: Abdominal pressure, fascia, finite element model, low-back pain, muscle activation, paraspinals, simulation, spine, spine stability, thoracolumbar fascia.

5.2.2. INTRODUCTION

Spine's stability is believed to be maintained through the coordination of adjacent tissues[1,2]. In essence, paraspinal muscles are always thought of as first stabilizers, whereby spinal stability is

supported by a combination of muscle effort. Paraspinal muscle co-activation increases spine's compressive forces, stiffening the spine in all potential instability modes[3,4]. However, although muscle internal pressure, commonly referred to as intra-muscular pressure (IMP), has been proven to play an essential role in muscle contraction[5,6], the harmony between IMP and the muscle structure in potentially providing spinal stability is usually disregarded[7,8]. In addition, intra-abdominal pressure (IAP) is believed to stabilize the spine as illustrated via experimental[9] and analytical[8,10,11] studies. However, the coordination between the abdominal wall and IAP towards stability is often overlooked. Recently, the thoracolumbar fascia (TLF) has enticed researchers to investigate its role in load transfer mechanism, providing a foundational support to contacting tissues[12,13]. Although TLF has been mainly explored via mathematical modelling[14,15] and rather simplified geometries[16], its role as a static spinal stabilizer is gaining in acceptance.

The clinical quantification of spinal stability, as provided by the coordination of spinal muscles with their IMP, IAP, and TLF, is an arduous task due to the high number of tissues involved[17]. This limits *in vivo* studies but highlights the use of modelling, mainly finite elements (FE), as an excellent experimental platform to explore complex biomechanical problems[18]. Consequently, a timely, accurate, and fully representative FE human spine model has been previously developed and extensively validated by the authors for the purpose of carrying out spinal stability analyses[19], which are otherwise not possible *via ex vivo* and *in vivo* platforms.

Therefore, the purpose of the present study was to objectively investigate, via a fully controlled research platform, the individual and collective contribution of major torso tissues, mainly TLF, abdominal wall with its IAP, and spinal muscles with their IMP, towards static spinal stability.

5.2.3. MATERIALS AND METHODS

A. Brief FE Model Description

The developed FE model was based on MRI-scans acquired from an anatomography; a database of 3D MRI-based human body parts, namely, "BodyParts3D/Anatomography". It consisted of 17 vertebral bodies (12 thoracic and 5 lumbar) linked by 16 intervertebral discs, modelled as deformable volumetric bodies. The TLF was segmented from multiple scans and also modelled as

a deformable body. The longissimus, multifidus, psoas major, lateral intertransversarius, and latissimus dorsi muscles were included and modelled as fluid-filled pressurized tissues comprised of two-state, fluid and structure fields, as previously shown to be valid[20]. Lastly, IAP was modelled as a pressure build-up enclosed by an abdominal cavity, defined by the abdominal muscles. The full model is shown in Fig. 5–1. The model was then meshed via a novel technique, forcing adjacent surfaces to share the same nodes, whereby FE fixed contacts computations would be eliminated. This was achieved in steps using SpaceClaim (v.19.1, Concord, Massachusetts, United States) to define geometrical components and their associated visual meshes, then Blender (v.2.83.5, Netherlands) to align mesh nodes on contacting objects, and lastly ANSYS (v.19.1, Canonsburg, Pennsylvania, United States) to combine and transform visual into numerical meshes (Fig. 5–2). The resulting element size was 3mm, with tetrahedral elements created for volumetric bodies while triangular elements for surfaces of fluid-filled tissues. Detailed mesh characteristics can be found in another complementary study[19]. Lastly, material properties were incorporated[19].

B. Boundary and Loading Conditions

The model was previously validated against a numerical model, amongst many, constructed in LifeMOD[21], whereby a flexion force ranging from 0 to 350N was applied on the first thoracic vertebra (T_1), and displacements of vertebral bodies T_{10} to L_5 were recorded. The pressure in the intervertebral discs (IVDs) was recorded and validated against normal physiological ranges.

Static spinal stability, or equilibrium stability of the spine, is defined as the spine's ability to retrieve its initial position following an applied external perturbation[22]. That is, the contribution of spinal soft tissues to oppose external static loads dictates spinal equilibrium stability levels. As such, for the current study, the validated maximum T_1 force of 350N, imposing a flexion, was used as the external perturbation (Fig. 5–1). Thereafter, a specific set of soft tissues were activated to investigate their ability to restore the spine to its initial, unperturbed, position. Those activated tissues were based on a series of case-studies to be detailed. During each test, the sacrum's position was fixed. Furthermore, in tests where the TLF was included, the extremities of the tendons attached to the latissimus dorsi, the back muscle in contact with the TLF, were also fixed. All other tissues were free to deform, translate, and rotate in all degrees of freedom.

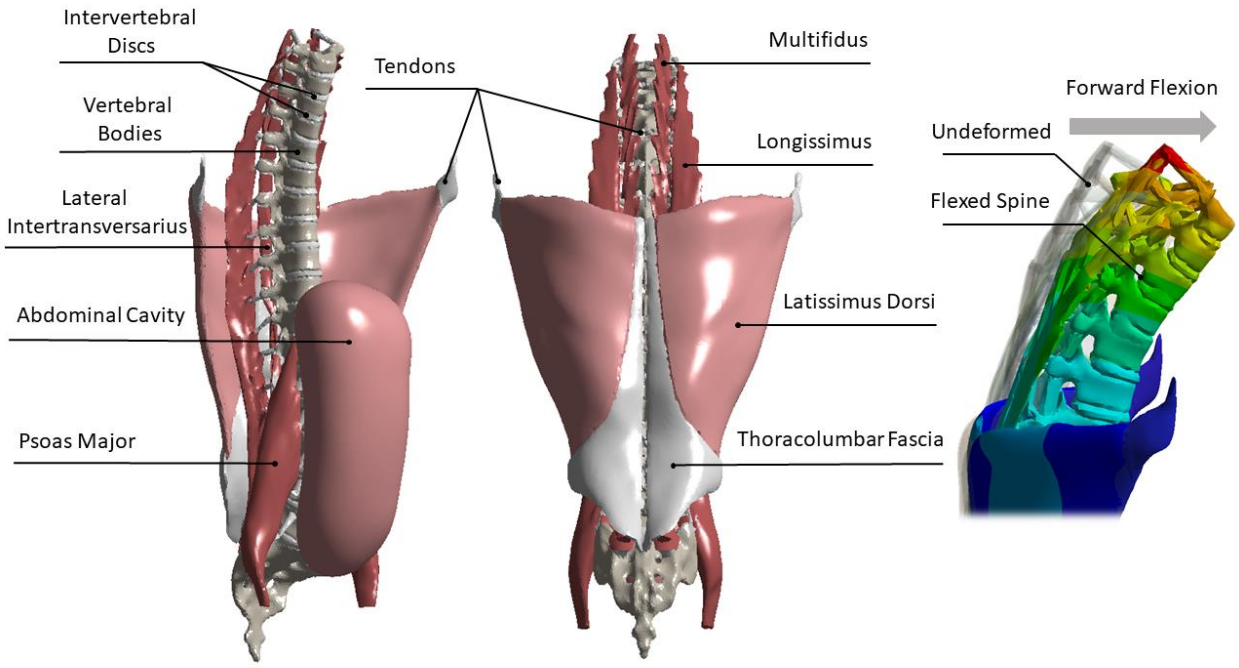

Figure 5–1: Depiction of the utilized spine model form.

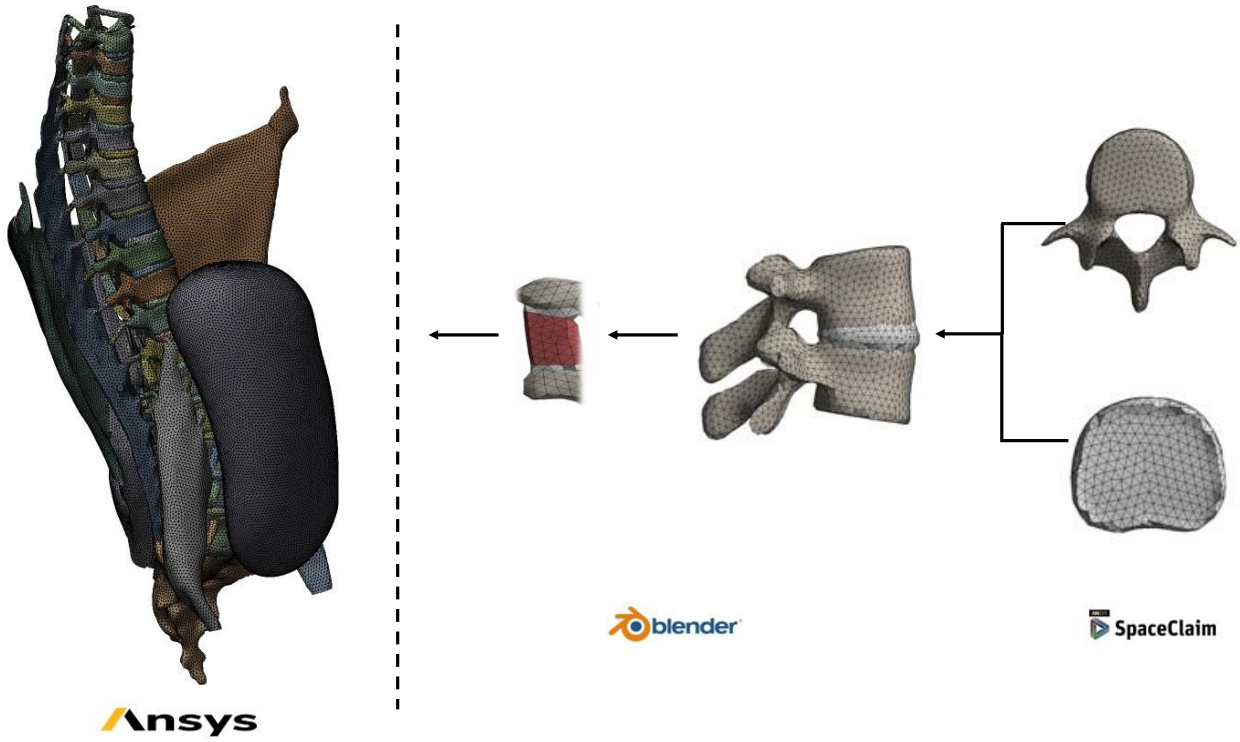

Figure 5–2: Depiction and steps realized to generate the finite element mesh.

C. Tests

- Case 0 (baseline): In this test, none of the tissues were activated. This served as the comparator, whereby under a forward flexion of 350N, L_1 to L_5 vertebral forward displacements, and IVD_1 to IVD_5 pressures were recorded.

The results of all subsequent tests were compared to case 0 in order to find the involvement of the tissue of interest to spinal stability, thus finding a percentage stability contribution computed by:

$$\%_{Stability\ Contribution} = \frac{|(Average\ Vertebral\ Displacements)_i - (Average\ Vertebral\ Displacements)_0|}{(Average\ Vertebral\ Displacements)_0} \times 100 \qquad (5.1)$$

where, *i is case 1, 2, …, or 8; while 0 is the baseline (case 0).*

- Case 1: Muscles were included as passive tissues only to investigate their individual stability contribution under passive conditions. With IMP being coded as active pressurized fluidic component inside each muscle, all such inputs were disabled in this case. Furthermore, all muscular force inputs, modelled as actin-myosin active components, were deactivated. This limits muscles' capabilities to only passive contraction generated by inherent material behavior and properties.
- Case 2: Muscles were included and activated for tensional force and corresponding IMP. In this test, along with subsequent ones inclusive of muscles, recorded EMG muscle forces[23] were introduced in each corresponding muscle as an antagonistic effect to the applied perturbation. These forces were also previously utilized to validate the model.
- Case 3: The thoracolumbar fascia (TLF) was solely engaged to investigate its individual stability contribution.
- Case 4: The abdominal wall, via its IAP, was solely activated to investigate its individual stability contribution. In this particular case, along with all subsequent ones where IAP was included, a 30 mmHg abdominal pressure was introduced[19,24].
- Case 5: Muscles were activated and the TLF was included.
- Case 6: Muscles and IAP were both activated.
- Case 7: IAP was activated and the TLF was included.
- Case 8: All tissues were included. With the muscles and IAP activated, as well as the inclusion of TLF, the overall stability contribution of the major torso tissues was investigated.

5.2.4. RESULTS

In accordance with previously validated results[19], for the baseline (case 0), forward vertebral body displacements were between 6.1 to 1cm, in the anterior direction, from L_1 to L_5 respectively and in a decreasing trend. IVD pressure increased from 0.50 to 0.54MPa between IVD_1 to IVD_5, also mimicking physiological documented values[19,25].

Under the identical conditions, case 1 recorded slightly smaller vertebral displacements (8% stability contribution) and IVD pressures (2%) when muscles were included as passive tissues only (Figs. 5–3 and 5–4). However, when muscles were activated, as per test 2, displacement results decreased to almost half of the baseline (53% stability contribution), with measured vertebral displacements between 2.9 and 0.4cm. Whereas an increasing IVDs pressure from 0.28 to 0.34MPa in the lumbar region was measured (Figs. 5–3 and 5–4), accounting for a 40% average difference from the baseline. Muscles activations were accompanied with an intramuscular pressure (IMP) varying from 258mmHg for the psoas major (P), 372mmHg for the longissimus (L), 94mmHg for the multifidus (M), to barely 12mmHg for all intertransversarius (I) muscles (Figure 5–5).

On the other hand, disregarding the muscular system, activating only the TLF, as per test 3, vertebral displacements decreased to a range of 1.4 to 0.3cm (75% stability contribution). The measured IVD pressures were between 0.24 to 0.29MPa, an average 49% decrease from the baseline (Figs. 5–3 and 5–4). As for test 4, solely activating the abdomen with a 30mmHg IAP showed the least individual tissue stability contribution (25%), recording a range of 4.6 to 0.7cm vertebral body displacements and 0.32 to 0.42MPa IVDs pressure with a 29% change from the baseline (Figs. 5–3 and 5–4).

As explained, tests 5 through 7 investigated a combination of the tissues of interest while test 8 included all tissues and activation together. Figs. 5–6 and 5–7 present these results, with Fig. 5–5 reporting the developed IMP for cases where muscles were activated. All aforementioned results were also numerically quantified in Table 5–1. As introduced earlier, stability contribution is the ability of a specific tissue to participate towards spine static stability, calculated in Table 5–1 as a percentage stability contribution relative to the baseline (case 0) using the average vertebral body displacements of each case as explained in the materials and methods section.

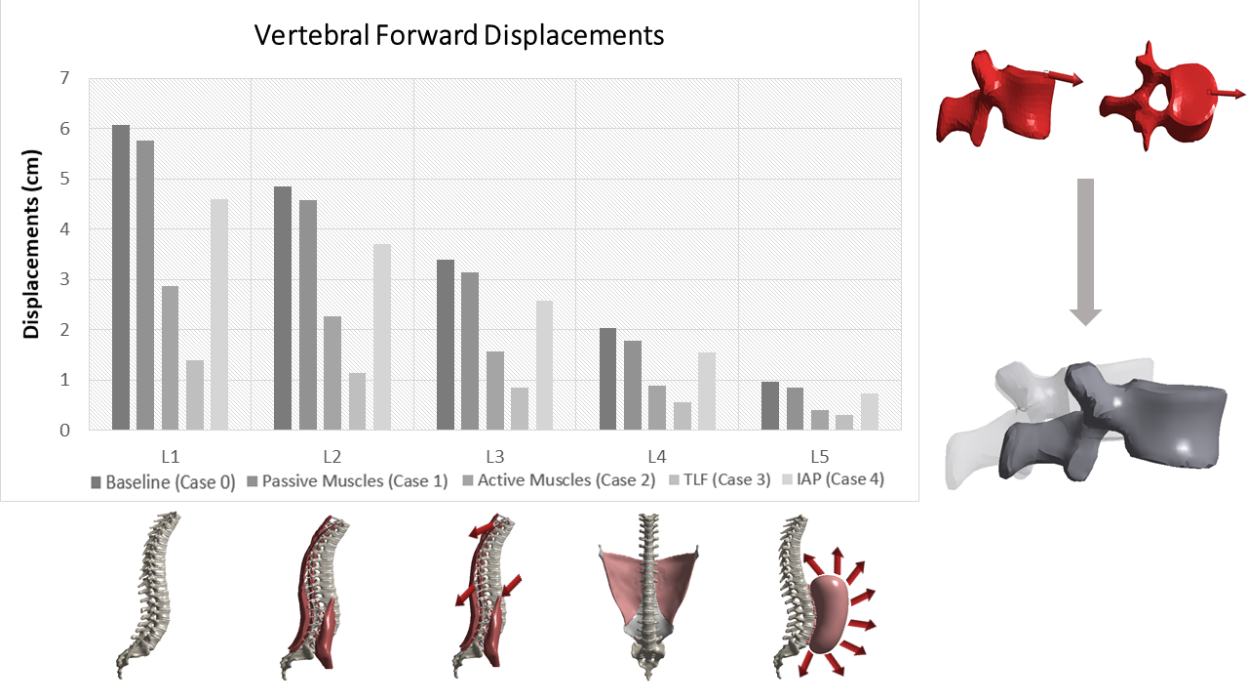

Figure 5–3: Vertebral forward displacements results for both the passive (case 1) and active (case 2) muscles conditions, thoracolumbar fascia 'TLF' inclusion (case 3), and intra-abdominal pressure 'IAP' activation (case 4), as compared to the baseline (case 0). L_1, L_2, L_3, L_4, and L_5 represent the first, second, third, fourth, and fifth lumbar vertebral bodies respectively.

5.2.5. DISCUSSION

Computational biomechanics by means of finite element models offers an objective and controlled platform to accurately represent and study the behavior of the human torso. When such models are appropriately validated and credible, they offer a complementary experimental platform to other *ex vivo* or *in vivo* studies. A number of prior research studies have analyzed spine stability, laying the foundations for this perplexing problem. Given the high number of tissues coordinating to achieve stability, simplifications are often required in experimental studies. These often include neglecting IMP and the TLF, or focusing only on active tissues, which may hinder results. Consequently, in the present study, a previously constructed and extensively validated novel three-dimensional full-scale FE model of the spine was leveraged towards analyzing individual and synergistic tissue contribution to static spinal stability. The model not only extends

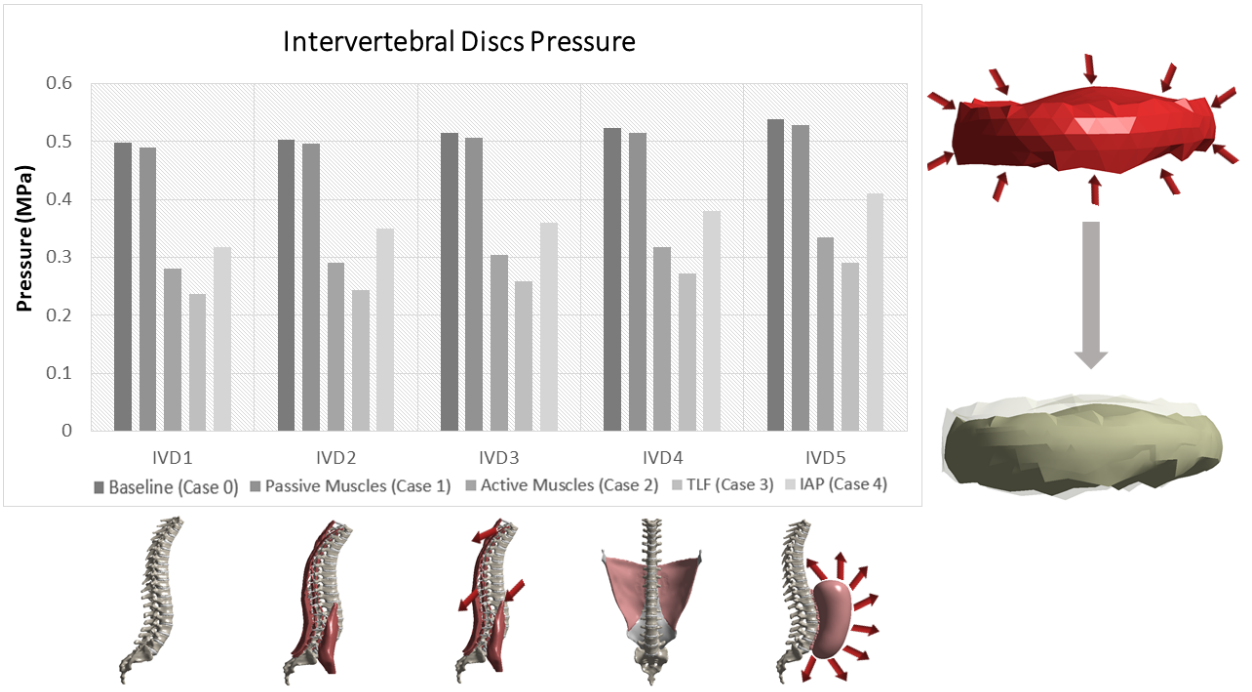

Figure 5–4: Intervertebral discs pressure results for both the passive (case 1) and active (case 2) muscles conditions, thoracolumbar fascia 'TLF' inclusion (case 3), and intra-abdominal pressure 'IAP' activation (case 4), as compared to the baseline (case 0). IVD_1, IVD_2, IVD_3, IVD_4, and IVD_5 represent the first, second, third, fourth, and fifth lumbar intervertebral discs respectively.

beyond the lumbar region and includes full thoracic spine, but also accurately represents IMP involved in active muscle contraction, IAP buildup inside the abdomen, and the full TLF tissue[19]. In the present study, each of the aforementioned tissue inclusions were considered individually and in combinations to explore their contribution to stability of the spine under external perturbations.

Under a 350N forward flexion force causing a perturbation, case 0 was performed to provide a reference or a validated comparator for all other cases, both in terms of vertebral displacements[21] and IVD pressures[25]. When investigating passive conditions (case 1), passive muscles contributed to about 8% of the simulated spine stability (Table 5–1), supporting previous claims made regarding the role of muscles coordination as active tissues towards stability and locomotion[26]. This was further emphasized by the results of case 2 when muscles were actively engaged, showing an individual contribution of 53% towards spine stability. This agrees with the potential

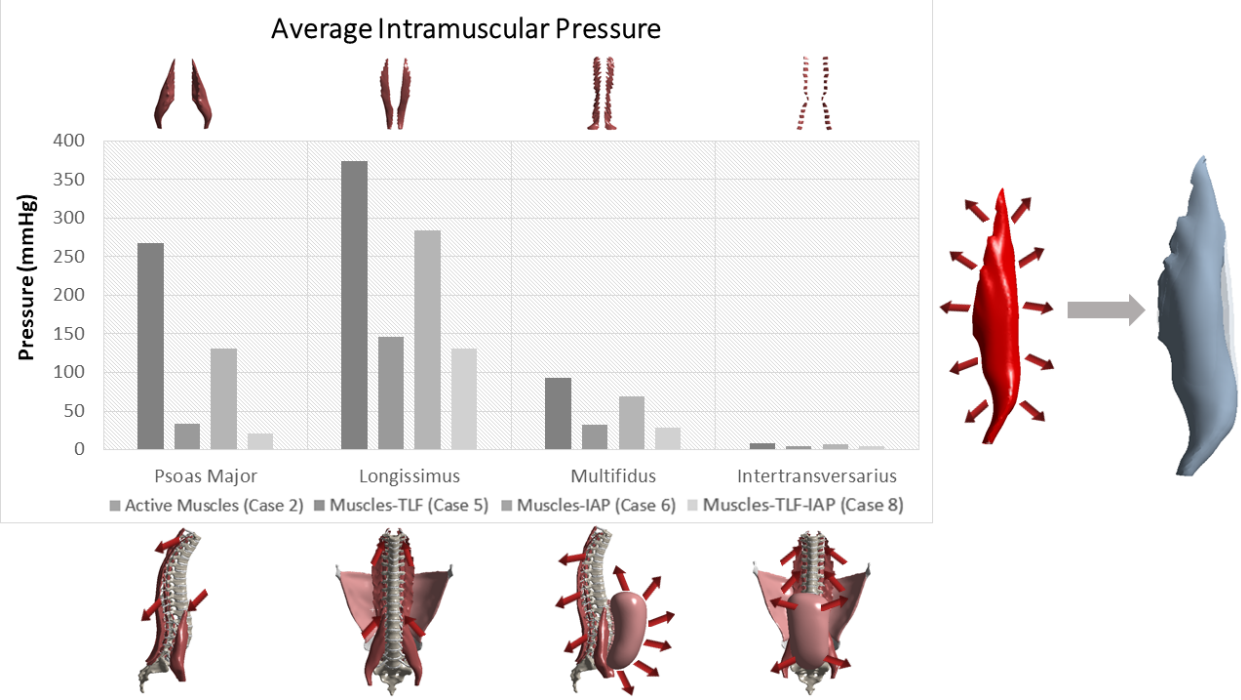

Figure 5–5: Intramuscular pressure 'IMP' results for the different cases in which muscles were activated. P, L, M, and I represent the psoas major, longissimus, multifidus, and intertransversarius muscles respectively.

antagonistic role of muscles to counter excessive loads faced by the spine under external perturbations. Such results, as well as previous studies[4,27], show the importance of increased muscle endurance to maintain spinal stability and as a protective measure against spinal deformities and conditions, such as low back pain (LBP). In other words, rehabilitation and clinical strengthening procedures of back muscles would increase muscular endurance, providing higher spinal stability, which would potentially help LBP patients. Besides, since a scoliotic spine is characterized by intrinsic instability[28], increasing spinal stability via muscle activation exercises can be a therapeutic strategy. However, spinal deformities are attributed to different causes, and are characterized by different bony alignments, to which physiotherapists should be careful which muscle groups, if any, to activate.

The results of individually including the TLF (case 3), showed a significant 75% contribution to stabilizing the spine as defined by static equilibrium. This contribution agrees with others who have researched or alluded the implications of the TLF in support of the spine[12–14]. To better

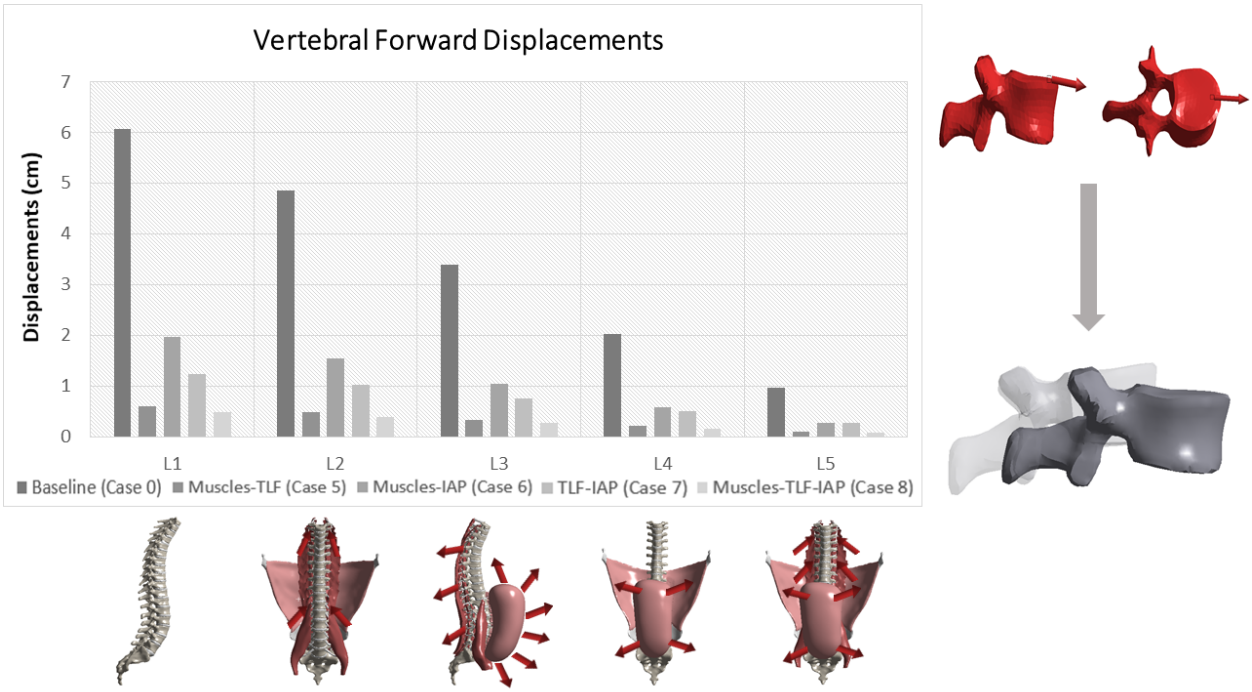

Figure 5–6: Vertebral forward displacements results for the different tissue combinations, cases 5 through 8, as compared to the baseline (case 0).

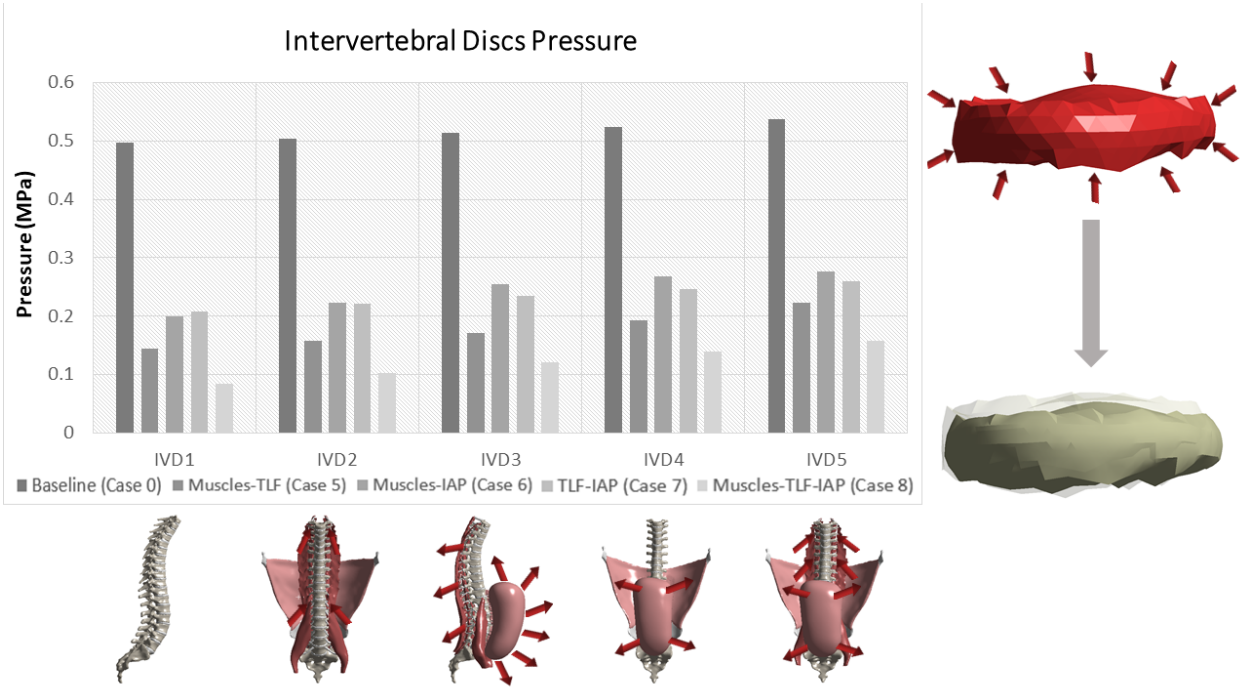

Figure 5–7: Intervertebral discs pressure results for the different tissue combinations, cases 5 through 8, as compared to the baseline (case 0).

Table 5-1: Results summary for all cases along with stability contribution

Cases	VBs Displacements (cm)					IVDs Pressure (MPa)					IMP (mmHg)				Stability Contribution
	L_1	L_2	L_3	L_4	L_5	IVD_1	IVD_2	IVD_3	IVD_4	IVD_5	P	L	M	I	
0	6.1	4.9	3.4	2	1	0.497	0.502	0.514	0.523	0.538	-	-	-	-	-
1	5.8	4.5	3.1	1.8	0.8	0.49	0.496	0.506	0.513	0.528	-	-	-	-	8%
2	2.9	2.3	1.6	0.9	0.4	0.28	0.29	0.304	0.318	0.337	258	372	94	12	53%
3	1.4	1.13	0.88	0.58	0.3	0.238	0.244	0.258	0.272	0.29	-	-	-	-	75%
4	4.6	3.7	2.5	1.5	0.7	0.321	0.348	0.353	0.376	0.418	-	-	-	-	25%
5	0.6	0.48	0.34	0.22	0.11	0.145	0.158	0.17	0.192	0.223	37	146	32	7	89%
6	1.9	1.55	1.1	0.65	0.25	0.2	0.22	0.258	0.268	0.279	132	287	31	10	69%
7	1.24	1.03	0.76	0.5	0.27	0.206	0.22	0.237	0.246	0.26	-	-	-	-	78%
8	0.47	0.37	0.26	0.16	0.08	0.084	0.103	0.12	0.137	0.158	21	128	26	6	93%

L_1, L_2, L_3, L_4, and L_5 represent the results for the first, second, third, fourth, and fifth lumbar vertebral bodies respectively. IVD_1, IVD_2, IVD_3, IVD_4, and IVD_5 represent the first, second, third, fourth, and fifth lumbar intervertebral disc respectively. P, L, M, and I represent the psoas major, longissimus, multifidus, and intertransversarius muscles respectively.

understand its role, the spine-TLF junctions were analyzed, showing elevated levels of tension developing at the contact points, which also agree with prior TLF studies[16]. As such, disrupting the fascial anatomy at TLF joints could reflect much less tensile forces, prohibiting the TLF from performing its stability role. Surgeons are thus advised to conduct minimally invasive spinal surgeries, such as IVD discectomy, without much TLF disruption, especially at its attachment points, to maintain higher spinal stability. Besides, stability provided by the TLF could have important clinical rehabilitation implications for patients with LBP. Studies have shown that fascia is the most sensitive deep tissue to pain in the lower back[29], and its dysfunction may hence play a major role in acute localized LBP. Physiotherapeutic exercises to strengthen the TLF, following spinal surgeries, could thus be of great help to limit the possibility of developing LBP episodes.

When including the abdomen with its IAP, results also support its growing understanding towards its potential role in spinal stability[30–32]. This measured 25% stability contribution is significant for a relatively small 30mmHg pressure build-up. Taking a closer look at the frontal side of the spine, the IAP vectors, by which it provided force interaction to the spine, seemed to have developed and converged to the anterior faces of the vertebrae bodies. As such, this suggests the resistive role of the IAP, exerting a counter effort to the spine during external perturbations imparting flexion. Thus, breathing and abdominal muscles activation exercises could be of great help to impose elevated IAP levels, within normal physiological ranges[33], to increase spinal stability.

When tissues were iteratively activated together, the spine stability increased but to different proportions when compared to those observed with individual tissues. This selective approach lends insight on the inter-coordination between these tissues in concert towards providing spinal stability and what influence they have on each other. That is, the TLF-muscle (case 5) combination led to a significant increase in stability but observed decrease in the muscle IMP. This may support the role of the TLF in support of the muscles as well as the spine, whereby the presence of the TLF may lead to less stress being imparted on the muscles. This is otherwise interpretable as requiring less muscle force to maintain stability as others have implied in the past[14,15]. The same appears to apply for cases 6 and 7 where the activation of IAP and muscles, as well as the TLF with IAP, may achieve a point where both tissues coordinate to stabilize the spine while their prior measure individual efforts are reduced consequently. Lastly, the activation of all tissues together, as

explored with case 8, supports this coordinative load sharing notion provided the individual effort of each tissue drops compared to all other cases explored. Specifically, an example is the drop in IMP for case 8, compared to cases 2, 5, and 6 (Table 5–1), while maintaining a 93% stability contribution. Case 8 does not only shine light on a potential optimized tissue activation, but further supports the notion that the tissues under consideration in the present study can be considered major players in static spinal stability.

Given the impact on stability of the tissues explored herein, accurate inclusion and modelling of such spinal tissues would provide great insights regarding designing and optimizing spinal instrumentations. Such efforts are in sync with growing trends that leverage numerical models in medical device design[34]. That is, validated models with representative spinal tissues can be used to compliment bench and clinical data towards the improvement and reliability of spinal instrumentation. Many research groups utilize modeling within their device design framework or assessment strategies[35–43]. The authors thus opine that as modeling and computing power progresses, it presents an opportunity to improve numerical models to be as physiologically accurate conditions as possible, to clinical initial and boundary conditions, perhaps leading to improve biomechanical understandings and corresponding device design.

A. Limitations

Similar to any *in silico* or finite element model, limitations are always present due to the model's numerical approach. However, with assumptions kept to a minimum, this does not limit model's ability to approximate and critically explore the overall biomechanical behavior of the spine. Some common modelling approximations, such as material properties, mesh, and model application, were justified and supported via previous successful validation efforts[19]. Another potential limitation is neglecting the contribution of the other torso tissues not explored herein such as ligaments and the rib cage. With the ligaments' role mostly coming into effect under high deformations[44], their elimination is a reasonable assumption as the present study only considered small static physiological loadings. In addition, the stabilizing action of the rib cage is mostly described by the dynamic respiration process[45], where it is believed to apply supportive spinal load as the lungs inflate. This effect is beyond the scope of this research, with static conditions being the primary focus. Under the above limitations, the model proved robust and underwent extensive

validation thus lending credibility and confidence to the relative tissue contribution towards static spine stability discussed herein.

In conclusion, this study leveraged a novel validated 3-dimensional finite element model of the spine inclusive of vertebral bodies, intervertebral discs, thoracolumbar fascia, accurate modelling of the abdominal pressure, and a fully representative model of the torso muscles to investigate their individual and combined contribution to static spinal stability. Several on-off case tests of these tissues were conducted and each revealed their respective and combined stability contribution. These novel analyses may provide insight towards how static spinal stability, as perceived in the present study, can be in part achieved or attempted via individual and/or combined torso tissue engagements.

5.2.6. KEY POINTS

- This study evaluated static spinal stability as provided by the synergistic activation of torso tissues.
- Thoracolumbar fascia, major torso muscles, and intra-abdominal pressure were major stabilizers, with a 93% overall stability contribution.
- The explored model suggested an optimized behavior provided by the surrounding active and passive tissues.

5.2.7. ACKNOWLEDGMENTS

We gratefully acknowledge funding by McGill University (MEDA), the Fonds de Recherche du Québec – Nature et Technologies (FRQNT), and the Natural Sciences and Engineering Research Center (NSERC). The authors also acknowledge that the 3D CAD model is based on a parametric 3D model from the Japanese Database ‘BodyParts3D/Anatomography’.

5.2.8. REFERENCES

1. Kavcic, N., Grenier, S. & McGill, S. M. Quantifying tissue loads and spine stability while performing commonly prescribed low back stabilization exercises. Spine (Phila. Pa. 1976). (2004). doi:10.1097/01.brs.0000142222.62203.67

2. Vera-Garcia, F. J., Brown, S. H. M., Gray, J. R. & McGill, S. M. Effects of different levels of torso coactivation on trunk muscular and kinematic responses to posteriorly applied sudden loads. Clin. Biomech. (2006). doi:10.1016/j.clinbiomech.2005.12.006

3. Gardner-Morse, M., Stokes, I. A. F. & Laible, J. P. Role of muscles in lumbar spine stability in maximum extension efforts. J. Orthop. Res. (1995). doi:10.1002/jor.1100130521

4. McGill, S. M., Grenier, S., Kavcic, N. & Cholewicki, J. Coordination of muscle activity to assure stability of the lumbar spine. J. Electromyogr. Kinesiol. (2003). doi:10.1016/S1050-6411(03)00043-9

5. Degens, H., Salmons, S. & Jarvis, J. C. Intramuscular pressure, force and blood flow in rabbit tibialis anterior muscles during single and repetitive contractions. Eur. J. Appl. Physiol. Occup. Physiol. (1998). doi:10.1007/s004210050381

6. Davis, J., Kaufman, K. R. & Lieber, R. L. Correlation between active and passive isometric force and intramuscular pressure in the isolated rabbit tibialis anterior muscle. J. Biomech. (2003). doi:10.1016/S0021-9290(02)00430-X

7. Cholewicki, J. & VanVliet Iv, J. J. Relative contribution of trunk muscles to the stability of the lumbar spine during isometric exertions. Clin. Biomech. (2002). doi:10.1016/S0268-0033(01)00118-8

8. Kavcic, N., Grenier, S. & McGill, S. M. Determining the stabilizing role of individual torso muscles during rehabilitation exercises. Spine (Phila. Pa. 1976). (2004). doi:10.1097/00007632-200406010-00016

9. Hodges, P. et al. Intervertebral Stiffness of the Spine Is Increased by Evoked Contraction of Transversus Abdominis and the Diaphragm: In Vivo Porcine Studies. Spine (Phila. Pa. 1976). (2003). doi:10.1097/01.BRS.0000096676.14323.25

10. Gardner-Morse, M. G. & Stokes, I. A. F. The effects of abdominal muscle coactivation on lumbar spine stability. Spine (Phila. Pa. 1976). (1998). doi:10.1097/00007632-199801010-00019

11. Cholewicki, J., Juluru, K. & McGill, S. M. Intra-abdominal pressure mechanism for stabilizing the lumbar spine. J. Biomech. (1999). doi:10.1016/S0021-9290(98)00129-8

12. Willard, F. H., Vleeming, A., Schuenke, M. D., Danneels, L. & Schleip, R. The thoracolumbar fascia: Anatomy, function and clinical considerations. Journal of Anatomy (2012). doi:10.1111/j.1469-7580.2012.01511.x

13. Driscoll, M. Fascia – The unsung hero of spine biomechanics. Journal of Bodywork and Movement Therapies (2018). doi:10.1016/j.jbmt.2017.10.014

14. Gracovetsky, S., Farfan, H. F. & Lamy, C. The mechanism of the lumbar spine. Spine (Phila. Pa. 1976). (1981). doi:10.1097/00007632-198105000-00007

15. Macintosh, J. E., Bogduk, N. & Gracovetsky, S. The biomechanics of the thoracolumbar fascia. Clin. Biomech. (1987). doi:10.1016/0268-0033(87)90132-X

16. El-Monajjed, K. & Driscoll, M. A finite element analysis of the intra-abdominal pressure and paraspinal muscle compartment pressure interaction through the thoracolumbar fascia. Comput. Methods Biomech. Biomed. Engin. (2020). doi:10.1080/10255842.2020.1752682

17. Panjabi, M. M. Clinical spinal instability and low back pain. J. Electromyogr. Kinesiol. 13, 371–379 (2003).

18. Trivedi, S. Finite element analysis: A boon to dentistry. Journal of Oral Biology and Craniofacial Research (2014). doi:10.1016/j.jobcr.2014.11.008

19. El Bojairami, I., El-Monajjed, K. & Driscoll, M. Development and validation of a timely and representative finite element human spine model for biomechanical simulations. Sci. Rep. (2020). doi:10.1038/s41598-020-77469-1

20. El-Bojairami, I. & Driscoll, M. Correlating Skeletal Muscle Output Force and Intramuscular Pressure via a 3-Dimensional Finite Element Muscle Model. J. Biomech. Eng. (In Submission)

21. Huynh, K. T., Gibson, I., Jagdish, B. N. & Lu, W. F. Development and validation of a discretised multi-body spine model in LifeMOD for biodynamic behaviour simulation. Comput. Methods Biomech. Biomed. Engin. (2015). doi:10.1080/10255842.2013.786049

22. Peter Reeves, N., Narendra, K. S. & Cholewicki, J. Spine stability: The six blind men and the elephant. Clinical Biomechanics (2007). doi:10.1016/j.clinbiomech.2006.11.011

23. Cholewicki, J., McGill, S. M. & Norman, R. W. Comparison of muscle forces and joint load from an optimization and EMG assisted lumbar spine model: Towards development of a hybrid approach. J. Biomech. 28, (1995).

24. Mueller, G. et al. Intramuscular pressure in the erector spinae and intra-abdominal pressure related to posture and load. Spine 23, 2580–2590 (1998).

25. Wang, S. et al. In vivo loads in the lumbar L3-4 disc during a weight lifting extension. Clin. Biomech. (2014). doi:10.1016/j.clinbiomech.2013.11.018

26. Van Dieën, J. H., Cholewicki, J. & Radebold, A. Trunk muscle recruitment patterns in patients with low back pain enhance the stability of the lumbar spine. Spine (Phila. Pa. 1976). (2003). doi:10.1097/01.BRS.0000058939.51147.55

27. Sajko, S. & Stuber, K. Psoas Major: a case report and review of its anatomy, biomechanics, and clinical implications. J. Can. Chiropr. Assoc. (2009).

28. Fusco, C. et al. Physical exercises in the treatment of adolescent idiopathic scoliosis: An updated systematic review. Physiotherapy Theory and Practice (2011). doi:10.3109/09593985.2010.533342

29. Schilder, A. et al. Sensory findings after stimulation of the thoracolumbar fascia with hypertonic saline suggest its contribution to low back pain. Pain (2014). doi:10.1016/j.pain.2013.09.025

30. Hodges, P. W., Shirley, D., Gandevia, S. C. & Physiotherapy, R. Lumbar spine stiffness is increased by elevation of intra- abdominal pressure 1. 3–5 (1999).

31. Kumar, S. & Davis, P. R. Spinal loading in static and dynamic postures : EMG and intra-abdominal pressure study. 0139, (2007).

32. McGill, S. M. & Norman, R. W. Reassessment of the role of intra-abdominal pressure in spinal compression. Ergonomics (1987). doi:10.1080/00140138708966048

33. Munns, S. L., Hartzler, L. K., Bennett, A. F. & Hicks, J. W. Elevated intra-abdominal pressure limits venous return during exercise in Varanus exanthematicus. J. Exp. Biol. (2004). doi:10.1242/jeb.01279

34. Driscoll, M. The Impact of the Finite Element Method on Medical Device Design. Journal of Medical and Biological Engineering (2019). doi:10.1007/s40846-018-0428-4

35. Guo, L. X. & Yin, J. Y. Finite element analysis and design of an interspinous device using topology optimization. Med. Biol. Eng. Comput. (2019). doi:10.1007/s11517-018-1838-8

36. Guan, W. et al. Spinal biomechanics modeling and finite element analysis of surgical instrument interaction. Comput. Assist. Surg. (2019). doi:10.1080/24699322.2018.1560086

37. Lin, H. M. et al. Biomechanical analysis and design of a dynamic spinal fixator using topology optimization: A finite element analysis. Med. Biol. Eng. Comput. (2014). doi:10.1007/s11517-014-1154-x

38. Robinson, Y., Lison Almkvist, V., Olerud, C., Halldin, P. & Fahlstedt, M. Finite Element Analysis of Long Posterior Transpedicular Instrumentation for Cervicothoracic Fractures Related to Ankylosing Spondylitis. Glob. Spine J. (2018). doi:10.1177/2192568217745068

39. Hsieh, Y. Y. et al. Removal of fixation construct could mitigate adjacent segment stress after lumbosacral fusion: A finite element analysis. Clin. Biomech. (2017). doi:10.1016/j.clinbiomech.2017.02.011

40. Karayannis, N. V., Jull, G. A. & Hodges, P. W. Physiotherapy movement based classification approaches to low back pain: Comparison of subgroups through review and developer/expert survey. BMC Musculoskelet. Disord. 13, 24 (2012).

41. Driscoll, M. et al. Biomechanical Comparison of 2 Different Pedicle Screw Systems During the Surgical Correction of Adult Spinal Deformities. Spine Deform. 3, 114–121 (2015).

42. Driscoll, M., Aubin, C. E., Moreau, A. & Parent, S. Biomechanical comparison of fusionless growth modulation corrective techniques in pediatric scoliosis. Med. Biol. Eng. Comput. (2011). doi:10.1007/s11517-011-0801-8

43. Clin, J. et al. Biomechanical Comparison of the Load-Sharing Capacity of High and Low Implant Density Constructs With Three Types of Pedicle Screws for the Instrumentation of Adolescent Idiopathic Scoliosis. Spine Deform. (2019). doi:10.1016/j.jspd.2018.06.007

44. Sharma, M., Langrana, N. A. & Rodriguez, J. Role of ligaments and facets in lumbar spinal stability. Spine (Phila. Pa. 1976). (1995). doi:10.1097/00007632-199504150-00003

45. Morris, J. M., Lucas, D. B. & Bresler, B. Role of the Trunk in Stability of the Spine. J. Bone Jt. Surg. (1961). doi:10.2106/00004623-196143030-00001

5.3. ADDITIONAL STUDIES RELATED TO SPINAL STABILITY

Coordinated activation and contribution of the set of soft tissues under study enhanced our understanding of the mechanisms at play to maintain equilibrium static spinal stability. Among which was the abdominal pressure, which appeared to produce supportive forces applied directly on the spine to limit its movement. The results of the 4th study gave further insights into an increased stability effort exhibited by the activation of the abdominal cavity when synergistically combined with other spinal tissues. However, the variabilities observed in anatomical and anthropometric data necessitated creating a patient-specific model of the abdominal cavity. In other words, the abdominal cavity is enclosed by a set of soft tissues, including the abdominal muscles and diaphragm, which exhibit very different properties from person to person. As such, abdominal data, reported in the literature review presented herein, from which abdominal models are generated, cover a wide range, to which end-results might show to be inconclusive. These collective variabilities can be explained by a person's 'abdominal compliance', or the measure of ease of abdominal expansion, which dictates if a person can sustain elevated abdominal pressure levels based on abdominal physiological properties. This presented the opportunity to investigate the effects of different physiologies on abdominal compliance in a static spine stability model.

In essence, an elevated abdominal compliance dictates that the abdomen can expand relatively freely, and vice versa. It is a parameter that is directly related to abdominal pressure and abdominal volume. As such, the proposed framework to evaluate spinal stability as a result of changes in abdominal compliance relies on abdominal cavity's governing physiological properties. Those primarily include modelled abdominal wall stiffness, thickness, and abdominal cavity's cross-sectional area. Equilibrium spinal stability, assessed in article 4, was thus further evaluated *via* supportive forces developed at the spinal connection levels with the abdominal wall and thoracolumbar fascia. This, in turn, would permit formulating a more comprehensive picture on

the mechanisms and physiologies maintaining stability, whereby the findings presented herein could allow to associate abdominal compliance, exercise, fat, and obesity conditions to spinal stability. Thus, patient-specific clinical recommendations to rehabilitate such conditions and improve stability become potentially possible. The outcomes of this investigation are presented in the manuscript entitled "Development and evaluation of a numerical spine model comprising intra-abdominal pressure for use in assessing physiological changes on abdominal compliance and spinal stability" for which the contribution of the first author is considered to be 65%. This manuscript was submitted to the *Clinical Biomechanics* journal on December 14, 2021.

5.3.1 ARTICLE 5: DEVELOPMENT AND EVALUATION OF A NUMERICAL SPINE MODEL COMPRISING INTRA-ABDOMINAL PRESSURE FOR USE IN ASSESSING PHYSIOLOGICAL CHANGES ON ABDOMINAL COMPLIANCE AND SPINAL STABILITY

Ibrahim El Bojairami[1,2]; Natasha Jacobson, Ph.D., P.Eng.[1,2]; Mark Driscoll, Ph.D., P.Eng.[1,2]

[1]*Musculoskeletal Biomechanics Research Lab, Department of Mechanical Engineering, McGill University, Montréal, Quebec, Canada*

[2]*Orthopaedic Research Laboratory, Department of Surgery, McGill University, Montréal, Quebec, Canada*

Address for notification, correspondence, and reprints:

Mark Driscoll, Ph.D., P.Eng., Assistant Professor

Associate Member, Biomedical Engineering

Canada NSERC Chair Design Engineering for Interdisciplinary Innovation of Medical Technologies

Department of Mechanical Engineering

817 Sherbrooke St. West

Montréal, QC, H3A 0C3 Canada

T: +1 (514) 398 – 6299

F: +1 (514) 398 – 7365

E-Mail: mark.driscoll@mcgill.ca

5.3.1.1 ABSTRACT

Background: Abdominal compliance is the "measure of ease of abdominal expansion" and determines whether a patient can withstand high intra-abdominal pressures. Thus, high compliance indicates that the abdomen can expand relatively freely, while low compliance restricts abdominal expansion.

Objective: The global objective of the present work is to evaluate the effect of physiological changes on abdominal compliance using a comprehensive spine finite element model inclusive of an abdominal model.

Methods: The effect of changing Young's modulus, abdominal wall thickness, and abdominal radii on abdominal compliance were evaluated. Intra-abdominal pressure and thoracolumbar fascia forces were also evaluated to assess abdominal physiological changes effects on overall static spinal stability.

Findings: Results showed that as wall thickness increased, compliance decreased. Similar findings were made with an increase in abdominal radius and Young's modulus. Furthermore, the active reduction in compliance, caused by increased elasticity and abdominal radius, resulted in an increase in spinal supportive forces originating from the thoracolumbar fascia and intra-abdominal pressurization, along with an increase in spine displacement from its original stable position. There was no clear stability identifiable trend for the case of changing abdominal wall thickness as fluctuations were present.

Interpretation: Investigated mechanics and data trends suggest that if one altered their active abdominal compliance, by way of increasing elasticity, they may have an improved stabilizing role on their spine.

Keywords: Intra-abdominal pressure, abdominal compliance, finite element modeling, spine stability, elasticity.

5.3.1.2 INTRODUCTION

Unhealthy abdominal mechanics have negative clinical implications. High levels of intra-abdominal pressure (IAP) are often caused by peritoneal inflammation and/or abdominal fluid build-up, typically as a result of acute abdominal injury or surgery[1]. Rates of high IAP, or, intra-abdominal hypertension, have been recorded in between 20 and 50% of intensive care unit patients, with rates increasing further in ventilated patients[2]. This increased IAP can reduce blood flow to vital organs, perpetuating further pressure build-up as organs become unable to drain excess fluids[1]. If a patient has low abdominal compliance (C_{ab}), the abdomen is unable to accommodate these high pressures and, thus, IAP may rise. Furthermore, low levels of IAP can be associated to poor spinal stability, a phenomenon linked to the onset of low back pain[3]. Thus, measuring and understanding a patient's C_{ab} may improve existing knowledge of diagnostics, monitoring, or treatment of unhealthy (high or low) levels of IAP, as well as provide insight toward static spinal stability.

Abdominal compliance is the "measure of ease of abdominal expansion"[1]. Thus, high C_{ab} indicates that the abdomen can expand relatively freely, while low C_{ab} restricts abdominal expansion. According to the World Society on Abdominal Compartment Syndrome (WSACS), C_{ab} can be determined given a change in intra-abdominal volume (IAV) and IAP [mL/mmHg][1,4]. This definition is not to be confused with its mechanical counterpart: the inverse of stiffness (S)[5]. Given that the stiffness matrix (modulus of elasticity) [kPa] describes a material's response to strain (ε), the mechanical compliance matrix [1/kPa] describes a material's response to stress (σ)[5]. Either stiffness or compliance, however, can be used to describe a material's overall behaviour[5]. More

comparable to the clinical definition for compliance is bulk modulus (or, modulus of compressibility [kN/m^2 or kPa])[6]. Bulk modulus describes a material's resistance to strain under hydrostatic pressure[6]. Given discrepancies between mechanical and clinical definitions, the definition identified by WSACS[1] will be used to describe C_{ab} for the purposes of the project put forth herein.

C_{ab} is a variable mechanical property directly affected by the elasticity of the abdominal wall (AW) and, to a lesser extent, the diaphragm[4]. As IAV increases, AW stiffness increases, resulting in a decrease in C_{ab}[4,7]. C_{ab}, as opposed to elastance, is the preferred medical term due to clinicians' familiarity with a similar measure, respiratory compliance[7]. Given the linear to exponential shape of the abdominal pressure-volume curve, it can be said that C_{ab} is constant until a critical IAV, at which time it begins to decrease[8,9]. Animals do not exhibit the same P-V curve shape as humans[10]. In animals, non-linearity is evident from baseline IAV[10]. As such, animal studies are not a reliable source of information when discussing C_{ab}. "Normal" C_{ab} values have been published as between 250 and 450mL/mmHg[8] in supine position, and reduce to 48mL/mmHg at sitting position[11]. Low C_{ab} prevents abdominal expansion, thus reducing the critical IAV at which IAP increases exponentially. Since C_{ab} is dependent on both the volume and pressurization of the abdominal cavity, distinction between passive and active compliance components can be discussed. In other words, passive respiration and stretching of the abdominal wall, for example, alter the passive component of compliance[12]. As such, "improving" passive C_{ab} is synonymous with increasing it, and can be accomplished with a healthy lifestyle, or, more immediately, with pharmaceutical intervention (such as neuromuscular blockers)[4,13]. Alternatively, women who have given birth have demonstrated increased passive C_{ab} due to the fascial stretching that accompanies pregnancy[13]. On the other hand, the active component of compliance can be altered *via* active inspiration and contraction of abdominal muscles[12]. A decreased compliance, in this case, could be beneficial due to abdominal role in subjecting the spine to higher supportive forces, and thus, increasing its stability[14]. As such, in contrast to the passive component, “improving” active C_{ab} can be though as synonymous with decreasing it. This can be accomplished by activating the abdominal muscles (muscles tone and their content inertia) in order to stiffen the abdominal cavity and increase IAP, which in turn decreases C_{ab}[15]. Thus, it was suggested that subjects who actively engage their abdominal muscles can improve their localized, instantaneous, active C_{ab} due to a decrease in apparent abdominal dimensions and an increase in IAP[12].

Computational techniques, namely Finite Elements (FE), have been extensively used in literature to analyze and understand human biomechanics[16]. Although C_{ab} has been mostly investigated via laparoscopy and clinical measurements[9,15,17], numerous FE models incorporating the AW and IAP have been developed due to the robustness and accuracy of the technique[18-20]. Some FE models introduced the effects of IAP as force vectors without inflation in the diaphragm/abdomen[21]. These models, however, prohibited C_{ab} analysis due to the absence of volumetric effects. On the other hand, other studies were successful in physiologically representing IAP as incompressible fluid embedded in a closed cavity[22], as well as representing the abdominal cavity encapsulated by three membrane layers[23].

Arguably, the inclusion of an abdominal model in a representative model of the spine would result in more accurate IAP findings[20]. To that matter, Meijer *et. al.* was the first to build a FE model of the trunk inclusive of the spine, ribcage, and the abdominal cavity[19]. Later, in a study developed by Ouaaid *et. al.*, an iterative kinematic-driven FE model to compute the muscular forces under different IAP levels was studied[24]. Another novel and comprehensive FE spine model, that fully represent spine tissues inclusive of an accurate cavity-based IAP model, is the one put forth by El Bojairami *et. al.*[20]. In this study, the abdominal cavity was modelled from MRI-scans of abdominal muscles and then coupled with pressure-based FE elements. This produced an accurate two-state, fluid-structure, IAP field and builds on this previously validated full spine model. This not only allows to assess C_{ab} under different physiological changes, but also discuss significance regarding static spinal stability.

The adoption of this accurate FE model was motivated by the "crude estimate" description of existing C_{ab} measurement methods[9]. Some studies have calculated C_{ab} given a change in IAV and corresponding change in IAP (typically measured during either abdominal drainage or peritoneal dialysis procedures), which was quantified as an inaccurate depiction of physiological conditions[7]. In Blaser *et. al.*'s review of C_{ab}, a wide variation in study results was presented[7]. This inconsistency suggests the need for further research to better understand abdominal mechanics related to compliance.

As such, the global objective of the present work is to evaluate the effect of physiological changes on C_{ab} using a fully representative FE spine model inclusive of an accurate fluid-structure IAP model. Evaluation of the effects of abdominal elasticity, wall thickness, and radius on C_{ab}

allows to assess such physiological conditions effects further objectively on static spinal stability observed from resultant supportive forces and spine displacements. The main contributions of this study can be summarized as follows:

- The adopted model, to the best of authors' knowledge, is the first to use a validated, two-state, fluid structure field of intra-abdominal pressure to assess abdominal elasticity, wall thickness, and radius physiological effects on abdominal compliance.

5.3.1.3 METHODS

A. Brief FE Model Description

The developed FE model was based on MRI-scans acquired from an anatomography; a database of 3D MRI-based human body parts, namely, "BodyParts3D/Anatomography". It consisted of 17 vertebral bodies (12 thoracic and 5 lumbar) linked by 16 intervertebral discs, modelled as deformable volumetric bodies. The thoracolumbar fascia (TLF) was segmented from multiple scans and modelled as a deformable body. IAP was modelled as fluid-filled pressurized cavity, enclosed by abdominal muscles, and comprised of two-state fluid and structure fields as previously shown to be valid[20]. Presented muscles followed a similar modeling procedure as that of IAP. The full model is shown in Fig. 5–8. The model was then meshed via a novel technique, forcing adjacent surfaces to share the same nodes, whereby FE fixed contacts computations would be eliminated. This was achieved in steps using SpaceClaim (v.19.1, Concord, Massachusetts, United States) to define geometrical components and their associated visual meshes, then Blender (v.2.83.5, Netherlands) to align mesh nodes on contacting objects, and lastly ANSYS (v.19.1, Canonsburg, Pennsylvania, United States) to combine and transform visual into numerical meshes. The resulting element size was 3mm, with tetrahedral elements created for volumetric bodies while triangular elements for surfaces of fluid-filled tissues.

The model then underwent rigorous credibility, verification, and validation assessments as detailed in another complementary study[20]. This served to assess model's decision influence and consequence in the context of use (CoU). In essence, a brief model risk assessment was first

conducted as per the American Society of Mechanical Engineer's (ASME's) V&V40 standard; a credibility assessment framework for computational models in medical applications[25]. Model form was firstly verified utilizing volume changes between the original scans and modelled numerical meshes, along a series of sensitivity analyses to verify numerical code, discretization error, and CoU discrepancies, as also suggested by Viceconti *et al*[26]. Thereafter, a series of 6 validation tests in efforts of methodically conducting a structure-by-structure validation, two for the muscle modelling procedure[27] and four for the whole spine model[20], were explored using previously validated *ex vivo*, *in vivo*, and *in situ* investigations. Additional model details, mesh characteristics, and prior material properties used in verification and validation can be found in another complementary studies[20,27].

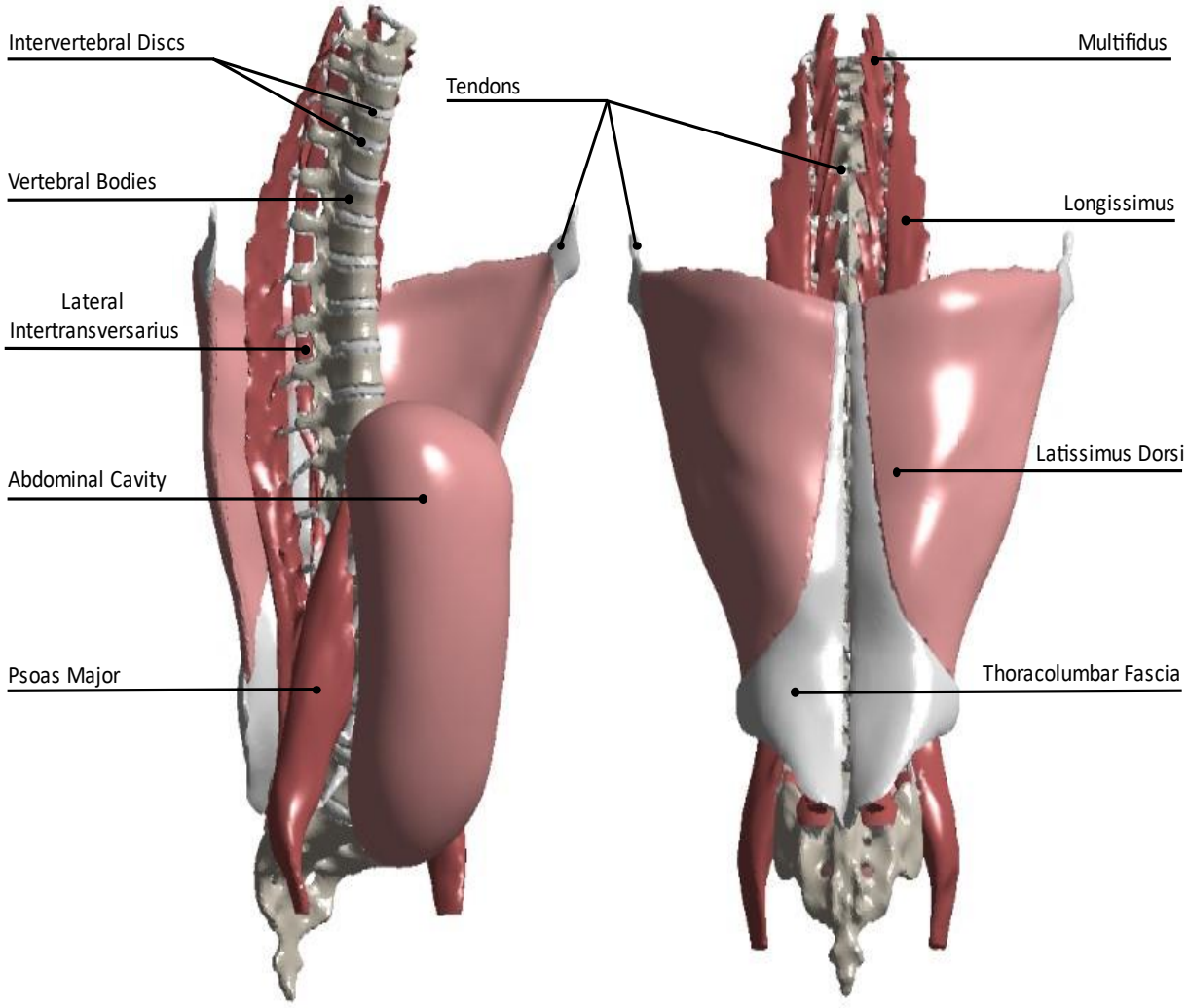

Figure 5–8: Finite element depiction of the utilized spine model.

B. Boundary and Loading Conditions

To simulate a static spine position, extremities of the latissimus dorsi as well as the sacrum were fixed. All other tissues were free to deform, translate, and rotate in all degrees of freedom. The only input was the IAP inside the abdominal cavity. This was coded via accurate special fluid elements, namely HSFLD242, in the commercial software ANSYS. Changes in abdominal cavity volume (ΔV), in response to IAP variations (ΔIAP), were measured to assess abdominal compliance using the following equation[9]:

$$C_{ab} = \frac{\Delta V}{\Delta IAP} \tag{5.2}$$

In order to assess the effect of abdominal physiological changes on C_{ab}, indirect validation was first carried out against the two prominent studies by Abu-Rafea *et. al.*[28] and McDougall *et. al.*[29]. As such, the model's ability to reproduce *in vivo* results was first assessed. To that matter, previously validated abdominal cavity material properties were adopted: Young's modulus of 25kPa and abdominal wall thickness (AWTh) of 9.7mm[20]. Thereafter, IAP was increased from 1.5 to 30mmHg, to which volume changes, and thus C_{ab}, were recorded and compared against Abu-Rafea *et. al.*[28] and McDougall *et. al*[29].

Tissue elasticity, defined by the Young's modulus (E), was the first physiological parameter of interest to investigate. As such, a wide range of E values, from as low as 10kPa, were collected[30-32]. While keeping other boundary conditions the same, including the same 9.7mm AWTh, the range of E (10kPa to 60kPa, in steps between 5 and 20kPa) was investigated. For each E value, IAP was similarly increased from 1.5 to 30mmHg in steps between 2.25 and 3.75mmHg, for which it was plotted against abdominal volume changes [L]. Thus, a set of C_{ab} curves were collected.

The second physiological parameter of interest was AWTh, for which reported values were collected[30,33,34] and a range of 5 to 20mm was simulated, in steps between 2.5 and 5mm. Similarly, other boundary conditions and material properties were maintained as the validation test, and thus, another set of C_{ab} curves were simulated. The last physiological parameter of interest was abdominal size, which translated into abdominal radius. As such, a range of 30 to 100mm abdominal radii was simulated in steps between 10 and 15mm while keeping other conditions similar to the validation case.

Lastly, the activation of IAP, alone, causes deviations from the initial spine static position. In response, this introduces radial forces on the spine (F_{IAP}), at the connection levels, in efforts of actively supporting the structure. This, by means of load transfer properties, in turn, puts the deep fibers of passive supportive tissues in tension mode. As such, the deep fibers of the TLF, one of the major supportive fascia of the spine, experience elevated tension forces in response to muscular or IAP activation. These sum up to an overall TLF reaction force (F_{TLF}) at the TLF-spine connection areas to counter the enforced relative spine displacement, *i.e.* in efforts of providing passive spinal stability. Static spinal stability is defined as the spine's ability to retrieve its initial position following an applied external perturbation[35]. As such, in the present study, IAP and TLF forces, along an average vertebral bodies' displacement, were defined as follows:

$$F_{IAP} = \left| \sum_{n=1}^{N} (\overrightarrow{F_n})_{elemental} \right| \tag{5.3}$$

$$F_{TLF} = \left| \sum_{m=1}^{M} (\overrightarrow{F_m})_{elemental} \right| \tag{5.4}$$

$$U = \frac{\left| \sum_{j=1}^{J} \left(\frac{\sum_{q=1}^{Q} (\overrightarrow{Uq})_{elemental}}{Q} \right)_j \right|}{J} \tag{5.5}$$

where F_{IAP} and F_{TLF} is the magnitude of the total amount of IAP and TLF forces exerted in efforts of supporting the spine, respectively. Variable U is the absolute average spine displacement caused by IAP activation as well as the difference between TLF and IAP supportive forces. The summations m and n are carried out over all FE elements in contact with the spine, while that of q is carried out over all vertebral bodies' elements. Lastly, the summation j is carried out over all vertebral bodies, *i.e.* up to a J = 17 (12 thoracic and 5 lumbar), to find an average spine displacement. These parameters allow to indirectly investigate the effect of changing E, AWTh, and radius on overall static spinal stability perceived by spine's supportive forces and displacement from its initial position.

5.3.1.4 RESULTS

A. Verification and Validation

Previously conducted verification tests, for the overall model, exhibited a maximum error of 8.7% corresponding to numerical mesh verification[20]. The first two validation tests, corresponding to muscles modelling procedure, showed a maximum discrepancy from the *ex vivo* comparators of 7.25%[27], recorded in terms of input muscle force and output muscular pressure. The four structure-by-structure, previously conducted, validation tests recorded a maximum difference of 13% from the comparators, recorded in terms of applied flexion and resultant lumbar vertebrae displacements[20]. Lastly, in one CoU whereby equilibrium spinal stability was examined, TLF behavior showed to be in line with previous observations in terms of developed and stored tensional forces[14].

On the other hand, in the current CoU of examining abdominal compliance, the presented simulations were validated against the works of Abu-Rafea *et. al.*[28] and McDougall *et. al.*[29] to confirm correct model function against experimental values. Fig. 5–9 illustrates the simulation results juxtaposed with validation data. Simulating the abdominal cavity with an increased pressure from 1.5mmHg to 30mmHg caused an increase in volume from 0.58 to 6.96L. Results of Abu-Rafea showed an increase in volume from 1.7 to 4.72L when the pressure increased from around 10 to 30mmHg. Although large discrepancies were observed with an average registered error of 13.1%, almost all simulated data points fell within reported standard deviations[28]. Similarly, for McDougall *et. al.*, for an increase in IAP from 5 to 30mmHg, a corresponding volumetric change of 0.66 to 6.75L was reported. Smaller discrepancies were observed, with an average error of 6.9%, and simulated data points also fell within reported standard deviations[29]. Widespread in validation data is indicative of the wide variation of patient-to-patient physiologies.

B. Changes in Abdominal Wall Elasticity

Changes in abdominal elasticity (Young's modulus, E) were made between E of 10kPa and 60kPa, with results summarized in Table 5–2. For each value of E, IAP was adjusted from 1.5 to 30mmHg, with the resulting abdominal volume measured. As E was increased, the range of resulting abdominal volumes decreased, from a maximum of 9.9L at an E of 10kPa, to a maximum

of 4L at an E of 60kPa. Fig. 5–10 illustrates the compiled data for each change in abdominal elasticity.

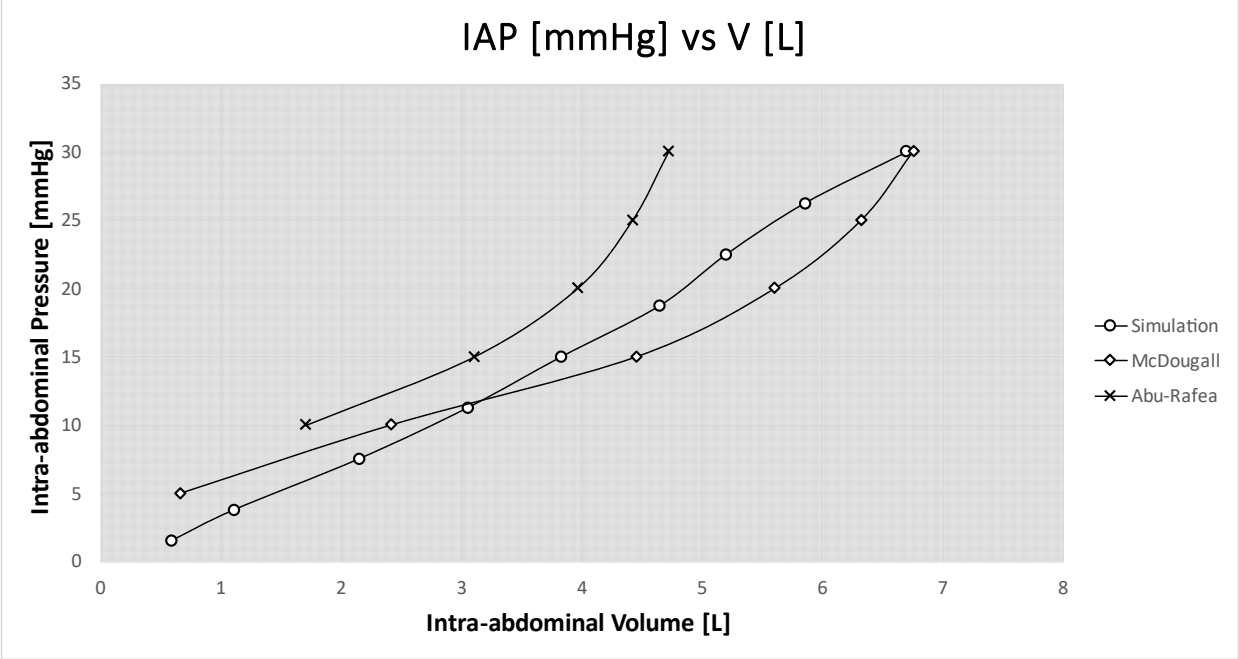

Figure 5–9: Simulated intra-abdominal pressure [mmHg] versus intra-abdominal volume [L] as compared against validation studies[28,29].

Table 5–2: Changes in abdominal elasticity and resulting abdominal compliance, stability, and force analyses

E [kPa]	C_{ab} [ml/mmHg]	F_{IAP} [N]	F_{TLF} [N]	U [mm]
10	340	20	15.4	7.05
15	290	26.7	20.1	11.02
20	250	29.2	22.7	15.35
30	200	33.6	26.6	19.87
40	180	36.1	28.8	20.59
60	160	42.7	34.5	25.83

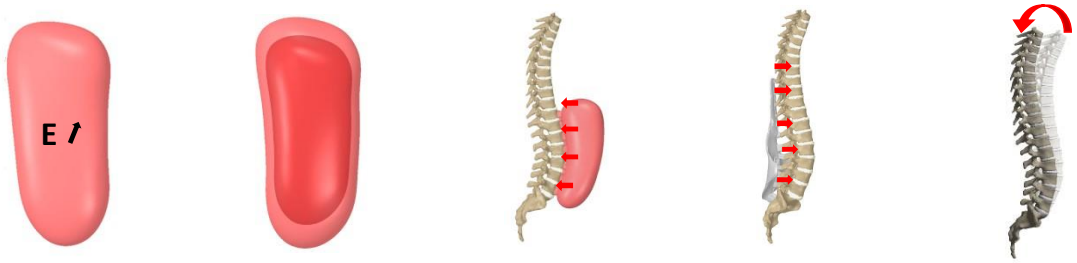

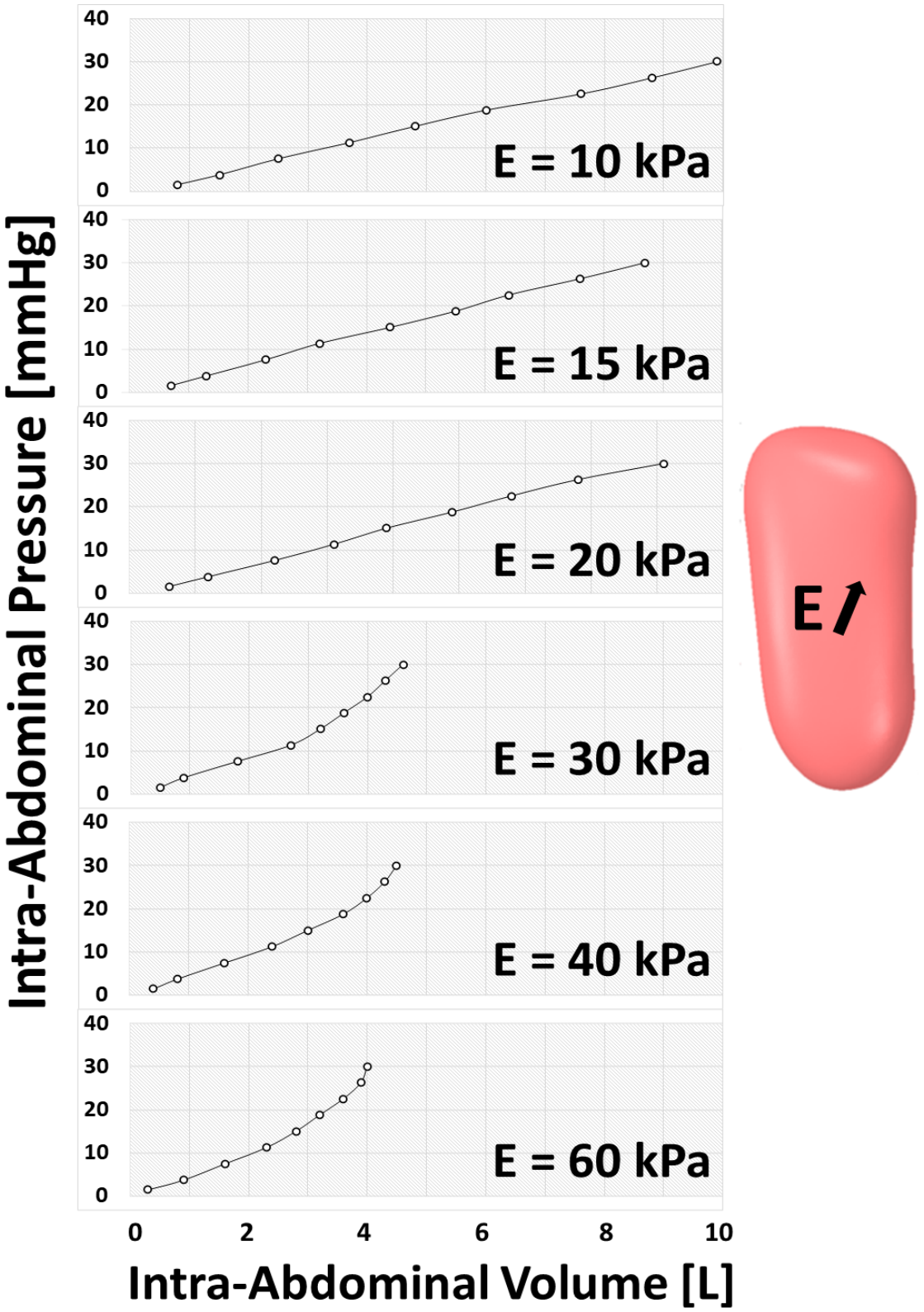

Figure 5–10: Intra-abdominal pressure [mmHg] versus intra-abdominal volume [L] for varying abdominal elasticities, as noted.

On the other hand, as E was increased, which led to a reduction in C_{ab}, IAP activation subjected the spine to F_{IAP} increasing in value from an average of 20 to 42.7N. Correspondingly, the TLF experienced an increase in fibers tensile forces, within the TLF tissue itself, resulting from the displacement imposed on the spine caused by IAP activation. These were translated by an overall TLF-spine contact forces ranging between 15.4 to 34.5N, opposite to the direction of displacement. Notably, as C_{ab} decreased, the spine experienced an average planar displacement increasing in value from 7.05 to 25.83mm (Table 5–2).

C. Changes in Abdominal Wall Thickness

Similarly, effect of changing abdominal wall thickness (AWTh) between AWTh of 5 and 20mm was investigated, with results summarized in Table 5–3. For each value of AWTh, IAP was adjusted from 1.5 to 30mmHg, with the resulting abdominal volume measured. As AWTh was increased, the range of resulting abdominal volumes decreased, from a maximum of 7.6L at an AWTh of 5mm, to a maximum of 5.4L at an AWTh of 20mm. Fig. 5–11 illustrates the compiled data for each change in abdominal wall thickness.

Table 5–3: Changes in abdominal wall thickness (AWTh) and resulting abdominal compliance, stability, and force analyses

AWTh [mm]	C_{ab} [ml/mmHg]	F_{IAP} [N]	F_{TLF} [N]	U [mm]
5	240	30.3	23.1	15.72
7.5	230	31.7	22.9	14.63
9.7	220	29.9	25.6	16.80
12.5	200	33.9	25.1	19.15
15	190	34.4	25.3	18.97
20	180	34.2	27.5	20.23

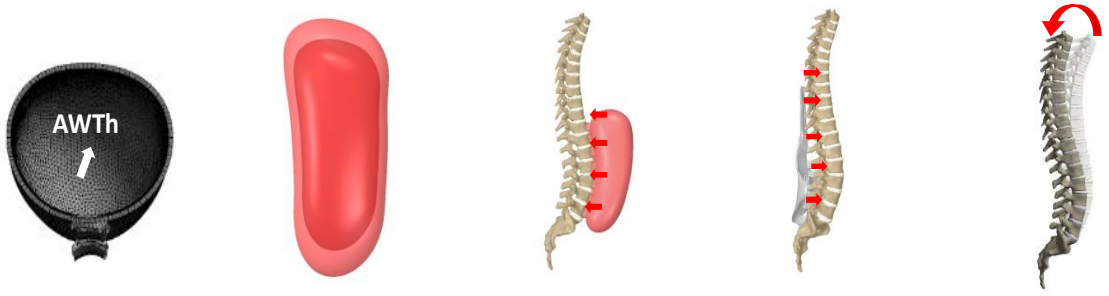

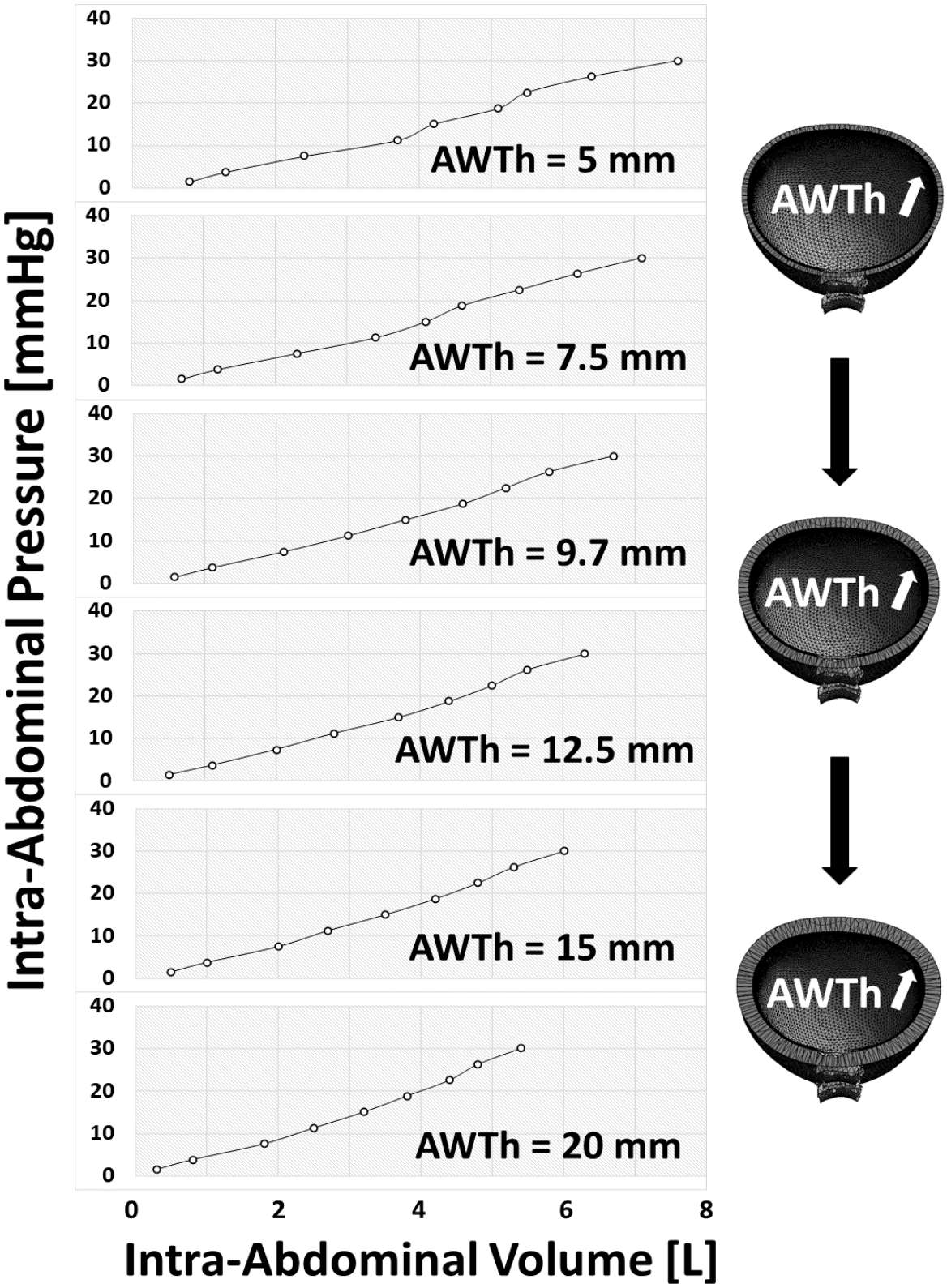

Figure 5–11: Intra-abdominal pressure [mmHg] versus intra-abdominal volume [L] for varying abdominal wall thickness (AWTh), as noted.

Furthermore, supportive spinal forces coming from the TLF and IAP activation, as well as resultant spine displacement, were also investigated as reported in Table 5–3. An increase in AWTh, accompanied with a reduction in C_{ab}, resulted in IAP forces fluctuating between 29.9 and 34.4N while between 22.9 and 27.5N for TLF forces, opposite to the direction of resultant displacement. As C_{ab} decreased, there was also no identifiable trend in spine displacement, with values ranging between 14.63 and 20.23mm (Table 5–3).

D. Changes in Abdominal Cross-Section

Lastly, effect of changing abdominal circumference between abdominal radii of 30 and 100mm was investigated, with results summarized in Table 5–4. For each value of abdominal radii, IAP was similarly adjusted from 1.5 to 30mmHg, with the resulting abdominal volume also measured. As abdominal radius was increased, the range of resulting abdominal volumes decreased, from a maximum of 7.2L at an abdominal radius of 30mm, to a maximum of 5.5L at an abdominal radius of 100mm. Fig. 5–12 illustrates the compiled data for each change in abdominal radii.

Table 5–4: Changes in abdominal radius and resulting abdominal compliance, stability, and force analyses

Radius [mm]	C_{ab} [ml/mmHg]	F_{IAP} [N]	F_{TLF} [N]	U [mm]
30	260	25.4	19.2	11.56
45	230	27.7	21	15.35
61.82	220	29.9	22.6	16.80
75	190	31	23.9	19.15
90	180	31.7	24.4	20.41
100	170	32	24.5	21.14

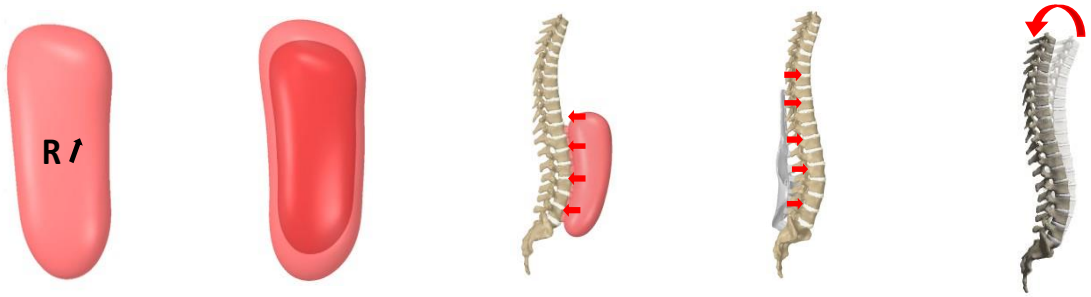

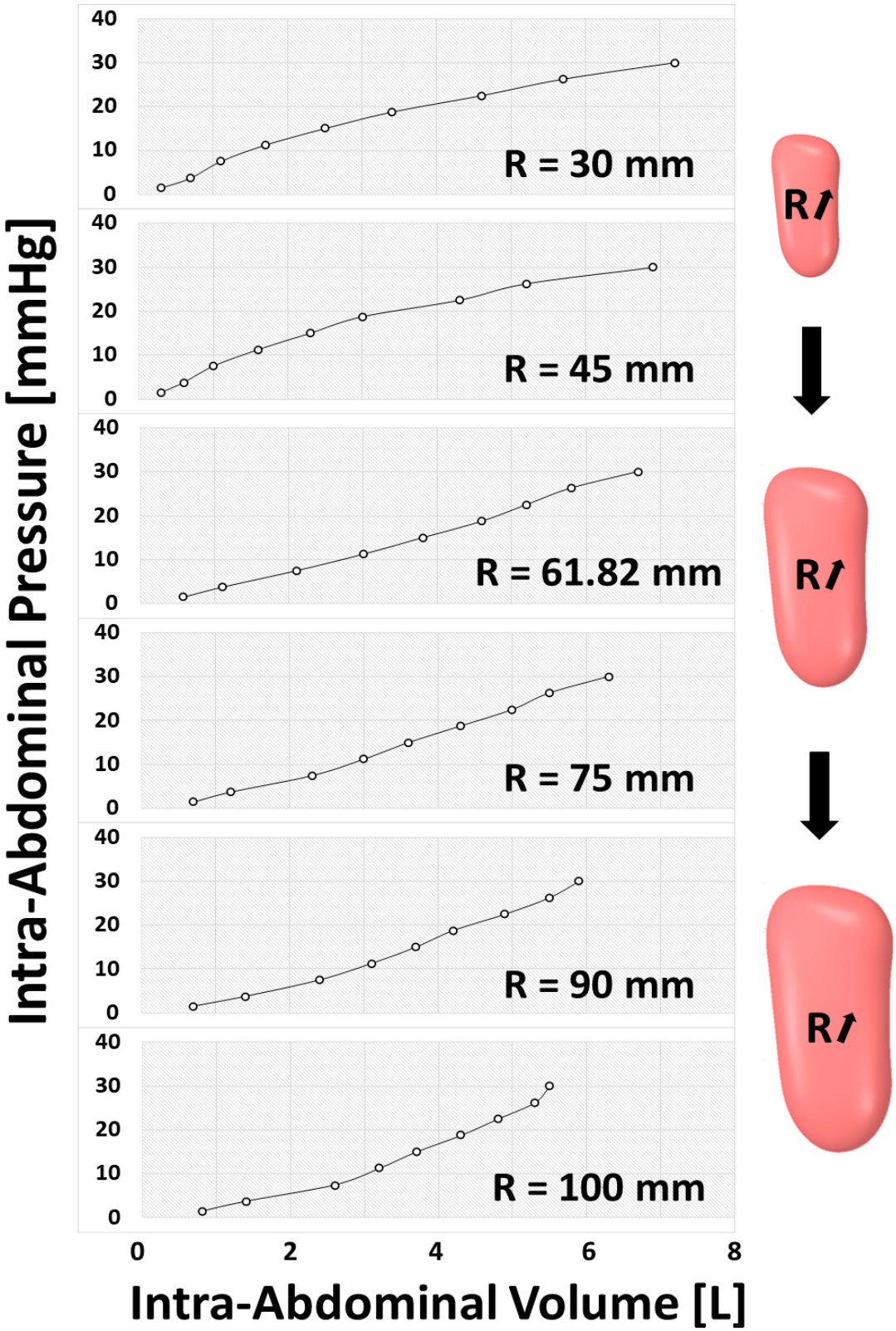

Figure 5–12: Intra-abdominal pressure [mmHg] versus intra-abdominal volume [L] for varying abdominal radii, as noted.

Spinal stability reflected by TLF and IAP forces supporting the spine, as well as overall spine displacement, were also investigated in this scenario, as reported in Table 5–4. Changes in abdominal radii, accompanied with a reduction in C_{ab}, resulted in an increase in IAP forces from 25.4 to 32N while from 19.2 to 24.5N for TLF forces, also opposite to the direction of resultant displacement. Similar to the first case, a reduction in C_{ab} was accompanied with an increase in overall spine displacement from 11.56 to 21.14mm (Table 5–4).

5.3.1.5 DISCUSSION

The purpose of this study was to exploit and validate a fully representative finite elements spine model, inclusive of an abdominal representation, in order to evaluate the effects of abdominal anatomical changes on abdominal compliance and static spine stability. The present model was successfully previously verified and validated within its CoU[20]. In particular, extensive carried out validation showed that the model may be potentially used to estimate muscle forces in a clinical setting[27] and permitted investigating equilibrium spinal stability[14]. This allowed examining the put forth CoU, namely investigating abdominal physiological changes on compliance and spinal stability. However, the model still underwent an additional validation test whereby its abdominal pressure and volume results were compared against previous work[28,29]. Simulated results were in good agreement and fell within standard deviations reported in the validation studies[28,29]. Specifically, a maximum discrepancy of 13.1% was registered against the study of Abu-Rafea, while 6.9% against the study of McDougall. Widespread in validation data was observed, which seemed to be indicative of the wide variation of patient-to-patient physiologies. Overall, simulated results closely resembled those of the compared studies, potentially validating the implemented methodology, and thus, the model can be used to investigate abdominal physiological parameters of interest.

A. Primary Findings

Investigated physiological changes included abdominal elasticity (Young's modulus), wall thickness, and cross-section. Findings suggested that C_{ab} is inversely related to AWTh, elasticity,

and cross-section. Of particular interest in results was the changes in non-linearity in circumferential data. Below a radius of 30mm, non-linearities presented a concave structure, whereas convex structures existed at radii above 60mm. In all results, the same IAP was applied. Therefore, it can be said that if there is a greater baseline volume, for the same amount of applied pressure (IAP), the abdomen is unable to inflate as much as its smaller counterparts. Clinically, this relates to a discussion on obesity. Greater resting IAP has been shown repeatedly in literature for patients with greater body mass indices (BMIs)[36,37]. However, perhaps of even greater interest is the combination of AWTh and circumference results, which may be viewed as stretching the abdomen and are thus translated into the passive component of C_{ab}. This could directly speak to the difference between gynoid and android obesity. Gynoid and android obesity refer to the cross-sectional shape and fat distribution in the abdomen. Gynoid obesity presents with an elliptical cross-section (thus, smaller net radii than its circular counterpart) and greater subcutaneous fat layer, whereas android obesity shows a circular cross-section and greater visceral fat layer[9]. It may be said that thickening fat layers at the abdomen, compounded with widening circumferences, as presented in android obesity, yield dangerously low levels of C_{ab} due to changes in its passive counterparts. This impression has been supported in previous clinical research[8,9].

Furthermore, results lend insight into the relationship between C_{ab} and AW elasticity. At increasing E, or stiffening, C_{ab} decreased. These results speak to the fact that, for the same IAP, patients are unable to create as much volume with stiffer abdomens. This finding has been supported, clinically, with research suggesting improved passive C_{ab} with fascial stretching of the AW due to pregnancy or exercise[7–9]. Conversely, poor passive C_{ab} (or low C_{ab}) has been shown in patients with greater AW scar tissue that has stiffened their AW[7–9]. Thus, it is recommended to practice stretching of the AW through exercise to support a healthier passive C_{ab} component.

On the other hand, IAP activation has been previously shown to directly affect spinal loadings and stability[38-40]. Besides, the thoracolumbar fascia is believed to be one of the strongest passive tissues supporting the spine. It has always enticed researchers to investigate its role in load transfer mechanism, providing a foundational support to contacting tissues[41,42], to which its role as a static spinal stabilizer is gaining in acceptance. As such, in efforts of assessing the effect of abdominal physiological changes on static spinal stability, vertebral IAP forces, TLF forces, and vertebral displacements were investigated. Findings showed that applying the same ranges of IAP while

increasing abdominal elasticity had the highest impact on load transmission and potentially stability. The reduction in C_{ab}, related to active augmentation of abdominal wall's elasticity, subjected the spine to IAP supportive forces ranging from 20 to as high as 42.7N with an accompanied spine displacement increasing from 7.05 to 25.83mm (Table 5–2). Changes in abdominal radius exhibited a similar trend but with a tighter range of 25.4 to 32N IAP forces and 11.56 to 21.14mm (Table 5–4). On the other hand, although the AW case was accompanied with a reduction in active C_{ab}, abdominal wall thickness did not seem to have a direct effect as fluctuations, but within an even a tighter range, were observed for both IAP forces and spine displacement (Table 5–3). Such findings may allow to associate abdominal compliance, exercise, fat, and obesity conditions to spinal stability as perceived by vertebral displacements from a stable static position. Based on the results, individuals who show improved active abdominal compliance, elasticity, and anatomy may further benefit from stabilizing effects as reported herein. In other words, should an external perturbation be applied on the spine trying to destabilize it, decreased compliance by means of active engagement of IAP can restabilize it *via* subjecting the spine to the high supportive forces and counter displacements reported herein. Furthermore, of particular interest were the results of the TLF which showed to store and redistribute excessive loads transmitted by nearby tissues. In all cases, the TLF showed elevated levels of fiber tensile forces, summed up and transferred to its contact areas, in efforts of providing passive spine stability. This significant contribution to stability agrees with others who have researched or alluded the implications of the TLF in support of the spine[41-45]. Therefore, stability provided by the TLF could have significant rehabilitation implications for patients with lower back pain, a condition that has also been associated with poor abdominal compliance[46,47].

Nevertheless, the results presented, herein, are of particular interest to a laparoscopic application. During laparoscopy, the abdomen is insufflated to create a chamber from which an operation can be performed[9]. With the given simulation, the prospect of individualized models is realized. Perhaps the present work may support the design of insufflation maxima and minima for a safe work environment, considering a patient's anthropometry, AW elasticity, and how these factors relate to C_{ab}, spinal loadings, and stability. At this time, recommendations can be made to limit insufflation in patients presenting with stiffer abdomens, larger abdominal cross-sections, and higher AW thicknesses. However, numerics on "healthy" ranges are not yet available.

B. Limitations

Similar to any *in silico* or finite element model, limitations are always present due to the model's numerical approach. However, with assumptions kept to a minimum, this does not limit model's ability to approximate and critically explore IAP, abdominal physiological changes, and associated spinal stability. Thus, given the underlying limitations, physiological effects on abdominal compliance and stability were still explored to a high accuracy level. Some common modelling approximations, such as material properties, mesh, and model application, were justified and supported via previous successful validation efforts[20,30-34]. Although most major tissues surrounding and affecting abdominal pressure build-up were included in the model, some other torso tissues were still not explored, such as ligaments. The elimination of ligaments was supported by the fact that their role mostly comes into effect under high deformations[48], to which the current research explored abdominal changes under static spine conditions. Lastly, IAP build-up was achieved via special fluid elements, creating a two-state, fluid and structure, field. Although this approach was previously validated by the current authors[20], an improvement could be to consider a fluid finite elements solver to model pressure streamlines inside the abdominal cavity more accurately. Yet, under the above limitations, the model proved robust and underwent extensive validation thus lending credibility and confidence to the effect of physiological changes on stability and abdominal compliance, as discussed.

5.3.1.6 CONCLUSION

The present work demonstrates the mechanical workings of abdominal compliance and suggests the efficacy of physiological changes to improve mechanical outcomes. To support the findings, herein, further research into a standardized C_{ab} meter is recommended for *in vivo* validation. Care was taken however to validate the model while the trends discussed agree with clinical observations. Developing such *in silico* models is a first step towards improving knowledge of local biomechanical implications of the abdominal cavity. Furthermore, it is an important step towards having complete numerical models of the torso, inclusive of abdominal compliance, as

the results herein highlight important model initial conditions that would impact the structural integrity of the abdominal region.

5.3.1.7 ACKNOWLEDGMENT

We gratefully acknowledge funding by McGill University (MEDA), the Fonds de Recherche du Québec – Nature et Technologies (FRQNT), and the Natural Sciences and Engineering Research Center (NSERC).

5.3.1.8 REFERENCES

1. Roberts, D. J., De Waele, J. J., Kirkpatrick, A. W. & Malbrain, M. L. N. G. Intra-abdominal hypertension and the abdominal compartment syndrome. in Surgical Intensive Care Medicine, Third Edition (2016). doi:10.1007/978-3-319-19668-8_46

2. Reintam Blaser, A. et al. Incidence, Risk Factors, and Outcomes of Intra-Abdominal Hypertension in Critically Ill Patients - A Prospective Multicenter Study (IROI Study). Crit. Care Med. (2019). doi:10.1097/CCM.0000000000003623

3. Stokes, I. A. F., Gardner-Morse, M. G. & Henry, S. M. Abdominal muscle activation increases lumbar spinal stability: Analysis of contributions of different muscle groups. Clin. Biomech. (2011). doi:10.1016/j.clinbiomech.2011.04.006

4. Malbrain, M. L. N. G. et al. The role of abdominal compliance, the neglected parameter in critically ill patients - A consensus review of 16. Part 1: Definitions and pathophysiology. Anaesthesiol. Intensive Ther. (2014). doi:10.5603/AIT.2014.0062

5. Hosford, W. F. MECHANICAL BEHAVIOR OF MATERIALS - SECOND EDITION. Zhurnal Eksperimental'noi i Teoreticheskoi Fiziki (2009).

6. Gere, J. M. Mechanics of Materials. 5th. Brooks Cole (2001).

7. Blaser, A. R., Björck, M., De Keulenaer, B. & Regli, A. Abdominal compliance: A bench-to-bedside review. J. Trauma Acute Care Surg. (2015). doi:10.1097/TA.0000000000000616

8. Malbrain, M. L. N. G., Peeters, Y. & Wise, R. The neglected role of abdominal compliance in organ-organ interactions. Critical Care (2016). doi:10.1186/s13054-016-1220-x

9. Ott, D. E. Abdominal compliance and laparoscopy: A review. Journal of the Society of Laparoendoscopic Surgeons (2019). doi:10.4293/JSLS.2018.00080

10. Yoshino, O., Quail, A., Oldmeadow, C. & Balogh, Z. J. The interpretation of intra-abdominal pressures from animal models: The rabbit to human example. Injury (2012). doi:10.1016/j.injury.2011.04.011

11. Tayebi, S. et al. A concise overview of non-invasive intra-abdominal pressure measurement techniques: from bench to bedside. Journal of Clinical Monitoring and Computing (2021). doi:10.1007/s10877-020-00561-4

12. Goldman, J. M., Rose, L. S., Morgan, M. D. L. & Denison, D. M. Measurement of abdominal wall compliance in normal subjects and tetraplegic patients. Thorax (1986). doi:10.1136/thx.41.7.513

13. On the abdominal pressure volume relationship. Internet J. Anesthesiol. (2012). doi:10.5580/892

14. El Bojairami, I. & Driscoll, M. Coordination Between Trunk Muscles, Thoracolumbar Fascia, and Intra-Abdominal Pressure Toward Static Spine Stability. Spine (Phila. Pa. 1976). (2021). doi:10.1097/BRS.0000000000004223

15. Sturini, E. et al. Respiratory variation of intra-abdominal pressure: Indirect indicator of abdominal compliance? Intensive Care Med. (2008). doi:10.1007/s00134-008-1155-z

16. Parashar, S. K. & Sharma, J. K. A review on application of finite element modelling in bone biomechanics. Perspect. Sci. (2016). doi:10.1016/j.pisc.2016.06.062

17. Papavramidis, T. S. et al. Abdominal compliance, linearity between abdominal pressure and ascitic fluid volume. J. Emergencies, Trauma Shock (2011). doi:10.4103/0974-2700.82205

18. Taylor, C. A., Hughes, T. J. R. & Zarins, C. K. Finite element modeling of three-dimensional pulsatile flow in the abdominal aorta: Relevance to atherosclerosis. Ann. Biomed. Eng. (1998). doi:10.1114/1.140

19. Meijer, G. Development of a non-fusion scoliosis correction device. Numerical modelling of scoliosis correction. (2011).

20. El Bojairami, I., El-Monajjed, K. & Driscoll, M. Development and validation of a timely and representative finite element human spine model for biomechanical simulations. Sci. Rep. (2020). doi:10.1038/s41598-020-77469-1

21. Stokes, I. A. F. & Gardner-Morse, M. Quantitative anatomy of the lumbar musculature. J. Biomech. (1999). doi:10.1016/S0021-9290(98)00164-X

22. Dietrich, M., Kedzior, K. & Zagrajek, T. Modeling of muscle action and stability of the human spine. in Multiple Muscle Systems 451–460 (Springer, 1990).

23. Arjmand, N., Shirazi-Adl, A. & Parnianpour, M. A finite element model study on the role of trunk muscles in generating intra-abdominal pressure. Biomed. Eng. Appl. Basis Commun. 13, 181–189 (2001).

24. El Ouaaid, Z., Shirazi-Adl, A., Plamondon, A. & Larivière, C. Trunk strength, muscle activity and spinal loads in maximum isometric flexion and extension exertions: A combined in vivo-computational study. J. Biomech. (2013). doi:10.1016/j.jbiomech.2013.06.018

25. ASME. Assessing Credibility of Computational Modeling and Simulation Results through Verification and Validation : Application to Medical Devices. Asme V&V 40-2018 (2018).

26. Viceconti, M., Olsen, S. & Burton, K. Extracting clinically relevant data from finite element simulations. Clin. Biomech. 20, 451–454 (2005).

27. El Bojairami, I. & Driscoll, M. Correlating Skeletal Muscle Output Force and Intramuscular Pressure via a 3-Dimensional Finite Element Muscle Model. J. Biomech. Eng.

28. Abu-Rafea, B., Vilos, G. A., Vilos, A. G., Hollett-Caines, J. & Al-Omran, M. Effect of body habitus and parity on insufflated CO2 volume at various intraabdominal pressures during laparoscopic access in women. J. Minim. Invasive Gynecol. (2006). doi:10.1016/j.jmig.2006.02.004

29. McDougall, E. M., Figenshau, R. S., Clayman, R. V., Monk, T. G. & Smith, D. S. Laparoscopic Pneumoperitoneum: Impact of Body Habitus. J. Laparoendosc. Surg. (1994). doi:10.1089/lps.1994.4.385

30. Song, C., Alijani, A., Frank, T., Hanna, G. B. & Cuschieri, A. Mechanical properties of the human abdominal wall measured in vivo during insufflation for laparoscopic surgery. Surg. Endosc. Other Interv. Tech. 20, 987–990 (2006).

31. Song, C., Alijani, A., Frank, T., Hanna, G. & Cuschieri, A. Elasticity of the living abdominal wall in laparoscopic surgery. J. Biomech. 39, 587–591 (2006).

32. Deeken, C. R. & Lake, S. P. Mechanical properties of the abdominal wall and biomaterials utilized for hernia repair. J. Mech. Behav. Biomed. Mater. 74, 411–427 (2017).

33. Tongyoo, A., Chatthamrak, P., Sriussadaporn, E., Limpavitayaporn, P. & Mingmalairak, C. Risk assessment of abdominal wall thickness measured on pre-operative computerized tomography for incisional surgical site infection after abdominal surgery. J. Med. Assoc. Thail. (2015).

34. Arjmand, N. Role of intra-abdominal pressure in the unloading and stabilization of the human spine during static lifting tasks. 1265–1275 (2006). doi:10.1007/s00586-005-0012-9

35. Peter Reeves, N., Narendra, K. S. & Cholewicki, J. Spine stability: The six blind men and the elephant. Clinical Biomechanics (2007). doi:10.1016/j.clinbiomech.2006.11.011

36. De Keulenaer, B. L., De Waele, J. J., Powell, B. & Malbrain, M. L. N. G. What is normal intra-abdominal pressure and how is it affected by positioning, body mass and positive end-expiratory pressure? in Applied Physiology in Intensive Care Medicine 2: Physiological Reviews and Editorials (2012). doi:10.1007/978-3-642-28233-1_22

37. Cobb, W. S. et al. Normal intraabdominal pressure in healthy adults. J. Surg. Res. (2005). doi:10.1016/j.jss.2005.06.015

38. Aspden, R. M. Intra-abdominal pressure and its role in spinal mechanics. Clinical Biomechanics (1987). doi:10.1016/0268-0033(87)90010-6

39. Daggfeldt, K. & Thorstensson, A. The role of intra-abdominal pressure in spinal unloading. J. Biomech. (1997). doi:10.1016/S0021-9290(97)00096-1

40. Hodges, P. W., Cresswell, A. G., Daggfeldt, K. & Thorstensson, A. In vivo measurement of the effect of intra-abdominal pressure on the human spine. J. Biomech. (2001). doi:10.1016/S0021-9290(00)00206-2

41. Willard, F. H., Vleeming, A., Schuenke, M. D., Danneels, L. & Schleip, R. The thoracolumbar fascia: Anatomy, function and clinical considerations. Journal of Anatomy (2012). doi:10.1111/j.1469-7580.2012.01511.x

42. Driscoll, M. Fascia – The unsung hero of spine biomechanics. Journal of Bodywork and Movement Therapies (2018). doi:10.1016/j.jbmt.2017.10.014

43. Gracovetsky, S., Farfan, H. F. & Lamy, C. The mechanism of the lumbar spine. Spine (Phila. Pa. 1976). (1981). doi:10.1097/00007632-198105000-00007

44. El-Monajjed, K. & Driscoll, M. A finite element analysis of the intra-abdominal pressure and paraspinal muscle compartment pressure interaction through the thoracolumbar fascia. Comput. Methods Biomech. Biomed. Engin. (2020). doi:10.1080/10255842.2020.1752682

45. El-Monajjed, K. & Driscoll, M. Investigation of Reaction Forces in the Thoracolumbar Fascia during Different Activities: A Mechanistic Numerical Study. Life 11, 779 (2021).

46. O'Sullivan, P. et al. Altered patterns of abdominal muscle activation in patients with chronic low back pain. Aust. J. Physiother. (1997). doi:10.1016/S0004-9514(14)60403-7

47. Helewa, A., Goldsmith, C. H., Lee, P., Smythe, H. A. & Forwell, L. Does strengthening the abdominal muscles prevent low back pain - A randomized controlled trial. J. Rheumatol. (1999).

48. Sharma, M., Langrana, N. A. & Rodriguez, J. Role of ligaments and facets in lumbar spinal stability. Spine (Phila. Pa. 1976). (1995). doi:10.1097/00007632-199504150-00003

5.4. SUMMARY

The central idea in this chapter was to advance the physiological notion of spinal stability by exploiting the validated spine model developed in chapter 4. The focus was on equilibrium, or static, spinal stability whereby the spine maintains a posture relatively similar to a starting one after an external perturbation is applied. This is the result of coordinated activation of a specific set of spinal tissues supporting the spine. Spinal muscles, thoracolumbar fascia, and abdominal pressure are believed to be major spinal stabilizers, to which their contribution to equilibrium spinal stability was examined in this chapter. This was achieved by applying a previously validated external forward flexion on the spine preceded by activating a tissue of interest. As such, case-scenarios of individual and combined activations of the aforementioned effects were executed

whereby the end-result, being spinal stability contribution, was evaluated *via* vertebral forward displacements. The study demonstrated that torso tissues exhibit different roles to stabilize the spine, among which is the antagonistic muscle effect and the thoracolumbar fascia force dissipation role. Lastly, the increase in intra-abdominal pressure showed to limit spinal movements and stiffen the abdominal cavity due to pressure increase accompanied with abdominal volume preservation. This produced a net effect of supportive forces applied directly on the spine.

The stabilizing role of the intra-abdominal pressure is governed by a number of physiological factors, which are key inputs to modelling the abdominal cavity. Those are mainly the stiffness, wall thickness, and cross-sectional are of the abdomen, which can be lumped into a parameter called the abdominal compliance. This motivated an additional study whereby the effect of changing these physiological factors on abdominal compliance, and further on spinal stability, was examined. In essence, the study showed that a decrease in abdominal active compliance, as a result of mainly augmenting stiffness and activation of abdominal cavity, was accompanied with increased stability along elevated tensioning of the thoracolumbar fascia. The study, thus, supported the efficacy of physiological changes to improve mechanical outcomes, among which is equilibrium spinal stability.

This chapter successfully completed objective 3, to which several research and application advances were achieved by means of confirming hypothesis 3. Firstly, stability results support the notion of increased muscle endurance to improve stability and protect against spinal deformities. Furthermore, the strong engagement of the thoracolumbar fascia towards maintaining spinal stability suggests the need for physiotherapeutic exercises, if possible, after a spinal surgery to strengthen its fibers and, in turn, decrease the possibility of experiencing low back pain. In addition, abdominal activation and the association between abdominal compliance and spinal stability suggests practicing breathing and abdominal activation exercises to limit spinal movement. Lastly, the experienced antagonistic role of muscles to counter excessive loads endured by the spine resulted in questioning the mechanisms governing such muscle activations. This directly led to investigating objective 4 as presented in chapter 6. All things considered, such advancements present insight into the accuracy and physiology of biomechanical computational models as means of improving biomechanical understandings and corresponding device design.

6

EXAMINATION OF MUSCLE ACTIVATION STRATEGIES IN A SPINE STABILITY MODEL

6.1. FRAMEWORK OF THE SIXTH ARTICLE

The successful completion of chapters 4 and 5 resulted in a validated, physiologically-representative, spine model exploited to investigate equilibrium spinal stability achieved by spinal tissues. In this context, preliminary assessments showed significant muscle contribution to maintain a stable spine posture, as defined in the dissertation herein. However, the spine is a statically undetermined system with a number of muscles exceeding its kinematic degrees of freedom. In other words, with muscles being the core of body's motor system, a spinal motor task can be executed in an infinite number of ways. This led to the general consensus in the scientific community that a musculoskeletal structure works in an optimized way to conduct a task. As a result of this, in the context of this dissertation, estimating individual muscle forces required to achieve stability became possible. However, conventional optimization approaches generally model muscles as force components, disregarding intramuscular pressure and other physiologies. At this point in this research, it has been already argued, and potentially shown, that such notions significantly contribute to the mechanics of muscles contraction and force transmission. As such, the study put forth aimed to exploit the spine model developed in chapter 4, and the preliminary results achieved in chapter 5, to investigate muscle activation and optimization strategies with the global objective of maintaining equilibrium spinal stability. Three conventional strategies were explored to further examine model's validity prior to formulating and exploring two novel pressure-based recruitment patterns. In all formulations, normal physiological constraints were placed on muscles activations with the global objective of maximizing spinal stability. The study

yielded insights on the activation of intramuscular pressure to execute efficient movements, minimize other spinal tissues efforts, and lead to less muscular fatigue. The outcome of this chapter marked the completion of objective 4, as well as affirmed hypotheses 4 and 5, as presented in the manuscript entitled "Formulation and Exploration of Novel, Intramuscular Pressure Based, Muscle Activation Strategies in a Spine Stability Model" for which the contribution of the first author is considered to be 85%. This manuscript was accepted at the journal of *Computers in Biology and Medicine* on March 21, 2022.

6.2. ARTICLE 6: FORMULATION AND EXPLORATION OF NOVEL, INTRAMUSCULAR PRESSURE BASED, MUSCLE ACTIVATION STRATEGIES IN A SPINE STABILITY MODEL

Ibrahim El Bojairami[1]; Mark Driscoll, Ph.D., P.Eng.[1]

[1]*Musculoskeletal Biomechanics Research Lab, Department of Mechanical Engineering, McGill University, Montréal, Quebec, Canada*

Address for notification, correspondence, and reprints:

Mark Driscoll, Ph.D., P.Eng., Assistant Professor

Associate Member, Biomedical Engineering

Canada NSERC Chair Design Engineering for Interdisciplinary Innovation of Medical Technologies

Department of Mechanical Engineering

817 Sherbrooke St. West

Montréal, QC, H3A 0C3 Canada

T: +1 (514) 398 – 6299

F: +1 (514) 398 – 7365

E-Mail: mark.driscoll@mcgill.ca

6.2.1. ABSTRACT

The spine is a naturally redundant, inherently unstable, and statically indeterminate biomechanical structure. To assess its stability, optimization models are often devised to determine spinal muscle recruitment patterns *via* estimating individual muscle forces. However, neglecting

muscles' fluidic behavior remains an approximation due to the role of muscle pressure in force transmission. The purpose of this study was to leverage a validated finite element (FE) model of the spine, inclusive of intramuscular pressure (IMP), to explore muscle recruitment patterns maintaining spinal stability. Three conventional strategies governing minimizing muscle effort, minimizing intervertebral discs compressive forces, and maintaining stability at all costs were first investigated to explore model's validity. Thereafter, two novel IMP-based strategies were devised and explored, specifically minimizing and maximizing IMP. Firstly, the model was previously shown valid in light of *in vivo* and *in silico* observations with an average discrepancy of 6%. This being the case, the conventional strategies dictated maximum muscular endurance while maintaining a stable position. A difference of up to 9.8% was observed against documented studies, whereby average vertebral bodies displacements, dictating a stable position, were as low as 0.04cm. In addition, the explored novel strategies suggested that an IMP of up to 1533mmHg potentially leads to sharing loads with surrounding tissues, whilst limiting the contraction of underlying muscles perceived by reaching a maximum constant force of 850N. This was supported by observations on the thoracolumbar fascia (TLF), whereby its fibers were subjected to extra tensional loads, reaching between 45 and 56.9N, under excessive IMP. This study validated a FE spine model inclusive of primary spinal supportive tissues, mainly pressurized muscles and the TLF. This validation further supported the notion of muscle activation strategies based on pressure, which the model was then leveraged to investigate. The explored IMP strategies may potentially serve to inform clinical applications such as motion analysis, device design for spine pathologies, rehabilitation, and functional electrical stimulation of muscles.

Keywords: Muscle activation strategies, muscle recruitment patterns, muscle optimization models, spine stability, finite element modelling, intramuscular pressure, thoracolumbar fascia, simulation, spine.

6.2.2. INTRODUCTION

A conservative estimate of the human body skeletal muscles is 630[1]. This greatly exceeds the number of kinematic degrees of freedom of the human motor system (roughly 244), thus producing

a redundant structure[1]. As such, each joint is considered a statically indeterminate system, to which there exists an infinite number of solution and ways to perform a motor task[2]. This has led to the development of optimization and electromyography (EMG) methods to estimate individual muscles force activation[3]. Optimization methods assume a specific muscle activation pattern in a way to optimize an objective function under physiological constraints[3]. Over the years, two distinct optimization types have been implemented for this problem: static and dynamic[4–8]. On the other hand, the EMG method exploits surface EMG recorded signals to compute individual muscle forces[3,9,10].

EMG approach requires a well-designed experimental setup, and are thus limited to laboratory based investigations[11]. In addition, EMG methods suffer from major shortcomings, are complex to design and maintain, and are susceptible to errors due to many reasons. Specifically, it is difficult to accurately measure EMG activity of deep and big muscles[12]. They require validated EMG-force relationships to estimate individual muscles effort[13]. Lastly, they suffer from cross-talk signals[14], signal processing issues and accuracy[15], and difficulties in measurement of maximal voluntary contraction required to normalize the signals[16]. Therefore, although EMG methods are widely used and advantageous in predicting antagonist muscle activation[17–20], their use is impractical in clinical, ergonomics, equilibrium, and stability applications[21,22]. On the other hand, optimization methods are easy to use, easy to develop, and can produce highly accurate results under physiological constraints[23,24]. Such physiological constraints are often bounds placed on muscle loads to prevent the adopted optimization from returning theoretical exaggerated forces[3]. Besides, in stability studies, additional constraints may be defined to limit the motion of the structure to within the scope of the research[25]. This would prevent excessive movements and allow the optimization to stay within a defined equilibrium stable position.

Over the years, special attention has been given to the spine due to its highly biomechanically redundant structure[1]. It is inherently unstable and requires recruitment of numerous muscles to ensure static stability and prevent buckling[3]. Numerous objective functions have been examined thus far to investigate muscle activation surrounding the spine. Those included: minimizing the sum of cubic muscle forces[26], minimizing total muscle stress[27], minimizing intervertebral discs (IVDs) forces[28], maintaining equilibrium stability at all costs[29], and minimizing or reversing a spinal deformity[24]. In addition, combining multiples of these objective functions for an overall

stability have been investigated[3]. However, no optimization model to date has accounted for muscle internal pressure, let alone investigating spinal stability achieved by intramuscular pressure-based optimization objective functions.

Skeletal muscles are biological soft tissues composed of about 80% fluidic content by volume[30]. Upon contraction, this enclosed fluid creates a regional hydrostatic stress inside muscles called intramuscular pressure (IMP)[31–33]. IMP has been shown to be an important parameter that is directly correlated to EMG measurements[34], estimated muscle force[35], as well as isokinetic[36] and dynamic[37] exercises. IMP is also believed to influence muscle performance by directly opposing sarcomere shortening forces[38]. Besides, it is an important metric in tissue nutrition, viability, and diagnosis of compartment syndrome[39–41]. As such, researchers have been able to create custom finite elements (FE) models of skeletal muscles to account for and incorporate IMP behavior. In fact, a handful of state-of-the-art muscle FE models have been developed to represent the biphasic, fluid-structure interaction, behavior of skeletal muscles brought about by their internal fluidic content[42–44]. However, despite the proven significant role of IMP during muscle activation, as well as its available custom and accurate depiction, this fluidic behavior is omitted when conducting stability, muscle recruitment, activation, and force optimization analyses.

As such, the purpose of the present study was to leverage a state-of-the-art, validated, representative, and IMP-inclusive, FE model of the spine[42] (Fig. 6–1), to investigate muscle activation and optimization strategies towards maintaining spinal stability. Three conventional objective functions were first studied to ensure model validity in this context of use and serve as a baseline. This included minimizing muscle effort (sum of cubic muscle forces), minimizing IVD compression (sum of squared IVD forces at the L_4-L_5 level), and absolute stability at all costs (minimum spine displacement within physiological range of activation). Lastly, two new and novel IMP-based objective functions were formulated to investigate the effect of pressure inclusion on muscle activations around the spine. This included minimizing and maximizing IMP levels during muscular contraction.

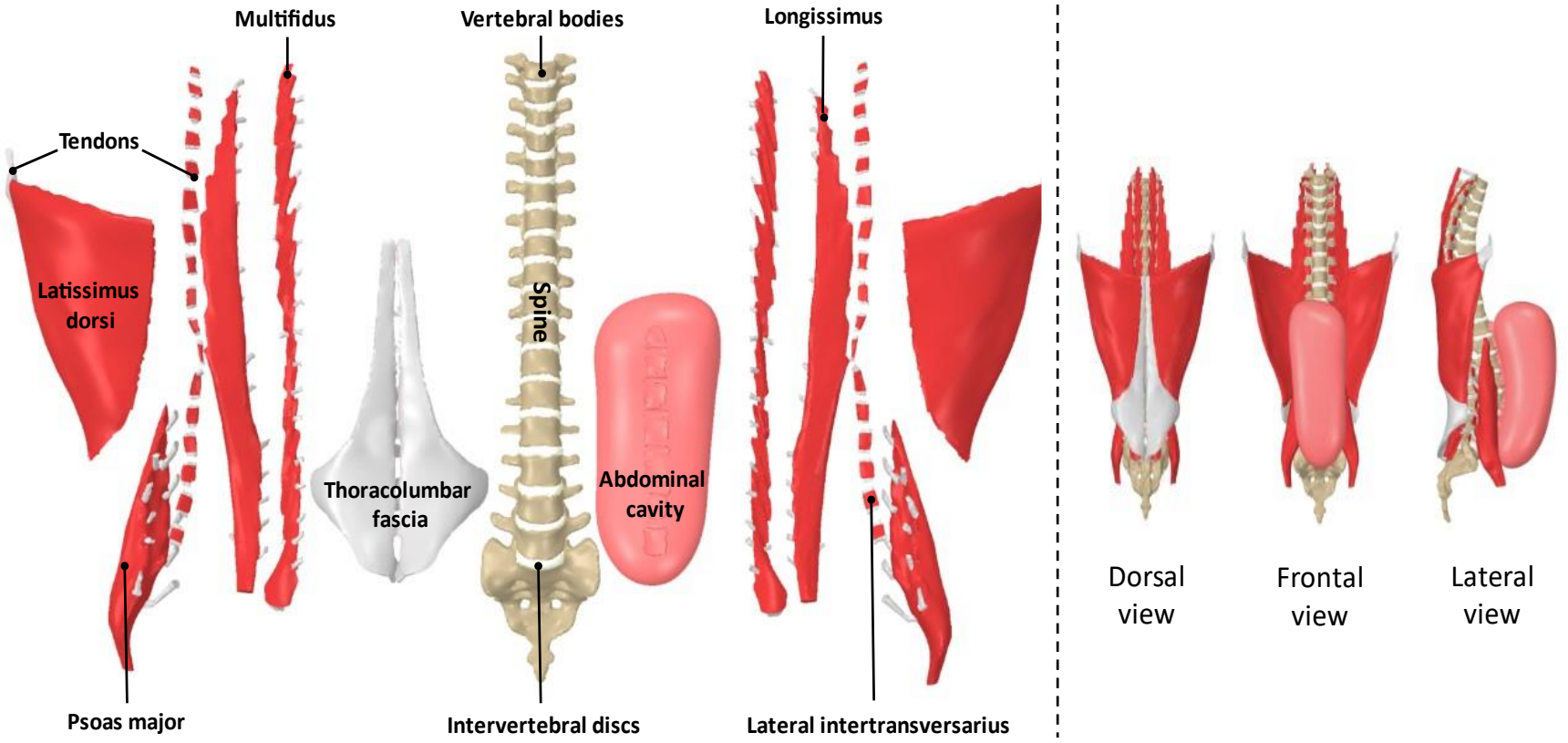

Figure 6–1: Overview and breakdown of the utilized spine model.

6.2.3. METHODS

A. Brief Overview of the Spine FE Model

The spine model form was based on magnetic resonance imaging (MRI) scans acquired from an anatomography; a database of three-dimensional MRI-based human body parts named "BodyParts3D/Anatomography". The developed FE spine model, using ANSYS (v.19.1, Canonsburg, PA), combines 17 vertebral bodies (thoracic and lumbar regions) interconnected by 16 IVDs, all modeled as volumetric deformable bodies. The model includes the thoracolumbar fascia (TLF), a tissue that previously validated spine models explored its contribution to stability[45]. The TLF was based on segmented scans and also modeled as a deformable structure. Furthermore, the model also included the longissimus, multifidus, psoas major, lateral intertransversarius, and latissimus dorsi as previously explored[45]. These skeletal muscles followed a previously developed and validated biphasic model, whereby muscles were modeled as fluid-filled pressurized tissues comprised of two-state, fluid and structure fields[42,46]. This would permit to engage, measure, and manipulate skeletal muscles' internal pressure, or what is referred to as intramuscular pressure (IMP). Lastly, intra-abdominal pressure (IAP) was modeled as a pressure build-up enclosed by an abdominal cavity, defined by the abdominal muscles. A depiction of the full model and involved tissues is shown in Fig. 6–1.

The numerical mesh was then generated *via* a previously employed technique, whereby adjacent surfaces are forced to share the same nodes, and thus, FE fixed contacts computations would be eliminated. The result was a uniform and smooth 3 mm element size mesh, with tetrahedral elements generated for volumetric bodies while triangular elements for surfaces of fluid-filled tissues. Further details on model description and mesh characteristics can be found in another complementary study[42]. Lastly, material properties were incorporated, again reflective of prior validated model[42]. This included a modulus/Poisson's ratio of 12GPa/0.3 for vertebral bodies and 25kPa/0.45 for the abdominal wall. The rest were modelled as incompressible with a modulus of 1GPa for tendons, 450MPa for the TLF, 42.7MPa for IVDs, 0.52MPa for the psoas major, and 36.87kPa for the rest of the muscles.

B. Loading and Boundary Conditions

The model loading conditions followed a previously conducted study on muscular optimization strategies while constraining spinal stability[3]. The authors examined a number of experimental static conditions comprising anterior and lateral bending. In short, the subjects performed a number of tasks which produced an average flexion moment of around 30N.m. Thereafter, the authors examined numerous objective functions conditions, among which are to minimize muscle and IVD forces, which permitted to explore individual muscle forces in order to achieve stability. This was examined using EMG data and a vectoral muscle-fascicle model that they developed based on a study by Cholewicki and McGill[47]. As such, the same loading condition was utilized in the present study.

For the purpose of the present study, static spinal stability is defined as the ability of select tissues to restore the spine's initial position following an applied external perturbation[48]. As such, for the current study, the validated experimental flexion moment of 30N.m was used as the external perturbation (Fig. 6–2) attempting to impart a flexed spine position. Thereafter, a specific muscle strategy is activated, with an objective function, and subject to bounds and constraints. Using feedback and the Multi-objective Genetic Optimization, 100 design points were investigated to find a Pareto-Optimal solution. Based on defined constraints, a feasible range of stability was examined to deduce the point of highest optimization, and thus, the most optimal statically stable spine position (Fig. 6–2).

For all strategies, universal boundary conditions included fixing the positions of the sacrum and the tendons attached to the latissimus dorsi, the back muscle in contact with the TLF. Furthermore, in all strategies, universal bounds were placed on muscle forces according to physiologically plausible limiting values[29]. Specifically, muscle forces were constrained such that maximum muscle normal stress is bounded between 0 and 460kPa. Based on present average cross-sectional area, muscular force bounds were approximated as follows: All other tissues were free to deform, translate, and rotate in all degrees of freedom.

Lastly, the feasible optimization region was defined based on a global stability constraint. This was the extent to which the final spine position, after optimization, is allowed to differ from the original stable position. This was assessed based on the average vertebral bodies' final displacements from the original position as follows:

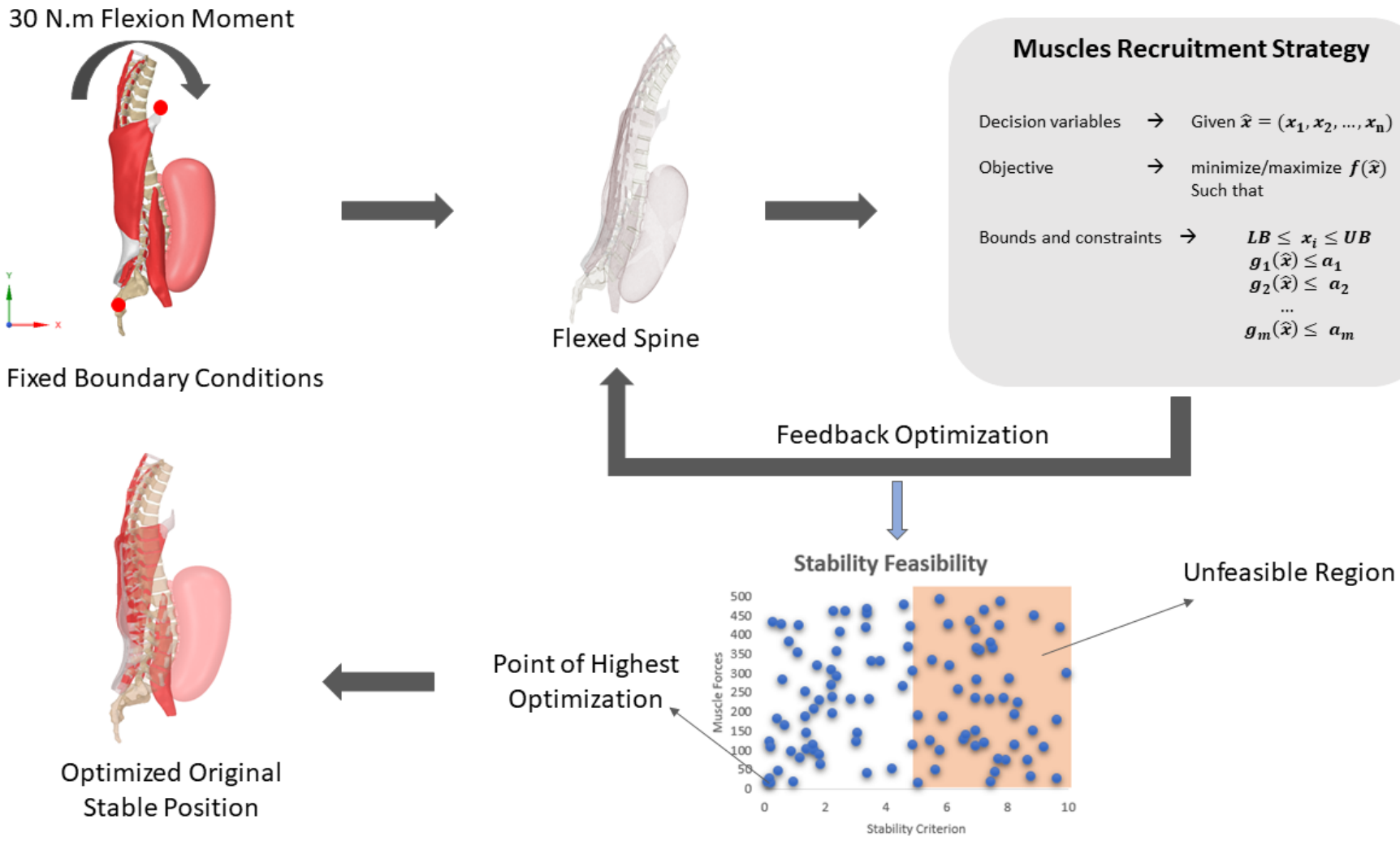

Figure 6–2: Overview of boundary and loading conditions, as well as optimization algorithm

$$U = \frac{\left| \sum_{j=1}^{J} \left(\frac{\sum_{q=1}^{Q} (\overrightarrow{Uq})_{elemental}}{Q} \right)_j \right|}{J} \quad (6.1)$$

where U is the absolute average spine displacement, mapped in the transverse plane in the x-direction (Fig. 6–2), following the 30N.m flexion moment and activated optimization strategy. Q is the number of FE elements on each vertebral body (VB) while J represents all available 17 VBs (12 thoracic and 5 lumbar).

C. Activation Strategies

Five different strategies, three conventional and two novel, were examined:

- *Conventional Strategies:*

1. **Minimize muscle effort.** This strategy aims to minimize the sum of cubic muscle forces upon activation. For each muscle, forces across all tendon attachments are minimized as per the following objective function:

$$min\left(\sum_{n=1}^{N} \left(\sum_{i=1}^{J} f_i \right)_n^3 \right) \quad (6.2)$$

where f_i is the tensional force applied at the i^{th} tendon attachment, along the longitudinal direction of the i^{th} tendon, for the n^{th} spinal muscle.

This strategy is thought to be compatible with maximizing muscle endurance, which might provide results that are similar to EMG data.

2. **Minimize intervertebral discs compression.** This strategy aims to minimize the sum of squared IVD forces at the L4-L5 level. The vector form of all elemental IVD forces is minimized as per the following objective function:

$$min\left(\left| \sum_{n=1}^{N} (\overrightarrow{F_n})_{elemental} \right| \right) \quad (6.3)$$

where F_n is the elemental IVD compressive force along the gravity y-direction (Fig. 6–2) and N is the number of FE elements in the L_4-L_5 IVD.

3. **Absolute Stability.** This strategy aims to minimize the spine's displacement from its original position following optimization. The average magnitude of all 17 VB displacements is minimized within physiological range of muscle activation as follows:

$$min(U) \tag{6.4}$$

where U is defined by Eq. (6.1).

This strategy is thought to be compatible with drastic measures taken by the musculoskeletal system to stabilize the spine at all costs in cases of emergencies.

- *Novel Strategies:*

4. **Minimize intramuscular pressure levels.** This strategy aims to minimize IMP built up around the spine. IMP is minimized inside each muscle followed by minimizing the total IMP as per the following objective function:

$$min(\sum_{n=1}^{N}[min(IMP)_n]) \tag{6.5}$$

where N represents all available muscles.

IMP has been previously shown to linearly correlate to muscle force[42,49,50]. As such, an additional constraint is added to maintain this correlation to within 5% difference.

This strategy is also thought to be compatible with maximizing muscle endurance, which might provide more insights into EMG recorded data.

5. **Maximize intramuscular pressure levels.** This strategy aims to maximize IMP built up around the spine. IMP is maximized inside each muscle with no bounds, other than physiological muscle forces constraints, as follows:

$$\sum_{n=1}^{N}[max(IMP)_n] \tag{6.6}$$

where N represents all available muscles.

Although IMP is linearly correlated to muscle force, this constraint was not maintained in this strategy to investigate what would occur should this be lost.

This strategy is thought to be compatible with exerting extra effort by the muscles whenever necessary or as required by the musculoskeletal system.

For all strategies, IAP was activated with a pressure of 30mmHg to be compatible with normal physiological ranges during spinal flexion. One last constraint was imposed to determine the feasibility of obtained data points. For strategies 1, 2, 4, and 5, a feasible optimization region was defined such that U does not exceed 5cm. However, since the interest behind the 3rd strategy is to maintain maximum stability, the feasible region has been tightened to a U of less than or equal 2cm.

D. Data Collection

For each strategy, a scatter tradeoff plot between the objective function and the displacement stability constraint (U) was first obtained for the 100 data points in order to identify the most optimal point. Based on the previously highlighted 460kPa muscle normal stress constraint, bounds for initial and final muscle forces were determined and inputted into the optimization. Those were [0, 148]N with an increment of 1.495N for the intertransversarius, [0, 194]N with an increment of 1.96N for the psoas major, [0, 233]N with an increment of 2.35N for the multifidus, and [0, 350]N with an increment of 3.54N for the longissimus thoracis. For the Pareto-Optimal case, 4 different parameters were of interest: individual muscle forces, individual muscle IMP, resistive/supportive forces measured at each TLF attachment with lumbar vertebrae's spinous processes (TLF-VB attachment), and total compressive forces measured at each lumbar IVD. Each of these parameters were plotted to identify trends, validate the approach, and compare between the conducted activation strategies.

6.2.4. RESULTS

A. Conventional Strategies

The first strategy *(Strategy 1: minimizing muscle forces)* exhibited a handful of data points with a final displacement below 1cm and an overall muscle force below 370N (Fig. 6–3). In accordance with published data[3], the most optimized point showed a U of 0.47cm with a total muscle force of 307N, broken down to a 134N for the longissimus (L), 71N for the multifidus (M), 68N for the

psoas major (P), and 34N for the lumbar lateral intertransversarius (I). Such results were in line with the same minimum force stability criterion whereby an average difference of barely 3.8% was observed when compared to published data[3]. In addition, for the same strategy, a total of 250.5 IMP was observed such that the IMP build-up was 107.5, 54.5, 68, and 20.5mmHg inside L, M, P, and I, respectively. Furthermore, forces observed at TLF-VB attachments were between 9.5 and 17N, adding up to around 62.8N total TLF force across all lumbar vertebral bodies. Lastly, IVD compressive forces fluctuated between 5.2 and 17.7N for each lumbar IVD, adding up to a total of around 55.8N IVD compressive forces (Fig. 6–3).

The second strategy *(Strategy 2: minimizing IVD forces)* showed concentrated results converging towards the optimal point of 9.1N L_4-L_5 IVD compressive force and *U* of 0.22cm (Fig. 6–4). Muscle forces and accompanied IMP were 147N and 139mmHg for L, 79N and 60mmHg for M, 93N and 98.5mmHg for P, and 81N and 49.5mmHg for I, adding up to a total muscle force of 400N and a total IMP of 347mmHg. Such results were also in line with the same minimum IVD force stability criterion whereby an average difference of 9.8% was observed when compared to published optimization data[3]. Lastly, TLF forces fluctuated between 17 and 41N whereas between 4 and 9.1N for IVD forces (Fig. 6–4).

The third and last conventional strategy *(Strategy 3: stability at all costs)* showed a tendency towards increasing muscle forces to achieve higher spinal stability (Fig. 6–5). The most optimal case was able to achieve a *U* of barely 0.04cm (around a 91% less VB displacement) when compared to the first two strategies but at the cost of almost doubling muscle forces to about 734N. Accompanied IMP recorded a total value of about 739.7mmHg, TLF forces ranged between 13.4 and 26.3N, while IVD compressive forces fluctuated between 7 and 15.4N (Fig. 6–5).

B. Novel Strategies

The first novel strategy *(Strategy 4: minimizing IMP)* exhibited a significant drop in summed IMP across present muscles to about 180mmHg along a significantly high stability with a *U* of 0.18cm. Individually, IMP and forces recorded for each muscle were 163N and 77mmHg for L, 99N and 53mmHg for M, 88N and 41mmHg for P, and 42N and 9mmHg for I (Fig. 6–6). Although forces were comparable to the first strategy, IMP results were significantly low along almost twice the stability. Besides, TLF forces were the highest recorded thus far, with values ranging between

29 and 45N for each TLF-VB attachment. Lastly, IVD compressive forces showed an increasing trend from 6.9 to 16N between L_1-L_2 IVD and L_4-L_5 IVD, with the exception of L_2-L_3 IVD being slightly off this rising trend, comparable to the first and third strategies (Fig. 6–6).

The second novel strategy *(Strategy 5: maximizing IMP)*, the tradeoff plot between IMP and stability did not show any apparent trend, with the data points diverging on both ends of the scatter plot (Fig. 6–7). In line with the objective function, the Pareto-Maximum case exhibited relatively high IMP values while recording a total muscle force comparable to that of strategy 3. Specifically, this case showed ability to re-establish stability with a U of around 0.25cm, total IMP of 1533mmHg, and total muscle force of 850N. Individually, IMP and forces observed for each muscle were 322N and 818mmHg for L, 218N and 257mmHg for M, 176N and 315mmHg for P, and 134N and 143mmHg for I (Fig. 6–7). Although forces did not increase much from the third strategy, IMP results were multiples of other cases, with conflicting results of almost equal stability but very different IMP (numerous points at the top and bottom part for U values below 1cm for example). In addition, TLF-VB attachments and IVDs' elements recorded the highest forces among all other strategies, with values ranging from 45 to 56.9N and from 7.1 to 26N, respectively (Fig. 6–7).

6.2.5. DISCUSSION

Physics-based numerical biomechanical analyses, by means of finite element modelling, serve as objective and controlled framework to accurately represent and study the behavior of the human spine. Appropriate validation can lend credibility to such models and offer a complementary or even alternate experimental platform to *ex vivo* and *in vivo* studies. The spine, is a biomechanically redundant structure, possessing an enormous number of kinematic degrees of freedom, to which its movement can be executed in an infinite number of ways. This has led to the formulation of optimization methods as a way to study the motor response (*i.e.* muscle recruitment patterns) surrounding the spine, as an approach to determining underlying muscle forces. With numerous tissues coordinating to execute a task while achieving spinal stability, simplifications are often made in experimental studies and those that employ optimization models. Conventionally, such

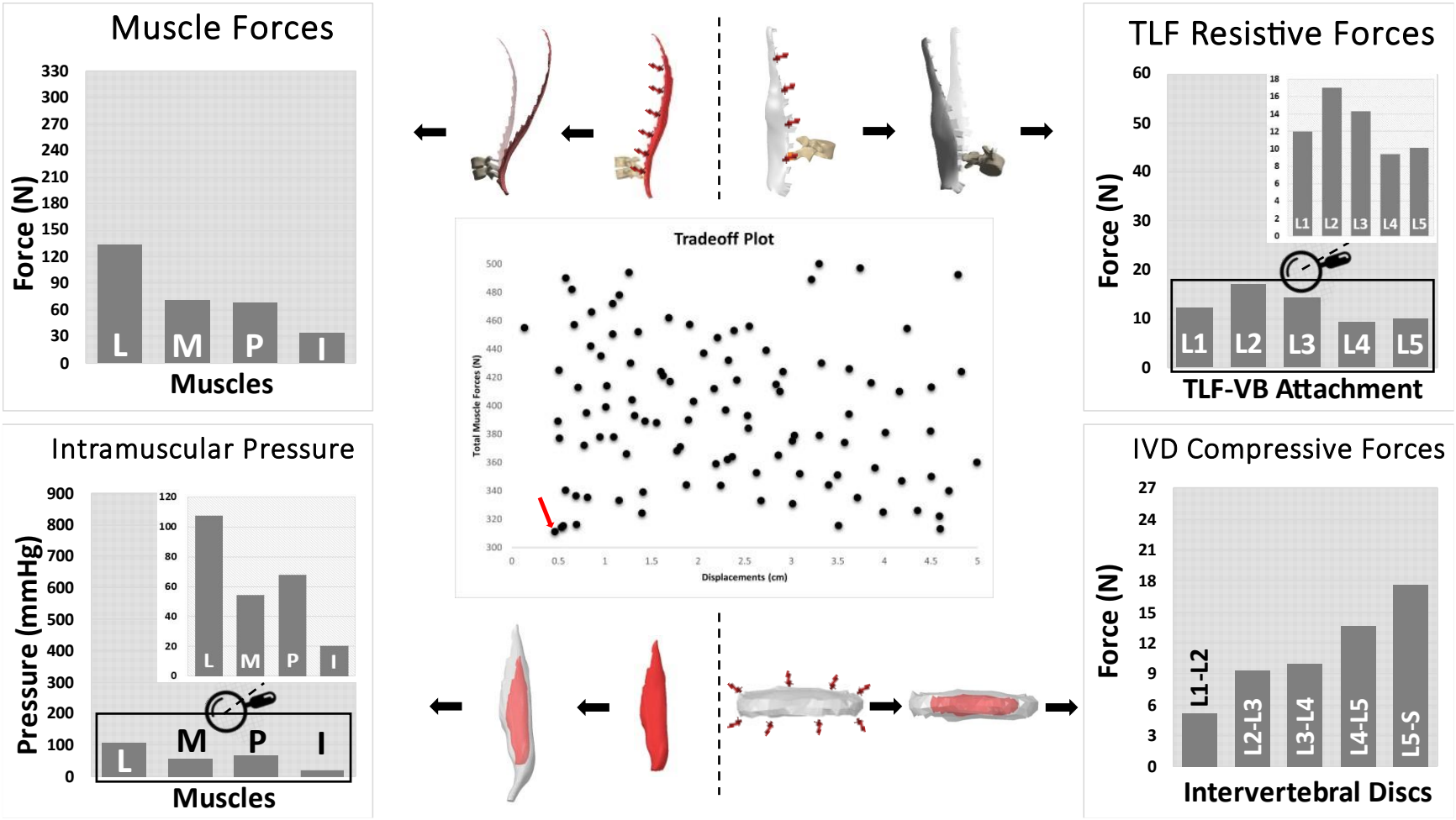

Figure 6–3: Muscles, TLF, and IVD forces, along IMP results, for the first optimization strategy (**Min Muscle Force**).

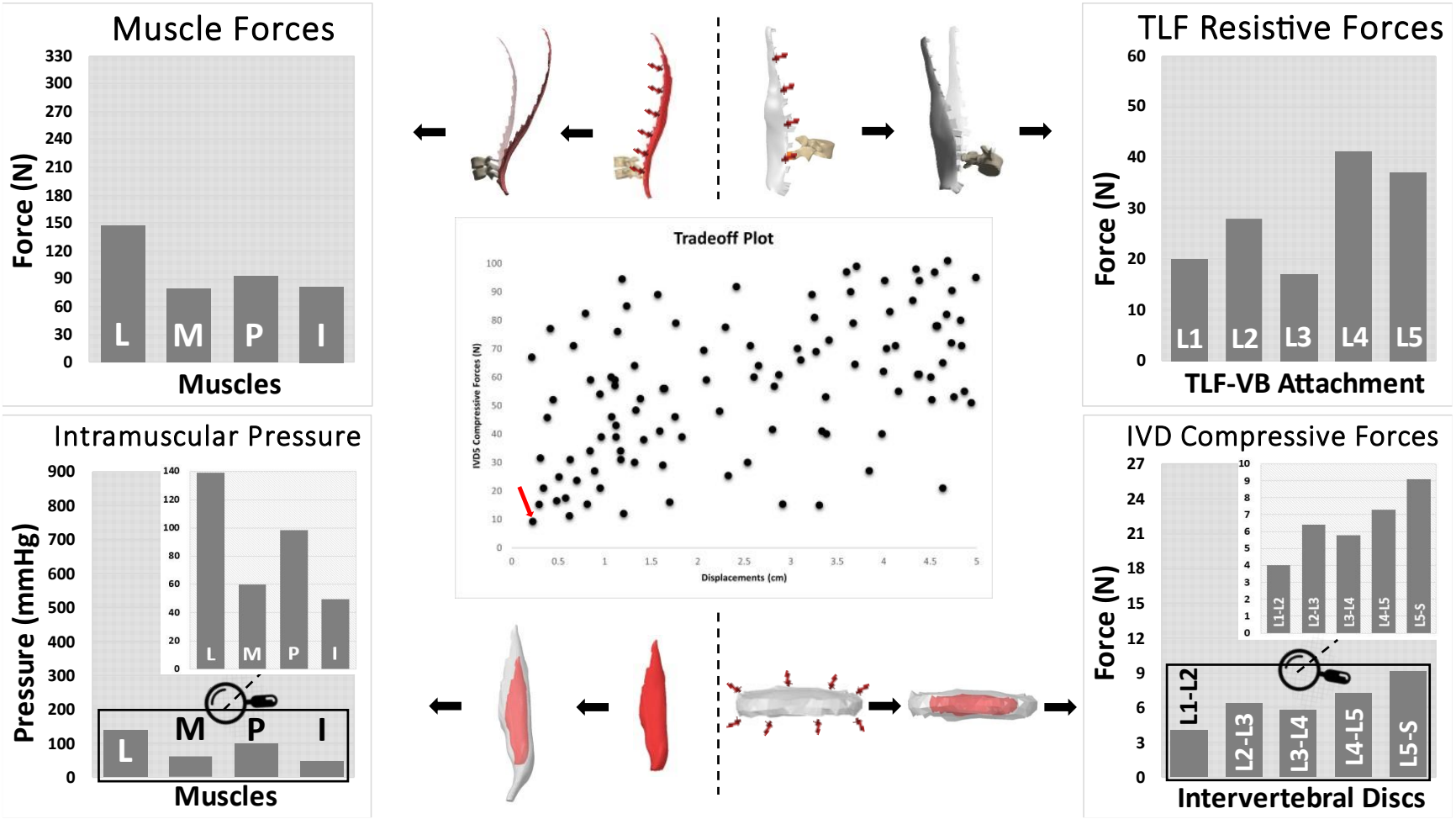

Figure 6–4: Muscles, TLF, and IVD forces, along IMP results, for the second optimization strategy (**Min IVD Force**).

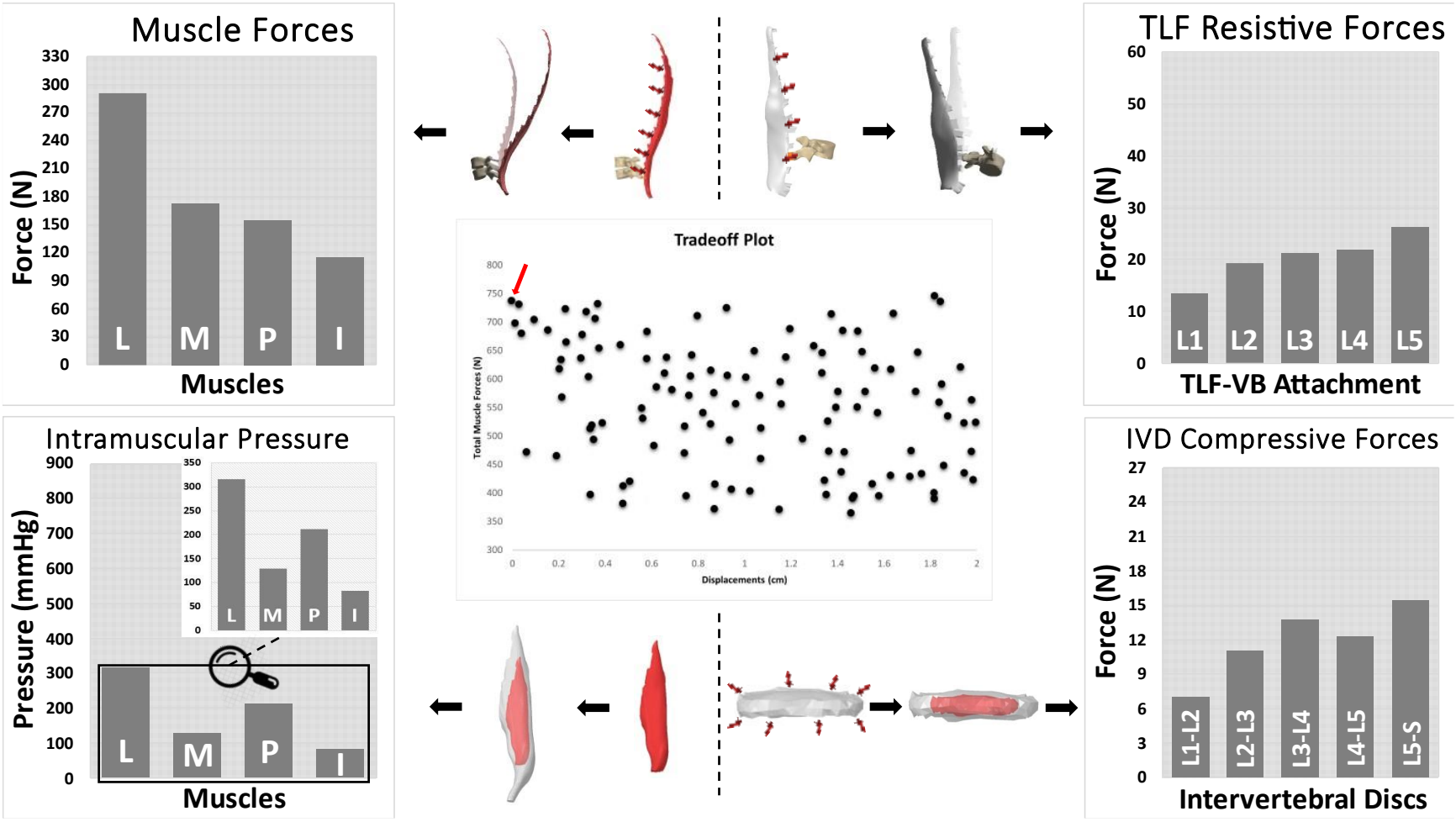

Figure 6–5: Muscles, TLF, and IVD forces, along IMP results, for the third optimization strategy (**Absolute Stability**).

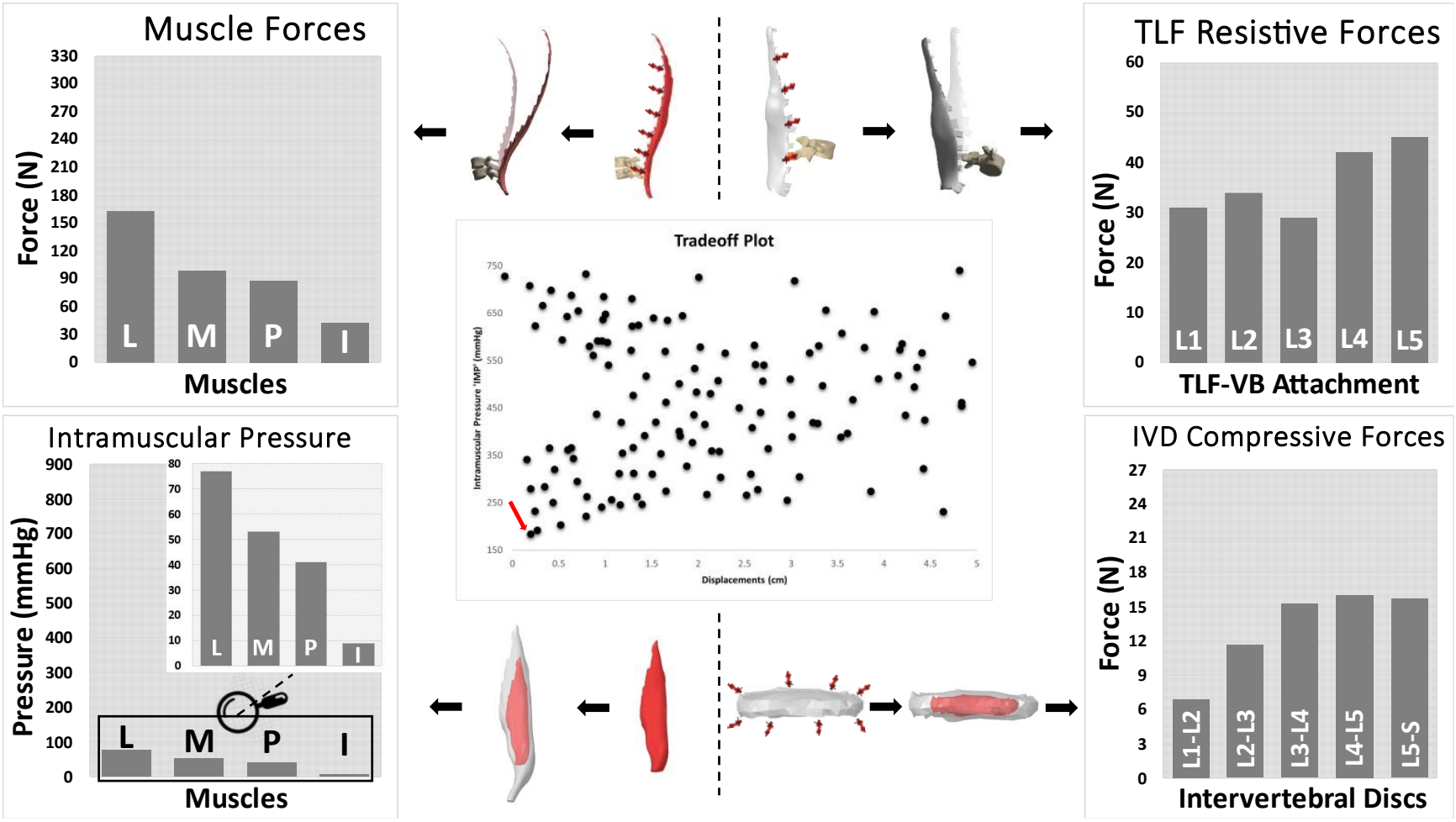

Figure 6–6: Muscles, TLF, and IVD forces, along IMP results, for the fourth optimization strategy (**Minimum IMP**).

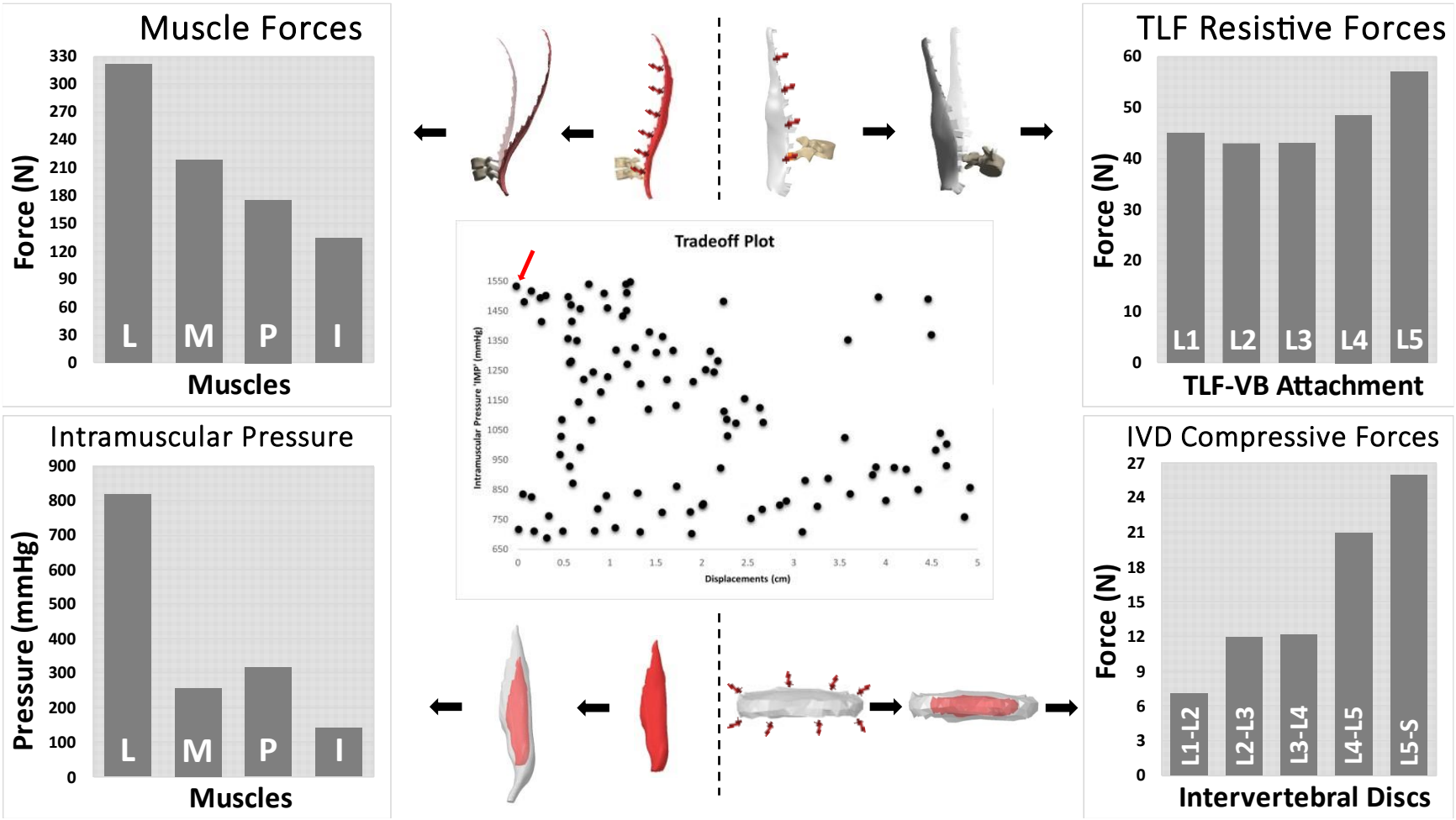

Figure 6–7: Muscles, TLF, and IVD forces, along IMP results, for the fifth optimization strategy (**Maximum IMP**).

models omit to include the roles of fascia (such as the TLF), internal pressures (such as abdominal pressure and IMP), or specific muscles' contraction types. Furthermore, to the authors' knowledge, IMP is a potentially important muscle physiology that has not previously been accounted for in muscle activation models. Consequently, in the present study, a previously constructed and extensively validated novel three-dimensional full-scale FE model of the spine was leveraged, inclusive of a novel two-state, fluid-structure IMP model, towards investigating five different muscle activation strategies. With a global constraint of maintaining spinal stability, three strategies were considered conventional: covering minimum muscle effort, minimum IVD compression, and absolute stability. Two explored strategies were novel: spanning minimizing and maximizing IMP, activation strategies. All strategies were successfully implemented, analyzed, and contrasted.

Elevated spinal loads have always been associated with risk factors such as the development of low-back pain and injuries[51]. This has led to the reasonable hypothesis that the central nervous system attempts to limit spinal loads to within tolerable levels when adopting muscle activation patterns. In addition, among other effects, *in vivo* and *in situ* observations suggest that spinal muscle coactivation is also governed by the mechanism and contribution of other tissues to spinal stability[52–54,45]. This motivated the present research to adopt all major trunk tissues known to contribute to stability, as well as a representative biphasic model of trunk muscles to account for IMP, in an attempt to better understand underlying activation strategies.

A. Conventional Strategies

Under loading conditions representative of the study of Stephen *et. al.*[3], the first two strategies exhibited a stable spine position with a total muscle force of 307N and 147N, respectively. The results of the first strategy, in line with the minimum force stability criterion in Stephen's, exhibited individual muscles forces that differed by as much as 14.4% from reported individual forces[3]. However, when averaged together for a total muscle force, an average difference of barely 3.8%, for the first strategy, whereas 9.8% for the second strategy, which mimicked that of Stephen's minimum IVD force criterion, were observed. This speaks to model's capability or validity in predicting *ex vivo* and/or *in vivo* muscle activation results with high accuracy. Despite such discrepancies between individual and total force averages suggest the mode of action and

mechanism of including IMP to redistribute and share loads. Although not significant, observed discrepancies were likely due to major differences between both utilized models, mainly the inclusion of TLF, IAP, and more importantly, IMP in the present study.

The third strategy *(absolute stability)* was of particular interest due to its severe conditions of maintaining stability at all physiological costs. This is considered relevant when the central nervous system aims to protect the musculoskeletal system against sudden external threats[55]. In addition to its physiological implications, this strategy served as a baseline to the others explored herein due to its maximum stability criterion. In other words, all other strategies are expected to achieve less stability, assessed by VBs displacements, to which all other parameters, such as exerted muscle forces, could be compared to this maximum stability strategy. It is with no surprise that relatively high muscle forces, as high as 291N for the longissimus, were required to achieve a near absolute stable position having only 0.04cm average VB displacement. Under the programed force-IMP correlation constraint, those forces were accompanied with elevated IMP values, which may support the importance of including this parameter for improved physiological muscle representation. In addition, the TLF also provided considerable support with tensional forces as high as 26.3N posteriorly at the L_5 spinous process attachment. In line with this, El-Monajjed and Driscoll recorded approximately 27N TLF force for a kyphotic back holding 10Kg[56]. In another study, the same authors simulated a similar task for a kyphotic back, but with a 20Kg load combined with applying a follower load of 3185N. This led to TLF forces at the L_5 level to triple to around 71N[57]. The 30 N.m applied moment in the present study reflects a moment arm of around 30cm for a 10Kg load, which physiologically represent the present model. This explains, and further supports, the similarities observed with the first paper. Observed differences with the second paper seem to be best explained by the added follower load, to which the TLF potentially developed further tensional forces to support it. Lastly, IVDs were subjected to relatively average-to-low compression forces, supporting the notion that a stable spine may present as a position of relief and, potentially, free of pain[58]. In short, elevated tissue forces, mainly from active muscles and indirectly from the TLF, speaks to measures practiced by sensory systems to stabilize musculoskeletal structures at all physiological costs in cases of sudden external stimuli[55].

In comparison to the third, the first two strategies *(minimizing muscle and IVD forces)* experienced the lowest activated muscle forces, not exceeding 134N for the first strategy while

147N for the second, both recorded for the longissimus muscle. Those were also correspondingly accompanied with average-to-low IMP values across all muscles. Although less stability was observed, 0.47cm and 0.25cm displacements for the first and second strategies respectively, global stability was still relatively achieved, in terms of spine deflections, in comparison to other studies[45]. This may speak to agonist and antagonist muscle activations, as well as the role of the muscular system, in efficient mobility and achieving joint stability, *i.e.* maximizing muscular endurance while maintaining a stable position[24]. On the other hand, the first two strategies experienced opposite trends, almost a tradeoff, in terms of TLF connective supportive loads and IVDs' compression forces, which were also below and beyond the limits of the baseline *(strategy 3)*. Such forces have been previously suggested to assist in spinal stabilization by way of posteriorly oriented tensions[56,57]. Specifically, the *minimum muscle effort* strategy showed fluctuations in TLF force, but with loads below 17N, whereas for the *minimum IVD compression* strategy, these went up to 41N, with the minimum being 17N. In contrast, the *minimum muscle effort* strategy showed an increasing trend of IVD compression loads from 5.2 to 17.7N, higher than those recorded for the *minimum IVD compression* strategy, which were between 4 and 9.1N. Although IVD results were not surprising as the second strategy aimed to minimize such loads, TLF results were of particular interest due to the huge variabilities observed between the supportive forces of both strategies. This might be potentially explained by the TLF developing high tensional forces in response to the external load. In other words, with less muscle activity opposing the applied load, the TLF plays an important role to passively support the spine.

B. Novel Intramuscular Pressure based Strategies

Considering the condensed fluidic content of skeletal muscles, the regional hydrostatic pressure build-up plays a significant role in force generation and transmission. Besides, IMP influences muscle and activity performance at the sarcomere level[38]. Thus, not including the IMP field and replacing it by means of muscle force vectors could be a significant simplification in activation and optimization models.

Under the same loading conditions, the fourth strategy had the objective of *minimizing IMP* while maintaining physiological and stability constraints. This led to the lowest registered IMP results, in comparison to all other strategies, with the longissimus recording barely 77mmHg. This

was accompanied with small, almost half of the baseline, muscle forces ranging between 42 and 163 N. This speaks to the potential of muscles exerting less effort by means of better load transmission *via* the enclosed fluidic field[43]. Although forces and IMP were relatively low, tensional forces developed in the TLF, especially at the connective regions, were extremely high, even higher than those of the baseline strategy of *absolute stability*. Taking a closer look at those regions, the small amount of IMP caused a slight curvature instead of maintaining linear axial insertions between muscles and vertebrae. This seems to have led to extra tensional forces being transmitted to the TLF, thus explaining the high TLF forces observed. In addition, depending on the magnitude and direction of muscle generated forces, force transmission is not exclusive to a serial process from muscle fibers to tendons. It has been shown that an additional component of force transmission occurs laterally *via* surrounding and contacting connective tissues[54]. Therefore, inflating the muscles caused by IMP might have resulted in lateral loads transmitting into TLF fibers, thus increasing TLF forces to such levels. In summary, the inclusion of IMP, with the objective of its minimization, seemed to have significant impact on neuromuscular activations; namely, exerting minimal muscular effort by means of engaging passive tissues, such as the TLF, perhaps in the interest of providing more efficient spinal stability from the perspective of muscle contribution.

The last novel strategy aimed to maximize IMP within normal physiological ranges whilst maintaining spinal stability. No apparent trend was identified whereby high and relatively low IMP values resulted in similar stability ranges. In line with the objective function, the highest IMP recorded reached 1533mmHg, accompanied with a total muscle force of 850N. This was an interesting observation in the sense that, although IMP results almost doubled, accompanied muscle forces only increased a little (an increase of about 116N only). To better understand this phenomenon, total muscle force vs. pressure profile, for all data points in the feasible optimization region, has been plotted, as shown in Fig. 6–8.

Results show that the increase in IMP caused an increase in muscle forces until reaching a top, fluctuating around it, and then starting to slightly decrease in response to further elevated IMP values. Taking a closer look at the simulation files, it seems that the excessive increase in IMP caused muscles to bump into each other, and into other surrounding soft tissues, which resulted in building compartmental pressure, or what is called intermuscular pressure, between muscles. This

caused a deterioration in muscles' capabilities to generate more tension. Thus, force transmission through tendons was significantly affected whereby forces had to be shared with adjacent soft tissues. A phenomenon that lines up with this observation has been previously discussed by Creze *et. al*[59]. They noticed a paradox in the anatomy of paraspinal muscles whereby those trunk muscles seemed to have a high volume but tiny tendons, to which they cannot pull strongly on their tendons. The findings of the last activation strategy *(maximizing IMP)* support Creze's observation by suggesting that the contraction of spinal muscles does not act to strictly pull on effector tendons only, but also increases the stiffness of the underlying muscles, share lateral loads with adjacent tissues, and provide more spine stabilization[59]. This is further supported by the extremely elevated observed TLF supportive loads, ranging from 45 to 56.9N, as well as the relatively high IVD compressive forces, in efforts of increasing spinal stability. Thus, it would appear that muscle pressures can both support *via* engaging soft tissues, such as the TLF, and abutting adjacent muscles via intra-muscular pressure.

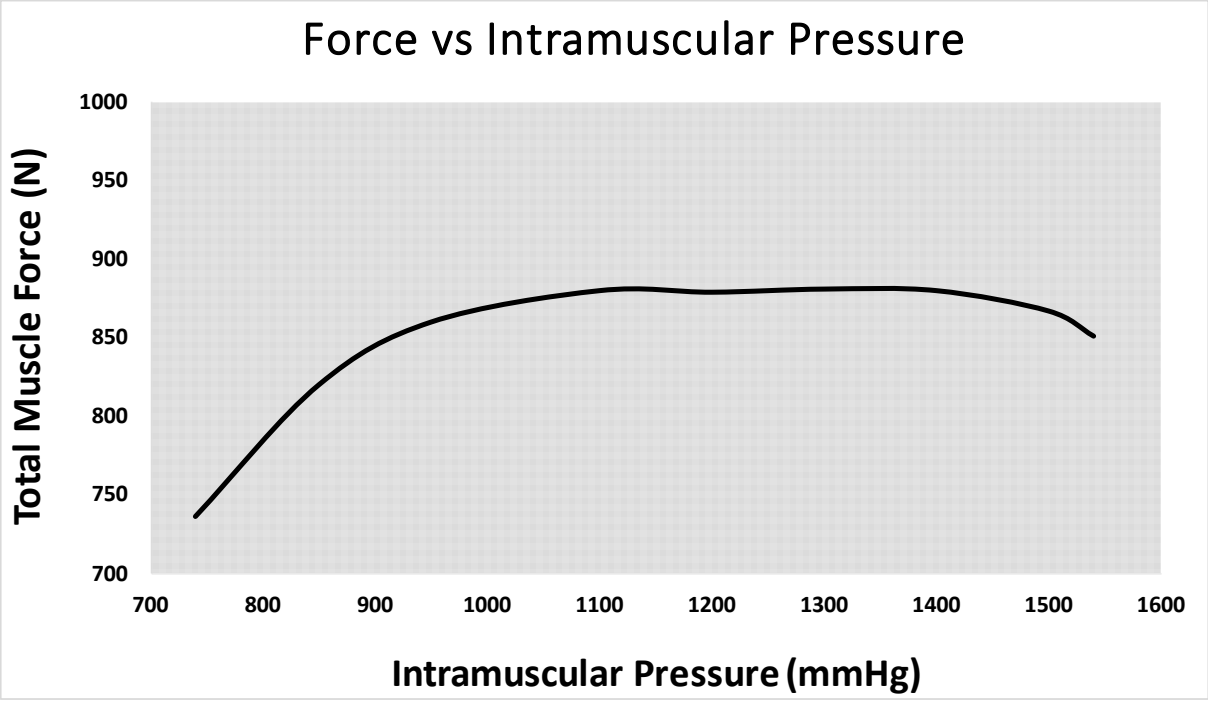

Figure 6–8: Total muscle force vs. IMP profile for all cases within the feasible optimization region of the fifth strategy (**Maximum IMP)**.

In accordance with other investigations[54,57,60,45], the TLF presents itself as an important passive tissue to withstand and store elevated tensional forces *via* load-sharing with the spine and muscles.

The findings of this paper also support the need to account for IMP in muscle recruitment strategies and optimization models. Specifically, the neuromuscular system appears to engage IMP to aid muscles in minimizing their tensile effort. In line with previous discussions on neuromuscular activation[61], this not only ensures better efficacy to support and stabilize the spine and surrounding tissues, but also may lead to less muscular fatigue in the long term. Lastly, the devised novel IMP-based activation strategies suggest that there potentially exists an optimized range of IMP values, in between the extreme values explored herein, whereby efficient movements are executed whilst minimizing spinal tissues effort.

C. Limitations

Similar to other FE models, the undertaken numerical approach caries some limitations. Nonetheless, with assumptions significantly minimized, this gives the model greater credibility of approximating, with high accuracy, underlying biomechanical behavior of the spine. Some common modelling approximations practiced in this paper, such as material properties, mesh, and model application, were explained and supported by means of previous successful validation efforts[42,62]. The stabilization effect of the rib cage, where it is believed to offer supportive spinal loads as the lungs inflate, was neglected[63]. This was a justifiable assumption as muscle activations are the primary interest of the present research study, with all other tissue engagement being representative of static conditions. Lastly, muscular activations were assumed to follow an optimized model. Although this permit evaluation of exact individual muscle contributions, the degree of activation relative to real experimental levels might have been misrepresented. Thus, such governed imposition may have led to underestimating optimized muscle forces and spinal stability levels. Nonetheless, under the mentioned limitations, the model proved robust and underwent extensive validation, thus lending credibility and confidence to explored muscular activation levels, in their interest towards maintaining a stable spine position, discussed herein.

6.2.6. CONCLUSION

In conclusion, this study leveraged a novel validated, fully representative, three-dimensional, FE model of the spine, inclusive of an accurate biphasic model of skeletal muscles and their enclosed IMP, to explore muscle recruitment patterns maintaining spinal stability. Three conventional strategies governing *minimizing muscle effort*, *minimizing IVD compressive forces*, and *maintaining stability at all costs* were firstly investigated to show model validation and discuss the supportive role of tissues surrounding the spine. Thereafter, two novel IMP-based strategies were devised, namely *minimizing* and *maximizing IMP*, and explored lending significance to the inclusion of IMP in muscle recruitment patterns due to suggested load-sharing role with surrounding tissues. The novel scenarios explored may greatly inform clinical applications such as motion analysis, device design for spine pathologies, and rehabilitation.

6.2.7. ACKNOWLEDGMENTS

We gratefully acknowledge funding by McGill University (MEDA), the Fonds de Recherche du Québec – Nature et Technologies (FRQNT), and the Natural Sciences and Engineering Research Center (NSERC).

6.2.8. REFERENCES

1. Prilutsky, B. I. & Zatsiorsky, V. M. Optimization-based models of muscle coordination. Exerc. Sport Sci. Rev. (2002). doi:10.1097/00003677-200201000-00007

2. Heintz, S. Muscular forces from static optimization. (2006).

3. Brown, S. H. M. & Potvin, J. R. Constraining spine stability levels in an optimization model leads to the prediction of trunk muscle cocontraction and improved spine compression force estimates. J. Biomech. (2005). doi:10.1016/j.jbiomech.2004.05.011

4. Anderson, F. C. & Pandy, M. G. Static and dynamic optimization solutions for gait are practically equivalent. J. Biomech. (2001). doi:10.1016/S0021-9290(00)00155-X

5. Crowninshield, R. D. & Brand, R. A. A physiologically based criterion of muscle force prediction in locomotion. J. Biomech. (1981). doi:10.1016/0021-9290(81)90035-X

6. Menegaldo, L. L., Fleury, A. D. T. & Weber, H. I. Biomechanical modeling and optimal control of human posture. J. Biomech. (2003). doi:10.1016/S0021-9290(03)00170-2

7. Raikova, R. A model of the flexion - Extension motion in the elbow joint - Some problems concerning muscle forces modelling and computation. J. Biomech. (1996). doi:10.1016/0021-9290(95)00072-0

8. Yamaguchi, G. T., Moran, D. W. & Si, J. A computationally efficient method for solving the redundant problem in biomechanics. J. Biomech. (1995). doi:10.1016/0021-9290(94)00145-T

9. Solomonow, M., Baratta, R. V. & D'Ambrosia, R. EMG-force relations of a single skeletal muscle acting across a joint: Dependence on joint angle. J. Electromyogr. Kinesiol. (1991). doi:10.1016/1050-6411(91)90027-3

10. Isear, J. A., Erickson, J. C. & Worrell, T. W. EMG analysis of lower extremity muscle recruitment patterns during an unloaded squat. Med. Sci. Sports Exerc. (1997). doi:10.1097/00005768-199704000-00016

11. Hajihosseinali, M., Arjmand, N., Shirazi-Adl, A., Farahmand, F. & Ghiasi, M. S. A novel stability and kinematics-driven trunk biomechanical model to estimate muscle and spinal forces. Med. Eng. Phys. (2014). doi:10.1016/j.medengphy.2014.07.009

12. Stokes, I. A. F., Henry, S. M. & Single, R. M. Surface EMG electrodes do not accurately record from lumbar multifidus muscles. Clin. Biomech. (2003). doi:10.1016/S0268-0033(02)00140-7

13. Uliam, H. et al. The Relationship Between Electromyography and Muscle Force. in EMG Methods for Evaluating Muscle and Nerve Function (2012). doi:10.5772/25381

14. Koh, T. J. & Grabiner, M. D. Evaluation of methods to minimize cross talk in surface electromyography. J. Biomech. (1993). doi:10.1016/0021-9290(93)90086-T

15. Li, G., Li, Y., Yu, L. & Geng, Y. Conditioning and sampling issues of EMG signals in motion recognition of multifunctional myoelectric prostheses. Ann. Biomed. Eng. (2011). doi:10.1007/s10439-011-0265-x

16. Cannan, J. A. R. & Hu, H. Automatic circumference measurement for aiding in the estimation of Maximum Voluntary Contraction (MVC) in EMG systems. in Lecture Notes in Computer Science (including subseries Lecture Notes in Artificial Intelligence and Lecture Notes in Bioinformatics) (2011). doi:10.1007/978-3-642-25486-4_21

17. Pope, M. H., Svenssonm, M., Andersson, G. B. J., Broman, H. & Zetterbeg, C. The role of prerotation of the trunk in axial twisting efforts. Spine (Phila. Pa. 1976). (1987). doi:10.1097/00007632-198712000-00016

18. Andersson, G. B. J., Zetterberg, C. & Schultz, A. B. The activity of individual trunk muscles during heavy physical loading. Spine (Phila. Pa. 1976). (1987). doi:10.1097/00007632-198712000-00015

19. McGill, S. M. A myoelectrically based dynamic three-dimensional model to predict loads on lumbar spine tissues during lateral bending. J. Biomech. (1992). doi:10.1016/0021-9290(92)90259-4

20. Granata, K. P. & Marras, W. S. The influence of trunk muscle coactivity on dynamic spinal loads. Spine (Phila. Pa. 1976). (1995). doi:10.1097/00007632-199504150-00006

21. van Dieën, J. H. Effects of antagonistic co-contraction on differences between electromyography based and optimization based estimates of spinal forces. Ergonomics (2005). doi:10.1080/00140130512331332918

22. Calisse, J., Rohlmann, A. & Bergmann, G. Estimation of trunk muscle forces using the finite element method and in vivo loads measured by telemeterized internal spinal fixation devices. J. Biomech. (1999). doi:10.1016/S0021-9290(99)00052-4

23. Stokes, I. A. F., Gardner-Morse, M. G. & Henry, S. M. Intra-abdominal pressure and abdominal wall muscular function: Spinal unloading mechanism. Clin. Biomech. (2010). doi:10.1016/j.clinbiomech.2010.06.018

24. Stokes, I. A. F. & Gardner-Morse, M. Muscle activation strategies and symmetry of spinal loading in the lumbar spine with scoliosis. Spine (Phila. Pa. 1976). (2004). doi:10.1097/01.brs.0000141182.42544.1f

25. Granata, K. P. & Wilson, S. E. Trunk posture and spinal stability. Clin. Biomech. (2001). doi:10.1016/S0268-0033(01)00064-X

26. Hughes, R. E., Chaffin, D. B., Lavender, S. A. & Andersson, G. B. J. Evaluation of muscle force prediction models of the lumbar trunk using surface electromyography. J. Orthop. Res. (1994). doi:10.1002/jor.1100120512

27. An, K. N., Kwak, B. M., Chao, E. Y. & Morrey, B. F. Determination of muscle and joint forces: A new technique to solve the indeterminate problem. J. Biomech. Eng. (1984). doi:10.1115/1.3138507

28. Stokes, I. A. F. & Gardner-Morse, M. Lumbar spinal muscle activation synergies predicted by multi-criteria cost function. J. Biomech. 34, 733–740 (2001).

29. Stokes, I. A. F. & Gardner-Morse, M. Lumbar spine maximum efforts and muscle recruitment patterns predicted by a model with multijoint muscles and joints with stiffness. J. Biomech. (1995). doi:10.1016/0021-9290(94)E0040-A

30. Sjogaard, G. & Saltin, B. Extra- and intracellular water spaces in muscles of man at rest and with dynamic exercise. Am. J. Physiol. - Regul. Integr. Comp. Physiol. (1982). doi:10.1152/ajpregu.1982.243.3.r271

31. Sejersted, O. M. et al. Intramuscular fluid pressure during isometric contraction of human skeletal muscle. J Appl Physiol Respir Env. Exerc Physiol 56, 287–295 (1984).

32. Ates, F. et al. Intramuscular pressure of tibialis anterior reflects ankle torque but does not follow joint angle-torque relationship. Front. Physiol. (2018). doi:10.3389/fphys.2018.00022

33. Nakhostine, M., Styf, J. R., van Leuven, S., Hargens, A. R. & Gershuni, D. H. Intramuscular pressure varies with depth: the tibialis anterior muscle studied in 12 volunteers. Acta Orthop. (1993). doi:10.3109/17453679308993649

34. Körner, L. et al. Relation of intramuscular pressure to the force output and myoelectric signal of skeletal muscle. J. Orthop. Res. (1984). doi:10.1002/jor.1100020311

35. Parker, P. A., Körner, L. & Kadefors, R. Estimation of muscle force from intramuscular total pressure. Med. Biol. Eng. Comput. (1984). doi:10.1007/BF02447706

36. Aratow, M. et al. Intramuscular pressure and electromyography as indexes of force during isokinetic exercise. J. Appl. Physiol. 74, 2634–40 (1993).

37. Ballard, R. E. et al. Leg intramuscular pressures during locomotion in humans. J. Appl. Physiol. 84, 1976–1981 (1998).

38. Daggfeldt, K. Muscle bulging reduces muscle force and limits the maximal effective muscle size. J. Mech. Med. Biol. (2006). doi:10.1142/s0219519406001947

39. Hargens, A. R., Mubarak, S. J., Owen, C. A., Garetto, L. P. & Akeson, W. H. Interstitial fluid pressure in muscle and compartment syndromes in man. Microvasc. Res. (1977). doi:10.1016/0026-2862(77)90136-4

40. Matsen, F. A., Mayo, K. A., Sheridan, G. W. & Krugmire, R. B. Monitoring of intramuscular pressure. Surgery (1976). doi:10.5555/uri:pii:0039606076902385

41. Hargens, A. R. et al. Tissue fluid pressures: From basic research tools to clinical applications. J. Orthop. Res. (1989). doi:10.1002/jor.1100070617

42. El Bojairami, I., El-Monajjed, K. & Driscoll, M. Development and validation of a timely and representative finite element human spine model for biomechanical simulations. Sci. Rep. (2020). doi:10.1038/s41598-020-77469-1

43. Jenkyn, T. R., Koopman, B., Huijing, P., Lieber, R. L. & Kaufman, K. R. Finite element model of intramuscular pressure during isometric contraction of skeletal muscle. Phys. Med. Biol. (2002). doi:10.1088/0031-9155/47/22/309

44. Wheatley, B. B., Odegard, G. M., Kaufman, K. R. & Haut Donahue, T. L. A validated model of passive skeletal muscle to predict force and intramuscular pressure. Biomech. Model. Mechanobiol. (2017). doi:10.1007/s10237-016-0869-z

45. Bojairami, I. El & Driscoll, M. Coordination Between Trunk Muscles, Thoracolumbar Fascia, and Intra-Abdominal Pressure Toward Static Spine Stability. Spine (Phila. Pa. 1976). (2021). doi:10.1097/BRS.0000000000004223

46. El-Bojairami, I. & Driscoll, M. Correlating Skeletal Muscle Output Force and Intramuscular Pressure via a 3-Dimensional Finite Element Muscle Model. J. Biomech. Eng. (In Submission)

47. Cholewicki, J. & McGill, S. M. Mechanical stability of the in vivo lumbar spine : implications for injury and chronic low back pain. J. Clin. Biomech. 11, 1–15 (1996).

48. Peter Reeves, N., Narendra, K. S. & Cholewicki, J. Spine stability: The six blind men and the elephant. Clinical Biomechanics (2007). doi:10.1016/j.clinbiomech.2006.11.011

49. Evertz, L. Q., Bulstra, L. F., Shin, A. Y. & Kaufman, K. R. Evaluate muscle tension using intramuscular pressure device in rabbit tibialis anterior model for improved tendon transfer surgery. Physiol. Meas. (2017). doi:10.1088/1361-6579/aa6739

50. Winters, T. M. et al. Correlation between isometric force and intramuscular pressure in rabbit tibialis anterior muscle with an intact anterior compartment. Muscle and Nerve (2009). doi:10.1002/mus.21298

51. Anton, D. Occupational biomechanics. Occup. Environ. Med. (1986). doi:10.1136/oem.43.1.70-b

52. Kavcic, N., Grenier, S. & McGill, S. M. Determining the stabilizing role of individual torso muscles during rehabilitation exercises. Spine (Phila. Pa. 1976). (2004). doi:10.1097/00007632-200406010-00016

53. Hodges, P. et al. Intervertebral Stiffness of the Spine Is Increased by Evoked Contraction of Transversus Abdominis and the Diaphragm: In Vivo Porcine Studies. Spine (Phila. Pa. 1976). (2003). doi:10.1097/01.BRS.0000096676.14323.25

54. Willard, F. H., Vleeming, A., Schuenke, M. D., Danneels, L. & Schleip, R. The thoracolumbar fascia: Anatomy, function and clinical considerations. Journal of Anatomy (2012). doi:10.1111/j.1469-7580.2012.01511.x

55. Shemmell, J., Krutky, M. A. & Perreault, E. J. Stretch sensitive reflexes as an adaptive mechanism for maintaining limb stability. Clinical Neurophysiology (2010). doi:10.1016/j.clinph.2010.02.166

56. El-Monajjed, K. & Driscoll, M. A finite element analysis of the intra-abdominal pressure and paraspinal muscle compartment pressure interaction through the thoracolumbar fascia. Comput. Methods Biomech. Biomed. Engin. (2020). doi:10.1080/10255842.2020.1752682

57. El-Monajjed, K. & Driscoll, M. Investigation of Reaction Forces in the Thoracolumbar Fascia during Different Activities: A Mechanistic Numerical Study. Life 11, 779 (2021).

58. O'Sullivan, P. B. et al. The effect of different standing and sitting postures on trunk muscle activity in a pain-free population. Spine (Phila. Pa. 1976). (2002). doi:10.1097/00007632-200206010-00019

59. Creze, M., Soubeyrand, M. & Gagey, O. The paraspinal muscle-tendon system: Its paradoxical anatomy. PLoS One (2019). doi:10.1371/journal.pone.0214812

60. Driscoll, M. Fascia – The unsung hero of spine biomechanics. Journal of Bodywork and Movement Therapies (2018). doi:10.1016/j.jbmt.2017.10.014

61. Kaufman, K. R., An, K. N., Litchy, W. J. & Chao, E. Y. S. Physiological prediction of muscle forces-I. Theoretical formulation. Neuroscience (1991). doi:10.1016/0306-4522(91)90012-D

62. Bojairami, I. El, Hamedzadeh, A. & Driscoll, M. Feasibility of extracting tissue material properties via cohesive elements: a finite element approach to probe insertion procedures in non-invasive spine surgeries. Med. Biol. Eng. Comput. (2021). doi:10.1007/s11517-021-02432-9

63. Morris, J. M., Lucas, D. B. & Bresler, B. Role of the Trunk in Stability of the Spine. J. Bone Jt. Surg. (1961). doi:10.2106/00004623-196143030-00001

6.3. SUMMARY

The central idea in this chapter was to advance the physiology of muscle activation strategies, executed to maintain equilibrium spinal stability, *via* exploiting the spine model developed in chapter 4 and the results collected in chapter 5. The focus was on the physiology of intramuscular pressure whereby two novel pressure-based strategies were devised and explored. This was due to the merits of including muscular pressure and its role in sharing and distributing loads with surrounding tissues. However, three conventional strategies were firstly examined in efforts of testing and validating the spine model. Those were mainly to minimize muscular force, minimize intervertebral discs compression, and maximum spinal stability at all costs. In addition to adding confidence to model's validity, these formulations gave insights into maximum muscular endurance while achieving a stable spine position. The novel recruitment patterns explored thereafter consisted of minimizing and maximizing intramuscular pressure in efforts of increasing spinal stability. The results of these strategies were interesting in the sense that muscular forces were efficiently transmitted *via* the enclosed fluidic field. Furthermore, an excessive increase in intramuscular pressure showed to build compartmental pressure between surrounding tissues, which prevented muscles from generating more tensional forces.

This chapter successfully completed the last objective, to which several research and application advances were achieved by means of confirming the last 2 hypotheses. Firstly, conventional strategies results confirmed the agonistic and antagonistic role of the muscular system in efficient mobility and achieving joint stability. Secondly, these further supported a role of the thoracolumbar fascia, being to passively develop high tensional forces in efforts of supporting the spine. Furthermore, the minimum intramuscular pressure novel strategy showed an impact on neuromuscular activations, whereby muscles exert minimal effort by means of efficiently engaging surrounding passive tissues. Lastly, the maximum pressure strategy suggested the potential existence of an optimized range of pressure to execute motor tasks. Such advances may carry considerable consequences in rehabilitation and designing devices for various spine pathologies.

7

GENERAL DISCUSSION

Spinal stability is a controversial notion governed by spinal tissues activations and passive contribution. Although it generally dictates the spine's capability to carry out its essential functions within physiological ranges of motion, it is a parameter of debate in the scientific community with little information on its mechanism and quantification. As highlighted in the literature review, loss in stability is indicative of developing spinal conditions, among which is low back pain. Thus, there remains a huge interest in further exploring and understanding this notion, which could lay the steppingstones towards improved treatments and corrective avenues of spinal conditions.

In an attempt to address these issues, motivated by the limitations identified in the literature review, and to bring an improved theoretical base to spinal stability and underlying activations, the field of finite elements modelling was exploited. In essence, the purpose of this thesis, in part, and this research, in whole, was to develop, verify, and validate a spine FE model representative of major spine soft tissues as a potential platform to exploring biomechanical mechanisms. In specific, the goal was to utilize this spine model to investigate the contribution of spinal muscles, their enclosed intramuscular pressure, intra-abdominal pressure, and thoracolumbar fascia towards stabilizing the spine under static equilibrium conditions. Besides, muscles contribution is generally governed by specific activation patterns, to which evaluating IMP-dependent stability-based activation strategies was also of interest. At the heart of this strategic methodology was the aim to advance our biomechanical perception of spinal stability and give comprehensive insights for future research.

The development of the spine computational platform was an integral aspect of this dissertation. Numerous decision factors had to be first considered and a thorough analysis on the exact model formulation was conducted. First and foremost was the modelling of skeletal muscles given their

fundamental role in force generation, transmission, and body locomotion[253]. Literature revealed that only a handful of numerical models take into account 2D and volumetric anatomy of muscles, along inner physiological factors, such as IMP[75,76]. The majority, however, consider simplified models, as extensive as linear force vectors, to simply quantify muscle forces[73,74,152]. This, in no means, imply that such models are ill-representations or faulty; they in fact serve their context of use, such as free-body kinematics. Besides, computational complexity and simulation power perhaps enforce such assumptions in order to develop a feasible model. All factors considered though, an accurate representation of the spine, along its interaction with muscles, requires more anatomically representative muscle models with a valid depiction of force transmission factors. To this matter, the merits of modelling enclosed muscle pressure, or IMP, could potentially be a plausible avenue.

As highlighted in paper 1, IMP has been shown to linearly correlate with muscle force and influence muscle performance. As such, integrating it with muscle force properties would create two complementary, fluid and structure, fields to enhance the representation of muscular contraction and improve the realism of volumetric FE muscle models. Therefore, it was believed that the accurate depiction of IMP might create a realistic and physiological model capable of interacting with the spine and other surrounding tissues. To test this theory, an anatomical model, based on the tibialis anterior muscle, was created and two custom fields, modelling the structural behavior of muscles and the fluidic pressure enclosed within were coded. Model results showed the existence of linear correlation between muscle contractile force and internal IMP, to which estimating one parameter *via* the other became possible.

To assess model's accuracy, indirect validation and verification case-scenarios were then conducted. The model showed to be valid, in light of previous published *ex vivo* and *in vivo* measurements, with a maximum discrepancy of 7.25%. Considering the wide range of variability in input parameters, mesh discretization, material properties, and tendon stiffness, sensitivity analyses supported that the model was robust, with a maximum verification discrepancy of 11.2%. Together, the differences in validation and verification results confirmed the first hypothesis. The fact that the author did not set up a direct experimental study to verify and validate the model depended on several factors. Firstly, published measurement studies on the same muscle were abundant and conclusive of the same linear correlation. Secondly, the muscle was modelled from

an MRI-scan with being mindful of the architecture and physiology of the comparators. Furthermore, methodical verification steps, highlighted by the sensitivity studies, were realized to ensure accurate formulation and simulation. Lastly, in all subsequent analyses, an initial validation step was carried out to further assess the model prior to conducting biomechanical simulations of interest. Such confidence levels must be kept in mind according to the context of use of the model.

Paper 1 achieved the development of the first scalable, custom-coded, biphasic FE model inclusive of an IMP enclosed fluidic field (objective 1). Since skeletal muscles are often distinguished by their length-tension property curves, the developed model also showed to abide by this inherent physiological relationship. From the author's understanding, the physiological link between IMP and resultant muscle force would allow replicating inner-body radial interaction between muscles and surrounding tissues. In other words, with the build-up of IMP, muscles would communicate with surrounding tissues by transmitting radial loads, which can be captured by the model put forth. Lastly, in fulfilling the global stability objective, chapter 3 successfully developed a muscle model that can be scaled to all paraspinal muscles, in order to initiate the development of a fully representative spine model, as proposed in chapter 4.

This led to evaluating whether the integration of pressurized spinal muscles, abdominal pressure, and thoracolumbar fascia in a uniform spine model would create an enhanced platform to analyze the mechanics of the spine. The inclusion of the aforementioned effects was motivated by their potential role in spinal stability, as put forth in the literature review. Other soft tissues were not explored herein, such as ligaments and the rib cage, due to their insignificant effect on this phenomenon and within the explored range of motion. That is, with all subsequent analyses adopting static physiological loadings, the ligaments have minimal effect as their role substantially appears at high deformations[254]. Besides, the stabilizing action of the rib cage mostly comes into effect under dynamic respiration processes[255], which is out of scope of the present thesis. On the other hand, the modelled tissues were based on a patient-specific MRI-scans obtained from an open-source Japanese database. That is, little to no alterations to the original anatomy were made in order to maintain model's credibility, which the author recommends for future models.

The resultant spine model, once put together, presented several challenges, among which was the computational mesh. The complexity of the model, being composed of hundreds of components, was accompanied with the hard decision of how to discretize the numerical field

while maintaining accuracy and computational feasibility. The author admits that numerous techniques were first developed and tested but with each requiring weeks and months to solve for a single simulation case. At this point, a decision was made to eliminate contacts computations by creating a uniform, unitary, spine structure with conforming meshes. Taking into account the biomechanics of the human body, this is actually recommended to execute homogenous motion and deformation across all tissues. In other words, tendons are extensions to muscle fascicles[256], whereby modelling those as one complex with no contacts in between is reasonable. In addition, under normal physiological ranges, tissues in interaction with the spine structure experience little to no separation or sliding[257], to which a uniform system with no contacts in between may be a feasible option. Therefore, a manual user-generated, non-conventional, meshing technique was created for this model to ease simulation time. As described in paper 2, this was done by creating a uniform mesh with conforming nodes between contacting objects, thus eliminating all unnecessary FE contacts. The second decision was to adopt linear material properties representative of static deformation associated with the spine. Although inherent response of soft tissue experiences nonlinear properties, the adopted set of material properties were previously validated and were adopted from the selected validation comparators. Besides, the decision to not consider nonlinear and viscoelastic properties was also, in part, motivated by the quasi-static nature and small range of motion of simulated scenarios of interest, all in the sake of enhancing model's feasibility and computational time. That is, under quasi-static conditions, it may be reasonable to ignore time-dependent parameters including viscoelasticity, whereas given the simulated range of motion, it may be feasible to assume that the material will behave within the linear regime. Still, to confirm this, as presented in paper 2, a strain analysis within the simulated range was conducted to which its results were in high agreement with the linear regime of the stress-strain curves of the included tissues[96,131,258–260], thus further supporting the use of a linear behavior. However, due to computational limitations, this study still lacked a material property sensitivity case-study, which presented the potential for the additional study presented in chapter 4.

In essence, the use of material properties representative of underlined mechanics is perhaps one of the most critical decisions in any engineering/biomechanical problem. Specifically, the material response of a soft tissue is governed by numerous factors including age, medical conditions, lifestyle, amongst other factors. That being the case, it comes with no surprise that literature reports large variabilities and discrepancies in this field. As such, in efforts of further verifying the inputs

of the spine model, in terms of material properties, paper 3 presents a feasibility study on reverse-engineering such properties of any soft tissue under consideration. This study was motivated by a virtual reality simulator, for surgical training purposes, developed in the musculoskeletal biomechanics research lab at McGill university. During such procedures, a needle is inserted into a tissue, which could be modelled in FE using fracture mechanics and cohesive elements. When this is coupled with a material behavior optimization scheme, the use of cohesive elements can be exploited to extract the mechanical response of the tissue. As such, paper 3 presented this novel approach using a hybrid gradient descent optimization algorithm to minimize the resultant material-based error function, which permitted capturing underlying fracture properties as well as hyperelastic material shear modulus. The author opines that this procedure, once further enhanced, can serve as a database for different soft tissues force-insertion profiles to be used by surgeons and physicians in clinical training purposes. However, there remains a need to cross-examine the results against *in vivo* tests to find meaningful correlations prior to building material properties databases. Still, with a maximum difference of 15% from experimental curves, as shown in paper 3, the adopted framework seemed promising should one need to verify adopted material properties, as the case with the FE spine model and future applications towards patient specific FE model tailoring.

After numerous discussed verification steps, the FE spine model still required sequential validation. In other words, the model was at the state-of-the-art, so to speak, in terms of integrating a unique set of soft tissues that have never been, together, modelled before. For that reason, a structure-by-structure or component-based approach towards validation was conducted from validating the pressurized muscle procedure, intervertebral discs pressure, the lumbar spine region, and the whole spine structure. The power of such a methodical procedure is the added validity of comparing against several comparators from different studies and with different experimental platforms. With results showing a maximum discrepancy of 13% in regard to IMP and IAP values required to achieve similar displacements, as entitled in the full spine validation test in paper 2, the model was deemed valid and capable of simulating spinal mechanics within the planned context of use and considering the adopted risk-based credibility assessment plan (hypothesis 2). Thus, a full-scale spine model, inclusive of the TLF, major spine muscles, IMP, and IAP was successfully developed, verified, and extensively validated in light of previous studies, to which objective 2 was accomplished. From the perspective of the author, the impact of this fully

representative FE spine model extends beyond numerical modelling and validation. In essence, the model can help in numerous industrial and biomechanical frameworks such as assessing spine injuries, investigating low-back pain, and designing spinal instrumentation. Perhaps more importantly, in the context of this dissertation, it serves as the ideal foundation to examine equilibrium spinal stability, as proposed in chapter 5.

The successful development and validation of the spine model allowed to test hypothesis 3, whereby modelled IAP, TLF, and included spinal muscles were activated in efforts of maintaining equilibrium spinal stability. With a multitude of stability quantification methods available, the one most convenient to the targeted context of use, under equilibrium static conditions, was adopted[261]. That is, the capability of a specific soft tissues to retrieve the spine within the vicinity of its initial position dictates the underlined tissue stability contribution. The reason behind focusing on IAP, TLF, and major spinal muscles is their believed role in supporting the spine under static loadings as well as in motion[262]. That is, the agonistic and antagonistic coactivation role of spinal muscles generally increase spinal compressive loads[263], thus increasing spine's apparent stiffness. Furthermore, one reason for taking into account muscles' enclosed IMP is the harmony enforced by this fluidic field to transfer generated loads, as shown in paper 1, in order for muscles to efficiently support the spine. Lastly, the contribution of IAP and TLF to spinal stability is often overlooked, though have been shown to provide foundational support to surrounding tissues, among which is the spine[87,264]. As such, activations of such tissues and their contribution to maintain equilibrium spinal stability was assessed *via* vertebral forward displacements, to which results showed a stability increase of up to 93% when the underlined tissues were synergistically activated, as shown in paper 4 (hypothesis 3).

In addition, the explored scenarios suggested an optimized behavior with different activation patterns exhibited by each investigated tissue. The 53% increase in stability achieved by spinal muscles speaks to their antagonistic role against excessive spinal external loads, forward flexion in this case. Besides, the inter-relation between IMP and muscle force supported the observation of muscles developing and tolerating high tensional forces under increased IMP, which may relate to enhanced muscular endurance on the long term. Such observations lead the author to recommend, from a purely mechanistic perspective, strengthening exercises of spinal muscles as a potential avenue to counter spinal deformities, due to such high stability effort. On the other

hand, of particular interest were the results of the TLF which showed a significant contribution of up to 75% stability effort. This agrees with previous observations on the passive strength of the TLF which permits it to store elevated tensional forces as a relief mechanism and to assist back muscles during contraction[265,266]. Lastly, although relatively smaller than other tissues, the IAP still contributed to about 25% of total equilibrium spinal stability by exerting frontal supportive forces on the spine. Since the model of the abdominal cavity was based on the anatomy of abdominal muscles, one recommendation can be to practice abdominal activation rehabilitative exercises to increase the efficacy of activating the IAP, and thus increase spinal stability. Nevertheless, with such an impact on stability, accurate modelling of the explored tissues herein could benefit the formulation of rehabilitation programs in efforts of countering spinal deformities, and perhaps, low back pain.

The activation of spinal muscles and abdominal pressure are governed by several factors which dictate their potential involvement in spine stability. A thorough investigation of this does not only complement our understanding of spinal stability, but also may lend insights into the passive engagement of the TLF. As such, an additional study in chapter 5 was conducted to investigate abdominal physiological factors affecting abdominal compliance, and indirectly spinal stability, whereas muscle activations were reserved for chapter 6. In essence, the stiffness, wall thickness, and cross-sectional area of the abdomen dictate abdominal compliance, and further the level of IAP activation. Paper 5 first showed that the mechanisms governing abdominal activation were valid in light of two literature comparators with a maximum difference of 13.1%. The widespread in validation data were best interpreted by the wide variation in patient-to-patient physiologies, to which results further validated the FE spine model. On the other hand, abdominal compliance was shown to be inversely related to wall thickness, elasticity, and cross-section. This directly relate to clinical research on obesity in which the results support that such a condition yield dangerously low levels of passive abdominal compliance[267,268]. In addition, of particular interest to this dissertation is the relevance of results to spine stability. Paper 5 showed that improved abdominal active compliance, associated with augmented elasticity, tend to increase IAP supportive forces to levels up to 42.7N, thus improving overall stability. Furthermore, supporting the findings of paper 4, the TLF exhibited elevated passive tensional forces in efforts of further contributing to a more stable spine position. Thus, the study supported the efficacy of abdominal physiological changes to improve mechanical outcomes; more specifically, equilibrium spinal stability.

The successful completion of objective 3 presented insights of high significance pertaining to spinal stability achieved by the IAP, TLF, and spinal muscles. In this context, the closing of chapter 5 delivered preliminary assessments that showed significant levels of muscle contribution to achieve a relatively stable spine position. The fact of the matter remained, however, that it was still unknown as to what patterns exactly governed such muscle activations, which significantly enhanced equilibrium spinal stability. At this point in this dissertation, however, one could argue about the critical need to account for IMP in skeletal muscle models, which led to putting forth and testing the last 2 hypotheses (hypotheses 4 and 5). In specific, chapter 6 aimed to conclude the discussion on spinal stability, within the context of this thesis, by examining muscle strategies activated for an equilibrium spinal stability objective.

In light of paper 6, three conventional activation strategies were first examined, which added further confidence to the credibility and validity of the FE spine model. These included minimizing muscle effort perceived by muscular forces, minimizing IVD compressive forces, and maintaining maximum stability at all costs, to which the results of these investigations showed a maximum discrepancy of 9.8% from *ex vivo* and *in silico* comparators. Furthermore, the maximum stability strategy exhibited high muscle and TLF supportive forces in effort of achieving a nearly absolute stable position with only a 0.04cm vertebral displacement. The significance of this can be thought of as the extreme measures enforced by the neuromuscular system, in terms of exerting total muscle force as high as 734N, to stabilize the spine at all physiological costs, reaching a relatively absolute stable position with 0.04cm displacements, in cases of sudden external stimuli [269]. In comparison to this, the minimum muscle effort strategy experienced the least amount of muscle forces in support of the spine, but with a less stable position. In support to chapter 5, TLF forces seemed to have compensated for the minimum developed muscle forces, which in fact speaks to the efficacy of the motor system in improving muscle endurance *via* the engagement of other tissues[248]. Similar findings were observed with the minimum IVD compressive forces but with higher TLF tensional forces, which, in the author's opinion, might be indicative of a relief mechanism for low back pain. This topic is highly debatable, but the idea is that the less forces experienced by the IVDs, accompanied with high TLF supportive loads, is indicative of less compression on the discs, which might otherwise potentially reduce low back pain episodes associated with narrowed disc.

Following the examination of these three conventional strategies, two novel IMP-based activations were devised and evaluated to conclude the assessment of hypotheses 4 and 5. Those were primarily to minimize and maximize IMP, while respecting physiological muscles constraints, in the sake of maintaining a stable spine position. The physiological validity of these strategies, namely pressure-based muscle activations, is motivated by historical and literature evidence on the presence of pressure-sensitive mechanoreceptors in skeletal muscles[270] and the diaphragm[271]. That is, the core concept and fundamentals of these activation strategies are plausible whereby the neuromuscular system is capable of receiving pressure feedback from skeletal muscles, thus monitoring and executing controlled pressure-based muscular activations. That being the case, two IMP-based activation strategies, described earlier, were explored.

In specific, the minimal IMP strategy was accompanied with relatively low muscle forces (within 6% of those of the minimal muscle force conventional strategy) but with extremely high TLF forces. The small amount of developed IMP (29% decrease from the minimal muscle force strategy) caused a curvature in TLF fibers, which directly affected vectoral tension within the tissue. Both these results confirmed the fourth hypothesis. Considering the relatively good stability achieved, results potentially suggest the efficacy of enhanced force transmission *via* the enclosed fluidic field[75]. The last strategy of maximizing IMP carried results of particular interest whereby the excessive increase in IMP was accompanied with a plateau of almost a constant force of around 850N (within 16% of the absolute stability conventional strategy). This was accompanied with TLF passive forces as high as 56.9N (2.16 times the TLF forces of the absolute stability strategy). Both these results affirmed the last hypothesis (hypothesis 5). Observations further showed that elevated levels of IMP were coupled with a build-up of compartmental pressure between surrounding tissues, thus abutting adjacent muscles and the TLF *via* intra- and inter-muscular pressure. Such an observation supports the idea that muscles can also share radial loads, as previously discussed[272]. All things considered, the investigated IMP-based strategies support the inclusion of IMP in stability models due to roles in force transmission and load sharing. Besides, the TLF persists as a critical passive structure capable of withstanding and storing elevated tensional forces in efforts of improving equilibrium spinal stability. This concluded the last objective whereby such stability findings may inform clinical assessments, motion analysis, and medical device design for various spine pathologies.

The FE spine model put forth in chapter 4 presents a great potential for a wide range of other biomechanical analyses. Although successfully validated within the explored context of uses, other investigations might necessitate additional improvements, and thus further validation steps. In this research, it was exploited to advance our understanding of equilibrium spinal stability; however, there remains other aspects of stability not explored herein, such as dynamic and clinical stabilities[219,239]. For this purpose, the development of a model capable of executing time-dependent analyses remains of huge interest. At the time of writing this dissertation, a bench-top controllable spine model is under development at the musculoskeletal biomechanics research lab at McGill university. Once fully functional, this could provide a potential avenue to validating a dynamic numerical model with which more advanced analyses can be conducted. Besides, the investigated activation strategies in chapter 6 also assume static conditions, which is reasonable for quasi-static motion conditions. However, muscle activations are governed by more complex phenomena at the microstructural levels, mostly dynamic interactions, to which the availability of such a bench-top controllable spine could provide insights into developing and validating such dynamically driven muscle models.

To date, though, there has been no single finite elements spine model representative of spine's physiology and inclusive of developed primary spine tissues. The milestones achieved herein put forth the first scalable and feasible muscle model to account for IMP and a state-of-the-art physiologically accurate spine model. The availability and validity of the approach permitted to lay foundations for equilibrium spinal stability along underlying IMP-based activation strategies. Hence, this dissertation advanced the knowledge sphere enclosing spine's biomechanics, from theoretical and applied perspectives, as disseminated by the 6 scientific journal articles presented herein.

8

CONCLUSION AND PERSPECTIVES

From a personal experience of my father fracturing one of his lower back vertebral bodies, and my mother constantly experiencing painful low back pain episodes, I conducted this research to strengthen my background in order to strive towards developing patient-specific relief devices for such underlined conditions. However, a question that has travelled with me throughout my doctoral journey and has constantly challenged my approaches and vision is: with the huge industrial pace and constant shifts in individuals' lifestyles, are we ever capable of keeping track of the evolving pathomechanisms and, accordingly, putting forth biological and physiological treatments? Perhaps, and this is nothing but a personal vision and hope, the fields of modelling and virtual simulations present themselves as competitive candidates to expedite this process.

As such, this doctoral dissertation exploited the field of finite elements, putting forth a novel spine model, to explore, quantify, and interpret the notion of equilibrium spinal stability governed by the collaborative activation of spinal tissues. The adopted methodical route advanced the biomechanical perception of pressurized muscles, physiological spine models, muscle recruitment patterns mechanisms, and fundamentals of stability. The developed *in silico* models, in combination with thorough *in vivo*, *ex vivo*, and *in situ* validations, has led to novel explorations of biomechanical factors relating to spinal stability, deformities, and potentially low back pain.

The framework initiated with the development of a volumetric FE muscle model, which showed a direct correlation between muscle contractile forces and enclosed IMP. Conducted validation and verification scenarios lent credibility to model's applications, robustness, and scalability potential. Thus, the model may be integrated in clinical environments to assess muscle forces and

injuries *via* IMP non-invasive measurement tools. This creates the opportunity to formulate patient-specific models, from which simulated preliminary interpretations can be made. However, it is still recommended to expand the capabilities of model put forth, including the integration of dynamic processes, to capture contraction mechanisms.

The scaling of the model to major spine muscles, and in combination with physiological models of the abdominal cavity and the thoracolumbar fascia, permitted the development of a state-of-the-art, full-scale, FE spine model. Extensive validation and verification analyses concluded a credible and timely model, with which spinal biomechanical simulations of interest can be conducted. However, it was still recommended to consider the sensitivity of the adopted materials prior to making firm clinical biomechanical interpretations. To this matter, an optimization method to reverse-engineer the exact material behavior of soft tissues was formulated and tested against experimental force insertion curves, which showed the feasibility of this approach to verify an adopted set of properties. Furthermore, in order to overcome computational complexity and enhance simulation time, it is recommended to adopt the formulated meshing technique for systems acting as unitary structures. Although judged insignificant for the explored context of uses herein, one suggestion to improve the model in the future is to include other soft tissues, such as ligaments and the rib cage, which may prove to contribute to other spine mechanics. Lastly, the model can be potentially integrated into virtual reality simulators for an enhanced metaverse representation.

The novelties exhibited by the developed FE model served to explore the controversial notion of spinal stability. Combined synergistic activations of spinal muscles, abdominal pressure, and thoracolumbar fascia showed to majorly contribute to stability. Furthermore, a specific case-study on abdominal pressure and compliance showed that abdominal wall stiffness, thickness, and cross-section indirectly relate to spine's stability. Thus, it is recommended to practice rehabilitative strengthening exercises of the underlined tissues to improve spinal posture and equilibrium stability. Furthermore, surgeons are advised to conduct minimally invasive spinal surgeries without much disrupting the thoracolumbar fascia due to shown significant contribution to stability. Still, further investigations are required, among which is to examine other aspects of stability, in order to arrive at more clinically significant suggestions.

Lastly, muscle recruitment patterns lent insights into the efficacy of the motor system to execute motor tasks, while maximizing muscle endurance *via* engaging surrounding soft tissues. The IMP-based activation patterns suggested an efficient force transmission process through the enclosed fluidic field. They further supported the idea of muscles sharing radial loads by developing compartmental pressure between spinal tissues. From the author's perspective, the inclusion of IMP in recruitment patterns may potentially allow for a better estimate of individual muscle forces. Thus, it is recommended to complement stability-based electromyography measurements with IMP-based activations in order to arrive at improved spinal stability guidance. This, however, requires dynamic and time-dependent muscle models, combined with extensive validation experiments, for the feasibility of integrating this with electrical activity approaches, which the author thrives to accomplish in future research career.

This dissertation has offered several novelties, significances, and contributions to the advancement of knowledge. In specific, it integrated three influential frameworks being a biomechanical-based numerical modelling of soft tissues, mechanobiological assessment of spinal physiologies, and macrostructural mechanics of muscles. In specific, the global objective has been successfully met whereby physiologically representative finite element models of a volumetric muscle and full spine were developed, with a maximum of 7.25% and 13% validation accuracy, respectively; thus also confirming hypotheses 1 and 2. The second part of the central objective was also achieved in which equilibrium spinal stability, maintained by spinal muscles, intra-abdominal pressure, and TLF, was assessed. These included tissues contributed to 93% of overall spine's equilibrium stability, thus answering the third hypothesis. The last part of the global objective was also successfully met whereby the inclusion of intramuscular pressure in spine stability-based models was assessed, which further confirmed the last two hypotheses. A potential avenue, at this point, can be to address the suggested improvements presented herein in this research. Upon doing so, limitless opportunities would present itself to contribute to the public health and well-being of individuals.

REFERENCES

1. Rice, D. & Dietrich, S. The vertebral column. in Embryos, Genes and Birth Defects 411–462 (John Wiley and Sons Ltd Chichester, 2006).

2. Watanabe, G., Kawaguchi, S., Matsuyama, T. & Yamashita, T. Correlation of scoliotic curvature with Z-score bone mineral density and body mass index in patients with osteogenesis imperfecta. Spine (Phila. Pa. 1976). 32, E488–E494 (2007).

3. Cholewicki, J., Simons, A. P. D. & Radebold, A. Effects of external trunk loads on lumbar spine stability. J. Biomech. (2000). doi:10.1016/S0021-9290(00)00118-4

4. Zhou, J., Dai, B. & Ning, X. The assessment of material handling strategies in dealing with sudden loading: Influences of foot placement on trunk biomechanics. Ergonomics (2013). doi:10.1080/00140139.2013.822568

5. Galbusera, F. The spine: its evolution, function, and shape. in Biomechanics of the Spine 3–9 (Elsevier, 2018).

6. Panjabi, M. The Stabilizing System of the Spine. Part I. Function, Dysfunction, Adaptation, and Enhancement. J. Spinal Disord. 5, 383–389; discussion 397 (1992).

7. Singh, H., Chang Chien, G. C. & Bolash, R. Anatomy of the spine. Treat. Chronic Pain Cond. A Compr. Handb. 11–20 (2017). doi:10.1007/978-1-4939-6976-0_4

8. Whitten, G. Trauma to the Upper Thoracic Spine: Anatomy, Biomechanics, and Unique Imaging Features. Image (Rochester, N.Y.) (1993).

9. Pait, T. G., Elias, A. J. R. & Tribell, R. Thoracic, lumbar, and sacral spine anatomy for endoscopic surgery. Neurosurgery 51, 67–78 (2002).

10. Driscoll, M. Design, Optimization, and Evaluation of a Fusionless Device to induce Growth Modulation and Correct Spinal Curvatures in Adolescent Idiopathic Scoliosis. PhD diss., École Polytechnique de Montréal (2011).

11. Ritzel, H., Amling, M., Pösl, M., Hahn, M. & Delling, G. The thickness of human vertebral cortical bone and its changes in aging and osteoporosis: A histomorphometric analysis of the complete spinal column from thirty-seven autopsy specimens. J. Bone Miner. Res. 12, 89–95 (1997).

12. Roberts, S., Menage, J. & Eisenstein, S. M. The cartilage end-plate and intervertebral disc in scoliosis: Calcification and other sequelae. J. Orthop. Res. 11, 747–757 (1993).

13. Tomita, K., Kawahara, N., Toribatake, Y. & Heller, J. G. Expansive midline T-saw laminoplasty (Modified spinous process- splitting) for the management of cervical myelopathy. Spine (Phila. Pa. 1976). (1998). doi:10.1097/00007632-199801010-00007

14. Mollica, F., Preziosi, L. & Rajagopal, K. R. Modeling of biological materials. (Springer Science & Business Media, 2007).

15. Gibson, L. J. The mechanical behaviour of cancellous bone. J. Biomech. 18, 317–328 (1985).

16. Goel, V. K., Ramirez, S. A., Kong, W. & Gilbertson, L. G. Cancellous bone young's modulus variation within the vertebral body of a ligamentous lumbar spine—application of bone adaptive remodeling concepts. J. Biomech. Eng. (1995). doi:10.1115/1.2794180

17. Shirazi-Adl, S. A., Shrivastava, S. C. & Ahmed, A. M. Stress analysis of the lumbar disc-body unit in compression. A three-dimensional nonlinear finite element study. Spine (Phila. Pa. 1976). (1984). doi:10.1097/00007632-198403000-00003

18. Zander, T., Rohlmann, A., Burra, N. K. & Bergmann, G. Effect of a posterior dynamic implant adjacent to a rigid spinal fixator. Clin. Biomech. (2006). doi:10.1016/j.clinbiomech.2006.04.001

19. Argoubi, M. & Shirazi-Adl, A. Poroelastic creep response analysis of a lumbar motion segment in compression. J. Biomech. (1996). doi:10.1016/0021-9290(96)00035-8

20. Kumaresan, S., Yoganandan, N. & Pintar, F. A. Finite element analysis of the cervical spine: A material property sensitivity study. Clin. Biomech. (1999). doi:10.1016/S0268-0033(98)00036-9

21. Rohlmann, A., Zander, T., Schmidt, H., Wilke, H. J. & Bergmann, G. Analysis of the influence of disc degeneration on the mechanical behaviour of a lumbar motion segment using the finite element method. J. Biomech. (2006). doi:10.1016/j.jbiomech.2005.07.026

22. Tadano, S., Kanayama, M., Ukai, T. & Kaneda, K. Morphological Modeling and Growth Simulation of Idiopathic Scoliosis. in Computational Biomechanics (1996). doi:10.1007/978-4-431-66951-7_4

23. Chosa, E., Totoribe, K. & Tajima, N. A biomechanical study of lumbar spondylolysis based on a three-dimensional finite element method. J. Orthop. Res. (2004). doi:10.1016/S0736-0266(03)00160-8

24. Goto, K. et al. Effects of lumbar spinal fusion on the other lumbar intervertebral levels (three-dimensional finite element analysis). J. Orthop. Sci. (2003). doi:10.1007/s00776-003-0675-1

25. Lafage, V., Gangnet, N., Sénégas, J., Lavaste, F. & Skalli, W. New interspinous implant evaluation using an in vitro biomechanical study combined with a finite-element analysis. Spine (Phila. Pa. 1976). (2007). doi:10.1097/BRS.0b013e3180b9f429

26. Ivanov, A. A., Kiapour, A., Ebraheim, N. A. & Goel, V. Lumbar fusion leads to increases in angular motion and stress across sacroiliac joint: A finite element study. Spine (Phila. Pa. 1976). (2009). doi:10.1097/BRS.0b013e3181978ea3

27. Cassidy, J. J., Hiltner, A. & Baer, E. Hierarchical structure of the intervertebral disc. Connect. Tissue Res. (1989). doi:10.3109/03008208909103905

28. Bellini, C. M., Galbusera, F., Raimondi, M. T., Mineo, G. V. & Brayda-Bruno, M. Biomechanics of the lumbar spine after dynamic stabilization. J. Spinal Disord. Tech. (2007). doi:10.1097/BSD.0b013e318031af6f

29. Fantigrossi, A., Galbusera, F., Raimondi, M. T., Sassi, M. & Fornari, M. Biomechanical analysis of cages for posterior lumbar interbody fusion. Med. Eng. Phys. (2007). doi:10.1016/j.medengphy.2006.02.007

30. Lavaste, F., Skalli, W., Robin, S., Roy-Camille, R. & Mazel, C. Three-dimensional geometrical and mechanical modelling of the lumbar spine. J. Biomech. (1992). doi:10.1016/0021-9290(92)90071-8

31. Park, W. M., Kim, K. & Kim, Y. H. Effects of degenerated intervertebral discs on intersegmental rotations, intradiscal pressures, and facet joint forces of the whole lumbar spine. Comput. Biol. Med. (2013). doi:10.1016/j.compbiomed.2013.06.011

32. Wang, J. L., Parnianpour, M., Shirazi-Adl, A. & Engin, A. E. Viscoelastic finite-element analysis of a lumbar motion segment in combined compression and sagittal flexion: Effect of loading rate. Spine (Phila. Pa. 1976). (2000). doi:10.1097/00007632-200002010-00009

33. Baroud, G., Nemes, J., Heini, P. & Steffen, T. Load shift of the intervertebral disc after a vertebroplasty: A finite-element study. Eur. Spine J. (2003). doi:10.1007/s00586-002-0512-9

34. Zhong, Z. C. et al. Finite element analysis of the lumbar spine with a new cage using a topology optimization method. in Medical Engineering and Physics (2006). doi:10.1016/j.medengphy.2005.03.007

35. Ruberté, L. M., Natarajan, R. N. & Andersson, G. B. Influence of single-level lumbar degenerative disc disease on the behavior of the adjacent segments-A finite element model study. J. Biomech. (2009). doi:10.1016/j.jbiomech.2008.11.024

36. Kurutz, M. & Oroszváry, L. Finite element analysis of weightbath hydrotraction treatment of degenerated lumbar spine segments in elastic phase. J. Biomech. (2010). doi:10.1016/j.jbiomech.2009.10.004

37. Little, J. P., Izatt, M. T., Labrom, R. D., Askin, G. N. & Adam, C. J. An FE investigation simulating intra-operative corrective forces applied to correct scoliosis deformity. Scoliosis (2013). doi:10.1186/1748-7161-8-9

38. Salim, M. S., Jaapar, N. F. N., Salleh, A. F. & Daud, R. Effect of muscle on cortical bone layer by finite element modeling. in AIP Conference Proceedings (2021). doi:10.1063/5.0044604

39. Dong, X. N. & Guo, X. E. The dependence of transversely isotropic elasticity of human femoral cortical bone on porosity. J. Biomech. (2004). doi:10.1016/j.jbiomech.2003.12.011

40. Lu, Y. M., Hutton, W. C. & Gharpuray, V. M. Can variations in intervertebral disc height affect the mechanical function of the disc? Spine (Phila. Pa. 1976). (1996). doi:10.1097/00007632-199610010-00006

41. Schmidt, H., Heuer, F. & Wilke, H. J. Which axial and bending stiffnesses of posterior implants are required to design a flexible lumbar stabilization system? J. Biomech. (2009). doi:10.1016/j.jbiomech.2008.10.005

42. Chen, C.-S., Cheng, C.-K., Liu, C.-L. & Lo, W.-H. Stress analysis of the disc adjacent to interbody fusion in lumbar spine. Med. Eng. Phys. (2001). doi:10.1016/S1350-4533(01)00076-5

43. Bernard, S., Grimal, Q. & Laugier, P. Accurate measurement of cortical bone elasticity tensor with resonant ultrasound spectroscopy. J. Mech. Behav. Biomed. Mater. (2013). doi:10.1016/j.jmbbm.2012.09.017

44. Yoon, H. G., Heo, S. J., Koak, J. Y., Kim, S. K. & Lee, S. Y. Effect of bone quality and implant surgical technique on implant stability quotient (ISQ) value. J. Adv. Prosthodont. (2011). doi:10.4047/jap.2011.3.1.10

45. Semaan, M. et al. Assessment of elastic coefficients of child cortical bone using resonant ultrasound spectroscopy. J. Mech. Behav. Biomed. Mater. (2019). doi:10.1016/j.jmbbm.2018.09.044

46. Cai, X. et al. Anisotropic elastic properties of human cortical bone tissue inferred from inverse homogenization and resonant ultrasound spectroscopy. Materialia (2020). doi:10.1016/j.mtla.2020.100730

47. Lawrence Katz, J. et al. The effects of remodeling on the elastic properties of bone. Calcif. Tissue Int. (1984). doi:10.1007/BF02406131

48. Noailly, J., Wilke, H. J., Planell, J. A. & Lacroix, D. How does the geometry affect the internal biomechanics of a lumbar spine bi-segment finite element model? Consequences on the validation process. J. Biomech. (2007). doi:10.1016/j.jbiomech.2006.11.021

49. Malandrino, A., Planell, J. A. & Lacroix, D. Statistical factorial analysis on the poroelastic material properties sensitivity of the lumbar intervertebral disc under compression, flexion and axial rotation. J. Biomech. (2009). doi:10.1016/j.jbiomech.2009.07.039

50. Louna, Z., Goda, I. & Ganghoffer, J. F. Homogenized strain gradient remodeling model for trabecular bone microstructures. Contin. Mech. Thermodyn. (2019). doi:10.1007/s00161-019-00746-6

51. Humzah, M. D. & Soames, R. W. Human intervertebral disc: structure and function. Anat. Rec. 220, 337–356 (1988).

52. Helgason, B. et al. Mathematical relationships between bone density and mechanical properties: A literature review. Clinical Biomechanics (2008). doi:10.1016/j.clinbiomech.2007.08.024

53. Zhou, Z. et al. Shock absorbing function study on denucleated intervertebral disc with or without hydrogel injection through static and dynamic biomechanical tests in vitro. Biomed Res. Int. (2014). doi:10.1155/2014/461724

54. Roberts, F. The nature and functions of the intervertebral discs. Br. J. Radiol. 17, 54–59 (1944).

55. Nikkhoo, M., Hsu, Y. C., Haghpanahi, M., Parnianpour, M. & Wang, J. L. A meta-model analysis of a finite element simulation for defining poroelastic properties of intervertebral discs. Proc. Inst. Mech. Eng. Part H J. Eng. Med. (2013). doi:10.1177/0954411913480668

56. Moss, I. L., Gordon, L., Woodhouse, K. A., Whyne, C. M. & Yee, A. J. M. A novel thiol-modified hyaluronan and elastin-like polypetide composite material for tissue engineering of the

nucleus pulposus of the intervertebral disc. Spine (Phila. Pa. 1976). (2011). doi:10.1097/BRS.0b013e3181e7b705

57. Groth, K. M. & Granata, K. P. The viscoelastic standard nonlinear solid model: Predicting the response of the lumbar intervertebral disk to low-frequency vibrations. J. Biomech. Eng. (2008). doi:10.1115/1.2904464

58. Yang, H., Jekir, M. G., Davis, M. W. & Keaveny, T. M. Effective modulus of the human intervertebral disc and its effect on vertebral bone stress. J. Biomech. (2016). doi:10.1016/j.jbiomech.2016.02.045

59. Zhang, Q. H., Zhou, Y. L., Petit, D. & Teo, E. C. Evaluation of load transfer characteristics of a dynamic stabilization device on disc loading under compression. Med. Eng. Phys. (2009). doi:10.1016/j.medengphy.2008.09.011

60. Fagan, M. J., Julian, S., Siddall, D. J. & Mohsen, A. M. Patient-specific spine models. Part 1: Finite element analysis of the lumbar intervertebral disc - A material sensitivity study. in Proceedings of the Institution of Mechanical Engineers, Part H: Journal of Engineering in Medicine (2002). doi:10.1243/09544110260216577

61. Iatridis, J. C. & Ap Gwynn, I. Mechanisms for mechanical damage in the intervertebral disc annulus fibrosus. J. Biomech. (2004). doi:10.1016/j.jbiomech.2003.12.026

62. Ghezelbash, F., Shirazi-Adl, A., Baghani, M. & Eskandari, A. H. On the modeling of human intervertebral disc annulus fibrosus: Elastic, permanent deformation and failure responses. J. Biomech. (2020). doi:10.1016/j.jbiomech.2019.109463

63. Panjabi, M. M. Clinical spinal instability and low back pain. J. Electromyogr. Kinesiol. 13, 371–379 (2003).

64. Hansen, L. et al. Anatomy and biomechanics of the back muscles in the lumbar spine with reference to biomechanical modeling. Spine (Phila. Pa. 1976). 31, 1888–1899 (2006).

65. Smith, D. A. The theory of sliding filament models for muscle contraction. III. Dynamics of the five-state model. J. Theor. Biol. (1990). doi:10.1016/S0022-5193(05)80372-8

66. O'Brien, M. The anatomy of the achilles tendon. Foot Ankle Clin. 10, 225–238 (2005).

67. Henson, B. & Edens, M. A. Anatomy, back, muscles. (2019).

68. Ward, S. R. et al. Architectural analysis and intraoperative measurements demonstrate the unique design of the multifidus muscle for lumbar spine stability. J. Bone Jt. Surg. - Ser. A (2009). doi:10.2106/JBJS.G.01311

69. Bogduk, N., Pearcy, M. & Hadfield, G. Anatomy and biomechanics of psoas major. Clin. Biomech. (1992). doi:10.1016/0268-0033(92)90024-X

70. Han, K. S., Rohlmann, A., Yang, S. J., Kim, B. S. & Lim, T. H. Spinal muscles can create compressive follower loads in the lumbar spine in a neutral standing posture. Med. Eng. Phys. (2011). doi:10.1016/j.medengphy.2010.11.014

71. Gatton, M. L., Pearcy, M. J., Pettet, G. J. & Evans, J. H. A three-dimensional mathematical model of the thoracolumbar fascia and an estimate of its biomechanical effect. J. Biomech. (2010). doi:10.1016/j.jbiomech.2010.06.022

72. Röhrle, O., Davidson, J. B. & Pullan, A. J. A physiologically based, multi-scale model of skeletal muscle structure and function. Front. Physiol. (2012). doi:10.3389/fphys.2012.00358

73. Semwal, S. K. & Hallauer, J. J. Biomechanical modeling: Implementing line-of-action algorithm for human muscles and bones using generalized cylinders. Comput. Graph. (1994). doi:10.1016/0097-8493(94)90121-X

74. Nussbaum, M. A., Chaffin, D. B. & Rechtien, C. J. Muscle lines-of-action affect predicted forces in optimization-based spine muscle modeling. J. Biomech. (1995). doi:10.1016/0021-9290(94)00078-I

75. Jenkyn, T. R., Koopman, B., Huijing, P., Lieber, R. L. & Kaufman, K. R. Finite element model of intramuscular pressure during isometric contraction of skeletal muscle. Phys. Med. Biol. (2002). doi:10.1088/0031-9155/47/22/309

76. Wheatley, B. B., Odegard, G. M., Kaufman, K. R. & Haut Donahue, T. L. A validated model of passive skeletal muscle to predict force and intramuscular pressure. Biomech. Model. Mechanobiol. (2017). doi:10.1007/s10237-016-0869-z

77. Levinson, S. F., Shinagawa, M. & Sato, T. Sonoelastic determination of human skeletal muscle elasticity. J. Biomech. (1995). doi:10.1016/0021-9290(94)00173-2

78. Feng, Y. N., Li, Y. P., Liu, C. L. & Zhang, Z. J. Assessing the elastic properties of skeletal muscle and tendon using shearwave ultrasound elastography and MyotonPRO. Sci. Rep. (2018). doi:10.1038/s41598-018-34719-7

79. Ward, S. R. et al. Passive mechanical properties of the lumbar multifidus muscle support its role as a stabilizer. J. Biomech. (2009). doi:10.1016/j.jbiomech.2008.09.042

80. Regev, G. J. et al. Psoas muscle architectural design, in vivo sarcomere length range, and passive tensile properties support its role as a lumbar spine stabilizer. Spine (Phila. Pa. 1976). (2011). doi:10.1097/BRS.0b013e31821847b3

81. Deeken, C. R. & Lake, S. P. Mechanical properties of the abdominal wall and biomaterials utilized for hernia repair. J. Mech. Behav. Biomed. Mater. 74, 411–427 (2017).

82. Metan, S., Mohankumar, G. C. & Krishna, P. FEM an Effective Tool to Analyse the Knee Joint Muscles during Flexion. Am. J. Biomed. Eng. (2016).

83. Dao, T. T. & Tho, M. C. H. B. A systematic review of continuum modeling of skeletal muscles: Current trends, limitations, and recommendations. Applied Bionics and Biomechanics (2018). doi:10.1155/2018/7631818

84. Teklemariam, A., Hodson-Tole, E., Reeves, N. D. & Cooper, G. A micromechanical muscle model for determining the impact of motor unit fiber clustering on force transmission in aging skeletal muscle. Biomech. Model. Mechanobiol. (2019). doi:10.1007/s10237-019-01152-2

85. Bosboom, E. M. H. et al. Passive transverse mechanical properties of skeletal muscle under in vivo compression. J. Biomech. (2001). doi:10.1016/S0021-9290(01)00083-5

86. Takaza, M., Moerman, K. M. & Simms, C. K. Passive skeletal muscle response to impact loading: Experimental testing and inverse modelling. J. Mech. Behav. Biomed. Mater. (2013). doi:10.1016/j.jmbbm.2013.04.016

87. Willard, F. H., Vleeming, A., Schuenke, M. D., Danneels, L. & Schleip, R. The thoracolumbar fascia: Anatomy, function and clinical considerations. Journal of Anatomy (2012). doi:10.1111/j.1469-7580.2012.01511.x

88. Wilke, J., Macchi, V., De Caro, R. & Stecco, C. Fascia thickness, aging and flexibility: is there an association? J. Anat. (2019). doi:10.1111/joa.12902

89. Vleeming, A. & Stoeckart, R. The role of the pelvic girdle in coupling the spine and the legs: A clinical-anatomical perspective on pelvic stability. in Movement, Stability & Lumbopelvic Pain (2007). doi:10.1016/B978-044310178-6.50010-4

90. Willard, F. H. The muscular, ligamentous, and neural structure of the lumbosacrum and its relationship to low back pain. in Movement, Stability & Lumbopelvic Pain (2007). doi:10.1016/B978-044310178-6.50003-7

91. Gracovetsky, S., Farfan, H. F. & Lamy, C. The mechanism of the lumbar spine. Spine (Phila. Pa. 1976). (1981). doi:10.1097/00007632-198105000-00007

92. Moorhouse, K. M. & Granata, K. P. Trunk stiffness and dynamics during active extension exertions. 38, 2000–2007 (2007).

93. Barker, P. J. et al. Effects of tensioning the lumbar fasciae on segmental stiffness during flexion and extension: Young investigator award winner. Spine (Phila. Pa. 1976). (2006). doi:10.1097/01.brs.0000195869.18844.56

94. Ranger, T. A., Newell, N., Grant, C. A., Barker, P. J. & Pearcy, M. J. Role of the Middle Lumbar Fascia on Spinal Mechanics. Spine (Phila. Pa. 1976). (2017). doi:10.1097/BRS.0000000000001854

95. Tesh, K. M., Dunn, J. S. & Evans, J. H. The abdominal muscles and vertebral stability. Spine (Phila. Pa. 1976). (1987). doi:10.1097/00007632-198706000-00014

96. Kirilova, M., Stoytchev, S., Pashkouleva, D. & Kavardzhikov, V. Experimental study of the mechanical properties of human abdominal fascia. Med. Eng. Phys. (2011). doi:10.1016/j.medengphy.2010.07.017

97. Chen, B., Zhao, H., Liao, L., Zhang, Z. & Liu, C. Reliability of shear-wave elastography in assessing thoracolumbar fascia elasticity in healthy male. Sci. Rep. (2020). doi:10.1038/s41598-020-77123-w

98. Henderson, E. R., Friend, E. J., Toscano, M. J., Parsons, K. J. & Tarlton, J. F. Biomechanical Comparison of Canine Fascia Lata and Thoracolumbar Fascia: An In Vitro Evaluation of Replacement Tissues for Body Wall Reconstruction. Vet. Surg. (2015). doi:10.1111/j.1532-950X.2014.12247.x

99. Kureshi, A., Vaiude, P., Nazhat, S. N., Petrie, A. & Brown, R. A. Matrix mechanical properties of transversalis fascia in inguinal herniation as a model for tissue expansion. J. Biomech. 41, 3462–3468 (2008).

100. Butler, D. L., Grood, E. S., Noyes, F. R., Zernicke, R. F. & Brackett, K. Effects of structure and strain measurement technique on the material properties of young human tendons and fascia. J. Biomech. (1984). doi:10.1016/0021-9290(84)90090-3

101. Yahia, L. H., Pigeon, P. & DesRosiers, E. A. Viscoelastic properties of the human lumbodorsal fascia. J. Biomed. Eng. (1993). doi:10.1016/0141-5425(93)90081-9

102. Cholewicki, J., Juluru, K. & McGill, S. M. Intra-abdominal pressure mechanism for stabilizing the lumbar spine. J. Biomech. (1999). doi:10.1016/S0021-9290(98)00129-8

103. Arjmand, N. & Shirazi-Adl, A. Role of intra-abdominal pressure in the unloading and stabilization of the human spine during static lifting tasks. Eur. Spine J. (2006). doi:10.1007/s00586-005-0012-9

104. Stokes, I. A. F., Gardner-Morse, M. G. & Henry, S. M. Intra-abdominal pressure and abdominal wall muscular function: Spinal unloading mechanism. Clin. Biomech. (2010). doi:10.1016/j.clinbiomech.2010.06.018

105. Echlin, K. Functional anatomy of the abdominal wall. in Oxford Textbook of Plastic and Reconstructive Surgery (2021). doi:10.1093/med/9780199682874.003.0101

106. ARJMAND, N., SHIRAZI-ADL, A. & PARNIANPOUR, M. A finite element model study on the role of trunk muscles in generating intra-abdominal pressure. Biomed. Eng. Appl. Basis Commun. 13, 181–189 (2001).

107. Marras, W. S. & Mirka, G. A. Intra-abdominal pressure during trunk extension motions. Clin. Biomech. (1996). doi:10.1016/0268-0033(96)00006-X

108. Lubowiecka, I. et al. A novel in vivo approach to assess strains of the human abdominal wall under known intraabdominal pressure. J. Mech. Behav. Biomed. Mater. 104902 (2021).

109. Song, C., Alijani, A., Frank, T., Hanna, G. & Cuschieri, A. Elasticity of the living abdominal wall in laparoscopic surgery. J. Biomech. 39, 587–591 (2006).

110. Song, C., Alijani, A., Frank, T., Hanna, G. B. & Cuschieri, A. Mechanical properties of the human abdominal wall measured in vivo during insufflation for laparoscopic surgery. Surg. Endosc. Other Interv. Tech. 20, 987–990 (2006).

111. Tongyoo, A., Chatthamrak, P., Sriussadaporn, E., Limpavitayaporn, P. & Mingmalairak, C. Risk assessment of abdominal wall thickness measured on pre-operative computerized tomography for incisional surgical site infection after abdominal surgery. J. Med. Assoc. Thail. (2015).

112. Borelli & Pauwels. Iatrophysics to Biomechanics. J Bone Jt. Surg 74, 335–339 (1992).

113. Harvey, W. Exercitatio anatomica de motus cordis et sanguinis in animalibus. Frankfurt (1628).

114. Weber, W. & Weber, E. Ueber die Mechanik der menschlichen Gehwerkzeuge, nebst der Beschreibung eines Versuchs über das Herausfallen des Schenkelkopfs aus der Pfanne im luftverdünnten Raume. Ann. Phys. (1837). doi:10.1002/andp.18371160102

115. Ranavolo, A. et al. Modelling the spine as a deformable body : Feasibility of reconstruction using an optoelectronic system. Appl. Ergon. 44, 192–199 (2013).

116. Marras, W. S. et al. Spine loading as a function of lift frequency , exposure duration , and work experience. 21, 345–352 (2006).

117. Arjmand, N., Gagnon, D., Plamondon, A., Shirazi-adl, A. & Larivière, C. Comparison of trunk muscle forces and spinal loads estimated by two biomechanical models. Clin. Biomech. 24, 533–541 (2009).

118. Shojaei, I., Arjmand, N., Meakin, J. R. & Bazrgari, B. A model-based approach for estimation of changes in lumbar segmental kinematics associated with alterations in trunk muscle forces. J. Biomech. 70, 82–87 (2018).

119. Christophy, M., Adila, N., Senan, F., Lotz, J. C. & Reilly, O. M. O. A Musculoskeletal model for the lumbar spine. 19–34 (2012). doi:10.1007/s10237-011-0290-6

120. Williamson Jr, F. Richard courant and the finite element method: A further look. Historia Mathematica. 369-378 (1980).

121. Burks, A. W. The invention of the universal electronic computer — how the Electronic Computer Revolution began. 18, 871–892 (2002).

122. Demkowicz, L. & Oden, J. T. A new finite element method for solving compressible navier-stokes equations based on an operator splitting method and. (1990).

123. Brekelmans, W. A. M., Poort, H. W. & Slooff, T. J. J. H. A new method to analyse the mechanical behaviour of skeletal parts. 43, 301–317 (2019).

124. Fagan, M. J., Julian, S. & Mohsen, A. M. Finite element analysis in spine research. 216, 281–298

125. Orne, D. & LIU, Y. K. A Mathematical Model of Spinal Response to Impact. 4, 49–71 (1970).

126. Prasad, P. & King, A. I. An Experimentally Validated Dynamic Model of the Spine. 546–550 (2019).

127. Williams, J. L. A Three-Dimensional Model of the Human Cervical Spine for Impact Simulation. (2017).

128. Newell, N. et al. Biomechanics of the human intervertebral disc : a review of testing techniques and results. J. Mech. Behav. Biomed. Mater. 69, 420–434 (2017).

129. Beebe, P., Bartel, D. & Graf, N. A Study of the Biomechanics of Spondylolysis. (2002).

130. Zander, T. & Bergmann, Æ. G. Comparison of the effects of bilateral posterior dynamic and rigid fixation devices on the loads in the lumbar spine : a finite element analysis. 1223–1231 (2007). doi:10.1007/s00586-006-0292-8

131. Spyrou, L. A. & Aravas, N. Muscle and Tendon Tissues: Constitutive Modeling and Computational Issues. J. Appl. Mech. (2011). doi:10.1115/1.4003741

132. Eberlein, R., Holzapfel, G. A. & Fro, M. Multi-segment FEA of the human lumbar spine including the heterogeneity of the annulus fibrosus. 34, 147–163 (2004).

133. Tesh, K. M., Dunn, J. S. & Evans, J. H. The abdominal muscles and vertebral stability. Spine (Phila. Pa. 1976). (1987). doi:10.1097/00007632-198706000-00014

134. Adams, M. A. & Dolan, P. CHAPTER 11 - How to use the spine, pelvis, and legs effectively in lifting. in Movement, Stability & Lumbopelvic Pain (Second Edition) (2007). doi:10.1111/jfb.12473

135. Stokes, I. A. F. & Gardner-Morse, M. Quantitative anatomy of the lumbar musculature. J. Biomech. (1999). doi:10.1016/S0021-9290(98)00164-X

136. Speich, J. E. et al. Adjustable passive length-tension curve in rabbit detrusor smooth muscle. J. Appl. Physiol. (2007). doi:10.1152/japplphysiol.00548.2006

137. Degens, H., Salmons, S. & Jarvis, J. C. Intramuscular pressure, force and blood flow in rabbit tibialis anterior muscles during single and repetitive contractions. Eur. J. Appl. Physiol. Occup. Physiol. (1998). doi:10.1007/s004210050381

138. Evertz, L. Q., Bulstra, L. F., Shin, A. Y. & Kaufman, K. R. Evaluate muscle tension using intramuscular pressure device in rabbit tibialis anterior model for improved tendon transfer surgery. Physiol. Meas. (2017). doi:10.1088/1361-6579/aa6739

139. Winters, T. M. et al. Correlation between isometric force and intramuscular pressure in rabbit tibialis anterior muscle with an intact anterior compartment. Muscle and Nerve (2009). doi:10.1002/mus.21298

140. Go, S. A. et al. Design Considerations of a Fiber Optic Pressure Sensor Protective Housing for Intramuscular Pressure Measurements. Ann. Biomed. Eng. (2017). doi:10.1007/s10439-016-1703-6

141. Järvholm, U., Palmerud, G., Styf, J., Herberts, P. & Kadefors, R. Intramuscular pressure in the supraspinatus muscle. J. Orthop. Res. (1988). doi:10.1002/jor.1100060210

142. Körner, L., Parker, P., Almström, C., Herberts, P. & Kadefors, R. The relation between spectral changes of the myoelectric signal and the intramuscular pressure of human skeletal muscle. Eur. J. Appl. Physiol. Occup. Physiol. (1984). doi:10.1007/BF00433393

143. Hodgkin, A. L. & Huxley, A. F. A quantitative description of membrane current and its application to conduction and excitation in nerve. J. Physiol. (1952). doi:10.1113/jphysiol.1952.sp004764

144. Huxley, A. F. Muscle structure and theories of contraction. Prog. Biophys. Biophys. Chem. (1957). doi:10.1016/s0096-4174(18)30128-8

145. Hill, A. V. The Heat of Shortening and the Dynamic Constants of Muscle. Proc. R. Soc. B Biol. Sci. 126, 136–195 (1938).

146. Winters, J. M. & Stark, L. Muscle models: What is gained and what is lost by varying model complexity. Biol. Cybern. (1987). doi:10.1007/BF00318375

147. Hatze, H. A myocybernetic control model of skeletal muscle. Biol. Cybern. (1977). doi:10.1007/BF00337268

148. Podolsky, R. J., Nolan, A. C. & Zaveler, S. A. Cross-bridge properties derived from muscle isotonic velocity transients. Proc. Natl. Acad. Sci. U. S. A. (1969). doi:10.1073/pnas.64.2.504

149. Hill, T. L., Eisenberg, E., Chen, Y. D. & Podolsky, R. J. Some self-consistent two-state sliding filament models of muscle contraction. Biophys. J. (1975). doi:10.1016/S0006-3495(75)85823-1

150. van Kaam, F. A. M., de Beer, E. L., Stienen, G. J. M. & Blangé, T. The influence of velocity of length change on tension development in skeletal muscle: Model calculations and experimental results. J. Biomech. (1984). doi:10.1016/0021-9290(84)90018-6

151. Delp, S. L. et al. An Interactive Graphics-Based Model of the Lower Extremity to Study Orthopaedic Surgical Procedures. IEEE Trans. Biomed. Eng. 37, 757–767 (1990).

152. Chao, E. Y. S., Lynch, J. D. & Vanderploeg, M. J. Simulation and animation of musculoskeletal joint system. J. Biomech. Eng. 115, 562–568 (1993).

153. Gatton, M., Pearcy, M. & Pettet, G. Modelling the line of action for the oblique abdominal muscles using an elliptical torso model. J. Biomech. (2001). doi:10.1016/S0021-9290(01)00079-3

154. Pandy, M. G. Computer Modeling and Simulation of Human Movement. Annu. Rev. Biomed. Eng. (2001). doi:10.1146/annurev.bioeng.3.1.245

155. Dong, F., Clapworthy, G. J., Krokos, M. A. & Yao, J. An anatomy-based approach to human muscle modeling and deformation. IEEE Trans. Vis. Comput. Graph. (2002). doi:10.1109/2945.998668

156. Johansson, T., Meier, P. & Blickhan, R. A finite-element model for the mechanical analysis of skeletal muscles. J. Theor. Biol. (2000). doi:10.1006/jtbi.2000.2109

157. Oomens, C. W. J., Maenhout, M., Van Oijen, C. H., Drost, M. R. & Baaijens, F. P. Finite element modelling of contracting skeletal muscle. in Philosophical Transactions of the Royal Society B: Biological Sciences (2003). doi:10.1098/rstb.2003.1345

158. Blemker, S. S., Pinsky, P. M. & Delp, S. L. A 3D model of muscle reveals the causes of nonuniform strains in the biceps brachii. J. Biomech. (2005). doi:10.1016/j.jbiomech.2004.04.009

159. Lemos, R. R., Rokne, J., Baranoski, G. V. G., Kawakami, Y. & Kurihara, T. Modeling and simulating the deformation of human skeletal muscle based on anatomy and physiology. in Computer Animation and Virtual Worlds (2005). doi:10.1002/cav.83

160. Röhrle, O. & Pullan, A. J. Three-dimensional finite element modelling of muscle forces during mastication. J. Biomech. (2007). doi:10.1016/j.jbiomech.2007.05.011

161. Böl, M. & Reese, S. Micromechanical modelling of skeletal muscles based on the finite element method. Comput. Methods Biomech. Biomed. Engin. (2008). doi:10.1080/10255840701771750

162. Blemker, S. S. & Delp, S. L. Three-dimensional representation of complex muscle architectures and geometries. Ann. Biomed. Eng. (2005). doi:10.1007/s10439-005-1433-7

163. Röhrle, O., Davidson, J. B. & Pullan, A. J. Bridging scales: A three-dimensional electromechanical finite element model of skeletal muscle. SIAM J. Sci. Comput. (2008). doi:10.1137/070691504

164. Böl, M., Kruse, R., Ehret, A. E., Leichsenring, K. & Siebert, T. Compressive properties of passive skeletal muscle-The impact of precise sample geometry on parameter identification in inverse finite element analysis. J. Biomech. (2012). doi:10.1016/j.jbiomech.2012.08.023

165. Siebert, T., Till, O. & Blickhan, R. Work partitioning of transversally loaded muscle: Experimentation and simulation. Comput. Methods Biomech. Biomed. Engin. (2014). doi:10.1080/10255842.2012.675056

166. Odegard, G. M., Donahue, T. L. H., Morrow, D. A. & Kaufman, K. R. Constitutive modeling of skeletal muscle tissue with an explicit strain-energy function. J. Biomech. Eng. (2008). doi:10.1115/1.3002766

167. Davis, J., Kaufman, K. R. & Lieber, R. L. Correlation between active and passive isometric force and intramuscular pressure in the isolated rabbit tibialis anterior muscle. J. Biomech. (2003). doi:10.1016/S0021-9290(02)00430-X

168. Calvo, B. et al. Passive nonlinear elastic behaviour of skeletal muscle: Experimental results and model formulation. J. Biomech. (2010). doi:10.1016/j.jbiomech.2009.08.032

169. Spyrou, L. A. & Aravas, N. Muscle and Tendon Tissues: Constitutive Modeling and Computational Issues. J. Appl. Mech. 78, 041015 (2011).

170. Daggfeldt, K. Muscle bulging reduces muscle force and limits the maximal effective muscle size. J. Mech. Med. Biol. (2006). doi:10.1142/s0219519406001947

171. Hargens, A. R., Mubarak, S. J., Owen, C. A., Garetto, L. P. & Akeson, W. H. Interstitial fluid pressure in muscle and compartment syndromes in man. Microvasc. Res. (1977). doi:10.1016/0026-2862(77)90136-4

172. Matsen, F. A., Mayo, K. A., Sheridan, G. W. & Krugmire, R. B. Monitoring of intramuscular pressure. Surgery (1976). doi:10.5555/uri:pii:0039606076902385

173. Hargens, A. R. et al. Tissue fluid pressures: From basic research tools to clinical applications. J. Orthop. Res. (1989). doi:10.1002/jor.1100070617

174. Dietrich, M., Kedzior, K. & Zagrajek, T. Modeling of muscle action and stability of the human spine. in Multiple Muscle Systems 451–460 (Springer, 1990).

175. Dietrich, M., Kedzior, K. & Zagrajek, T. A Biomechanical Model of the Human Spinal System. Proc. Inst. Mech. Eng. Part H J. Eng. Med. (1991). doi:10.1243/PIME_PROC_1991_205_257_02

176. Daggfeldt, K. & Thorstensson, A. The role of intra-abdominal pressure in spinal unloading. J. Biomech. (1997). doi:10.1016/S0021-9290(97)00096-1

177. Meijer, G. Development of a non-fusion scoliosis correction device. Numerical modelling of scoliosis correction. (2011).

178. El Ouaaid, Z., Shirazi-Adl, A., Plamondon, A. & Larivière, C. Trunk strength, muscle activity and spinal loads in maximum isometric flexion and extension exertions: A combined in vivo-computational study. J. Biomech. (2013). doi:10.1016/j.jbiomech.2013.06.018

179. Driscoll, M. Fascia – The unsung hero of spine biomechanics. Journal of Bodywork and Movement Therapies (2018). doi:10.1016/j.jbmt.2017.10.014

180. El-Monajjed, K. & Driscoll, M. A finite element analysis of the intra-abdominal pressure and paraspinal muscle compartment pressure interaction through the thoracolumbar fascia. Comput. Methods Biomech. Biomed. Engin. (2020). doi:10.1080/10255842.2020.1752682

181. Vleeming, A., Schuenke, M. D., Danneels, L. & Willard, F. H. The functional coupling of the deep abdominal and paraspinal muscles: The effects of simulated paraspinal muscle contraction on force transfer to the middle and posterior layer of the thoracolumbar fascia. J. Anat. (2014). doi:10.1111/joa.12227

182. Dreischarf, M. et al. Comparison of eight published static fi nite element models of the intact lumbar spine : Predictive power of models improves when combined together. J. Biomech. 47, 1757–1766 (2014).

183. Schmidt, H., Galbusera, F., Rohlmann, A., Zander, T. & Wilke, H. J. Effect of multilevel lumbar disc arthroplasty on spine kinematics and facet joint loads in flexion and extension: A finite element analysis. Eur. Spine J. (2012). doi:10.1007/s00586-010-1382-1

184. Little, J. P. & Adam, C. J. Geometric sensitivity of patient-specific finite element models of the spine to variability in user-selected anatomical landmarks. Comput. Methods Biomech. Biomed. Engin. (2015). doi:10.1080/10255842.2013.843673

185. Goel, V. K. et al. Effects of Charité artificial disc on the implanted and adjacent spinal segments mechanics using a hybrid testing protocol. Spine (Phila. Pa. 1976). (2005). doi:10.1097/01.brs.0000195897.17277.67

186. Shirazi-Adl, A. & Parnianpour, M. Load-bearing and stress analysis of the human spine under a novel wrapping compression loading. Clin. Biomech. (2000). doi:10.1016/S0268-0033(00)00045-0

187. Jones, A. C. & Wilcox, R. K. Finite element analysis of the spine : Towards a framework of verification , validation and sensitivity analysis. 30, 1287–1304 (2008).

188. Cheung, J. T., Zhang, M., Leung, A. K. & Fan, Y. Three-dimensional finite element analysis of the foot during standing — a material sensitivity study. 38, 1045–1054 (2005).

189. Oreskes, N., Shrader-Frechette, K. & Belitz, K. Verification, validation, and confirmation of numerical models in the earth sciences. Science (80-.). (1994). doi:10.1126/science.263.5147.641

190. Lewandowski, A. Issues in model validation. Int. Inst. Appl. Syst. Anal. (1982).

191. Arjmand, N. Role of intra-abdominal pressure in the unloading and stabilization of the human spine during static lifting tasks. 1265–1275 (2006). doi:10.1007/s00586-005-0012-9

192. Viceconti, M., Olsen, S. & Burton, K. Extracting clinically relevant data from finite element simulations. Clin. Biomech. 20, 451–454 (2005).

193. Ross, C. F. et al. Modeling Masticatory Muscle Force in Finite Element Analysis: Sensitivity Analysis Using Principal Coordinates Analysis. 299, 288–299 (2005).

194. Freburger, J. K. et al. The Rising Prevalence of Chronic Low Back Pain. Natl. Institutes Heal. 169, 251–258 (2015).

195. Gatchel, R. J. Low Back Pain: Recent Advances and Perspectives.

196. Dipphysio, P. O. S. Acute Low Back Pain: Beyond Drug Therapies. (2014).

197. O'Sullivan, P., Smith, A., Beales, D. & Straker, L. Understanding Adolescent Low Back Pain From a Multidimensional Perspective: Implications for Management. J. Orthop. Sport. Phys. Ther. 47, 741–751 (2017).

198. Allan, D. B. & Waddell, G. An historical perspective on low back pain and disability. Acta Orthop. 60, 1–23 (1989).

199. Riihimäki, H. Back pain and heavy physical work: a comparative study of concrete reinforcement workers and maintenance house painters. Br. J. Ind. Med. 42, 226–232 (1985).

200. Jacobs, P. The cost of low-back pain : a review of the literature. Health Econ. 1–14 (2003). doi:10.1115/1.3101931

201. Johnson, C. L. et al. National health and nutrition examination survey: analytic guidelines, 1999-2010. Natl. Cent. Heal. Stat. Vital Heal. Stat (2013). doi:10.4103/0973-7847.194042

202. Epidemiological, A. N. Risk Factors in Low-Back. 65,

203. Cholewicki, J., Juluru, K., Radebold, A., Panjabi, M. & McGill, S. Lumbar spine stability can be augmented with an abdominal belt and/or increased intra-abdominal pressure. Eur spine J 8, 388–395 (1999).

204. Benyamina Douma, N., Côté, C. & Lacasse, A. Quebec Serve and Protect Low Back Pain Study: What About Mental Quality of Life? Saf. Health Work (2018). doi:10.1016/j.shaw.2018.08.006

205. Besen, E., Young, A. E. & Shaw, W. S. Returning to Work Following Low Back Pain: Towards a Model of Individual Psychosocial Factors. J. Occup. Rehabil. 25, 25–37 (2015).

206. Deyo, R. A. et al. Trajectories of symptoms and function in older adults with low back disorders. Spine (Phila. Pa. 1976). 40, 1352–1362 (2015).

207. Billis, E. V., McCarthy, C. J. & Oldham, J. A. Subclassification of low back pain: A cross-country comparison. Eur. Spine J. 16, 865–879 (2007).

208. Hyodo, H., Sato, T., Sasaki, H. & Tanaka, Y. Discogenic pain in acute nonspecific low-back pain. Eur. Spine J. 14, 573–577 (2005).

209. Schleip, R., Zorn, A. & Klingler, W. Biomechanical properties of fascial tissues and their role as pain generators. J. Musculoskelet. Pain 18, 393–395 (2010).

210. Panjabi, M. M. The stabilizing system of the spine. Part II. neutral zone and instability hypothesis. J. Spinal Disord. 5, 390–397 (1992).

211. Janzen, K. & Peters-Watral, B. Treating co-occurring chronic low back pain & generalized anxiety disorder. Nurse Pract. 41, 12–18 (2016).

212. Casazza, B. Diagnosis and Treatment of Acute Low Back Pain. Am. Fam. Physician (2012).

213. Koes, B. W. et al. An updated overview of clinical guidelines for the management of non-specific low back pain in primary care. Eur. Spine J. 19, 2075–2094 (2010).

214. Karayannis, N. V., Jull, G. A. & Hodges, P. W. Physiotherapy movement based classification approaches to low back pain: Comparison of subgroups through review and developer/expert survey. BMC Musculoskelet. Disord. 13, 24 (2012).

215. Cherkin, D. C., Deyo, R. A., Battié, M., Street, J. & Barlow, W. A Comparison of Physical Therapy, Chiropractic Manipulation, and Provision of an Educational Booklet for the Treatment of Patients with Low Back Pain. N. Engl. J. Med. 339, 1021–1029 (1998).

216. Rosenstiel, A. K. & Keefe, F. J. The use of coping strategies in chronic low back pain patients: Relationship to patient characteristics and current adjustment. Pain 17, 33–44 (1983).

217. Society, P. Interventional Therapies, Surgery, and Interdisciplinary Rehabilitation for Low Back Pain. Spine (Phila. Pa. 1976). 34, 1066–1077 (2009).

218. Beazell, J. R., Mullins, M. & Grindstaff, T. L. Lumbar instability: an evolving and challenging concept. J. Man. Manip. Ther. 18, 9–14 (2010).

219. White, A. A., Johnson, R. M., Panjabi, M. M. & Southwick, W. O. Biomechanical analysis of clinical stability in the cervical spine. Clin. Orthop. Relat. Res. (1975). doi:1132209

220. McGill, S. M. & Cholewicki, J. Biomechanical basis for stability: an explanation to enhance clinical utility. J. Orthop. Sports Phys. Ther. 31, 96–100 (2001).

221. Kirkaldy-Willis, W. H. Presidential symposium on instability of the lumbar spine: Introduction. Spine (1985). doi:10.1097/00007632-198504000-00012

222. Boden, S. D. & Wiesel, S. W. Lumbosacral segmental motion in normal individuals: Have we been measuring instability properly? Spine (Phila. Pa. 1976). (1990). doi:10.1097/00007632-199006000-00026

223. Pope, M. H. & Panjabi, M. M. Biomechanical Definitions of Spinal Instability. Spine (Phila. Pa. 1976). 10, 255–256 (1985).

224. Hukins, D. W. L. What is lumbar instability. Lumbar spine Disord. Curr. concepts 26–37 (1995).

225. White, A. A. & Panjabi, M. M. The basic kinematics of the human spine: A review of past and current knowledge. Spine (Phila. Pa. 1976). (1978). doi:10.1097/00007632-197803000-00003

226. Driscoll, M. et al. Biomechanical assessment of reduction forces measured during scoliotic instrumentation using two different screw designs. Spine Deform. 1, 94–101 (2013).

227. Driscoll, M. et al. Biomechanical Comparison of 2 Different Pedicle Screw Systems During the Surgical Correction of Adult Spinal Deformities. Spine Deform. 3, 114–121 (2015).

228. Dimnet, J., Fischer, L. P., Gonon, G. & Carret, J. P. Radiographic studies of lateral flexion in the lumbar spine. J. Biomech. (1978). doi:10.1016/0021-9290(78)90006-4

229. Rolander, S. D. Motion of the lumbar spine with special reference to the stabilizing effect of posterior fusion. An experimental study on autopsy specimens. Acta Orthop. Scand. Suppl 90:1-144 (1966).

230. Hodges, P. W., Shirley, D., Gandevia, S. C. & Physiotherapy, R. Lumbar spine stiffness is increased by elevation of intra- abdominal pressure 1. 3–5 (1999).

231. Kumar, S. & Davis, P. R. Spinal loading in static and dynamic postures : EMG and intra-abdominal pressure study. 0139, (2007).

232. Meakin, J. R. & Aspden, R. Static and dynamic stability of the spine. (2006). doi:10.1016/j.jbiomech.2006.07.014

233. McGill, S. M. & Norman, R. W. Reassessment of the role of intra-abdominal pressure in spinal compression. Ergonomics (1987). doi:10.1080/00140138708966048

234. Mengert, W. F. & Murphy, D. P. Intra-abdominal pressures created by voluntary muscular effort. Surg Gynecol Obs. 57, 745–751 (1933).

235. Keith, S. A. Man's Posture; Its Evolution and Disorders. (1923).

236. Bartelink, D. L. The role of abdominal pressure in relieving the pressure on the lumbar intervertebral discs. J. Bone Joint Surg. Br. (1957). doi:10.1016/S0140-6736(01)35637-4

237. Morris, J. M., Lucas, D. B. & Bresler, B. Role of the Trunk in Stability of the Spine. J. Bone Jt. Surg. (1961). doi:10.2106/00004623-196143030-00001

238. Peter Reeves, N., Narendra, K. S. & Cholewicki, J. Spine stability: The six blind men and the elephant. Clinical Biomechanics (2007). doi:10.1016/j.clinbiomech.2006.11.011

239. Diee, J. H. Van, Selen, L. P. J. & Cholewicki, J. Trunk muscle activation in low-back pain patients , an analysis of the literature. J. Electromyogr. Kinesiol. 13, 333–351 (2003).

240. Cholewicki, J. & McGill, S. M. Mechanical stability of the in vivo lumbar spine : implications for injury and chronic low back pain. J. Clin. Biomech. 11, 1–15 (1996).

241. Granata, K. & England, S. Stability of Dynamic Trunk Movement. Natl. Institutes Heal. 31, 1–13 (2006).

242. Meakin, J. R., Hukins, D. W. L. & Aspden, R. M. Euler buckling as a model for the curvature and flexion of the human lumbar spine. 1383–1387 (1996).

243. Schleip, R. & Klingler, W. Active fascial contractility : Fascia may be able to contract in a smooth muscle-like manner and thereby influence musculoskeletal dynamics. 273–277 (2005). doi:10.1016/j.mehy.2005.03.005

244. Mengiardi, B., Pfirrmann, C. W. A. & Gerber, C. Frozen Shoulder: MR Arthographic Findings. J. Musculoskelet. Imaging 233, 486–492 (2004).

245. Prilutsky, B. I. & Zatsiorsky, V. M. Optimization-based models of muscle coordination. Exerc. Sport Sci. Rev. (2002). doi:10.1097/00003677-200201000-00007

246. Heintz, S. Muscular forces from static optimization. (2006).

247. Brown, S. H. M. & Potvin, J. R. Constraining spine stability levels in an optimization model leads to the prediction of trunk muscle cocontraction and improved spine compression force estimates. J. Biomech. (2005). doi:10.1016/j.jbiomech.2004.05.011

248. Stokes, I. A. F. & Gardner-Morse, M. Muscle activation strategies and symmetry of spinal loading in the lumbar spine with scoliosis. Spine (Phila. Pa. 1976). (2004). doi:10.1097/01.brs.0000141182.42544.1f

249. Hughes, R. E., Chaffin, D. B., Lavender, S. A. & Andersson, G. B. J. Evaluation of muscle force prediction models of the lumbar trunk using surface electromyography. J. Orthop. Res. (1994). doi:10.1002/jor.1100120512

250. An, K. N., Kwak, B. M., Chao, E. Y. & Morrey, B. F. Determination of muscle and joint forces: A new technique to solve the indeterminate problem. J. Biomech. Eng. (1984). doi:10.1115/1.3138507

251. Stokes, I. A. F. & Gardner-Morse, M. Lumbar spinal muscle activation synergies predicted by multi-criteria cost function. J. Biomech. 34, 733–740 (2001).

252. Stokes, I. A. F. & Gardner-Morse, M. Lumbar spine maximum efforts and muscle recruitment patterns predicted by a model with multijoint muscles and joints with stiffness. J. Biomech. (1995). doi:10.1016/0021-9290(94)E0040-A

253. Roberts, T. J. The integrated function of muscles and tendons during locomotion. in Comparative Biochemistry and Physiology - A Molecular and Integrative Physiology (2002). doi:10.1016/S1095-6433(02)00244-1

254. Sharma, M., Langrana, N. A. & Rodriguez, J. Role of ligaments and facets in lumbar spinal stability. Spine (Phila. Pa. 1976). (1995). doi:10.1097/00007632-199504150-00003

255. Morris, J. M., Lucas, D. B. & Bresler, B. Role of the Trunk in Stability of the Spine. J. Bone Jt. Surg. (1961). doi:10.2106/00004623-196143030-00001

256. Alexander, R. M. N. Tendon elasticity and muscle function. in Comparative Biochemistry and Physiology - A Molecular and Integrative Physiology (2002). doi:10.1016/S1095-6433(02)00143-5

257. Adams, M. A. & Dolan, P. Spine biomechanics. J. Biomech. (2005). doi:10.1016/j.jbiomech.2005.03.028

258. Keaveny, T. M., Wachtel, E. F. & Kopperdahl, D. L. Mechanical behavior of human trabecular bone after overloading. J. Orthop. Res. (1999). doi:10.1002/jor.1100170308

259. Benedict, J. V., Walker, L. B. & Harris, E. H. Stress-strain characteristics and tensile strength of unembalmed human tendon. J. Biomech. (1968). doi:10.1016/0021-9290(68)90038-9

260. Yang, T. et al. The rule of strain in different stratification of the intervertebral disc under physiologic loading. Biomed. Res. (2017).

261. Peter Reeves, N., Narendra, K. S. & Cholewicki, J. Spine stability: The six blind men and the elephant. Clinical Biomechanics (2007). doi:10.1016/j.clinbiomech.2006.11.011

262. Kavcic, N., Grenier, S. & McGill, S. M. Quantifying tissue loads and spine stability while performing commonly prescribed low back stabilization exercises. Spine (Phila. Pa. 1976). (2004). doi:10.1097/01.brs.0000142222.62203.67

263. McGill, S. M., Grenier, S., Kavcic, N. & Cholewicki, J. Coordination of muscle activity to assure stability of the lumbar spine. J. Electromyogr. Kinesiol. (2003). doi:10.1016/S1050-6411(03)00043-9

264. Gardner-Morse, M. G. & Stokes, I. A. F. The effects of abdominal muscle coactivation on lumbar spine stability. Spine (Phila. Pa. 1976). (1998). doi:10.1097/00007632-199801010-00019

265. Hukins, D. W. L., Aspden, R. M. & Hickey, D. S. Thorecolumlbar fascia can increase the efficiency of the erector spinae muscles. Clin. Biomech. (1990). doi:10.1016/0268-0033(90)90029-6

266. Macintosh, J. E., Bogduk, N. & Gracovetsky, S. The biomechanics of the thoracolumbar fascia. Clin. Biomech. (1987). doi:10.1016/0268-0033(87)90132-X

267. Malbrain, M. L. N. G., Peeters, Y. & Wise, R. The neglected role of abdominal compliance in organ-organ interactions. Critical Care (2016). doi:10.1186/s13054-016-1220-x

268. Yoshino, O., Quail, A., Oldmeadow, C. & Balogh, Z. J. The interpretation of intra-abdominal pressures from animal models: The rabbit to human example. Injury (2012). doi:10.1016/j.injury.2011.04.011

269. Shemmell, J., Krutky, M. A. & Perreault, E. J. Stretch sensitive reflexes as an adaptive mechanism for maintaining limb stability. Clinical Neurophysiology (2010). doi:10.1016/j.clinph.2010.02.166

270. Watanabe, N. & Hotta, H. Heart rate changes in response to mechanical pressure stimulation of skeletal muscles are mediated by cardiac sympathetic nerve activity. Frontiers in neuroscience (2017).

271. Holt, G. A., Dalziel, D. J. & Davenport, P. W. The transduction properties of diaphragmatic mechanoreceptors. Neuroscience letters (1991).

272. Creze, M., Soubeyrand, M. & Gagey, O. The paraspinal muscle-tendon system: Its paradoxical anatomy. PLoS One (2019). doi:10.1371/journal.pone.0214812